The University of Nottingham
UNITED KINGDOM · CHINA · MALAYSIA
Faculty of Engineering - Civil Engineering Department

Multi-scale Response of Sustainable Self- Compacting Concrete (SCC) to Carbonation and Chloride Penetration

Thesis submitted to the University of Nottingham for the degree of Doctor of Philosophy in Civil Engineering

by

Mahmoud Kh. Mohammed
BSc Eng., MSc Eng.

Supervised by
Andrew R. Dawson and Nick H. Thom

July 2015

Dedication

This thesis is dedicated to her pure soul (my mother) who wasn't able to read or write during her life

Mom, I remember that day very well in my childhood when you told me: "One day I want to be proud of you my son"

Today, I hope that I achieved your desire .....

Mahmoud

May 2015

List of Abbreviation and Notations

ACI: American Concrete Institute
Afm, Aft: Ettringite (**Aft**: mono-sulfate or (Al_2O_3 -Fe_2O_3- mono, **Afm**: sulfoaluminate hydrates Al_2O_3 -Fe_2O_3- tri)
agg. : aggregate
APD: Average Pore Diameter
ASTM: American Society of Testing Materials
BJ: Step value (J-ring Test)
BSE: Back-Scattered Electron
C(x,t): chloride concentration at depth x
C: Calcite ($CaCO_3$)
C: concentration of CO_2 or Cl^-
C_0: initial chloride content
C_2S: Di calcium silicate
C_3A: Tri calcium aluminate
C_3S: Tri calcium silicate
C_4AF: Tetra calcium alumino-ferrite
C_{cr} : chloride threshold
CEMI: Portland cement (CEM I 52.5R)
CH: Calcium hydroxide
Cl^-: Chloride ion
CM: Cement Matrix
CO_2: Carbon Dioxide
CPD: Critical Pore Diameter
C_s: Surface chloride concentration
CSH: Calcium Silicate Hydrate
CSI: Cement Sustainability Initiative
CSTR61: Concrete Society Technical Report 61
***d* or X_c**: Depth of carbonation
D: diffusion coefficient
D_a (t): Time dependent chloride diffusion coefficient
D_a_0 (t): Achieved apparent chloride diffusion coefficient (D_{nss}) at maturity age t_0
D_0: migration coefficient of matrix alone
D_{cl}: migration coefficient of mortar
DEF: Delayed Ettringite formation
divJ_{cl} : the chloride flux term
D_{nss}: apparent chloride diffusion coefficient (non-steady state)
D_{nssm}: non-steady state migration coefficient
DTG: derivative of weight loss
EDS or EDX: Energy-Dispersive X-ray
EFNARC: European Guidelines for Self-Compacting Concrete
erf: error function
FA: Fly ash
FA-SCC: Fly Ash Self-compacting Concrete
FA-SF-SCC: Fly Ash- Silica Fume -Self-compacting Concrete

FTIR: Fourier transformation infrared spectroscopy
g: gram
g: in Eq. (acceleration due to gravity)
ggbs: Ground granulated blastfurnace slag
HPC: High Performance Concrete
IR: Insoluble residue
ITZ: Interfacial Transition Zone
J: flux of CO_2 or Cl^-
K: coefficient of (Permeability or Carbonation)
k: intrinsic permeability of materials
$\mathbf{K_{acc}}$: accelerated carbonation coefficient
$\mathbf{K_{act}}$: actual carbonation coefficient
$\mathbf{K_{cr}}$: Chloride penetration parameter
l: length
L: Liter
LOI: Loss on ignition
LP: limestone powder
LP-SCC: Limestone Self-compacting Concrete
M: Metakaolin
Ma-*P*%: Macro pores percentages
Mi-*P* %: Miacro pores percentages
MIP: Mercury Intrusion Porosimetry
n: curve fitting factor
NVC: Normal Vibrated Concrete
$\mathbf{OH^-}$: Hydroxyl ion
OPC: Ordinary Portland Cement
P: Intrusion pressure
P: Porosity
$\mathbf{P_c}$: Capillary pressure
PCE: polycarboxylic ether
PFA: Pulverized Fuel Ash
$\boldsymbol{P_V}$: Macro-porosity (vacuum)
Q: Flow rate
$\mathbf{Q_{cl}}$: sink term for modeling of equilibrium between free and bound chloride
r: Pore radius
RHA: Rice Husk Ash
RILEM: International Union of Laboratories and Experts in Construction Materials, Systems and Structures
RMT: Rapid Migration Test
R-SCC: Reference Self-compacting Concrete
SCC: Self Compacting Concrete
SCMs: Supplementary Cementitious Materials
SE: Secondary Electron
SEM: Scanning Electron Microscopy
SF: Silica Fume
SI: Segregation Index
Sp. Gr: Specific Gravity

SP: Super-Plasticizer
t: time
$\mathbf{t_0}$: Reference maturity age (when concrete exposed to chloride)
$\mathbf{T_{50}}$: Time to obtain 50cm flow
TGA: Thermo Gravimetric Analysis
v: Apparent velocity of flow of water per unit time per unit area
V: Volume
$\mathbf{V_f}$: aggregate volume fraction
w/c ratio: water to cement ratio
w/cm ratio: water to cementitious ratio
x: depth
XRD: X-ray Diffraction
α: Aging factor (reduction in D_{nss} with time due to continuous hydration plus binding effect
γ: Mercury surface tension
η: Dynamic viscosity of the liquid
θ: Contact angle (140º)
ρ: concrete/ fluid bulk density
$\mathbf{\varphi SC_{cl}}$: potential term, porosity and saturation is directly obtained by thermo-hygro physics

Abstract

The work described in this thesis has been performed in order to gain further understanding of the relationship between the microstructural characteristics of some common types of medium to high strength sustainable Self- Compacting Concretes (SCCs) (especially the internal pore structure, the interfacial transition zone (ITZ), and chemical composition) and the carbon dioxide and chloride diffusivities. This was done by evaluating the diffusion coefficients with the aid of some selected and modified accelerated tests at the macro scale. The internal composition and microstructure form were quantitatively analyzed for one normal vibrated concrete (NVC), one normal SCC mix (R-SCC) and three different types of sustainable SCCs with relatively high partial replacement of cement at micro and nano scales and linked with the macro scale tests. This was done by using a wide range of advanced techniques such as thermo gravimetric analysis (TGA), x-ray diffraction (XRD), mercury intrusion porosimetry (MIP) and scanning electron microscopy (SEM). In addition, the penetration parameters from the macro short term tests were used to simulate the results mathematically in order to assess the long term behavior of the concrete mixes.

Possible mechanisms, in multi-scale terms, are proposed to explain the overall response of both normal and sustainable medium to high strength grade SCCs to the degradation caused by carbonation and chloride penetration in harsh environments. The findings of the research will contribute to deeply understand the role of the internal microstructure of sustainable SCC in determining the carbonation and chloride penetration. The recommendations derived from this research are fundamental to achieving more durable sustainable SCC with longer service life for applications in aggressive environments.

At the macro scale, it was found that SCC exhibited lower carbonation resistance than NVC in the short term. However, the modification of the internal micro structure in this type of concrete enabled it to resist CO_2 penetration over the long term, during the service life, based on the modeling results. Overall, the research suggests that carbonation of SCC may not be chemically controlled, rather, the internal pore structure may play an important role. Furthermore, the effect of carbonation on the internal pore structure and the chemistry of the concrete matrices were more noticeable in SCC containing fly ash with silica fume than in those with limestone powder or fly ash replacements. The significant improvement of the internal pore structure by using multi-active fillers and mineral admixtures is not recommended for the sustainable SCC which might be exposed to severe combined

environments (carbonation and chloride). In aggressive chloride environments, sustainable SCC was more suitable than NVC except when using the unreactive (limestone) filler type.

At micro scales, it was deduced that the degree of percolation of the pores of the ITZ had a significant role in controlling the chloride penetration process. Further, it is proposed that the ITZ thickness might be, primarily, responsible in determining the chloride ions' migration velocity especially when coarse and unreactive filler are used. At nano scale, it is also suggested that the critical pore diameter in the cement matrix is more significant than is the average pore diameter in controlling the chloride resistance in SCC. Further, the features of the internal pore structure and the strength level at the macro scale had less effect than the micro-scale properties on the whole response of sustainable SCC to carbonation and chloride ingress in both short and long term tests.

The chloride numerical results indicated that the NVC at the same design strength level as the reference SCC showed lower service life and higher depth of cover design. For the sustainable SCC, the results showed that the incorporation of relatively high partial replacement of fly ash Class F and the combined high partial replacement of fly ash with the silica fume has little effect on the penetration parameter (K_{cr}) relative to that of reference-SCC. However, the incorporating of limestone powder at the same cement replacement ratio as other admixtures increased the K_{cr}, reduced the service life and increased the depth of cover design even when compared to the NVC at the same strength level.

Declaration

I declare that the contents and the work described in this thesis were performed at the University of Nottingham, Faculty of Engineering from October 2011 to May 2015. I hereby certify that this thesis is my own and has not been submitted in whole or in part to any other university or any other educational association for a higher degree.

Mahmoud Khashaa Mohammed

Nottingham, May 2015

Emails: evxmkm@nottingham.ac.uk, mahmoudkh_ani@yahoo.com

We declare that the contents and the work described in this thesis were performed at the University of Nottingham, Faculty of Engineering from October 2011 to May 2015 and under our supervision.

Andrew Dawson

Associate Professor,

Nottingham Transportation Engineering Centre

Faculty of Engineering

Email: andrew.dawson@nottingham.ac.uk,

Dr. Nick Thom

Lecturer,

Nottingham Transportation Engineering Centre

Faculty of Engineering

Email: nicholas.thom@nottingham.ac.uk,

Acknowledgement

First of all, I have to thank God "Allah" who gave me the power, the patience and the continuation to be able to complete my study.

By the end of my PhD, I can say that both acquiring of the knowledge and solving the research problems independently are the most enjoyable parts during the PhD journey. However, the support and the guidance of other people contribute effectively for a successful one. The current work was performed with the help of many people whom I would like to express my deepest appreciation.

The first two persons that I would like to offer my special thanks and sincere gratitude are my supervisors (**Andrew Dawson** and **Nick Thom**). They have been extraordinarily tolerant and supportive. Without their guidance and persistent help this thesis would not have been possible. I am particularly grateful for the great assistance, motivation and encouragement given by Andrew who gave me a lot of his professionalism, scientific and practical experience. From you as an exceptional supervisor I have learned a lot and my words are not enough to express my deepest gratitude. My supervisors (Andrew and Nick) I will never forget your help.

The author would like to express his gratitude for his PhD scholarship sponsored by Higher Committee for Education Development in Iraq (HCED). I am indebt to the all the staff of this committee for their help before and during the study. I am deeply grateful to all technical staff of NTEC (Nottingham Transportation Engineering Centre) and Structural & Concrete Laboratory for their help in the experimental work especially Mr. Mick Winfield, Mr. Richard Blakemore and Miss Nancy Milne. The author wish also thanks Mr. Keith Dinsdale (Chief Experimental Officer, University of Nottingham-Faculty of Engineering), Mrs Vikki Archibald (Analytical Technician, University of Nottingham- Faculty of Engineering) and Dr. Nigel Neate (University of Nottingham-Faculty of Engineering) for their help and guidance in conducting the MIP, TGA and SEM tests.

Thanks should also go to Mr Jason Heaton a member of the Department of Electrical and Electronic Engineering, University of Nottingham for his help in the arrangement of the accelerated chloride penetration test. The author would like to gratefully acknowledge Mr.

Saddam Al-Mudhady (PhD-student in the school of chemistry-Nottingham University), Mr. Mark Dale (Rock Mechanics Technician, and Mr. Matthew Lane (Technician) for their precious assistance in preparing the concrete powder samples and conducting the titration tests. My deepest heartfelt to all my colleagues: Dr Khalid, Dr Savas, Dr Pejman, Dr Marva, Dr Alan, Dr Adam, Dr Usama, Dr Rose, Dr Cinzia, Dr Mahmoud, Raheem, Ameer, KayC, Venon, Ahmed, Ayad, Waleed, Hasan, Hamed, Ahmed Nassar, Rami, Ahmed Ibrahim, Syed, Haneen, Tariq, Harith, Yasameen and all the PhD students who come thereafter to the NTEC. Thank you very much my friends and for all the others who I did not mention.

The author also would like to give his special thanks to the PhD examination committee for their valuable discussions and suggestions: Professor Peter Claisse for his acceptance to review the work and to do the final exam and Dr Mathew Hall as an internal examiner for his continues help and his suggestions during the PhD and during the correction process.

Finally, I owe my deepest gratitude to my whole lovely family for their continuous support. Dear wife Suzan and my little princesses (Doha, Doaa and Saja), I know that you wanted to spend holiday times in discovering this lovely country (UK) but I was busy most of the time. Please forgive me for this. Dad, brothers and sisters: I miss you a lot through the last three years and I never forget that you're praying for me to complete my study to meet you again. I pray to Allah to keep you in a safe condition during this difficult period in Iraq till we can meet again.

Mahmoud

May 2015

Tables of contents

List of Tables

List of Figures

Chapter 1:
Introduction

1.1 General background

Most of the people might not know a lot about it or at least do not like it too much but, concrete is around us everywhere. If you do not live alone in the middle of a desert or a sea!, please just turn your head around and you will discover this fact. There is no doubt that the concrete is of special importance in the buildings and constructions. Among the other building and construction materials (i.e. steel, brick asphalt, timber etc.), it is still in the top rank according to its highest consumption compared to others worldwide. According to the Cement Sustainability Initiative, CSI (2009), the consumption of the concrete is expected to be equal to 25 billion tons per year which means above 3.8 tons per person per year in the world.

On the one hand, it is so easy to mix cement, aggregate (fine + coarse) and water to produce fresh concrete mix. Again, it is so simple to cast this mix in any shape to produce an object with certain strength. On the other hand, it is very difficult to totally understand its characteristics in both its fresh and hardened conditions (De Schutter et al., 2008).

The ease of concrete production, with low cost, the availability of its raw material, and the excellent resistance against water might be considered as the key features that make concrete the most used construction materials. However, the high emission of the CO_2 to the atmosphere during the manufacturing process of cement increases the concern about using this material widely. Therefore, the use of novel and sustainable concrete with low cement content becomes a very attractive approach to reduce this concern.

Since it was introduced for the first time in the early nineties (De Schutter and Audenaert 2007), Self-Compacting Concrete (SCC) has become one of the most desirable types of concrete due to the benefits listed later on, and it has opened a new area of research in the field of concrete technology. Liu (2009) stated that the number of published research works which deal with the SCC topic has witnessed a significant increase, showing the interest in developing this type of concrete. Iureş and Bob (2010)

demonstrated that SCC can be considered as a modern construction material with wide applicability. Moreover, it represents the biggest innovation in concrete technology for many years because of both its performance and ease of installation.

SCC has been defined in different ways by many researchers and guidelines. However, SCC is a highly flowable concrete which can totally fill the formwork under the action of the gravity, even with a high congestion of steel reinforcement, and can compact totally under its own weight without segregation and bleeding. According to this definition, SCC in the fresh stage should meet three main criteria (De Schutter et al., 2008):

i: superior flowing ability

ii: good obstruction-passing ability

iii: sufficient resistance to segregation

Due to its excellent fresh features, the benefits of using SCC can be summarized as follows (Ouchi, 2001, De Schutter et al., 2003, CIP.37, 2004):

- Faster casting and better finishing with less effort.
- The omission of vibration, reducing the electricity consumption and the necessity of skilled workers.
- Improvements in the working environment and conditions by avoiding noise.
- Ability to pump for long distances, allowing its use in a wide range of structures.
- Incorporation of natural or artificial waste materials, making it an environmental-friendly material.
- Increase of the safety of the jobsite.
- Provision of uniform concrete surfaces for architectural purposes.
- Increase in the bond strength with the steel reinforcement, and
- Increase (theoretically) in the durability in comparison with the normal vibrated concrete (NVC).

However, one of the most important concerns of SCC is the high cost of production due to the use of high dosages of chemical admixtures and the larger content of binder (including cement). Nehdi et al.(2004) reported that the cost of materials in SCC is approximately 20-50 % higher than those for NVC and they proposed that the use of filler materials as a partial replacement of cement could effectively reduce the total cost.

One of the most recent potential developments that could contribute effectively to achieving low cost and sustainable SCC construction, and could improve both the mechanical and durability characteristics of concrete in general and SCC in particular, is the use of relatively high dosages of reactive and non-reactive natural fillers or manufacturing by-products as a partial replacement of cement (Coppola et al., 2004, Moriconi, 2007, Dinakar et al., 2008). This will be termed a sustainable SCC in this thesis. Such a mix might provide extra improvement in the fresh characteristics, produce more sustainable concrete and reduce the high materials cost by limiting the cement content. In spite of the above, the durability aspect of SCC and especially, of sustainable SCC with less cement to provide long-term strength remains a concern of many concrete researchers. This is especially so in terms of carbonation and chloride penetration where the available laboratory studies are somewhat controversial compared to that of NVC at medium to high strength grades.

Recently, Assié et al.(2007) asked the following question "*is SCC as durable as NVC, especially in terms of physicochemical durability, at the same level of compressive strength*?" The results of his laboratory tests kept the answer to this question uncertain. These results included a medium to high strength SCC grade which is preferable in producing many pre-stressed and precast concrete structural elements that is mostly used in harsh environments. Furthermore, the lack of practical information about the long term character of physicochemical durability aspects, due to the relatively young age of actual SCC structures, adds another complication in reaching the appropriate judgment. For sustainable concrete, the question of the interest is: *how does this type of concrete response to the degradation process in both the short and long term in comparison to plain concrete?* In order to attempt answering this question, the degradation process at macro scale should be correlated to the internal chemical composition and microstructure features at micro and even nano scales with the aid of advanced techniques.

Thus, the current research work is designed to provide further understanding of the relation between some durability features in terms of chemical composition and microstructural characteristics, chloride penetration and carbonation resistance of a normal vibrating concrete (NVC) mix, one normal SCC mix and three other sustainable SCC mixes. These special SCC mixes contain three common types of filler at a relatively

high rate of replacement of cement: Fly ash (FA), limestone powder (LP) and silica fume (SF). The work also examined the impact of the concrete pore structure at different scales and the local micro permeation properties of the Interfacial Transition Zone (ITZ) on the overall chloride penetrability resistance. Moreover, the impact of carbonation on the microstructure and associated chemical changes as well as the distribution of the pore structure is assessed. Finally, based on theoretical basics, the two physico-chemical phenomena (carbonation and chloride penetrations) were modeled and the service life in natural and severe conditions was predicted.

1.2 Significance of research

In severe environments, the corrosion of embedded steel in concrete as a result of both carbonation and chloride penetration has been considered as one of the most serious threat to concrete durability. Most concrete structures exposed to these harsh environments show a high deterioration rate of the concrete cover due to corrosion of embedded steel at some time after their construction. Fig. 1-1 show some example of steel corrosion in concrete.

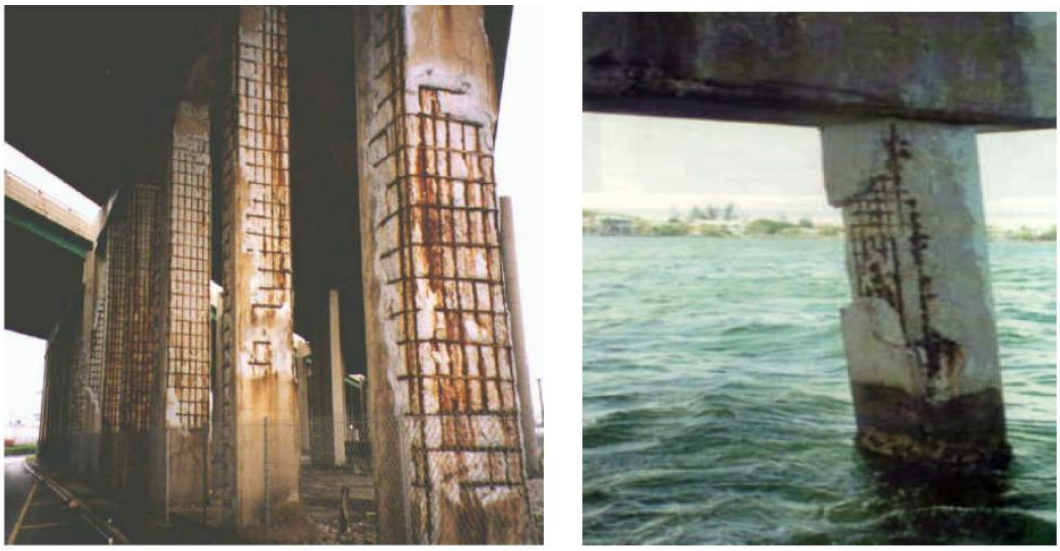

Figure 1-1 Bridge columns damaged by corrosion of reinforcing steel due to: a) de-icing chemical exposure b) severe environment
http://en.sxelade.com/upload/2011-2/FI2011022414572664 98.jpg
http://www.corrosionclinic.com/corrosion_courses/advanced_course_in_concrete_durability.htm

Due to the expensive cost of repair and maintenance, steel corrosion in concrete has a huge impact on the world economy. For example, the US Federal Highways Administration estimated in 2001 that $6.43 to $10.15 billion was required for maintenance and replacement of bridges in the USA due to corrosion of which

maintenance of concrete bridges was valued at $2.14 to $5.86 billion (Yunovich M. et al., 2001). In the UK particularly in England and Wales, the cost of bridge repair due to this problem only, was about £616.5 million in 1989 (El-Reedy, 2008). According to these cost statistics, therefore, the influence of concrete steel corrosion on the economy of countries is very significant. Recently, due to the corrosion of steel reinforcement, the US Federal Highway Administration has stated that, among 134,000 reinforced concrete bridges in the USA, 23% of them need repairing immediately, and 39 % are in a bad condition and about $90 billion would be the total cost of repair (Mehta and Monteiro, 2006).

The Arabian Gulf region is one of the world's most aggressive environments for concrete durability and, hence, many reinforced concrete structures that have recently been constructed in this region show a high deterioration rate due to corrosion of reinforcing steel in concrete. In Iraq, the author's home country, concrete structures are suffering from the same problem especially in the southern areas where high humidity, high temperature and aggressive salts are present.

The past decade has witnessed a rapid development of Self-Compacting Concrete (SCC) and its frequent use in many construction applications. Nowadays, SCC forms vital parts of infrastructure and substructures in the world that can be exposed to external environmental attack. In particular, medium strength SCC has been used widely for various precast concrete elements and it is planned for many other applications (Rodríguez Viacava et al., 2012). This widespread use of medium strength SCC could increase the probability of its exposure to severe natural environments. With the extensive use of this type of concrete, it is becoming increasingly difficult to ignore the influence of its microstructure and hydration on the durability. Further, understanding the transport characteristics such as fluid, gas and aggressive substances, which are the main factors that influence the steel corrosion, as a function of the internal microstructure and the chemical composition, as well as stimulating them experimentally and mathematically, are at the heart of a fundamental understanding of concrete durability.

1.3 Need for research

The work described in this thesis has been performed in order to gain further understanding of the relationship between the microstructural characteristics of some medium to high NVC and SCCs (especially the internal pore structure of the concrete, the ITZ, and chemical composition) and the carbon dioxide and chloride penetrations onto these mixes. The research approach is to combine both the experimental results with the mathematical and numerical works in order to achieve the aims of the study. It should be noted that the methodology is not to specify or to select an optimum dosage of cement replacement to produce different types of sustainable SCC. Extensive previous research work has already addressed this (Bouzoubaâ and Lachemi, 2001, Sonebi, 2004, Xie et al., 2002, Sukumar et al., 2008, Dinakar et al., 2008). The approach adopted in this dissertation is to try to give a deeper understanding of the overall response of a medium to high strength NVC and SCC at different scales, which are the types of mix most frequently used in aggressive environments, to the deterioration caused by carbonation and chloride penetration.

Before establishing the final aims, the objectives of the current study and some of important strategies are firstly delineated. These strategies were defined and agreed in the first year of this study on the bases of reviewing and analyzing the extensive previous research work on the subject of SCC. This was done in order to find the gaps in knowledge that have to be filled. However, due to the time limitations, some of them, regarding corrosion processes and the electrochemical behavior of the steel, are omitted and shifted to become recommendations for the future work. The research objectives were planned to achieve the aims given later in this chapter (Section 1.4) based on the following considerations:

- Extensive studies focused on the studying of the mix design, fresh and rheological properties of SCC and limited work has been done to investigate the durability in terms of steel corrosion, carbonation and chloride penetration in SCC in general and in sustainable SCC in particular.

- Limited researches addressed the carbonation and chloride penetration of SCC in comparison with NVC at the medium to high strength level. The physico-chemical durability aspects of SCC remained uncertain at this strength grade. Therefore, the

study considered SCC with medium to high design compressive strength, 50-60 MPa.

- Extensive research works are available for highly sustainable SCC with very high dosages of cement replacements, up to 80%, with different types of filler. However, the low design strengths obtained might not be enough to consider such mixes for structural applications in aggressive environments. Thus, the replacement of cement to make sustainable SCC was restricted to about 33% so as to achieve the desired compressive strength.

- There are many types of fillers that can be used for the production of SCC but, the most common fillers are fly ash (FA) and limestone powder (LP). Of the possible mineral admixtures, Silica fume (SF) is the most popular compared to others such us rice husk ash (RHA) and Metakaolin (M). The literature showed that the optimum dosage for partial cement replacement by silica fume was between (5-8) percent. For the above reasons, these three types of fillers/mineral admixture were used.

- The use of fillers and micro mineral admixtures as a partial replacement of cement may help to produce sustainable SCC and reduce the cost of SCC effectively. But much less is known about the ability of these modified SCCs to resist the deterioration caused by carbonation and the chloride ingress in the long term.

1.4 Aims and objectives of the research

1.4.1 Overall Aim

On the basis of the foregoing, the overall aim of the present investigation is to evaluate the effect of using different types of filler at relatively high partial replacement of cement on the microstructural characterization, carbonation and chloride penetrations of sustainable SCC. The idea of the research is to provide further understanding of the microstructural characteristics and the chemical composition of the SCC related to the carbonation and chloride ingress. More specifically, the impact of the local pore structure and micro permeation properties of the Interfacial Transition Zone (ITZ) and the percolation of these pores on the overall resistance to chloride penetration velocity will

be studied in addition to determining the change of some of the microstructural and chemical properties before and after carbonation.

1.4.2 Objectives

The specific aims of the research are summarized as follow:

- Investigate the progression of carbonation and chloride diffusion via the use of modified accelerating tests which can facilitate obtaining the results in a reasonable time-frame.
- Quantify the internal pore structure at the macro/microscopic and nano scales, the connectivity of these pores and the chemical composition, particularly of the matrices and the interfacial transition zone (ITZ), using a wide range of advanced techniques such as thermo gravimetric analysis (TGA), x-ray diffraction (XRD), mercury intrusion porosimetry (MIP) and scanning electron microscopy (SEM).
- Quantify the effect of the different fillers on the internal pore structure before and after carbonation.
- Quantify how the carbonation and chloride penetration are related to the overall chemical and microstructural form of the SCCs.
- Develop new research methodologies to predict the long term behavior of the produced concrete under naturally occurring aggressive conditions. These methodologies will be based on the short term laboratory testing via selected and modified accelerating tests and on the mathematical and theoretical foundations of both the carbonation and the chloride penetration.

1.4.3 Approaches and Tasks

The sequence of the research objectives can be defined in five steps:

- **Step one: Production and fresh properties**

1- To review the mix design procedures of both the NVC and SCC and to find the easiest way for the concrete production as the present investigation is not designed to examine the early age properties i.e the fresh properties.

2- To conduct a very simple parametric study for the purpose of optimizing the fresh properties and comparing the result with the available standards, ENV 206:1992 for slump classification of NVC and EFNARC: 2002 for the fresh requirements of SCC.

3- To obtain comparable and typical NVC, reference SCC and sustainable SCC mixes by defining their fresh and strength properties up to 28 days.

- **Step two: chemical composition and microstructural investigations**

1- To study the effect of using different fillers and mineral admixtures on the hydration characteristics of the produced concrete and to define the chemical composition at 28 days (before exposure to accelerated carbonation or chloride tests).
2- To experimentally analyze the local permeation characteristics of the ITZ.
3- To characterize the pore structure of the concrete at macro/micro and nano scales at 28 days and to investigate the effect of the curing time on the pore structure characterization at 56 days.
4- To determine the pore percolation of the cement matrices at the nano scale and the percolation degrees of the pores in the ITZ at micro scale.

- **Step three: Selection and modification of appropriate accelerated tests**

1- To review the existing accelerated tests for both carbonation and chloride penetration in concrete and to choose the appropriate methods.
2- To modify some of accelerated test methods in order to observe the progression of the carbonation and chloride in the concrete/mortar and determining their accelerated diffusion coefficients.

- **Step four: Microstructural and chemistry investigations after carbonation**

1- To study the long term behavior of the concrete after complete carbonation.
2- To determine the change of the pore structure at micro and nano scale and to identify the associated change of the matrices' chemistry.

- **Step five: Carbonation and chloride-structure property relationships and modelling**

1- To establish the macro/micro and nano internal pore structure property relationships with overall concrete response to carbonation and chloride penetration.
2- To model the carbonation and the chloride penetration process.
3- To assemble a method by which to predict the service life and the concrete cover designation.

The flowchart in Fig.1-2 shows the overall plan, the research activities and the interaction between them to meet the overall aim (black boxes are the input and the output of the research, blue boxes and lines represent the main topics covered, green boxes and lines briefly describe the purposes and the red boxes and lines summarize the aspects of the main topics and their purposes).

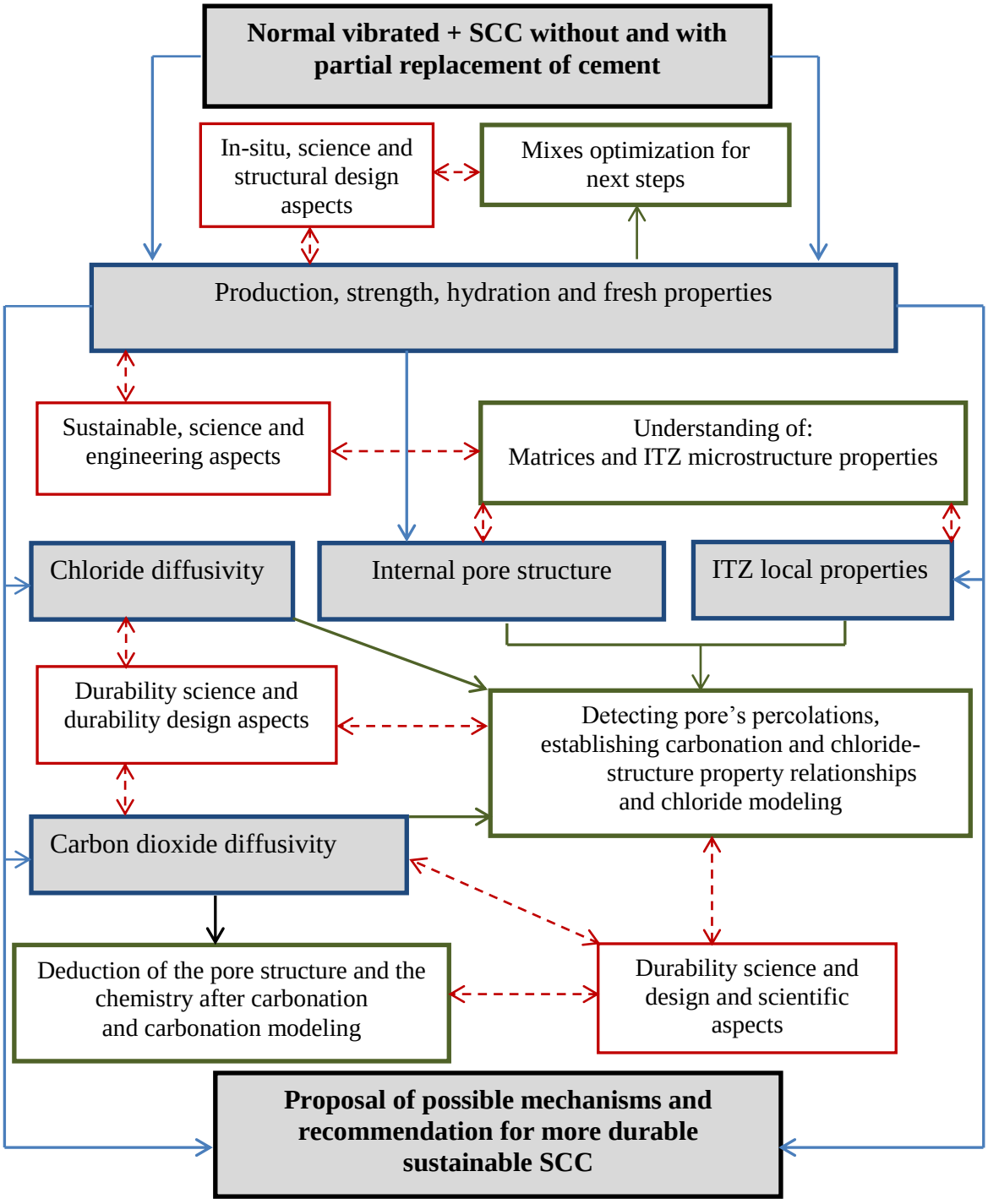

Figure 1-2 Schematic diagram - overall description of the whole research work and research activities

1.5 Published researches

The modified test methods, the developed research methodologies and the majority of the results obtained in this PhD thesis were published in a series of three papers in a well-respected journal (**Construction and Building Materials**) and one conference paper. These papers and the novelty of their contribution are as follow:

1- M.K. Mohammed, A.R. Dawson and N.H. Thom "Production, microstructure and hydration of sustainable self-compacting concrete with different types of filler". First work to analyze the internal pore structure and the micro characteristics of the interfacial transition zone (ITZ) of sustainable SCC quantitatively.

2- M.K. Mohammed, A.R. Dawson and N.H. Thom "Carbonation of filler typed self-compacting concrete and its impact on the microstructure by utilization of 100% CO2 accelerating techniques". First work to analyze the change of the microstructure of sustainable SCC after complete carbonation and present a new methodology to predict the actual carbonation depths by utilization of 100% CO_2 techniques.

3- M.K. Mohammed, A.R. Dawson and N.H. Thom "Macro/micro-pore structure characteristics and the chloride penetration of self-compacting concrete incorporating different types of filler and mineral admixture". Modification of rapid chloride migration test is achieved and chloride ingress-pore structure relationship is proposed for the first time.

4- M.K. Mohammed, A.R. Dawson and N.H. Thom "Improvement of the service life of sustainable self-compacting concrete SCC by integrating high dosage of cement replacement" **Second International Conference on Advances in Civil, Structural and Mechanical Engineering - CSM 2014 in Birmingham University**. A simplified service life model for the chloride ingress in concrete has been proposed using a numerical tool developed in Excel solver to calculate the diffusion coefficient and surface chloride content according to the NT build 443 accelerated tests.

During the PhD course, a MSc thesis entitled "**Carbonation of medium to high strength Portland cement concrete**" by (Dilovan M. Saeed, 2013) was supported by the author in line with the current research using the same unpressurised carbonation accelerating test as developed by the author with 100% CO_2 and with the same proposed methodology for service and cover designation, but for a shorter period.

1.6 Thesis layout

The existing research is organized in eight chapters. Chapter 1 presents an introduction, which mainly contains general background, research significance, the aims and the objectives, the overall research plan and layout. Chapters 2 and 3 cover the more relevant and up-to-date literature review to the present work. They were written in such a way that combines both an understanding of the fundamental background of all the aspects covered and which shows the points of contention and the gaps in knowledge in the previous research work. Chapter 4 consists of details of the material used and their characterizations, brief description and the basics of the techniques used, except those of the accelerated carbonation and chloride penetration tests. Very concise reviews of these tests and the need for the modification are embedded in the beginning of their related chapters (Chapters 6 and 7). Chapter 5 provides the results of the quantitative analysis of the internal concrete microstructure and chemical composition. Chapter 6 and 7 deliver the results related to the carbonation and chloride progressions, the response of the internal structure to them and the modeling works. Finally, Chapter 8 summarizes the main conclusions, suggestions to produce more durable sustainable SCC for severe environments and the recommendations for future work.

1.7 References

ASSIÉ, S., ESCADEILLAS, G. & WALLER, V. 2007. Estimates of self-compacting concrete 'potential'durability. Construction and Building Materials, 21, 1909-1917.

BOUZOUBAÂ, N. & LACHEMI, M. 2001. Self-compacting concrete incorporating high volumes of class F fly ash: Preliminary results. Cement and Concrete Research, 31, 413-420.

CIP.37. 2004. Self consolidating concrete [Online]. National ready mix concrete association. Available: http://www.nrmca.org/aboutconcrete/cips/37p.pdf [Accessed 28-10-2014].

COPPOLA, L., CERULLI, T. & SALVIONI, D. Year. Sustainable development and durability of self-compacting concretes. In: 8th CANMET/ACI Int. Conf. on Fly Ash, Silica Fume, Slag and Natural Pozzolans in Concrete, 2004. 29-50.

CSI. 2009. Available: http://www.wbcsdcement.org/index.php/key-issues/sustainability-with-concrete/concrete-recycling [Accessed 28-10-2014].

DE SCHUTTER, G. & AUDENAERT , K. 2007. Report 38: Durability of Self-Compacting Concrete-State-of-the-Art Report of RILEM Technical Committee 205-DSC, RILEM publications.

DE SCHUTTER, G., AUDENAERT, K., BOEL, V., VANDEWALLE, L., HEIRMAN, G., VANTOMME, J. & D'HEMRICOURT, J. Year. Transport properties in self-compacting concrete and relation with durability-overview of a Belgian research project (keynote paper). In: Proc. of the 3rd Int. Symp. on Self-Compacting Concrete (SCC2003), 2003. 799-807.

DE SCHUTTER, G., BARTOS, P. J. M., DOMONE, P. & GIBBS, J. 2008. Self-compacting concrete, Taylor and Francis Group.

DILOVAN M. SAEED. 2013. Carbonation of medium to high strength portland cement concrete. MSc, Nottingham University.

DINAKAR, P., BABU, K. G. & SANTHANAM, M. 2008. Durability properties of high volume fly ash self compacting concretes. Cement and Concrete Composites, 30, 880-886.

EL-REEDY, M. A. 2008. Steel-reinforced concrete structures: assessment and repair of corrosion, CRC.

IUREŞ, L. & BOB, C. 2010. The Future Concrete: Self-Compacting Concrete [Online]. Available: http://www.ce.tuiasi.ro/~bipcons/Archive/184.pdf [Accessed].

LIU, M. 2009. Wider application of additions in self-compacting concrete. PhD, UCL (University College London).

MEHTA, P. K. & MONTEIRO, P. J. M. 2006. Concrete: microstructure, properties and materials, McGraw-Hill.

MORICONI, G. Year. Recyclable materials in concrete technology: sustainability and durability. In: Sustainable Construction Materials and Technologies, Proc. Special Sessions of First inter. conf. on sustainable Construction Materials and Technologies, Coventry, UK, 2007. 11-13.

NEHDI, M., PARDHAN, M. & KOSHOWSKI, S. 2004. Durability of self-consolidating concrete incorporating high-volume replacement composite cements. Cement and Concrete Research, 34, 2103-2112.

OUCHI, M. Year. Self-compacting concrete-development, applications and key technologies. In: Proceedings of the Fourth International Conference on Materials Engineering for Resources, 2001. Akita: Society of Materials Science Japan.

RODRÍGUEZ VIACAVA, I., AGUADO DE CEA, A. & RODRÍGUEZ DE SENSALE, G. 2012. Self-compacting concrete of medium characteristic strength. Construction and Building Materials, 30, 776-782.

SONEBI, M. 2004. Medium strength self-compacting concrete containing fly ash: Modelling using factorial experimental plans. Cement and Concrete Research, 34, 1199-1208.

SUKUMAR, B., NAGAMANI, K. & SRINIVASA RAGHAVAN, R. 2008. Evaluation of strength at early ages of self-compacting concrete with high volume fly ash. Construction and Building Materials, 22, 1394-1401.

XIE, Y., LIU, B., YIN, J. & ZHOU, S. 2002. Optimum mix parameters of high-strength self-compacting concrete with ultrapulverized fly ash. Cement and Concrete Research, 32, 477-480.

YUNOVICH M., NEIL G, BALVANYOS T. & LAVE L. 2001. APPENDIX D, Corrosion Cost and Preventive Strategies in the United States; FHWA-RD-01-156; September 30, 2001.

Chapter 2:
Microstructure, hydration of concrete and the chloride ion penetrability

2.1 General

This chapter provides a brief and up-to-date literature review which can contribute to further understanding of the fundamental properties and the complexity of the concrete/mortar microstructure as a composite material in general and its phases specifically on the chloride penetration resistance. The first section will begin with a general overview of the complexity of the concrete microstructure following by explaining the microstructure and the hydration of the cement matrix and the associated change in the presence of the fillers and mineral admixtures. The second section will give a very brief description of the pore classification of the concrete/mortar as a composite material at different scales and will discuss the nature and the micro-features of the ITZ between the aggregate and the cement matrix. The third part will cover the effect and the role of each concrete phase in controlling the chloride transport property of the concrete.

2.2 Complexity of concrete microstructure (General overview)

In general, at the macro scale level, concrete is considered as an isotropic heterogeneous material with a very complex microstructure. At this scale, it consists of three different phases: the mortar phase (fine aggregate plus cement paste), the coarse aggregate phase and the interface between them which is normally called the interfacial transition zone (ITZ) (See Section 2.2.3). However, at the meso-scale, the mortar is considered as a three-phase composite material as the concrete itself as well: the fine aggregate phase, the cement matrix phase and the ITZ between the two.

For the transport properties of the concrete, the aggregate in both forms fine /coarse is defined as a solid material in the adhesive cement matrix. Thus, it is considered as an impermeable phase as compared to the cement matrix and ITZ phases (Shi et al., 2012). However, the influence of the aggregate phase on the permeation features of the concrete in general, and on chloride penetrability in particular, could be expressed as a function of its quantity and type (mineralogy composition) (See Section 2.3.1).

The ordinary cement paste itself could contain different interfaces between the solid hydration products such as un-hydrated or partially hydrated cement grains and the outer hydration products (cement paste) (Thomas and Jennings, 2008) as presented later in Fig. 4-4a. The use of high quantities of reacted or non-reacted fillers for the modern concrete types such as Self-Compacting Concrete (SCC) also produce other interfaces between the unreacted fillers and the other hydration products in the cement paste. These resulting interfaces in the high performance concrete (HPC) cement matrix could contribute significantly in increasing the heterogeneity of this concrete phase. Thus, for the HPC or SCC in certain, it might be possible to define the cement matrix as a third concrete scale level in addition to the concrete at the large macro scale and the mortar at the meso scale.

Sun et al.(2011) have recently explained the multi-scale microstructure of concrete/mortars and describe it as a four-phase composite material including the heterogeneity in the matrix phase. Fig 2.1 explains this modern standpoint for the different length scales of the concrete.

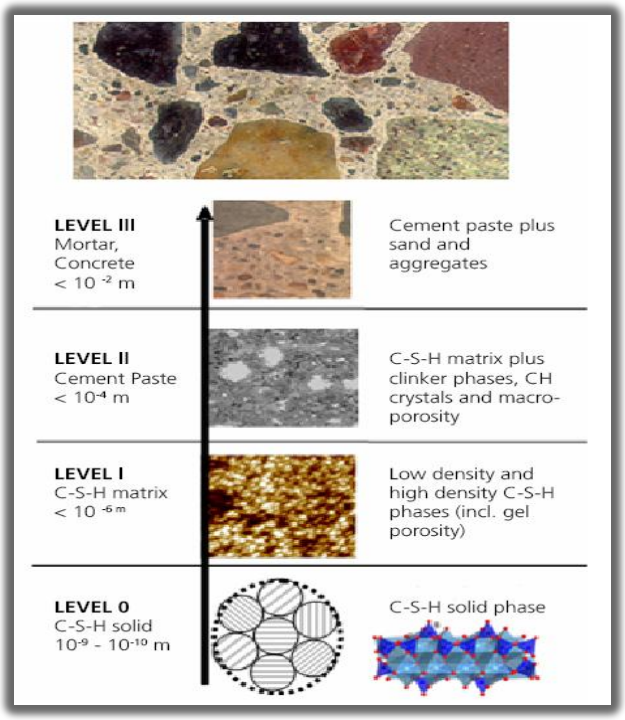

Figure 2-1 Levels of the concrete microstructure phases at macro, meso, micro and nano scales (CSM, 2009) http://www.csm-instruments.com/en/webfm_send/156

The heterogeneity of the cement matrix, and the associated changes in the hydration products due to the use of different fillers, will add another complexity which must be understood in order to predict the properties of such modern concrete types and, in

particular, to understand the multifaceted transport properties such as chloride penetration and carbonation reactions.

Most changes in both the chemistry and the microstructure of the concrete occur in the cement matrix and the ITZ regions as a result of using different cement matrix components. Thus, from a chemical and microstructural point of view, the degree of hydration and the micro/nano characteristics of these two phases are very important. Mondal (2008) concluded that in spite of the huge quantity of research that has been conducted to investigate the fundamental properties of the cementitious construction materials at large scale, work in the micro or even in the nano scales will achieve a better understanding of the multifaceted macroscopic phenomena in addition to providing ready input data for the multi-scale modeling.

The combination of the unique chemical composition, microstructure and completely different mix design procedure of the SCC relative to NVC adds another challenge to address in describing and understanding the impact of the internal microstructure on any particular tested property. The difference of the microstructure and the chemistry of the SCC as compared to the NVC is a result of using different materials and different casting process, i.e.

i) The use of the fillers and mineral admixture

ii) The higher quantity of superplastcizer (SP) usually with a low ratio of water to cementitious material.

iii) The absence of vibration during the casting process.

So that the specific requirements of the fresh characteristics necessitate different mix design procedures (De Schutter and Audenaert 2007). Figs 2-2 a,b shows the difference in the mix design of SCC in comparison with NVC and methods for achieving self-compactibility in the SCC mix, while Figs 2-3 explains the volumetric contents of the SCC mix according to the Japanese mix design method (Iureş and Bob, 2010, Hunger, 2010).

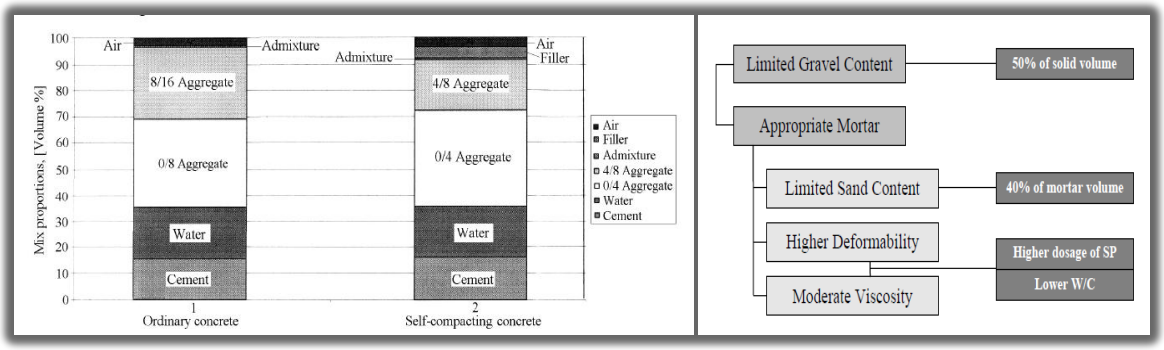

Figure 2-2 a) **Typical mix design of NVC and SCC (Iureş and Bob, 2010) b) Methods for achieving self-compactibility by Okamura and Ozawa, 1995 (Hunger, 2010)**

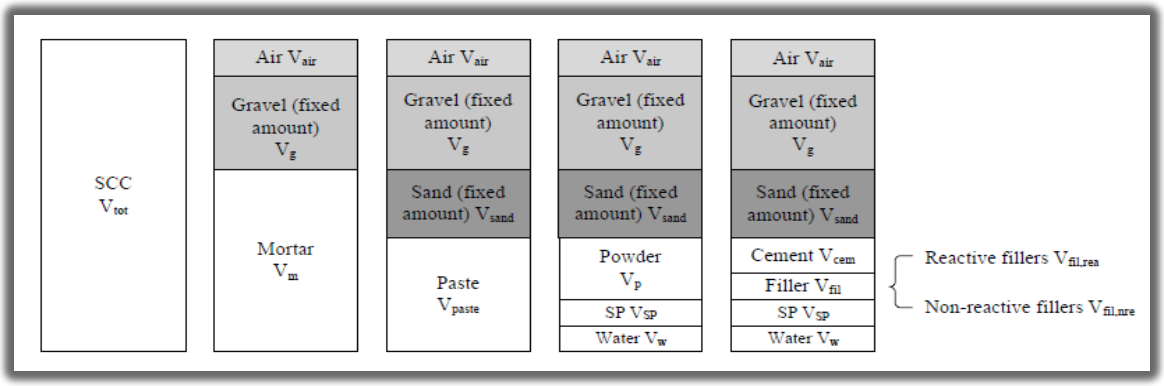

Figure 2-3 Volumetric contents according to the Japanese mix design method (Hunger, 2010)

The difficulty in defining the role and the effect of the concrete mix design, in terms of the internal microstructure on the concrete carbonation and chloride transport behavior is still a big challenge for concrete technologists, especially for the HPC or SCC. This is due to the different mix design, chemistry and the microstructure of the concrete, in particular the different macro/micro/nano scale characteristics and the complexities of the two physico-chemical phenomenons as well.

Based on above, a significant part of the current work uses a wide range of advanced techniques, such as SEM, MIP, TGA and XRD, in order to distinguish between the chemical and microstructure features of the different concrete phases, or even the interaction effects between them, on the overall macro/micro/nano-penetration features. Of special interest are the internal pore structure at different scales (macro to nano) and the micro permeation characteristics of this composite material in general and of the cement matrix and the ITZ in particular. This is to provide a better understanding of the role that microstructure and chemistry can play in influencing the multi-faceted

phenomena of carbonation and chloride migration and in determining the durability and environmental response of sustainable SCC.

2.2.1 Structure of hydrated cement paste

"*Anhydrous Portland cement is a grey powder composed of angular particles typically in the size range from 1 to 50 μm. It is produced by pulverizing a clinker then supplementing the resulting powder with a small amount of calcium sulfate, the clinker being a heterogeneous mixture of several compounds produced by high-temperature reactions between calcium oxide and silica, alumina, and iron oxide*" (Mehta and Monteiro, 2006). The main compounds of cement are given in Table 2-1.

Table 2-1 Main compounds of cement (Mehta and Monteiro, 2006, Neville, 2011)

Name of compound	Oxide composition	Abbreviation	Phase
Tri calcium silicate	$3CaO.SiO_2$	C_3S	Alite phase
Di calcium silicate	$2CaO.SiO_2$	C_2S	Belite phase
Tri calcium aluminate	$3CaO.Al_2O_3$	C_3A	Aluminate phase
Tetra calcium aluminoferrite	$4CaO.Al_2O_3.Fe_2O_3$	C_4AF	Ferrite phase

The main compounds in the cement grains undergo a complex reaction with water during the hydration process. The hydrated ordinary cement pastes can contain the following hydration products (Mehta and Monteiro, 2006):

- Calcium silicate hydrate (Tobermorite gel or CSH): for complete hydration of the C_2S and C_3S in the cement, it comprises 50-60 % of the volume of solids. Therefore, it has a significant role in determining the general properties of the cement paste such as the strength and permeation properties.
- Calcium hydroxide (Portlandite or CH): it occupies 20–25 % volume of solids in the hydrated paste and forms as a minor product from the hydration of silicates.
- Calcium sulfoaluminate hydrates (Afm and Ettringite): it comprises 15-20% of the solids volume in the hydrated paste and mainly results from the reaction of C_3A with the gypsum in the presence of water during the hydration process.
- Anhydrate clinker grains: these can be found, but their occurrence depends on the degree of hydration and the grain size of the cement.

The description of the geometry of these hydration products as an isolated or single element is not applicable when determining the solid characteristics or the overall generated porosity. Yet the interaction between these elements at the scale of microns and even nanometers is highly influential on many properties including the porosity, the pore distribution, the pore connectivity and percolation (Thomas and Jennings, 2008). Fig 2-4 shows a BSE image of an ordinary cement paste microstructure showing the interaction between various hydration products and the function of these different hydration products to determine the overall porosity and permeability during the cement hydration process.

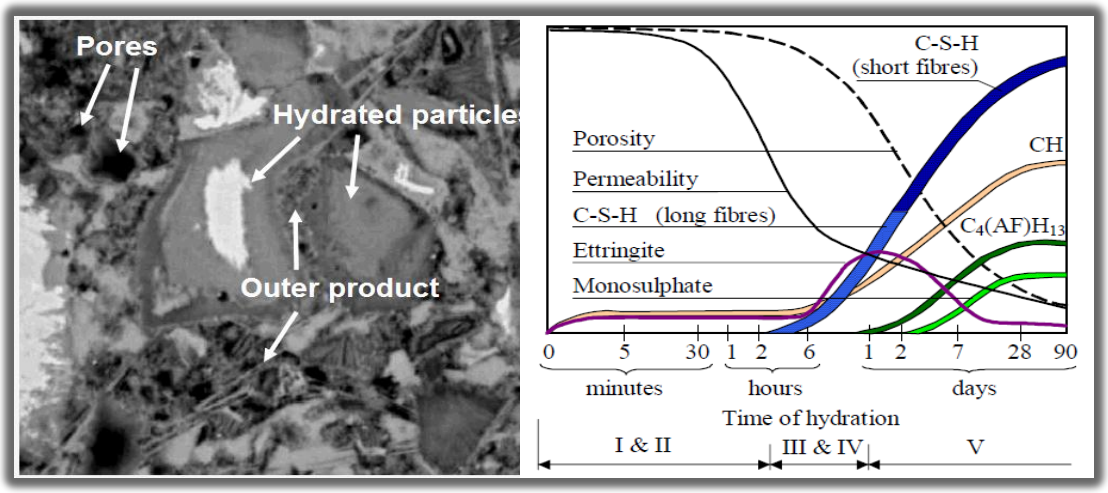

Figure 2-4 a) hydration products interconnection (SE image) (Thomas and Jennings, 2008) b) porosity and permeability as a function of hydration development (Esping 2007)

Generally, in SCC, the fillers can be classified into two types: reactive and non-reactive. However, for non-reactive fillers such as limestone powder (LP), there is no reliable evidence to date that indicates it can participate chemically to improve the structure of the hydrated cement paste (De Schutter G, 2011). For this reason, fly ash (FA) and other reactive fillers such as rice husk ash (RHA), metakaolin and silica fume (SF) have also been used as mineral additions in SCC production.

The use of active fillers or mineral admixtures in the HPC cement matrix, which are mainly active glassy siliceous pozzolan materials, generally alters the solid characteristics or the overall porosity of the cement matrix, the pore continuity and the pores' percolation as well. These materials are able to consume the CH phase in the cement matrix and produce an additional different form of CSH in the presence of water. However, the resulting product might have different features from the original CSH

($CaSiO_2.2H_2O$) depending on the resulting Ca/Si ratio and the available water molecules. The general reaction of the pozzolan materials can be expressed as in Eq.2-1 and 2-2 (Shi et al., 2012):

$$\text{Pozzolan} + \text{water} + Ca(OH)_2 \longrightarrow \text{CSH} \quad \text{..... Eq.2-1}$$

$$H_4SiO_4 + Ca(OH)_2 \longrightarrow H_2SiO_4^{--} + Ca^{++} + 2H_2O \quad \text{..... Eq.2-2}$$

$$\longrightarrow CaH_2SiO_4.2H_2O$$

However the reduction of the CH in the cement matrix due to the use of these pozzolanic materials could be affected by the nucleation of crystals, their growth at early ages and pozzolanic reactions later on as shown in Fig 2-5 (Canut, 2012).

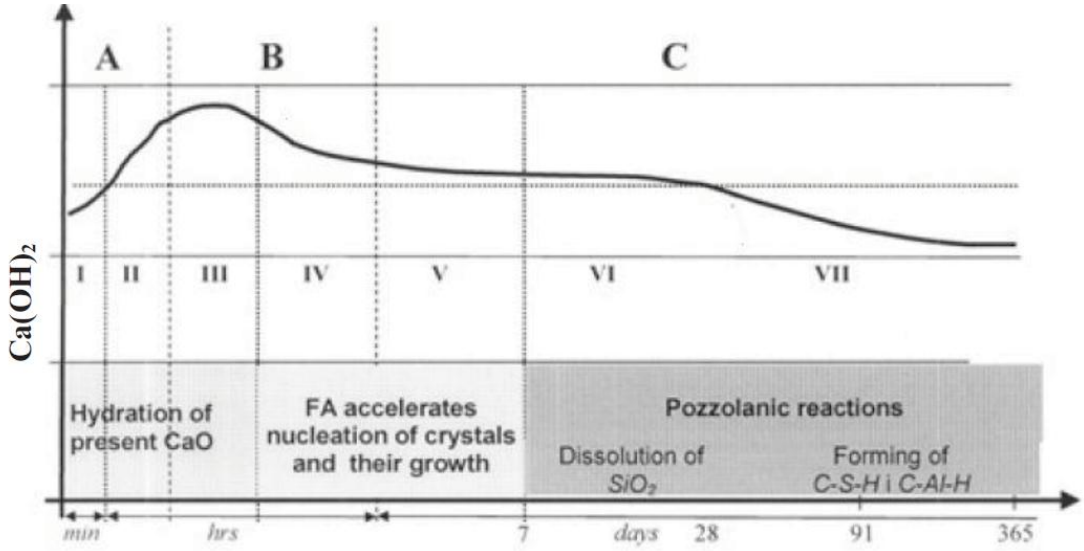

Figure 2-5 hydration of PC with fly ash FA addition (after Stefanovic et al. 2007) (Canut, 2012)

2.2.2 Classification of the pores in concrete

Hydrated cement paste contains different types of voids: first, separated big entrapped air voids which mainly depend on the water to cement ratio used and the degree of compaction during the casting process. Second, separated interlayer voids between CSH which typically form 28% porosity in otherwise solid CSH. These two types of voids are not responsible for the transport characteristics of the cement matrix yet the later type might have an essential role in determining the shrinkage or creep characteristics of the concrete in general (Mehta and Monteiro, 2006) (Table 2-2). Third, capillary voids between the solid contents. These voids play a vital role in determining the permeability and porosity of cement matrix alone or the permeability and porosity features of the

concrete as a composite material in the presence of the solid phase (aggregate). The distribution and continuity of these voids depends on the degree of hydration and water to cement ratio (Mehta and Monteiro, 2006).

The complex pore structure of the cement matrix alone might not explain the transport properties of the concrete as a composite porous material. Instead, the pore structure of the cement matrix, the local pore features of the porous ITZ region and the interaction between these pores might are likely to control the overall response to the penetration of the water and the other aggressive substances as will be explained in Section 2.3. Thus, the study of the internal pores structure of the concrete as a composite material is more important than the cement matrix alone to address the transport-microstructure property relationships.

As a composite porous material, Scanning Electron Microscopy (SEM) and Mercury Intrusion Porosimetry (MIP) techniques could be very useful tools in distinguishing these pores and in determining the combined of the complex pore structure. The combined use of advanced techniques such as SEM and MIP allows an informed understanding of the pore distribution, the pore geometry, the percolation and connectivity of these voids (Ying, 2013).

Fig 2-6 describes the distribution of the concrete pores at different scales from 1nm to 1cm while Table 2-2 listed the diameter ranges of these pores. It is obvious that the entrapped air voids at the large (macro) scale could affect the concrete strength characteristics only whereas the continuous capillary pores (in the range of 10 nm to 10 µm) could significantly determine both the strength and permeability characteristics.

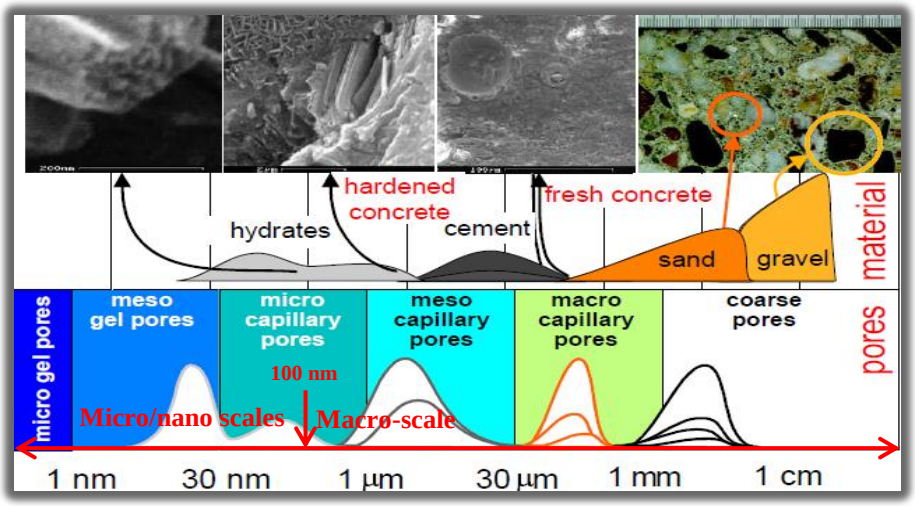

Figure 2-6 Distribution of the concrete pores at different scales in details

Table 2-2 Classification of pores in hydrated cement paste after (Ying, 2013)

Name		*Diameter*	*Paste properties affected*
Micropores "inter layer"	Gel Pores	Up to 0.5 nm	Shrinkage, creep at all RH
Micropores "inter layer"		0.5 nm to 2.5 nm	Shrinkage, creep at all RH
Small (gel) capillaries		2.5 nm to 10 nm	Shrinkage between 50% and 80% RH
Medium capillaries	Capillary Pores	10 nm to 50 nm	Strength, permeability, shrinkage at high RH, >80%
Large capillaries		50 nm to 10 µm	Strength, permeability
Entrained air		0.01 mm to 1 mm	Strength

Canut (2012) claimed that the term "porosity" was the misleading and could be avoided by the proper definition of the pore characteristics such as pore volume, pore size distribution and the pore threshold (critical pore diameter). Furthermore, the pore threshold can be relevant for assessing the concrete resistance to transport of substance in the cementations materials. These characteristics are shown in Fig.2-7.

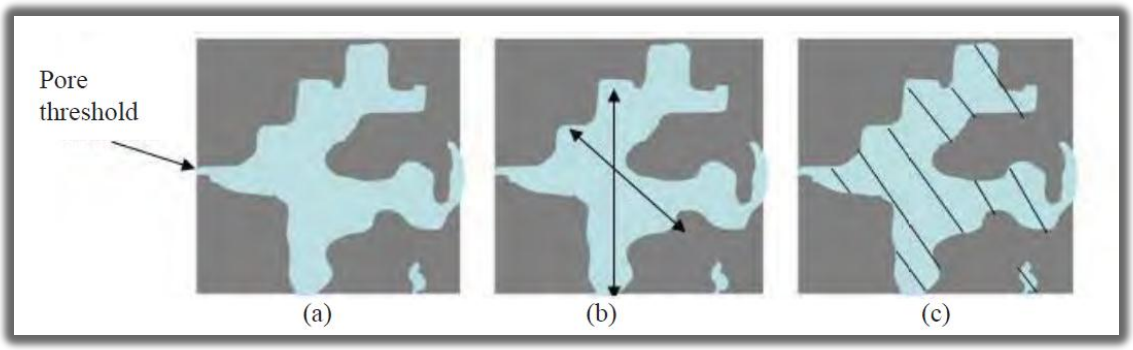

Figure 2-7 Pore characteristics a) pore throat b) pore feret and c) pore area fraction Canut (2012)

2.2.3 The interfacial transition zone (ITZ) in concrete

2.2.3.1 Definition and chemistry of an ITZ in concrete

In general the microstructure of the concrete is defined by both the porous structure and the development of the hydration products. However, the hydration reaction in the vicinity of the aggregate surface varies from the bulk cement matrix. This is mainly due to the greater volume of (local) water near the aggregate surface. Generally, this is

deriving from the inability of the cement grains to pack on the aggregate surface as shown in Fig 2-8.

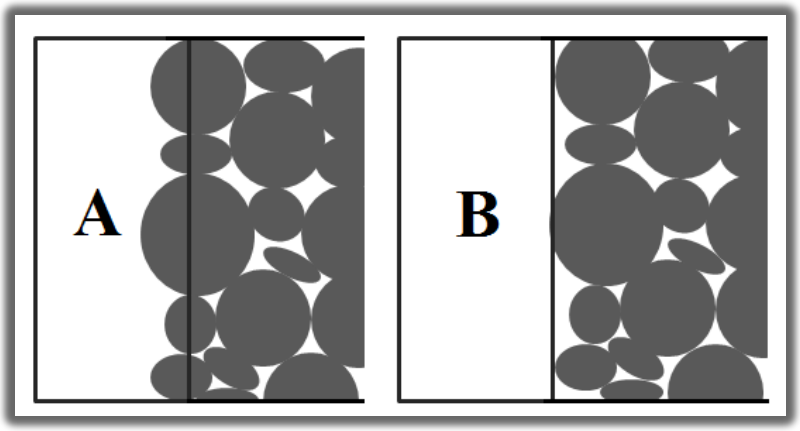

Figure 2-8 Illustration of the aggregate "wall effect" A) impossible packing of cement grains B) Possible packing produces higher porosity in the ITZ after (Scrivener et al., 2004)

After mixing and hydration of ordinary Portland cement, large amounts of Ettringite and hexagonal crystals of CH will be formed in a further porous framework between the aggregate-cement matrix interface and the bulk matrix. With the progress of hydration, this porous region might be filled with poorly crystalline CSH leading to a decrease in porosity. It is the resulting zone that is known as the Interfacial Transition Zone (ITZ). Fig 2-9 shows the boundary of this porous region (Scrivener et al., 2004, Mehta and Monteiro, 2006).

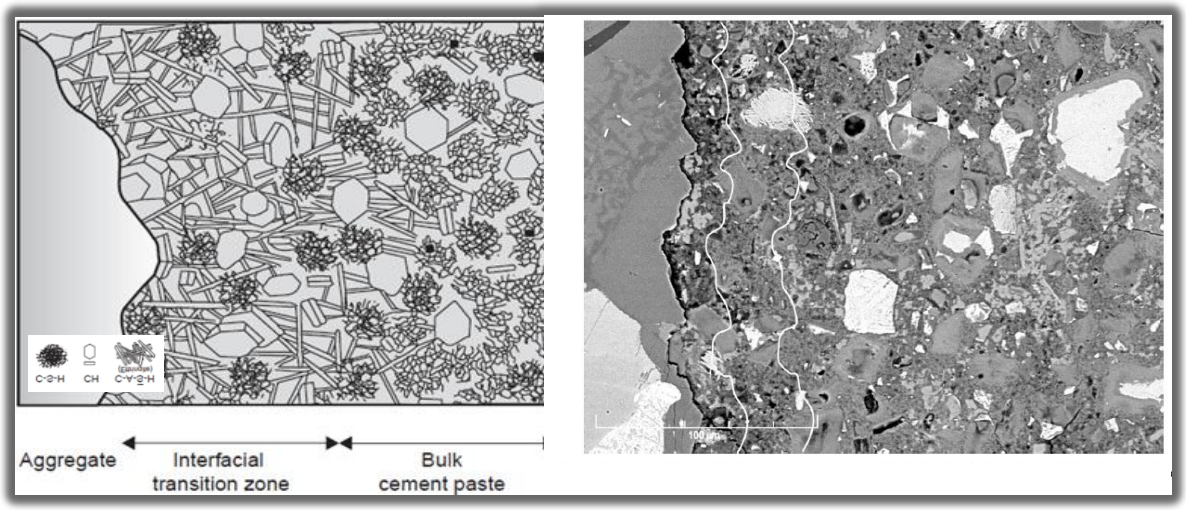

Figure 2-9 Basic microscopic views ITZ in concrete a) schematic diagram (Mehta and Monteiro, 2006) and b) actual BSE image (Scrivener et al., 2004)

Accordingly, the nature and the porosity of the ITZ region may be changed into two ways:

- ✓ Physically, as a result of the wall effect (See Fig. 2-8) (Scrivener et al., 2004). The presence of finer materials than the cement grains could reduce this effect considerably.
- ✓ Chemically, as a result of the continuous cement hydration progress with time. This is especially true in when using reactive cementitious material as a partial cement replacement (Larbi, 1991).

The above two aspects are related to the effect of changing the boundaries in the adhesive matrix of the ITZ (by changing mix design parameters such as w/c ratio, or binder type). However, Erdem et al.(2012) concluded that the change of the aggregate boundary (using different types of aggregate) significantly changed the nano and micro characteristics of the ITZ. This effect is excluded in the present investigation as the same type of fine and coarse aggregates are used for the normal vibrated concrete/ mortar mix and for the SCC concrete/ mortar mix.

2.2.3.2 ITZ porosity and thickness and the image analysis approach

It is postulated by Ollivier et al. (1995) that the wall effect explained earlier, creates a water to cement ratio gradient in the vicinity of the aggregate surface leading to the formation of a porosity inclines starting from the aggregate interface and extending approximately 50 µm towards the cement matrix as shown in Fig. 2-9. Scrivener and Nemati (1996) stated that other research work indicates that this effect might extend to about 100µm away from the aggregate interface while the migration of ions during the hydration causes a greater deposition of the hydration products near to aggregate and reduces the wall effect to only about 35 to 45µm (Scrivener and Nemati, 1996) which is approximately one third or one half the size of the largest cement grains. However, Ollivier et al. (1995) claims that the most significant effect of this re-arrangement of the localized water around the aggregate should be limited to about 15-20 µm only (the median diameter of cement grains).

Normally, the resulting porosity gradient in the ITZ region of the normal cement matrix (OPC) Fig. 2-10_1 can be obtained from analysis of the BSE images of this region, noting the different porosity bands in the cement matrix Fig. 2-10_2. By this means, the start point of the dense bulk cement matrix allows the ITZ thickness to be defined, although

there can be difficulty, in practice, in determining the point which can be considered as the boundary between the porosity of the ITZ and the near bulk matrix.

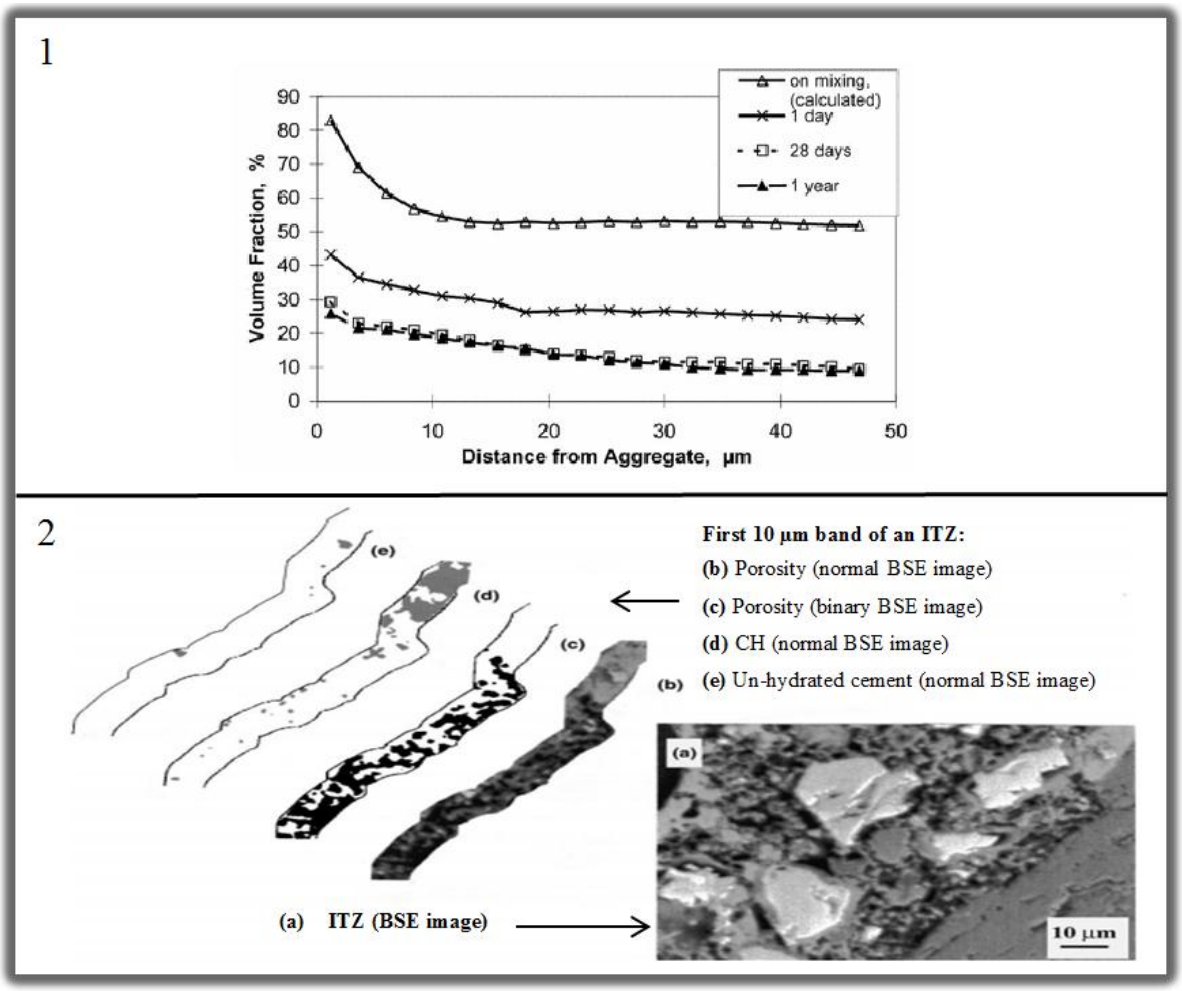

Figure 2-10 1) Porosity gradients in the ITZ region (Scrivener et al., 2004)
2) Porosity of the 1st band of an ITZ using image analysis after (Diamond and Huang, 2001)

Although the reported value of the ITZ thickness is usually between 10-50 µm, the thickness of the ITZ can vary from type of concrete to another. Basheer et al. (2005) used a more open approach to analyze the porosity gradient of the ITZ. They reported three sections for the porosity obtained across the ITZ using the image analysis technique and defined different thicknesses of ITZ (two types) as shown in Fig.2-11:

- Peak porosity region (n1) which is about 40 µm thick (ITZ_1).
- A transient porosity region (n2) which is about 160 µm thick (ITZ_2).
- The bulk porosity region (n).

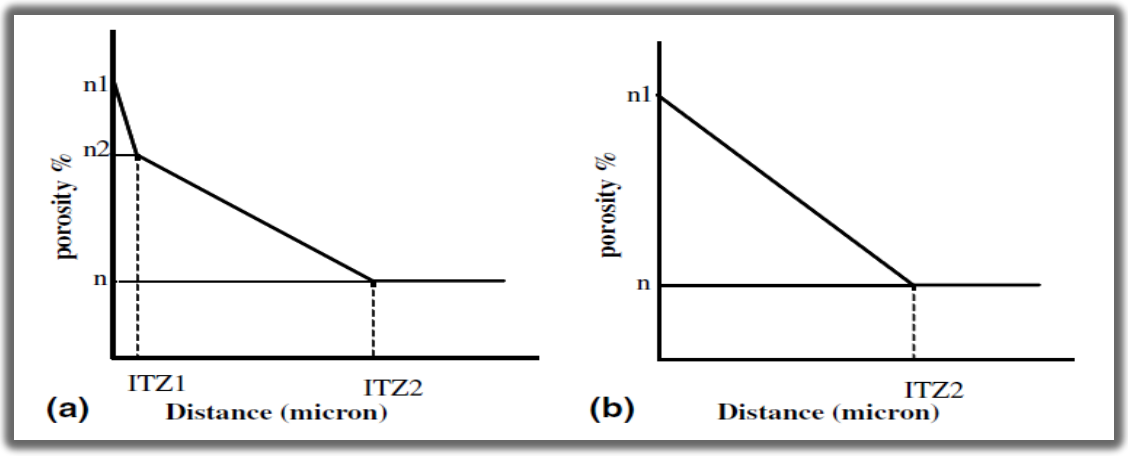

Figure 2-11 Approach to analyze the porosity and thickness of the ITZ Basheer et al. (2005)

However, for SCC made with different types of blended cement, Leemann et al.(2010) defined the ITZ thickness as the zone near the aggregate-matrix interface where the measured porosity is more than 15% greater than the average of the bulk matrix (assessed beyond 70 µm) while in a very recent work for blended cementitious material, Gao et al (2013) considered that the bulk cement matrix must commence somewhere between 15 µm and 50 µm from the aggregate interface. They used this definition for the purpose of simplicity and theoretically calculated the boundary of the ITZ as the distance from the aggregate at which the median gain size of binders observed, matched the median grain sizes of cement, slag and filler used(15.7 µm). The diameters of the cementitious binders were defined by the laser diffraction technique.

Gao et al. (2013) pointed out that, for the image analysis technique, the exact determination of the ITZ thickness is difficult and needs an elaborate and statistical analysis of the different porosity bands using the ITZ-BSE images. Generally, for characterizing the ITZ porosity and thickness for the complex blended cement matrix, the work proposed three main steps:

1- Determination of an exact threshold grey level value using the overflow criteria (obtained from a cumulative grey scale plot from the frequency count of grey scale histograms for the segmented ITZ-BSE images, Fig. 2-12.
2- Analysis of the porosity of each strip (band) from the aggregate interface towards the bulk matrix using the defined threshold grey level, Fig. 2-13.
3- The use of a statistical analysis, such as T-distribution, to examine the accuracy of the image analysis technique of each analyzed band.

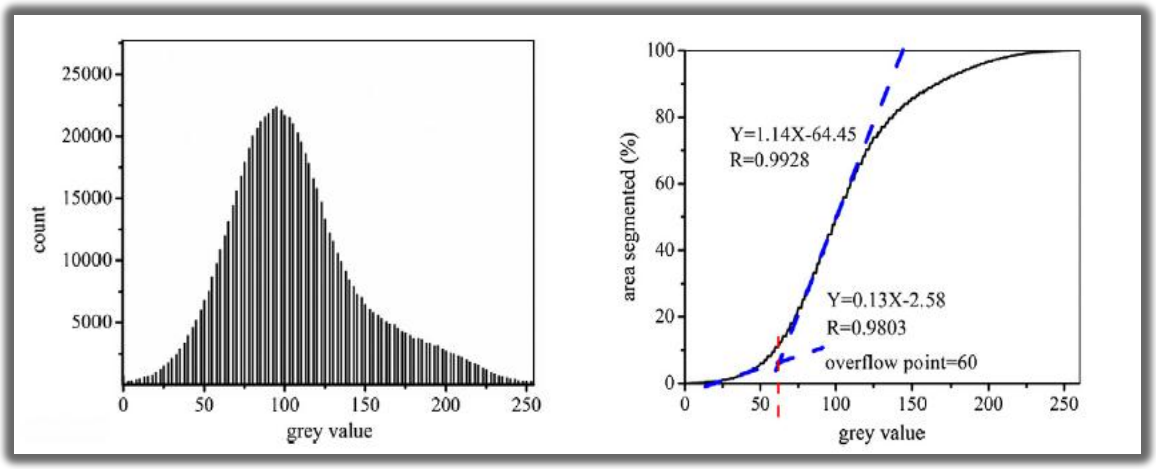

Figure 2-12 a) Frequency count of gray scale histogram for blended cement mortar

b) Cumulative grey scale for the blended cement mortar with the inflection point (Gao et al., 2013)

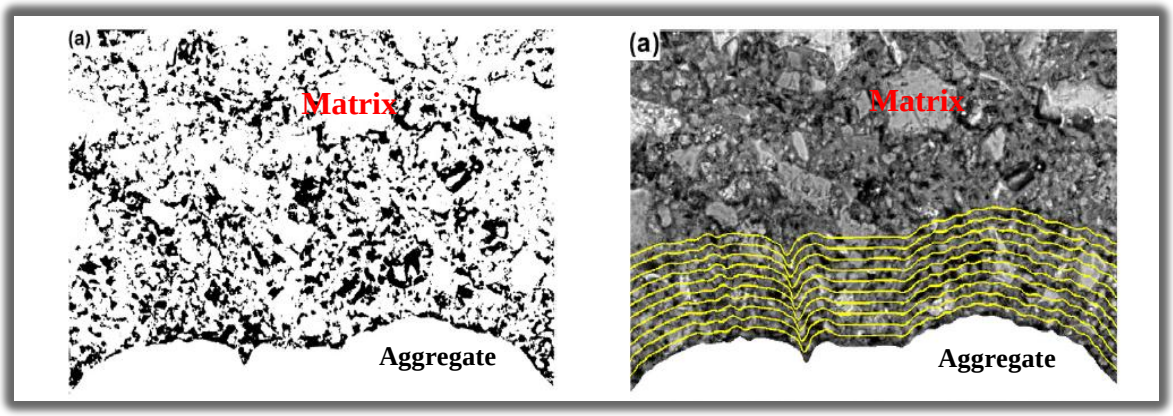

Figure 2-13 a) binary image using the defined threshold b) Delineated 10 successive 5 µm wide strips (Gao et al., 2013)

According to the work reviewed above, it seems that the last proposed method for analyzing the ITZ micro-features (thickness and porosity) using the image analysis is more accurate than others for the blended cement paste systems. Therefore, it was used with the aid of Image J program 1.45S (Image processing and Analysis by Java) for this purpose in the current study.

2.3 Relationships between the concrete phases, internal microstructure characteristics and chloride penetration phenomenon

A considerable amount of research work has been conducted to study the concrete mix design and the microstructure in relation to the normal transport properties such as water and other non-reactive liquid movement (Permeability) for both normal and high performance concrete. However, the micro-concrete chemistry, the macro/micro and

even nano internal microstructure property relationships with the complex transport properties such as carbonation and chloride penetration require detailed review.

In a very recent review paper, work concerning the durability of steel reinforced concrete in chloride-rich environments, Shi et al. (2012), claimed that complex concrete pore structure should be investigated in depth and more research work and tests are needed in order to define some of the existing knowledge gaps and to shed light on the fundamental chloride diffusivity-pore structure relationships. The authors pointed out that the concrete pore structure can be influenced by different mix design parameters, such as water to cement ratio, type and proportion of mineral admixtures and cement, compaction, curing, etc., and the presence of cracks as well. For modern types of concrete, it seems that the most of the mix design parameters mentioned would effectively change the micro and nano features of the concrete in the cement matrix and the ITZ phases much more than would any changes in the aggregate phase. However, this section gives a brief description and discussion of the role of each concrete phase, or the combined effect of these phases, on the chloride penetrability.

2.3.1 Effect of aggregate phase on the chloride penetrability

As reported by Delagrave et al. (1997), the existence of aggregates in a cement matrix could have two conflicting effects on the transport properties in general and the chloride penetration in particular as shown in Fig. 2-14. The incorporating of the aggregate increases the tortuosity of the matrix leading to a decrease in the chloride penetrability. However, it leads to the formation of numerous ITZs which can assist the movement of chloride ions through the concrete body.

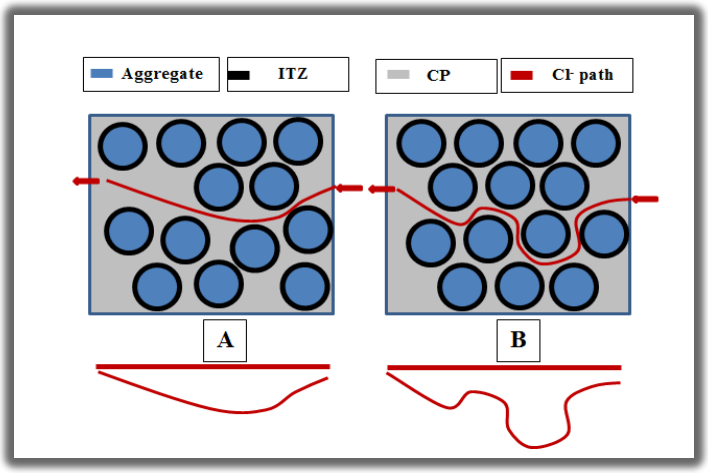

Figure 2-14 schematic representation of the effect of the aggregate volume fraction in the tortuosity path of the chloride penetration

Considering concrete/mortar as a composite material (in which the aggregate is relatively impermeable and chloride ion flow exists parallel to the aggregate surface), Yang and Su (2002) proposed a model explaining the combined dilution effect and tortuosity effect of the aggregate in the concrete mortar as shown in Fig 2-15. They suggest that the chloride migration coefficient of the mortar decreases as the aggregate volume fraction (V_f) increases, Eq. 2-3 (Bruggeman equation).

$$D_{cl} = D_o(1 - V_f)^{3/2} \quad \text{..... Eq. 2-3}$$

Where D_{cl}= the diffusion coefficient of mortar and D_0= the diffusion coefficient of matrix alone

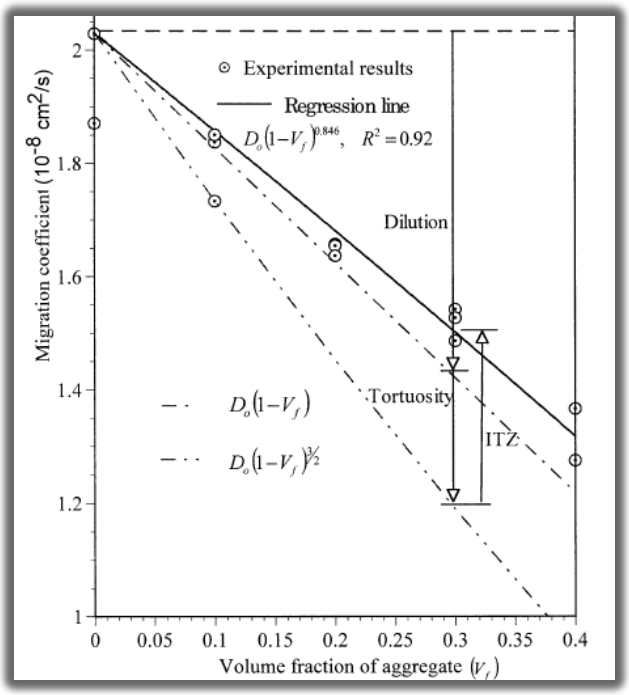

Figure 2-15 Chloride migration coefficient versus volume fraction of aggregate (Yang and Su, 2002)

However, the existence of numerous ITZs, when there is a high volume fraction of the fine aggregate, may have the effect on eliminating the improvement (i.e. reduction) in the chloride migration coefficient. Sun et al.(2011) revealed that the steady state chloride migration coefficient, which is used for validating a Multi-scale mesoscopic model to predict the effective chloride diffusion coefficient of concrete, increases as the volume fraction of the same size of the fine aggregate increases for different mortar specimens.

This disagreement between the above three references on the combined effect of using a high fine aggregate volume fraction, which is very important for the SCC mix design in order to obtain mix stability and flow characteristics, emphasizes the significance of

investigating the effect of the local ITZ micro characteristics on the overall chloride resistance in SCC.

As the SCC has a different mix design procedure and unique chemical composition and micro and nano characteristics in comparison to the NVC (as explained earlier in this chapter), questions have been raised as to which has the dominant role: *the micro permeation characteristics of the ITZ or the pore characteristics of the bulk cement matrix in determining the chloride penetration resistance?*

To attempt an answer to this question for SCC, the only available study in the literature is by Leemann et al.(2010). They studied the effect of using different types of cement on the porosity of the ITZ and its relationship to chloride resistance, using the rapid chloride migration test according to the Swiss standard SIA 262/1. In this study, the authors concluded that the change of the internal pore structure of the cement matrix, as caused by the use of different types of cement in four different SCC mixes, had a stronger effect on the non-steady state chloride migration coefficients obtained than did the pore volume in the ITZ.

However, the long curing time (62 days) used in this investigation might reduce any controlling effect of the local microstructure characteristics of the ITZs. Moreover, Leemann et al. made no attempt to address how the change of the internal pore structure, including the tortuosity effect of the aggregate and the percolation of pores in the ITZ, nor the nature of the pore system in the matrices, could affect the chloride resistance of SCC as only one technique was used (Image analysis) for characterizing the ITZ pores microstructure. This cannot give enough information about the effect of the internal capillary pores and their percolation to fully defend their conclusion.

2.3.2 Effect of cement matrix phase (pore characteristics and binding ability) on the chloride diffusion coefficient

In general, the chloride resistance of the concrete might largely depend on the pores geometry and their interconnectivity through the pore system of the concrete, and to a lesser extent on the chemical binding capacity of the cement paste (Shi et al., 2012). However, as the chloride penetration takes place, some chloride ions can be arrested by the cement hydration products while others (water soluble chloride) can penetrate further

causing the de-passivation of the embedded steel. This overlap between the chloride ions and the hydration products in the cement matrix is called the chloride binding ability. The chloride interaction with the cement paste can occur into two ways (Spiesz et al., 2011):

- ✓ The chemical interaction with the calcium aluminate hydrates (AFm and Aft) that resulted from the hydration of the aluminates in cement (C_3A and C_4AF).
- ✓ The physical absorption of the chloride ions on the surface of the CSH that resulted from the hydration of the silicates in cement (C_2S and C_3S).

To investigating the action(s) of the internal micro-structure on the chloride penetration resistance, including the calculation of the approximate ITZ chloride diffusion coefficient or the effect of different fine aggregate volume fractions of the cementitious mortars, most previous research works have been based on accelerated steady state measurements (Yang and Su, 2002, Yang, 2005, Zheng et al., 2009). The calculation of the steady state chloride migration coefficient could be affected by the chloride binding ability of the cement matrix, given the long-time needed to reach steady state conditions. However, if the steady state has been maintained, it can be assumed that all chloride binding has already been completed. In this case, the effect of this phenomenon can be neglected (Stanish et al., 2000). Therefore, the use of these types of tests instead of the non-steady state tests can prolong the time interval so that the effect of binding ability can be clearly observed. Electrically accelerated tests might not, therefore, give an accurate value of chloride diffusion coefficient that derives from the role of the internal pore structure alone. Instead results are likely to reflect of the combined role of the chemical composition of the cement matrix and the internal pores features.

On the other hand, test time is fairly fast in the non-steady state chloride migration test and chloride binding does not take place to a large extent (Castellote et al., 1999). Spiesz et al. (2011) claimed that, to some extent, the binding ability of chloride ions (which is highly dependent on the type of the filler or the use of supplementary cementations materials due to the change in ionic consumption (pH-value) of the pore water) is a function of the pH value of the pore solution and of the migration of the OH^- ions during the time of the non-steady state chloride accelerated test. More recent work in the rapid migration test using NT Build 492 (RCM) has been done by Spiesz and Brouwers (2012). They observed that there was no significant drop in the pH value of the pore

solution due to the effect of the external electrical field (30V) for 24 hours which would be expected if OH^- ions were being displaced by Cl^- ions. Pore pH was examined by spraying three different types of colorimetric pH indicators to the split surface of specimen broken after the RMT. The results indicate that the pH level of the OPC containing LP remained over 13.

This cement matrix's binding ability could be influenced by the use of different fillers or mineral admixtures, depending on the ability of these materials to alter the chemistry of the hydration products in the cement matrix, as explained in Section 2.2.1. Heirman et al. (2006) showed that it was not possible to reach the steady state for some SCC specimens even after 90 days of the test, and only an insignificant quantity of chloride ions moved in this time. Therefore, for SCC, the NT Build 492-Nordtest method (Nordtest,1999) was successfully used in order to determine the non-steady chloride migration coefficients for ranking eight types of SCC with different water to binder ratios and different filler types. Heirman et al. (2006) stated that, in spite of the absence of acceptance measures, evaluation of the chloride ingress resistance could be achieved by obtaining the non-steady state migration coefficient D_{nssm} which may be assessed using the criterion suggested by Tang et al. 2001 as shown in Table 2-3.

Table 2-3 Assessment of chloride resistance in SCC using D_{nssm} after (Heirman et al., 2006)

$D_{nssm} < 2\times10^{-12}$ m^2/sec	Very good resistance against chloride ingress
$D_{nssm} < 8\times10^{-12}$ m^2/sec	Good resistance against chloride ingress
$D_{nssm} < 16\times10^{-12}$ m^2/sec	Moderate resistance against chloride ingress
$D_{nssm} > 16\times10^{-12}$ m^2/sec	Not suitable for aggressive environment

For the above mentioned reasons, the non-steady state accelerated test was modified and used in the present study based on the recommendations of NT Build 492-Nordtest method (Nordtest,1999). The modification described in Chapter seven (Section 7.3) was mainly performed in order to reduce the time of the test to, as much as possible, avoid the change of the ionic composition of the pore water solution (pH value) due to the migration of the OH^- ions during the chloride migration test as this point still represents an argument between researchers (Spiesz et al., 2011, Spiesz and Brouwers, 2012). This may be especially important when the chemical composition of the cement matrix differs from test to another. The modification might limit to different extents the local chloride

binding ability due to the difference in reactivity levels of the fillers and the mineral admixtures used when assessed through the relatively long time of the standard test (6hr or more).

2.3.3 Effect of ITZ on the chloride transport

The ITZ between the aggregate and the cement matrix is usually the weakest phase of the concrete composite material. The influence of the ITZ characteristics on the mechanical properties of the concrete might be fully investigated. However, lots of questions have been raised on the role of this more porous zone on the transport properties of the concrete in general and on chloride penetration in particular (Ollivier et al., 1995). The inquiry addressed by Mehta and Monteiro (2006) about the higher value of the permeability coefficient of a concrete/mortar as a composite material than that of the corresponding cement matrix might reflects the effect of the ITZ between the aggregate and the cement matrix.

Theoretically, the porous nature of the ITZ is a favorite place for increasing the chemical reactions and facilitating ingress of the deleterious substances. In addition, the leaching and/or the dissolution of the CH in this region considerably affects the ion penetration (Ollivier et al., 1995). Concerning the estimation of the chloride ion diffusion coefficient of the ITZ in normal vibrated concrete, the assessed ITZ chloride diffusion coefficient alone was about 2.8 times the matrix chloride diffusion coefficient for 50 µm ITZ-thickness, 1.8 for 40 µm ITZ-thickness and 1.6 times for 20µm ITZ-thickness based on an experimental and regression analytical results obtained by Yang and Su (2002).
A further, recent, study performed by Jiang et al. (2013) concentrated on a numerical estimation of the diffusion coefficient of the ITZ and showed that the chloride diffusion coefficient of the bulk cement paste is of the order of 1 to 10 times of that of the ITZ. However, it should be emphasized here that the geometric arrangement of pores in both the ITZ and the bulk cement matrix, and the resulted continuous pathways from the interconnection of these pores in the presence of the aggregate, is very complex and it is not easy to numerically simulate them without obtaining vast experimental data that could quantitatively characterize these pores in a concrete.

2.4 Concluding remarks:

- The expected change in the cement matrix phase due to the use of reactive /non-reactive fillers and mineral admixtures in SCC could significantly alter both the chemical composition and the internal microstructure of the cement matrix especially in the case of cement replacement. This will add a further microstructure complexity to both the cement matrix phase alone and to the concrete/mortar as a composite material. For modern types of concrete, this should be quantitatively investigated to address the role of the internal chemical composition and microstructure in relation to the phenomenon such as carbonation and chloride penetration.

- There are conflicting arguments as to the effects of using different volume fractions of aggregate on the concrete transport properties in general, and on the chloride penetration in particular. Based on existing models for normal vibrated cement mortars, the importance of investigating the combined role of the ITZ micro-permeation characteristics in the presence of high volume fractions of fine aggregate in SCC evident.

- The exact determination of pore structure characteristics at different scales and the ITZ micro-permeation properties, especially for concrete with HPC cement matrices such as SCC, is too difficult and it would need an elaborate efforts. For the pore structure, there is need to combine the results from different advanced techniques such as saturated porosity at macro scale, MIP and SEM at micro and nano scales in order to obtain practical description. For the ITZ, advanced techniques such as image analysis and EDX analysis are required in order to investigate the micro-permeation features.

- In spite of previous studies which have extensively investigated the chemical and microstructure nature of the cement matrix and the ITZ of normal vibrated concrete, the role of fillers and mineral admixtures, as a relatively high partial cement replacements in SCC, in the development of the concrete pore structure, of the blended cement matrix and of the ITZ microstructure development is still unsatisfactory. Further, the role of the combined materials on the chloride penetrability resistance still unaddressed in the literature for this concrete type.

- The chloride diffusion coefficient assessed by non-steady state is more appropriate than the steady state one for investigating the functionality of the internal microstructure as related to the chloride resistance of the concrete, especially with HPC cement matrix. However, test modification is required to reduce the effect of the cement matrix chemistry (chloride binding ability) on the chloride ingress.
- The geometric arrangement of the capillary pores in both the ITZ and the bulk cement matrix, and the resulting continuous pathways from the interconnection of these pores in the presence of the aggregate, is very complex. The addition of different fillers and mineral admixtures might change the micro/nano pore structure characteristics especially for both the cement matrix and ITZ. Thus, more research work is needed to experimentally investigate the role of the internal pore structure at different scales on the chloride resistance of SCC.
- Understanding of the overall performance of the concrete against any structural response, durability property and environmental issue needs to be developed. The well-known advanced techniques and standards should be used as much as possible to examine the features of each concrete phase or to investigate the combined effect of these phases against the complex concrete transport properties such as chloride penetration.

2.5 References

BASHEER, L., BASHEER, P. & LONG, A. 2005. Influence of coarse aggregate on the permeation, durability and the microstructure characteristics of ordinary Portland cement concrete. Construction and Building Materials, 19, 682-690.

CANUT. 2012. Pore structure in blended cement pastes. PhD, Technical University of Denmark.

CASTELLOTE, M., ANDRADE, C. & ALONSO, C. 1999. Chloride-binding isotherms in concrete submitted to non-steady-state migration experiments. Cement and Concrete Research, 29, 1799-1806.

CSM. 2009. Mechanical Properties of Cementitious Materials by Grid Nanoindentation [Online]. Available: http://www.csm-instruments.com/en/webfm_send/156 [Accessed 29 June 2009].

DE SCHUTTER, G. & AUDENAERT , K. 2007. Report 38: Durability of Self-Compacting Concrete-State-of-the-Art Report of RILEM Technical Committee 205-DSC, RILEM publications.

DE SCHUTTER G. Year. Effect of limestone as mineral addition in self-compacting concrete. In, 2011. 6th Conference on our world in concrete & structures. Singapore;.

DELAGRAVE, A., BIGAS, J., OLLIVIER, J., MARCHAND, J. & PIGEON, M. 1997. Influence of the interfacial zone on the chloride diffusivity of mortars. Advanced Cement Based Materials, 5, 86-92.

DIAMOND, S. & HUANG, J. 2001. The ITZ in concrete–a different view based on image analysis and SEM observations. Cement and Concrete Composites, 23, 179-188.

ERDEM, S., DAWSON, A. R. & THOM, N. H. 2012. Impact load-induced micro-structural damage and micro-structure associated mechanical response of concrete made with different surface roughness and porosity aggregates. Cement and Concrete Research, 42, 291-305.

ESPING 2007. Early age properties of self-compacting concrete-Effects of fine aggregate and limestone filler. PhD, Göteborg, Sweden.

GAO, Y., DE SCHUTTER, G., YE, G., YU, Z., TAN, Z. & WU, K. 2013. A microscopic study on ternary blended cement based composites. Construction and Building Materials, 46, 28-38.

HEIRMAN, G., VANDEWALLE, L., BOEL, V., AUDENAERT, K. & DE, G. Year. Chloride penetration and carbonation in self-compacting concrete. In: ConcreteLife'06-International RILEM-JCI Seminar on Concrete Durability and Service Life Planning: Curing, Crack Control, Performance in Harsh Environments, 2006. RILEM Publications SARL, 13-23.

HUNGER, M. 2010. An integral design concept for ecological self-compacting concrete. PhD, Eindhoven University of Technology, The Netherlands.

IUREŞ, L. & BOB, C. 2010. The Future Concrete: Self-Compacting Concrete [Online]. Available: http://www.ce.tuiasi.ro/~bipcons/Archive/184.pdf [Accessed].

JIANG, J.-Y., SUN, G.-W. & WANG, C.-H. 2013. Numerical calculation on the porosity distribution and diffusion coefficient of interfacial transition zone in cement-based composite materials. Construction and Building Materials, 39, 134-138.

LARBI, J. A. 1991. The cement paste-aggregate interfacial zone in concrete. Technische Universiteit Delft.

LEEMANN, A., LOSER, R. & MÜNCH, B. 2010. Influence of cement type on ITZ porosity and chloride resistance of self-compacting concrete. Cement and Concrete Composites, 32, 116-120.

MEHTA, P. K. & MONTEIRO, P. J. M. 2006. Concrete: microstructure, properties and materials, McGraw-Hill.

MONDAL, P. 2008. Nanomechanical Properties of Cementitious Materials. PhD, Northweatern.

NEVILLE, A. M. 2011. Properties of Concrete, London, Pearson Education Limited.

NT BUILD 492 Nordtest,1999. Concrete mortar and cement based repair materials:chloride migration coefficient from non-steady-state migration experiments.

OLLIVIER, J., MASO, J. & BOURDETTE, B. 1995. Interfacial transition zone in concrete. Advanced Cement Based Materials, 2, 30-38.

SCRIVENER, K. L., CRUMBIE, A. K. & LAUGESEN, P. 2004. The interfacial transition zone (ITZ) between cement paste and aggregate in concrete. Interface Science, 12, 411-421.

SCRIVENER, K. L. & NEMATI, K. M. 1996. The percolation of pore space in the cement paste/aggregate interfacial zone of concrete. Cement and Concrete Research, 26, 35-40.

SHI, X., XIE, N., FORTUNE, K. & GONG, J. 2012. Durability of steel reinforced concrete in chloride environments: An overview. Construction and Building Materials, 30, 125-138.

SPIESZ, P., BALLARI, M. & BROUWERS, H. 2011. RCM: A new model accounting for the non-linear chloride binding isotherm and the non-equilibrium conditions between the free-and bound-chloride concentrations. Construction and Building Materials.

SPIESZ, P. & BROUWERS, H. 2012. Influnce of the electrical field applied in chloride migration tests on the properties of concrete [Online]. Available: http://josbrouwers.bwk.tue.nl/publications/Conference77.pdf [Accessed 25-02-2012 2013].

STANISH, K., HOOTON, R. D. & THOMAS, M. 2000. Testing the chloride penetration resistance of concrete: a literature review, Department of Civil Engineering, University of Toronto.

SUN, G., ZHANG, Y., SUN, W., LIU, Z. & WANG, C. 2011. Multi-scale prediction of the effective chloride diffusion coefficient of concrete. Construction and Building Materials, 25, 3820-3831.

THOMAS, J. & JENNINGS, H. 2008. The science of concrete [Online]. Available: http://iti.northwestern.edu/cement/index.html [Accessed 22-7-2014].

YANG, C. & SU, J. 2002. Approximate migration coefficient of interfacial transition zone and the effect of aggregate content on the migration coefficient of mortar. Cement and Concrete Research, 32, 1559-1565.

YANG, C. C. 2005. Effect of the percolated interfacial transition zone on the chloride migration coefficient of cement-based materials. Materials chemistry and physics, 91, 538-544.

YING, W. 2013. Performance assessment of cement-based materials blended with micronized sand: microstructure, durability and sustainability.

ZHENG, J.-J., WONG, H. S. & BUENFELD, N. R. 2009. Assessing the influence of ITZ on the steady-state chloride diffusivity of concrete using a numerical model. Cement and Concrete Research, 39, 805-813.

Chapter 3:
Carbonation, chloride penetration mechanisms and service life in concrete

3.1 General

The aim of this chapter is to provide review of literature on concrete on carbonation and chloride penetration of concrete in general and of SCC in particular. These two physico-chemical phenomena are the main factors of the corrosion of embedded steel reinforcement leading to reduced serviceability. Accordingly, although this thesis about concrete, the current chapter contains a short and condensed introduction to the service life and corrosion of steel as well.

The subjects covered in the literature review in this chapter can be classified into four main areas:

- Introduction to the service life and corrosion of steel in concrete.
- Carbonation in concrete in general and on carbonation of medium to high strength SCC in particular.
- Chloride penetration in concrete in general and on chloride penetration of medium to high strength SCC in particular.
- Theoretical background of carbonation and chloride penetration and their combined actions on concrete and steel.

3.2 Concrete service life and corrosion of steel phenomena in concrete

Everywhere in the world, corrosion of steel in concrete has been recognized as the main reason for concrete structure deterioration. Each type of concrete, even of poor quality, can offer a certain protection to the embedded steel. However, "*the question of interest in the use of steel is not whether this process will occur (it will!) but how fast it will occur in practice*"(Hansson et al., 2007).

One of the most important causes of steel corrosion is the presence of chloride ions either in the constituents as an internal source (contaminated concrete), or migrating inwards from an external source (sea, underground and de-icing water) which then leads to reduction in the serviceability life of the affected concrete structure. Chloride attack has

become an increasingly important area in the study of concrete durability since the middle of the last century (Angst et al., 2009). The problem related to the internal chloride content is more significant than the ingress from an external source because of the proximity of the chloride ions to the embedded steel surface. However, for such situation, the problem can be avoided by the selection of raw materials that satisfy the concentration limits set by available standards. The main source of chloride in contaminated concrete is the aggregate, so these require particularly carful sourcing. Thus, in practice, the ingress of the chloride from the external sources (Section 3.6) is still considered a big challenge for the durability of concrete which is exposed to aggressive chloride environments. It is critical to produce an appropriate concrete type in order to reduce or even to eliminate the chloride ingress effect during the concrete's design service life.

Another notable influence on the steel corrosion is the reduction of the concrete alkalinity which is induced by the reaction between carbon dioxide (CO_2) from the atmosphere and the cement hydration products (especially CH and later CSH and other hydration products) in the presence of humidity which is known as carbonation (Section 3.3). Recently, concrete researchers have shown an increased interest in this topic due to the global increase in concentration of carbon dioxide in the atmosphere.

3.2.1 Service life definition

ACI Committee 365 (2000) defines the durability by the ability of the concrete or its ingredients to maintain serviceability in certain surrounding conditions through a period of time which is called the service or span life. Although the concrete has been considered as a durable construction material for a long time, deterioration might occur under aggressive environments such as the exposure to chloride, sulfate, acids and carbon dioxide. In addition, actual concrete structures may be exposed to synergistic effects of one or more of these environments. However, the concrete element has to provide the embedded steel with adequate protection against corrosion to prolong the span life.

With regard to concrete service life, Tutti (1982) proposed a model which describes the corrosion process with time (**Fig. 3-1a**). He divided the process into two stages: initiation and propagation. The initiation stage can be defined as the time which is needed for the

ingress of aggressive substances such as CO_2 or Cl^- from the external environment to the embedded steel's surface indicating a time before which there is an absolute need for choosing a proper maintenance technique. The second stage is the time between de-passivation of steel until the end of the service life of the concrete structure (Bertolini et al., 2004).

In other words, the first phase is the time taken by the carbon dioxide or chloride penetration to destroy the steel protection provided by the high alkalinity nature of the concrete, while the second one is the time taken for the degradation of the embedded steel. In reality, the initiation stage usually takes a long time to happen especially for high quality concrete, and the steel remains in a passive state. However, the protection provided by the concrete cover can be destroyed in aggressive environments and the extent of corrosion damage increases with time as shown in **Fig. 3-1b**.

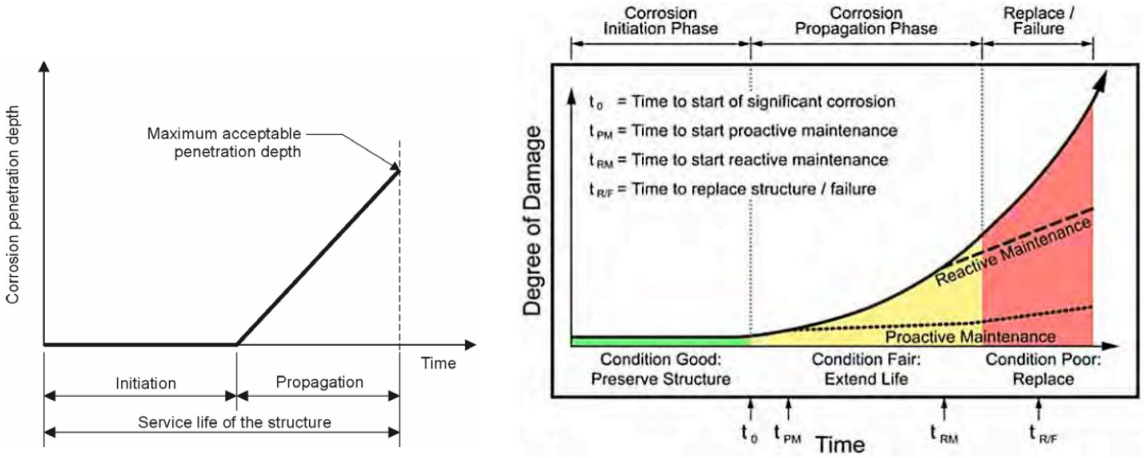

Figure 3-1 a) concrete service life definition (Bertolini et al., 2004) b) degree of damage against exposure time (The corrosion society. NACE, 2012)

3.2.2 Corrosion of steel phenomena in concrete

Although there are different types of concrete deterioration such as alkali silica reaction and freeze-thaw action, corrosion of steel reinforcement has a particularly harmful effect on the durability of concrete and is considered as the most serious threat to concrete structures due to its significant impact on the structures' safety and economy (Ferreira, 2004).

It is well known that the concrete is very weak under tensile stresses compared to the compression ones. Therefore, cracking and finally spalling of the concrete cover usually

occurs due to the formation of the internal tensile stresses as a result of the increase of the volume of rust on the steel surface as compared with the original steel (Mehta and Monteiro, 2006). Furthermore, the steel in reinforced concrete members will suffer a reduction in its cross-sectional area and may loss bond strength with the concrete due to corrosion and hence, structural failure might become possible (Mehta and Monteiro, 2006). Fig 3-2 shows the steps of in the internal stress initiation mechanism due to the steel corrosion while Fig.3-3 demonstrates the structural consequences of steel corrosion in reinforced concrete structures.

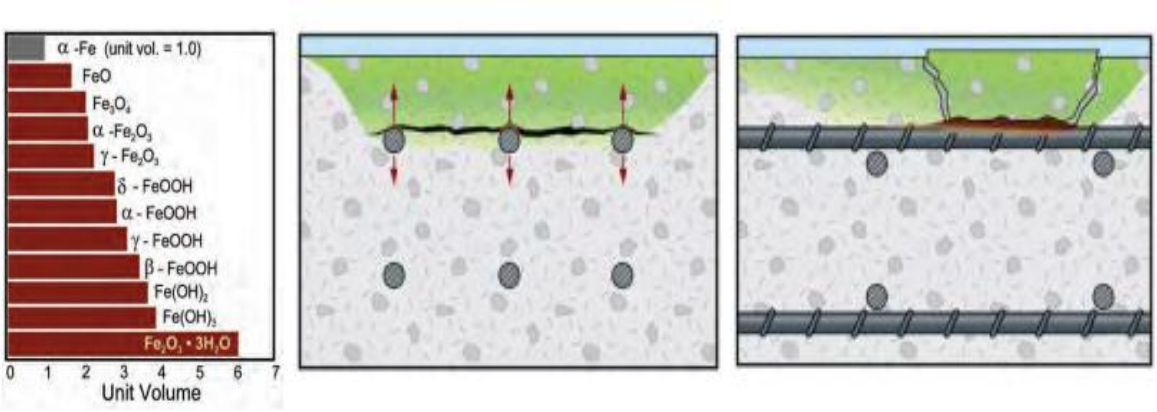

Figure 3-2 a) unit volume of the steel rust products b) initiation of the internal tensile stresses c) spalling of the concrete cover (The corrosion society. NACE, 2012)

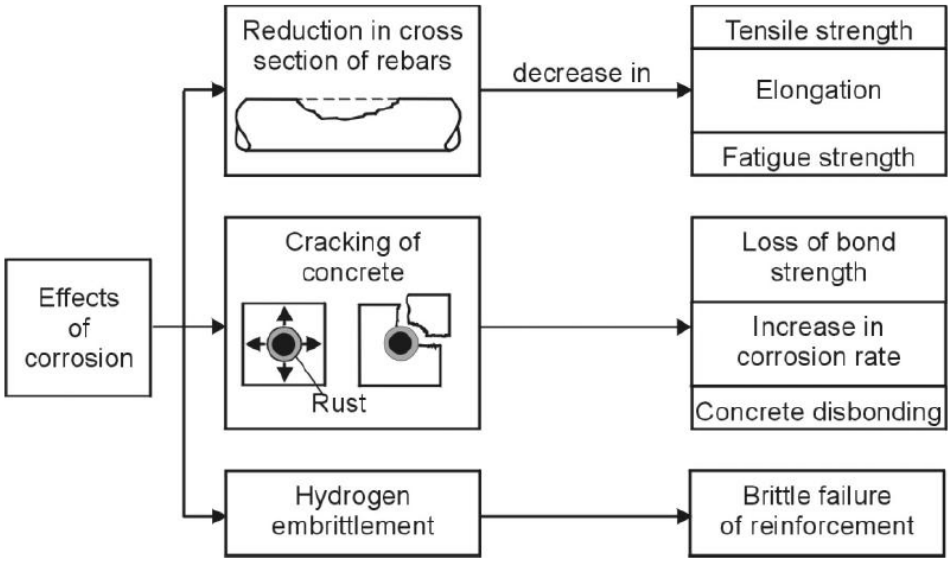

Figure 3-3 structural consequences of steel corrosion in reinforced concrete structures (Ferreira, 2004)

In general, the corrosion of steel reinforcement is an electrochemical process in which two main half-cell reactions must take place. The first one is called the anodic reaction while the second is called the cathodic reaction. In the anodic reaction, the production of electrons occurs due to the oxidization or dissolution of Iron to form ferrous ions Fe^{++} (Eq.3-1). In the cathodic reaction (Eq.3-2), consumption of these electrons occurs to form hydroxyl ions during the reduction of oxygen (ACI Committe 222, 2000).

$Fe \longrightarrow Fe^{++} + 2\,e^{-}$ Anodic reaction (Oxidation) ..... **Eq. 3-1**

$2H_2O + O_2 + 4e^{-} \longrightarrow 4\,(OH)^{-}$ cathodic reaction (Oxygen reduction) ..... **Eq. 3-2**

These two reactions are governed by the availability of oxygen, moisture and the pH value of the solution in the pores system of cement paste near the steel surface. Fig. 3-4 illustrates basic mechanism of steel corrosion in concrete.

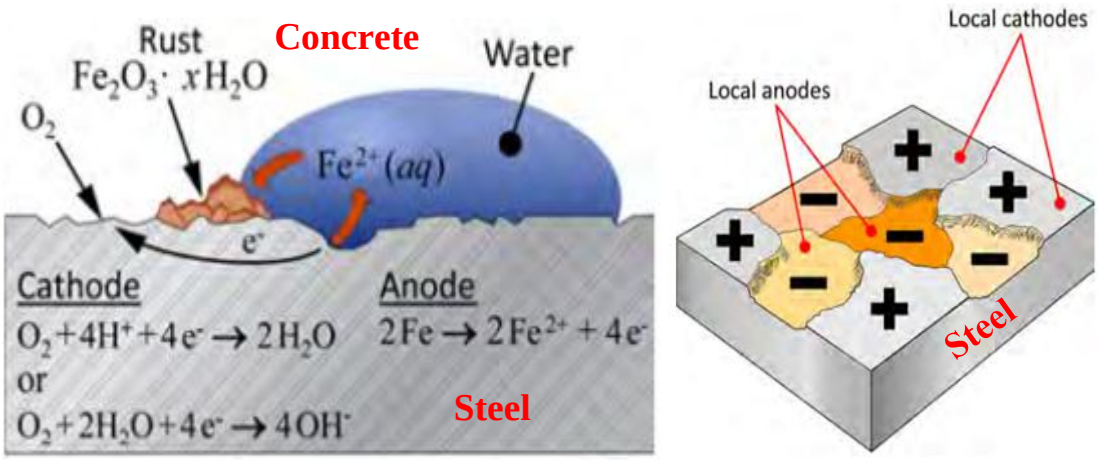

Figure 3-4 basic mechanism of steel corrosion in concrete a) cross section b) top view of anodes and cathodes area on steel (The corrosion society. NACE, 2012)

Two types of corrosion cell might occure. If the distance between the anode and the cathode is very small or cannot be distinguished (the anode and the cathode are on the same reinfircing bar), the microcell corrosion will occur. In contrast, if there is a clear distance between them (the anode and the cathode are separated), macro cell corrosion type will take place. The total rate of corrosion (macrocell + microcell) is about three times higher than macrocell corrosion alone (ACI Committe 222, 2000, Bertolini et al., 2004, Hansson et al., 2007).

3.2.3 Carbonation and chloride effect on steel corrosion

For sound concrete, the steel normally is in a passive state due to the formation of an iron oxide surface film in the high pH environment of the concrete. However, this protection film can be destroyed as a result of both carbonation of the concrete cover or chloride ions' appearing adjacent to the steel surface. These two effects will alter the pH value of the pore water solution near the steel surface leading to the destruction of its passive state.

The neutralization of CH from the cement paste by the carbonation reaction (Section 3.3) will reduce the pH value of the pore system significantly from around 12 to about 8. Consequently, if the cover of the reinforcement carbonates, the steel passivation might be destroyed totally, and the corrosion probability will increase in the presence of moisture and Oxygen. A pH value of 10 or less can affect the steel passivation considerably. However, the passive film might become unstable with even a pH value of 11.5 (Andrade et al., 1990, Rendell et al., 2002, Chang et al., 2003). For SCC containing fly ash and bottom ash, Siddique (2011) explained that the pH values of the pore solution has a significant control on steel corrosion and the carbonation degree as shown in Table 3-1.

Table 3-1 Degree of carbonation and the pH value of SCC (Siddique, 2011)

Degree of carbonation	100%	50-100 %	0-50 %	No carbonation
pH value	< 7.5	7.5-9.0	9.0-11.5	> 11.5

In comparison to chloride ion penetration (section 3.6), the corrosion of steel might be less dangerous due to the uniform steel de-passivation when the concrete cover is deteriorated by carbonation. In contrast, once the chloride ions reach the surface of the steel, the passive nature of the reinforcing steel is attacked in a severe manner (Eq.3-3 and Eq.3-4) (Ahmad, 2003). As a result, anodic conditions will be created and the corrosion process will be started. The pitting corrosion caused by the chloride ions as shown in Fig 3-5 might reduce the cross-sectional area of the steel and catastrophic failure of the structure could result.

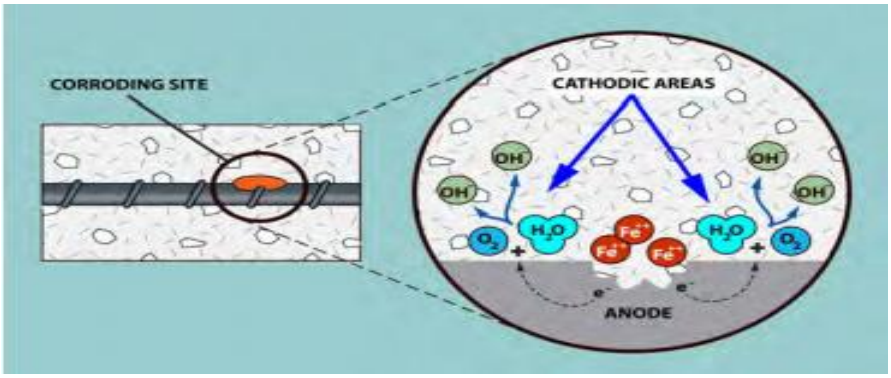

Figure 3-5 Reduction of the steel cross section area in the anaodic spot due ti chloride (The corrosion society. NACE, 2012)

The reaction between Cl^- ions and the ferrous ions at the anode area is summarized as:

$$Fe^{++} + 2Cl^- \longrightarrow Fe\,Cl_2 \quad \text{..... Eq. 3-3}$$

$$FeCl_2 + 2H_2O \longrightarrow Fe\,(OH)_2 + 2HCl \quad \text{..... Eq. 3-4}$$

The resulting Hydrochloric acid will deplete the pH value of the pore water solution. Another important effect of the chloride ions is the reduction in the electrical resistivity of concrete due to the increased chloride ionic content of the pore water solution. The electron transfer between the cathode and the anode for the corrosion cell will increase significantly in concrete with low electrical resistivity leading to high corrosion currents. As reported by Neville (2011), the distribution of pores in the cement paste, the moisture content and the chloride ionic content of the pore water solution are the main factors that can affect the concrete resistivity. Concrete which has an AC electrical resistivity between 500-700 Ω.mm might be able to resist the steel corrosion, but below this value corrosion can be anticipated (Mehta and Monteiro, 2006).

The minimum concentration of chloride ions on the steel surface to initiate the corrosion is called the chloride threshold (C_{cr}). This value depends on the pH value of the pore water solution and the concentration of Oxygen and sometimes is expressed by the Cl^-/OH^- ratio. In the presence of oxygen bubbles near the steel surface, the ratio is about 0.66 while it is about 1.4 in the presence of air (Stanish et al., 2000, Shi et al., 2012). There are many factors which affect the chloride threshold value and most of them are incompletely understood (Hansson et al., 2007, Neville, 2011), they include:

• Mixture proportions of the concrete.

• Type and specific surface area of the cement.

• Cement sulfate content and the use of any supplementary cementing materials (SCMs).

• W/c ratio, curing conditions, age and environmental history of the concrete.

• Degree of carbonation of the concrete.

• Temperature and relative humidity of the environment.

• Roughness and cleanliness of the reinforcement.

Despite the variability induced by the factor listed above, C_{cr} is normally taken as close to 0.05 by weight of concrete for durability design purposes (service life determination). Fig.3-6 shows how a higher C_{cr} can be tolerated by better quality concrete or when the humidity is low or close to saturation when oxygen access is reduced (Gjørv 2009). The average C_{cr} is 0.4% by weight of cement, which is equal to 0.07 by weight of concrete as listed in Table 3-2, and is often stated in codes and specifications for durability design purposes (Gjørv 2009).

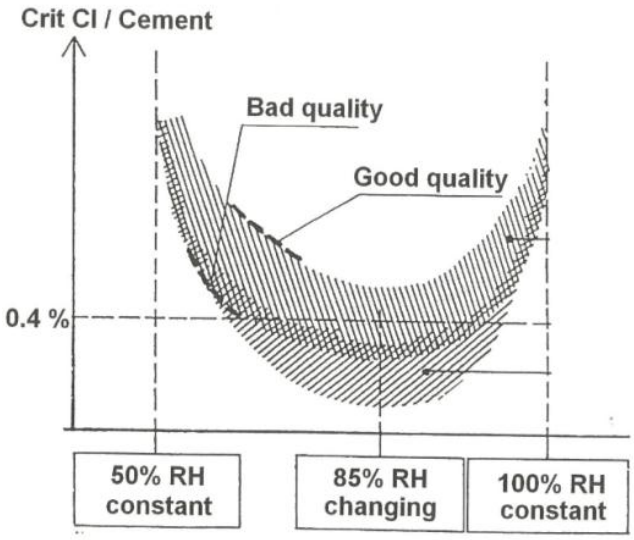

Figure 3-6 average C_{cr} in different humidity condition for bad and good quality concrete (Gjørv 2009)

Table 3-2 Probability of steel corrosion and critical chloride content (Gjørv 2009)

Chloride content %		Risk of corrosion
By wt. of cement	**By wt. of concrete**	
> 2.0	> 0.36	Certain
1.0-2.0	0.18-0.36	Probable
0.4-1.0	0.07-0.18	Possible
< 0.4	< 0.07	Negligible

3.2.4 Combined effect of carbonation and chloride effect on steel corrosion

The combined action of carbonation and chloride penetrations on concrete can be considered as one of the most severe degradation mechanisms. This severe exposure condition has very harmful effect on steel reinforcement protection as explained by Yoon (2007). However, this effect might depend on the sequence of the carbonation and chloride penetration and the status of the affected concrete cover as shown in Fig.3-7.

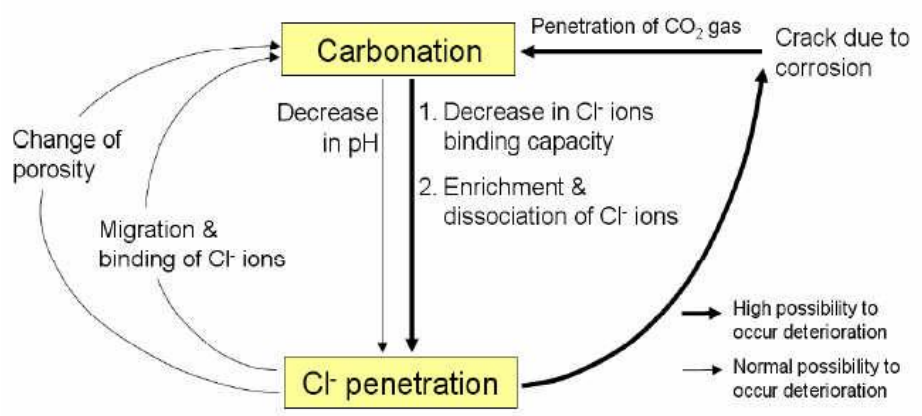

Figure 3-7 Mechanism of interaction between carbonation and chloride penetration (Yoon, 2007)

If the carbonation happened to a previously chloride contaminated concrete, considerable decrease in the binding capacity and an enrichment and dissolution of Cl^- ions might happen. Thus, in this case, a high probability of deterioration is expected. On the other hand, if carbonation has already decreased the pH value and altered the porosity of a healthy concrete, the binding capacity and the chloride ion migration following carbonation could be affected. In this case, a normal rate of deterioration is often anticipated.

Kayyali and Haque (1988) stated that the carbonation increases the free chloride in the carbonated mortars, especially those containing mineral admixture such as FA. Moreover, Ihekwaba et al (1996) indicated that the reduction of the pH value of the concrete due to carbonation reaction might have a catalyst effect for Cl^- ions to cause severe corrosion deterioration in contaminated concrete by chloride attack.

On the basis of inspection of a series of 25 year-old concrete structures, Costa and Appleton (2001), pointed out that the carbonation process has little effect if the concrete quality is medium or high. However, in low quality concrete, the interaction effect of

carbonation and chloride ingress caused an early steel de-passivation. Consequently, severe deterioration has then been recorded.

Hansson et al.(2007) pointed that the synergistic attack of carbonation and chloride can cause serious problems for concrete especially in hot coastal regions. Yoon (2007) tested the effect of the combined action of carbonation and chloride penetration on three NVC mixes with different w/c ratios (0.4, 0.5 and 0.55). The concrete was subjected to three different exposure conditions, single carbonation and single chloride, carbonation and chloride, and double carbonation with contaminated concrete by chloride. He concluded that the carbonation is a minor cause of concrete degradation under the double condition. However, the effect of carbonation was more pronounced on concrete contaminated by chloride.

In summary, it seems that the rate of corrosion of steel imbedded in concrete is controlled by many factors includes pH, humidity levels, oxygen, porosity and Cl^- concentration in pores. Many of these depend on classical concrete quality measures such as, density, mix proportion and water to cement/cementitious ratio and type of binder. However, in practice, the most important for initiated deterioration in aggressive natural environments, appear to be the reduction of the pH as a consequence of the ingress of either Cl^- or CO_2 from the surrounding environments towards the embedded steel. In addition, the interaction effect of these aggressive substances could cause substantial change in the electrical resistivity of the concrete leading to a high rate of deterioration to the reinforcing steel in short time.

3.3 Carbonation in concrete

3.3.1 Mechanism of carbonation and the change of the hydration products

In general, the pH value of normal concrete ranges from 12.6 to 13.5. This is mainly attributed to the presence of CH in the cement paste which is a product resulting from the hydration of Tri-calcium silicate (C_3S) and Di-calcium silicate (C_2S) in cement (Neville, 2011). The form of carbonation attack comprises the partial, but significant, neutralization of the alkalinity (pH value) of the hydrated cement paste. The process consists of the diffusion of the CO_2 gas through the pores system and then the reaction with the hydration products especially CH in the presence of water. Carbonation can cause the pH value of pore water inside the concrete to decrease to about 8 and this will

terminate the passive layer of the embedded steel and permit the corrosion of steel rebar to commence as explained earlier in Section 3.2.3.

The reaction starts from the surface of the concrete towards the inside and its velocity depends on several factors such as humidity, chemical composition of the cement paste, water/binder ratio, the degree of hydration, permeability and porosity of concrete, temperature and CO_2 concentration (Jiang et al., 2000, Bertolini et al., 2004). According to Jiang et al.(2000), the reaction of the diffused CO_2 and water in the pores of cement paste forms a weak carbonic acid, which dissolves CH and CSH. These general carbonation reactions can be summarized as in Eqs. 3-5 to 3-7.

$$CO_2 + H_2O \longrightarrow H_2CO_3 \quad \text{..... Eq. 3-5}$$

$$H_2CO_3 + Ca(OH)_2 \longrightarrow CaCO_3 + 2H_2O \quad \text{..... Eq. 3-6}$$

$$H_2CO_3 + CaO.SiO_2.H_2O \longrightarrow CaCO_3 + 2H_2O + SiO_2 \quad \text{..... Eq. 3-7}$$

For the carbonation of the CH, Matouek and Drochytka.1998 quoted by Stehlik and Novak (2011), describe four stages in the carbonation process. The first stage is the reaction between carbon dioxide and the calcium hydroxide in the presence of humidity as shown in Eq. 3-6. The second stage is the transformation of the insoluble resulting $CaCO_3$ into a soluble phase as shown in Eq. 3-6:

$$CaCO_3 + CO_2 + H_2O \longrightarrow Ca(HCO_3)_2 \quad \text{..... Eq. 3-8}$$

The third stage consists of recrystallizing the resulting insoluble carbonates to large calcite and aragonite crystals and the fourth stage is referred to as full carbonation (100% carbonation). It is important to highlight that the complete carbonation has a significant impact on the porosity and permeation properties of the concrete because of the crystallization of $CaCO_3$ in the concrete pores. However, not only the CH can suffer from the carbonation reaction but also all the other available hydration products. The major compounds in the unhydrated cement grains could react with the CO_2 as shown in Eq's 3-9 and 3-10 (Parrott and Hong, 1991).

$$C_3S + 3CO_2 + vH_2O \longrightarrow SiO_2 + vH_2O + CaCO_3 \quad \text{..... Eq. 3-9}$$

$$C_2S + 2CO_2 + vH_2O \longrightarrow SiO_2 + vH_2O + 2CaCO_3 \quad \text{..... Eq. 3-10}$$

For the hydration products, the resulting products after carbonation are a combination of water and the listed products in Table 3-3.

Table 3-3 Products formed when Portland cement hydration products carbonate after (Jana and Erlin, 2007)

Hydration products	CH	CSH	C_3A- Hydrates	C_4AF- Hydrates	AFt/ AFm
Carbonation products	C	C , CSH	C, alumina gel	C, ferric oxide, alumina	Gypsum, alumina gel

3.3.2 Impact of carbonation on the concrete microstructure and transport property

In addition to the significant disturbance to the pH level, the overall process of carbonation may also alter tortuosity, porosity and pores size distribution of the cement matrix. For the carbonation of NVC, the metastable calcium carbonate $Ca(HCO_3)_2$ is considered as one of the main causes of the changes in the pore sizes leading to a reduction in the porosity (Wowra et al., 2002). However, for HPC Borges et al. (2010) claimed that the overall porosity and permeability will potentially be slightly increased when the main phase (CSH) is also attacked by CO_2. As stated by Lagerblad (2005), the mode of carbonation and its effect on the porosity with mixtures containing pozzolans might be totally different from those made with OPC and this depends on the mechanism of carbonate (CO_3^{-2}) transformation and the mode of the nucleation of CO_3^{-2} on CH as well. To provide more understanding of carbonation impact on the porosity, this mechanism must be understood very well as shown in Fig. 3-8.

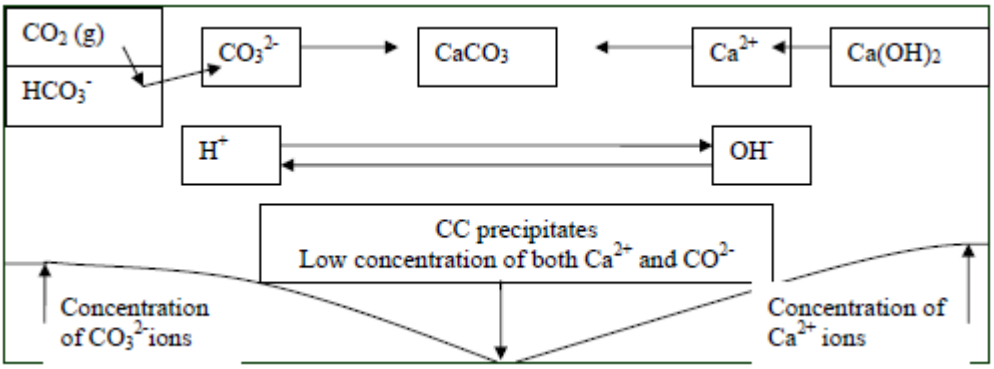

Figure 3-8 Schematic diagram of diffusion process in a single pore of a carbonating concrete (Lagerblad, 2005)

If the carbonate ions' concentration is high, it might participate on the surface of the CH compounds and with the pore solution or another high concentration phase (Ca^{+2}). This will have an impact on the porosity. In contrast, the porosity might not change under low

CO_3^{-2} concentration. However, this depends on the transmission speed of Ca^{++} and CO_3^{-2} ions in a single pore (Lagerblad, 2005).

The permeability, porosity and the pore volume features of a low to medium strength normal vibrated carbonated concrete with two strength grades (23 and 50 MPa) were investigated by Claisse et al. (1999) using air vacuum and MIP techniques respectively. In terms of permeability and porosity, the authors claimed that the carbonation led to a considerable reduction in these two characteristics, especially for low strength concrete. For the pore volume, they suggested that the total pore volume has only changed slightly and that the $CaCO_3$ precipitated on the pores didn't effect this change. Further, they concluded that the results obtained by surface permeability measurements and electrical connectivity characterization of the carbonated concrete give misleading indication of porosity.

The pore structure and chloride diffusion properties of hydrated high performance cement pastes after complete carbonation were studied by Ngala and Page (1997). They found that there was a decline in the total porosity of three cement paste systems (Ordinary Portland cement (OPC), fly ash and slag pastes) after carbonation, but the most interesting find of their research was the redistribution of the pore sizes; the percentage of large capillary pores (diameter >30 nm) was increased somewhat for the OPC pastes while it was increased considerably more for the fly ash and slag pastes. The results of this study might support the hypothesis provided later on by (Lagerblad, 2005) who proposed a different carbonation mechanism for blended cement used in HPC. In a very recent work on the carbonation of SCC conducted by Zdzisława O and Wioletta G (2013), a negative impact of carbonation has been recorded on the porosity of a SCC made with a 40 % partial replacement of cement with slag. Capillary pores greater than 25 nm was increased in size after carbonation leading to an increase in the absorption and water penetration and a reduction in the freezing-thawing cycles, in the presence of 3% NaCl solution.

For SCC, Mohammed et al.(2014) stated that the macro and micro diffusivity properties of the concrete as a composite material may alter due to the change of the porosity and the pore distribution caused by the carbonation process. Furthermore, carbonation might cause a significant alteration in the concrete properties that are strictly related to the

microstructure due to the change of cement matrix chemistry, such as the capillarity and connectivity of the pores in micro and nano scales in addition to the change of the pH of the pore solution.

The available research work of how the carbonation can alter the microstructure including the capillary pores, pore size distribution and the pore's connectivity characteristics is very limited especially for sustainable SCC. This might considerably affect the transport property in the cases of long term exposure and the combined action of carbonation and water or chloride penetration. Therefore, an attempt has been made in the present study to address both the impact of the carbonation on the microstructure (including capillary pores, pore size distribution and the associated chemistry change) in a quantitative manner in Chapter 6 and the impact of carbonation on the Chloride diffusion in Chapter 7.

3.3.3 Effect of pozzolanic materials on the progression of carbonation

The more recent investigations into the effects of using pozzolanic material as a partial replacement of cement on the progression of carbonation are reviewed in this section and their main conclusions are presented.

Papadakis (2000) concluded that the use of supplementary cementitious materials (SCMs) as a partial replacement of cement may shorten the time of carbonation to reach the steel bars and, hence, may increase the steel corrosion hazard. He claimed that the quantity of carbonatable materials decreases by replacing cement with SCMs, resulting in faster progression of carbonation front. The pozzolanic reaction means that there is less available CH phase that is available to react with the CO_2. Thus the same volume of CO_2 can penetrate to neutralize more concrete. Khan and Lynsdale (2002) carried out an investigation to study strength, permeability and carbonation of HPC with binary and ternary blended cement using PFA up to 40% and different percentages of SF (0-15)%. The w/c ratio varied from 0.27-0.5. They demonstrated that the carbonation depth increases with the increase of PFA percentage as a partial replacement of cement. The incorporating of SF led to a small increase in carbonation depth in comparison with OPC. However, after two years in natural condition, the maximum carbonation depth for 40% PFA concrete was only 2 mm indicating a reasonable resistance to carbonation.

In another study (Atiş, 2003), the carbonation of concrete containing high levels of FA (50-70) % as a partial replacement of cement was examined under an accelerated carbonation condition. The author claimed that there was a higher carbonation depth for the concrete with 70 % FA as compared with 50% FA and NVC. In addition, the effect of superplasticizer on the carbonation depth was insignificant in the assessed HPC. Sisomphon and Franke (2007), studied the effect of the curing age on the carbonation depth of concrete containing high volumes of pozzolanic materials and also modeled the carbonation phenomenon in HPC. They concluded that the depth of carbonation decreased with the increase of curing age (3, 7 and 28 days). However, after 28 days curing (a similar exposure to that reported in Chapter 6 of this thesis), all the HPC exhibited lower carbonation resistance as compared to the reference-HPC, as shown in **Fig. 3-9**. In addition, a new carbonation depth-time relationship were chosen for modeling of the carbonation in HPC ($X = K \times t^{0.4}$) as compared to **Eq. 3-18** in Section 3.4 which is normally used for this purpose.

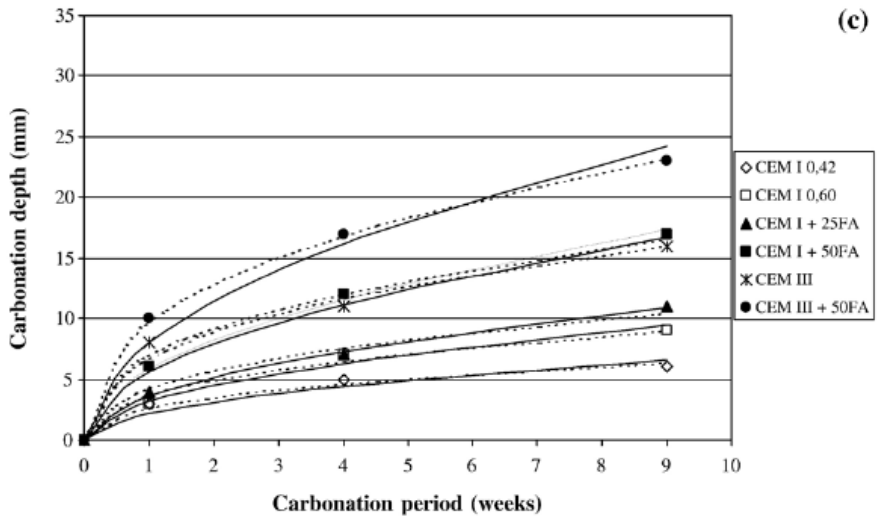

Figure 3-9 Relationship between the best fit and the expermintal result of carbonation depth of reference and HPC integrating high pozzolan contents (Sisomphon and Franke, 2007)

For the above perspective, Gjørv (2009) pointed out that the reactive materials can consume CH to form CSH owing to the pozzolanic reaction of these soft materials. Consequently, this reduces the amount of CH leading to a reduction in the pH value of the pore water even before carbonation. This reduction due to the use of these materials as a partial replacement of cement might also act to increase the carbonation progression hazard.

Younsi et al.(2011) recorded low resistance to carbonation in concrete made with 50% FA addition. Their results were based on accelerated carbonation and porosity tests. Although the porosity values of their reference mix and their 50% FA mix were approximately equal, the latter was more carbonated than the reference mixture. For SCC with a strength grade of 30-35 MPa and at various proportions of FA as a partial replacement of cement, the natural carbonation depth results indicated that the increase of the FA content beyond 25% had no effect on the carbonation depth at 90 days age while it increased very slightly for the long term exposure (365 days) as shown in Fig. 3-10 (Siddique, 2011).

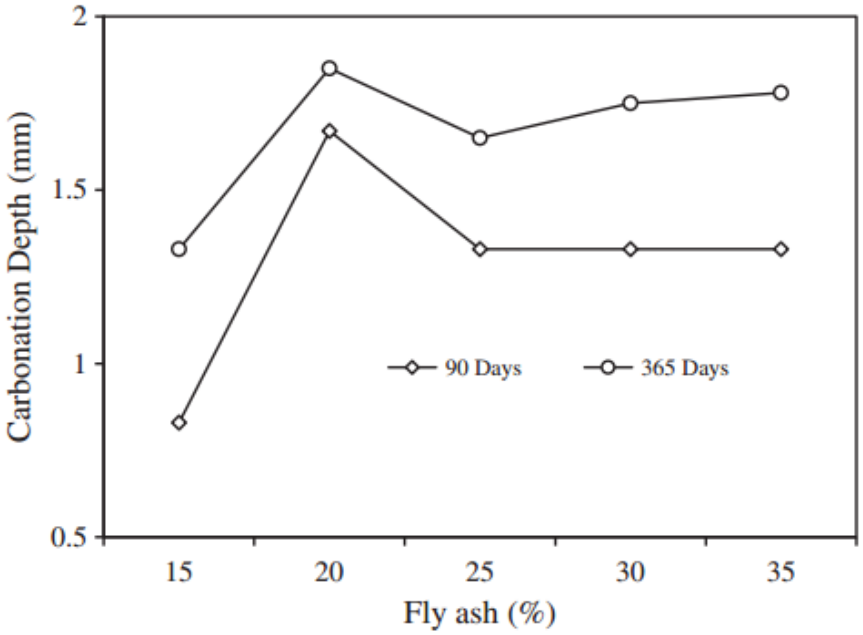

Figure 3-10 Effect of various FA contents on carbonation depth of SCC (30-35) MPa

3.3.4 Measurements of carbonation

Several measurement techniques have been proposed to evaluate the carbonation depth in concrete. In this section, existing techniques will be described and a comparison made.

3.3.4.1 Phenolphthalein indicator test and microscopic methods (Silva et al., 2002, Jana and Erlin, 2007)

Phenolphthalein solution (pH indicator) is conventionally used for carbonation depth measurements. It consists of spraying a new broken surface of concrete with the indicator. The color of the carbonated areas will not change while it will turn to pink in noncarbonated area as shown in Fig.3-11a.

More details of the carbonation front and its nature may be obtained using the petrographic microscope technique. In this technique, two types of specimens can be used. Small concrete or matrix pieces from the exposed concrete surface to the CO_2 should be mounted on slides or very thin sections should be prepared so they can be observed using petrographic microscope. The carbonated and non-carbonated areas in the matrix will exhibit a different colour spectrum under polarized light due to the different minerals present as shown in Fig.3-11b.

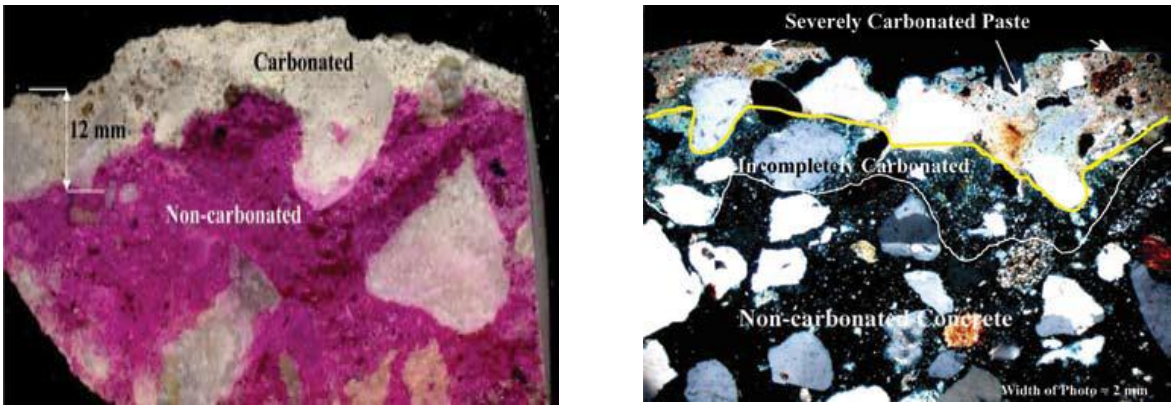

Figure 3-11 examining the carbonation front a) Phenolphthalein indicator b) petrographic microscope

For the concrete microstructural morphology observations of the carbonated concrete and the associated chemical changes of the hydration products due to carbonation, the secondary mode of the SEM was used by several investigators e.g. (Silva et al., 2002) as shown in Fig. 3-12.

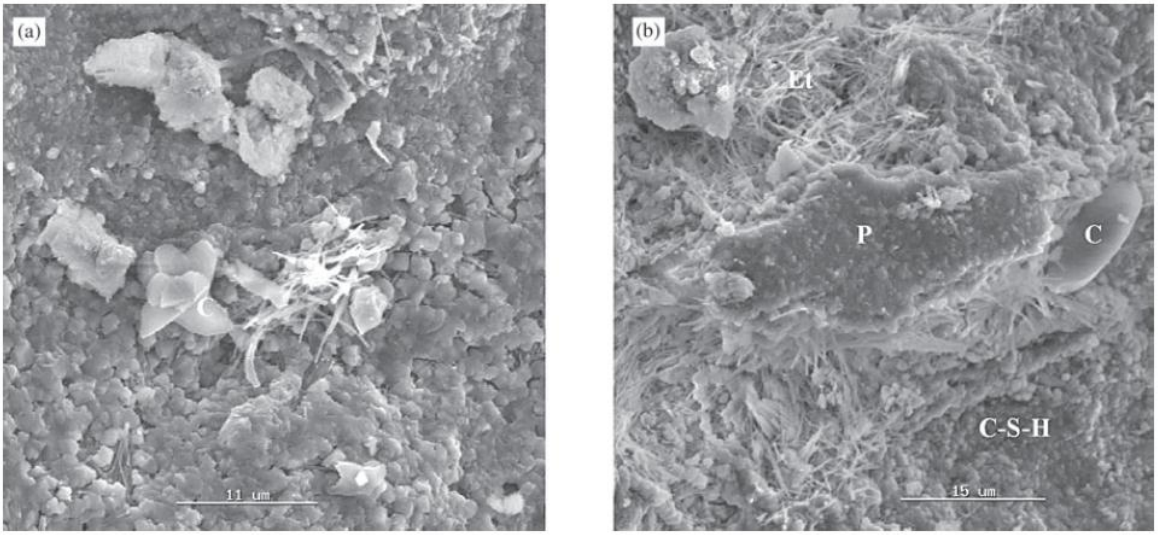

Photomicrographs of Concrete: a) presence of carbonates (C); b) several elements of the microstructure: carbonates (C), portlandite (P), calcium silicates (C-S-H) and ettringite (Et).

Figure 3-12 morphology and hydration products after carbonation of fracture specimens obtained from carbonation front (Silva et al., 2002)

3.3.4.2 Advanced use of Phenolphthalein indicator and other advanced techniques

In order to examine the accuracy of using the Phenolphthalein indicator, Chang and Chen (2006) used three different advanced techniques to examine the typical distribution of pH through the carbonation front:

- (TGA) method, which determines the concentration of CH and C.
- (XRD) tests which determine the intensity distribution of CH and C.
- Fourier transformation infrared spectroscopy (FTIR) test method which detects the presence of C–O in concrete samples as a basis for determining the presence of $CaCO_3$.

For the TGA and XRD analysis, the carbonation front Xc was determined when the concentration/relative intensity distributions of CH and C were horizontal whereas the point at which concentration/relative intensity gradient is steepest matches the position of the carbonation front as indicated by Phenolphthalein as shown in Fig. 3-13a and b. In the FTIR test, a carbonated concrete powder exhibits a peak, with a wave number in the range of 1410-1510 cm^{-1} as shown in Fig 3-13c, below the base line. The peak below, but nearest to this base line, indicate the position of the carbonation front.

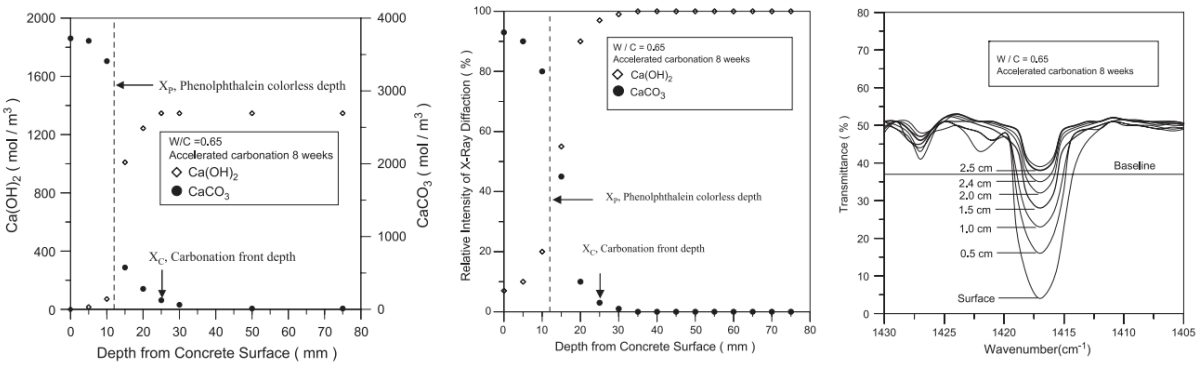

Figure 3-13 Comperasion of various advanced techniques a) TGA b) XRD c) FTIR and the Phenolphthalein indicator to detect the carbonation front profile (Chang and Chen, 2006)

Table 3-4 summarizes and compares the results of the carbonation depths from the above advanced technique in comparison to those obtained by Phenolphthalein.

Table 3-4 relationship between Phenolphthalein colorless depth and carbonation front using advanced technique (Chang and Chen, 2006)

Accelerated carbonation time	Phenolphthalein colorless depth (Xp mm)	Carbonation front (Xc, mm)		
		TGA	XRD	FTIR
8 weeks	12	25	25	24
16 weeks	17	35	35	35

3.4 Theoretical background of carbonation in concrete

Generally, carbonation has been recognized as a diffusion-based phenomenon as shown in Eq. 3-11 (Bertolini et al., 2004):

$$d = Kt^{1/n} \quad \text{..... Eq. 3-11}$$

d : Depth of carbonation, K: carbonation constant, : time and n : curve fitting factor

The equation only can be applied for steady concentrations of CO_2 and uniform paste properties and this might not be attained in actual exposure (Jana and Erlin, 2007). In addition, a considerable amount of diffused CO_2 will react with the hydration products in the cement paste during the carbonation progression. Taking into account the binding ability of the cement paste to capture CO_2 by the reaction with the hydration products, Papadakis (2000) proposed a more advanced mathematical model to define the constant, K, in a physico-chemical approach as shown in Eq. 3-12.

$$X_c = \sqrt{\frac{2D_{e,CO_2}\left(\frac{CO_2}{100}\right)t}{0.33CH + 0.214\,CSH}} \quad \text{..... Eq. 3-12}$$

X_c : depth of carbonation, D_{e,CO_2} : diffusivity of CO_2 in carbonated concrete, m^2/s, CO_2: carbon dioxide content of ambient air at concrete surface, t: time,s, CH : estimated calcium hydroxide content and CSH: estimated calcium-silicate-hydrate content

Because of the diffusion nature of the carbonation process, (Audenaert et al., 2007, De Schutter et al., 2008) reported that the carbonation can be considered as a Fickian problem for the SCC as well (based on the Fick's first law) and they proposed a simple

model based on the square-root time relationship Eq.3-18. This relationship is derived from the first Fick's law as follow:

$$J = -D\frac{dc}{dx} \quad \text{..... Eq. 3-13}$$

J is the flux of CO_2 (mol/m^2.s), *D* diffusion coefficient (m^2/sec), *C* is the concentration of CO_2 (mol/m^3) and x is a position variable being the distance travelled by the diffusing species (m).

At the carbonation depth, assuming the steady-state conditions, the concentration gradient of CO_2 is equal to C_1 (concentration on the concrete surface) - C_2 (concentration in un-carbonated zone) divided by the distance between these points (linear assumption). Therefore, the equation can be written as:

$$J = -D(C_1 - C_2)/x \quad \text{..... Eq. 3-14}$$

J can also be expressed as the amount of diffusing CO_2 molecules *dQ* (mol) divided by the time *t* (s) and passing across the exposed surface *S* (m^2)

$$J = dQ/Sd_t \quad \text{..... Eq. 3-15}$$

The amount of diffusing CO_2 molecules, *dQ* (mol), reacts with a certain amount of hydration products in concrete. This amount of reacting hydration products in a unit volume is given the symbol (mol/m^3), so:

$$dQ = a\,Sd_x \quad \text{..... Eq. 3-16}$$

Combining the Eqs. 3-14 to 3-16, leads to:

$$Xd_x = D/\,a\,(C_1 - C_2)d_t \quad \text{..... Eq. 3-17}$$

If *D*, a, C_1 and C_2 are assumed to be constant with time, integrating leads to:

$$x = A\sqrt{t} \quad \text{..... Eq. 3-18}$$

Where $A = \sqrt{\frac{2D}{a\,(C_1 - C_2)}}$ = constant with time

x: depth of carbonation (*mm*), *A*: carbonation coefficient ($mm/year^{0.5}$) and *t*: time (*year*)

3.5 Carbonation in medium to high strength SCC

Final report of RILEM TC205 on the durability of SCC RILEM (2008) claimed that SCC sometimes has a larger and sometimes a smaller carbonation depth as compared with NVC. Based on experimental works prior to 2008, they pointed out that due to the high amount of CH and CSH found in SCC, the carbonation hazard might be reduced, and this depends on the type of filler, the way of adding this filler and its effect on the composition of cement paste. However, the integration of high amounts of cement replacement by a certain filler types (reactive or non-reactive) could alter the porosity and the capillary pores' nature due to the change of the hydration products, especially CH and CSH contents in the hydrated cement matrix (as explained earlier in Chapter 2) leading to change in the carbonation progress.

For LP-SCC, the conclusion of the RILEM (2008) is in agreement with the subsequent work conducted by Valcuende and Parra (2010) who demonstrated that the SCC with limestone powder showed lower natural carbonation rates in comparison with NVC that contained limestone powder as well. This is due to the lower porosity and finer pore structure. However, the differences in the carbonation rate became very small when the fines content (cement plus LP) tended to be similar. The carbonation diffusion coefficient of the medium strength SCC was only 0.15 mm/month$^{0.5}$ less than the value for NVC at the same strength level, while it was 0.46 mm/month$^{0.5}$ for the low strength SCC less than the comparable. In contrast, Audenaert et al.(2007) concluded that at a constant w/c ratio and cement to powder ratio (c/p), the increase of the amount of the limestone powder results in a higher carbonation coefficient (mm/year$^{0.5}$) due to the increase in the total porosity as a result of high volume cement matrix in LP-SCC.

Assie et al.(2007) tried to estimate the self-compacting concrete 'potential' durability characteristics based on LP filler through answering some questions related to SCC in comparison to that of NVC, including carbonation and chloride penetrations. The authors considered three types of SCC and NVC according to the strength classes: 20 MPa for ordinary concrete, 40 MPa for structural concrete and 60 MPa for medium to high strength concrete. The accelerated carbonation depth results (50 ± 5% CO_2 concentration and 65 ± 5% relative humidity after 28 days curing), as shown in Fig.3-14, indicated that

the degradation of SCC by carbonation depth increased as fast as, or even slightly faster than, for the corresponding NVC, especially for normal and structural grades.

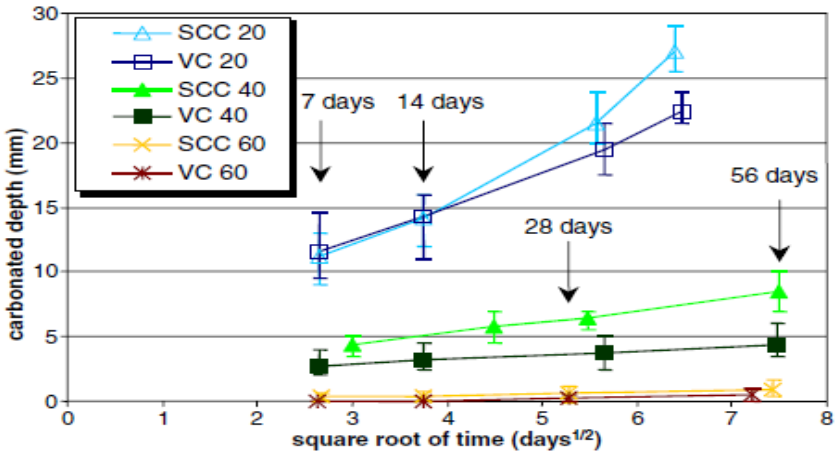

Figure 3-14 Carbonation depth versus the sequare root of time for various types of NVC and SCC (Assie et al., 2007)

The result of this study showed that medium to high strength SCC has a slightly lower or similar carbonation resistance. However, the use of 50% CO_2 concentration and the short term of the carbonation test (56 days after 28 days curing) might not be enough to obtain accurate and representative results for this high strength grade. 100% CO_2 concentration over a longer time scale (8 months) was adopted in the present study in observing the carbonation progress and resistance of the produced medium to high strength NVC and SCC (See Section 6.2.2).

For the medium to high strength SCC containing reactive and non-reactive filler such as LP and FA, Heirman et al.(2006) performed a long-term study (up to one year) to investigate the carbonation resistance of various type of SCC in comparison with NVC under accelerated condition (10 %CO_2 concentration, 20±2 ºC and 65 ± 5% relative humidity after 28 days curing). The strength grade of the NVC was 47.6 MPa while it varied from 39.9 to 73.3MPa for the various type of SCC as shown in Table 3-5.

Table 3-5 Overview of carbonation depths (mm) and accelerated carbonation constants [Acc (mm/year$^{0.5}$)] after (Heirman et al., 2006)

Time	NVC	SCC1	SCC3	SCC5	SCC14	SCC15	SCC16	SCC17
1 day (CC)	1.65	1.85	0.25	0.20	2.00	2.60	0.53	0.67
14 days (CC)	0.80	4.50	4.03	3.59	3.75	5.75	2.81	5.95
28 days (CC)	4.33	3.22	4.83	4.83	4.92	8.33	3.40	8.33
¼ year (CC)	8.33	7.00	8.50	4.67	7.33	13.92	4.00	11.83
½ year (CC)	15.75	12.08	15.00	15.17	8.33	18.25	10.50	20.33
1 year (CC)	12.75	12.00	19.83	18.67	10.67	23.17	14.00	25.50
A_{CC} (mm/year$^{0.5}$)	15.74	13.84	19.66	18.03	11.99	24.89	13.32	26.33
Comp. St. cube (MPa)	47.6	57.1	69.2	49.0	68.4	46.7	73.3	39.9

Their results indicated that NVC showed higher accelerated carbonation constant, A_{CC}, values in comparison with the all types of SCC at the same medium to high strength grade. Indeed, the results relating to the carbonation of medium to high strength SCC are a subject of controversy compared to the NVC at the medium to high strength grade. Medium to high strength grades are usually used in aggressive exposure environments and a key current question at the time of preparing this thesis as follows: *which has the dominant effect in determining the carbonation propensity: the chemical composition of cement matrix (pH value-mainly defined by the CH content) or the arrangement of the concrete pores*? The combined quantitative examinations of the chemistry of cement matrix and the internal microstructure (in terms of capillary pore nature, pore size distribution up to nano scale and the associated changes in these features before and after carbonation could provide a satisfying answer. The examination of above factors is one of the main aims of the present investigation (See Chapter6).

3.6 Chloride penetration in concrete

The section covers a particular literature area which can contribute to the understanding of the mechanisms of chloride transport in concrete.

3.6.1 Chloride penetration mechanisms

The chloride transport mechanism in concrete is a very complex phenomenon. It includes both the transport of the chloride inside the concrete by different mechanisms as will expand and the binding effect of the cement matrix to capture the chloride ions (binding ability) as explained in Chapter2 (Section 2.3.2). In general, there are three different mechanisms of chloride transport in concrete: permeability, capillary absorption and diffusion. The following sections summarize these three basic mechanisms and their theoretical backgrounds (Stanish et al., 2000, Cement Concrete & Aggregates Australia, 2009, Bioubakhsh, 2011).

3.6.1.1 Permeability

The movement and advection of a fluid through concrete in a certain time under a certain pressure gradient is described in terms of permeability. Eq. 3-20 (Darcy's law) defines the permeability of any porous media, including concrete. The flow of the liquid under steady state condition is proportional to the difference of the applied pressure (fluid gradient). Porosity, pore size distribution and the capillary pores' geometric features, such as tortuosity and connectivity, are related more or less directly, if non-explicitly, to the permeability of the concrete.

$$v = \frac{Q}{A} = -\frac{k\sigma g}{\eta}\ \frac{\Delta h}{L} \quad \text{..... Eq. 3-19}$$

v: Apparent velocity of flow of water per unit time per unit area (m/s) , Q: Volumetric flow rate (m^3/s) , A: Cross sectional area of the sample (m^2) , Δh: fluid head difference across the sample (m), L: Thickness of the sample (m), η: Dynamic viscosity of the liquid (kg/m.s), σ: density of the fluid (kg/m^3), g: acceleration due to gravity (m/s^2), and k : intrinsic permeability of materials (m^2).

The intrinsic permeability coefficient k is independent of the fluid involved:

$K = \frac{k\sigma g}{\eta}$ (m/s), therefore:

$$v = \frac{Q}{A} = -K\ .\frac{\Delta h}{L} \quad \text{..... Eq. 3-20}$$

Where: K is the coefficient of permeability of the fluid through concrete (m/s). Expressed in differential form this is written as:

$$v = -K\frac{dh}{dx} \quad \text{..... Eq. 3-21}$$

Darcy's law expresses the movement of the fluid only without any species. However, chloride movement through the cementitious materials is more complex and can be considered as an advective-diffusive phenomenon. This is because bulk movement or pore solution phase should be taken into account. Eq. 3.22 provides the mass balance equation for the chloride transport.

$$\frac{\partial}{\partial t}(\phi SC_{cl}) + divJ_{cl} - Q_{cl} = 0, \quad \text{..... Eq. 3-21}$$

$\boldsymbol{\varphi SC_{cl}}$ is the potential term, from which the porosity and saturation is directly obtained by thermo-hygro physics, $\boldsymbol{Q_{cl}}$ is the sink term for modeling of equilibrium between free and bound chloride, and $\boldsymbol{divJ_{cl}}$ is the chloride flux term

3.6.1.2 Absorption (Capillary suction):

Absorption is defined as the conveyance of liquids to the unsaturated concrete pores due to the surface tension. Thus, this feature is governed by the moisture content rather than pore structure only. Absorption can be expressed by Eq. 3-22:

$$A = b + S\sqrt{t} \quad \text{..... Eq. 3-22}$$

A: the mass or volume of liquid absorbed per unit of surface or the depth of liquid ingress, *S*: the sorptivity, *t*: the time and b: the initial surface absorption

The theory of the capillarity or unsaturated flow clarifies the relation between the absorption and the square root of time as follow:

$$P_c = \frac{2\gamma\cos\theta}{r} \quad \text{..... Eq. 3-23}$$

Pc: Capillary pressure (Pa), γ: surface tension (*Pa.m*), θ: wetting angle (equal to 0 for water) and *r*: effective radius of capillary tube (m)

According to Poiseuille's equation for the flow of liquid in a tube:

$$Q = \frac{dv}{dt} = \frac{\pi p r^4}{8l\eta} \quad \text{..... Eq. 3-24}$$

Q: Flow rate (m^3/s), *v*: Volume of liquid (m^3), *p*: pressure gradient (*Pa*) and *l*: length of tube (*m*)

Substitution for *dv* (*dv*= $\pi 2$ *dl*) in Eq. 3-24 leads to:

$\frac{ldl}{dt} = \frac{pr^2}{8\eta}$..... **Eq. 3-25**

Assuming the capillary pressure to be the only driving force and substituting for *p* using Eq. 3-24 yields:

$\frac{ldl}{dt} = \frac{\gamma}{4\eta}$ or $ldl = \frac{\gamma}{4\eta}\, dt$..... **Eq. 3-25**

Note $cos\theta = cos0 = 1$, therefore:

$l = S\sqrt{t}$..... **Eq. 3-26** Where $S = \sqrt{\frac{\gamma}{2\eta}}$ is sorptivity

3.6.1.3 Diffusion

Chloride can penetrate saturated concrete through the pore system of hydrated cement paste moving from high to low concentration through the water in the pores by diffusion. This process is governed by Fick's first law under steady state conditions (Eq. 3-13). However, a very long time is needed to achieve the steady-state chloride diffusion. Therefore, there is a need to adopt a non-steady-state diffusion interpretation, especially for HPC. The non-steady state process is controlled by Fick's second law (Eq. 3-27).

$J = -D\ \frac{dc}{dx}$..... **Eq. 3-13**

J is the flux of chloride ions ($mol/m^2.s$), *D* is diffusion coefficient (m^2/sec), *C* is the concentration of chloride ions (mol/m^3) and *x* is a position variable (m).

$\frac{\partial c}{\partial t} = D\ \frac{\partial c^2}{\partial x^2}$..... **Eq. 3-27**

Where: *t* is time (*sec*).

The typical general solution of this partial differential equation is:

$C(x,t) = C_s[1 - erf(\frac{x}{2\sqrt{Dt}})]$ ..... **Eq. 3-28**

$C(x,t)$ = chloride content measured at depth *x* at exposure time *t*, *% by weight of concrete*

C_s = surface chloride content, *% by weight of concrete*

x = depth, mm

D = apparent chloride diffusion coefficient, m^2/sec

t = exposure time, sec

erf = error function= $\mathrm{erf}(z) = \frac{2}{\sqrt{\pi}} \int_0^z \exp\ (-u^2)\, du$

Theoretically, the diffusion coefficient obtained from both cases should be the same. However, for concrete in practice the occurrence of steady state condition seems difficult.

3.6.1.3 Combined Transport Process

The above three basic mechanisms will interact with each other. Chloride conveyed by these mechanisms will also, likely, be affected by carbonation actions and occasionally by hygrothermal process (chloride transport by heat stresses), depending on the exposure type in natural conditions. Table 3-6 presents the primary chloride transport mechanisms for various exposures and example concrete structures.

Table 3-6 Chloride transport mechanisms as a function of exposure conditions
Adopted from (Cement Concrete & Aggregates Australia, 2009)

Exposure	Example of structure	Chloride transport mechanism
Submerged	Substructure below low tide	Diffusion
	Basement exterior walls or transport tunnel Liners below low tide. Liquid containing structures	Permeation, diffusion and, Possibility, capillary absorption
Tidal	Substructure and superstructures in the tidal zone	Capillary absorption and diffusion
Splash and spray	Superstructure about high tide in the open sea	Capillary absorption and diffusion (Also carbonation)
Coastal	Land based structure in coastal area or superstructures above high tide in river estuary or body of water in coastal area	Capillary absorption (Also carbonation)

From a practical point of view, the chloride transport due to the permeability is usually insignificant in reasonable or good quality concrete, due to the very low values of K (Eq. 3-20). However, diffusion can be considered as the main transport mechanism for chloride. The assessment of the internal microstructure at different scales as reviewed in details in Chapter 2 will be very helpful to understand the role of the combined chloride transport property.

3.6.2 Effect of pozzolanic materials on the chloride diffusion coefficient of concrete

The type of cement, the w/c ratio and the age of the concrete are the main factors that affect the chloride ingress in concrete. The effects of these factors on the non-steady state chloride migration coefficient (D_{nssm}), as determined by NT Built 492 standard, are have been extensively investigated in the literature by many concrete researchers. For HPC concrete containing various types and proportions of pozzolanic materials, Hassan (2012), summarized the effect of above factors from different previous investigations as shown in Figs. 3-15 and 3-16. The results in these figures demonstrate that the D_{nssm} generally decreased for the reference-HPC and those containing pozzolans with the use of low w/c ratio. In addition, the value of the D_{nssm} decreased with time for all the types of concrete except in the case of NVC as reported by Andrade et al. 2011 and in the HPC containing 8% SF Blezinsky et al. 2002 in the above figures.

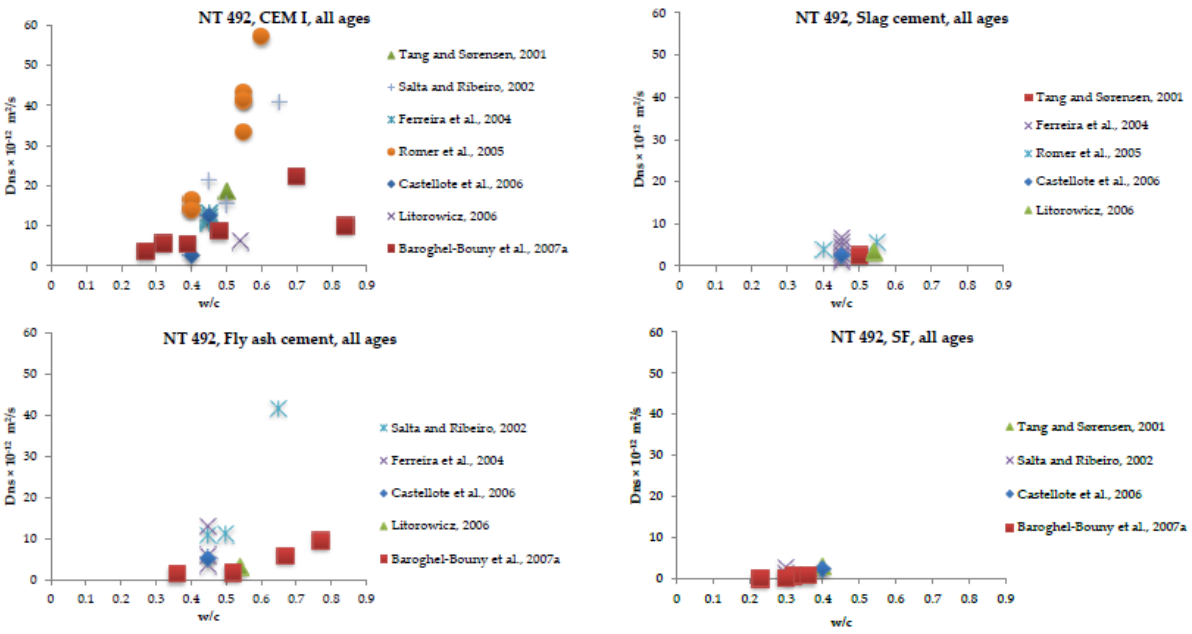

Figure 3-15 Effect of w/c on D_{nssm} a) CEM I concrete b) ggbs concrete c) FA concrete and d) silica fume concrete (Hassan, 2012)

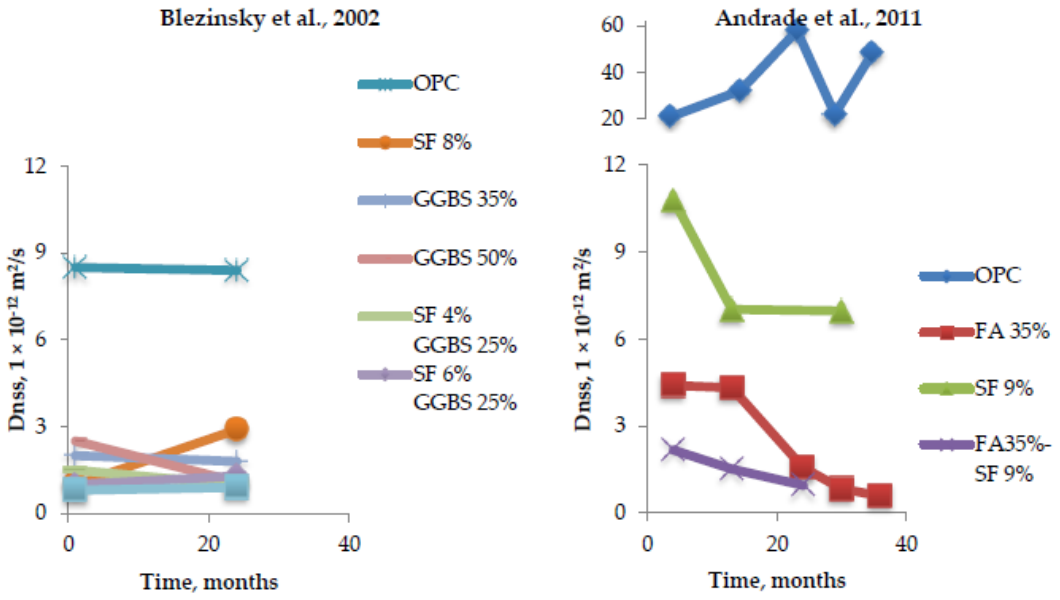

Figure 3-16 Aging effects on D_{nssm} in concrete incorporating different pozzolans materials (Hassan, 2012)

3.6.3 Chloride diffusion coefficient - time dependency

The reduction of the D_{nssm} with time seems to indicate that the chloride diffusion reduces with time. In practice, this may be caused, in part, by binding to and reactions with the active binders; the effect depending on the type (activity) and quantity of the cement and pozzolans in the HPC especially in those HPCs containing relatively high partial replacement of cement with pozzolans. Fig. 3-17 explains the effect of chloride binding capacity on the reduction of the measured chloride diffusion coefficient as a function of the cement replacement proportion by FA.

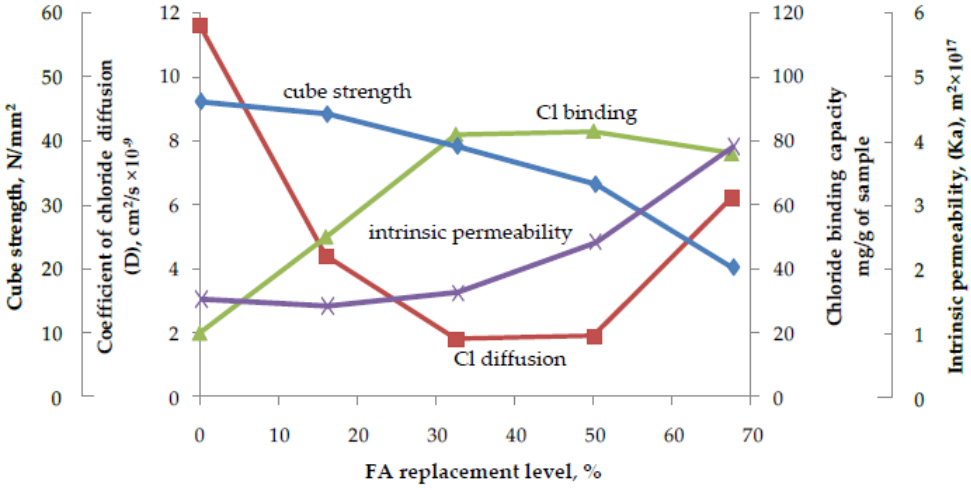

Figure 3-17 Chloride binding capacity as a function of cement replacement by FA (Hassan, 2012)

Hassan (2012) studied a wide range of concrete mixtures containing CEM I concrete and different SCMs. Values of the non-steady state chloride diffusion coefficients (D_{nssn}) in this study were obtained from both accelerated and natural ponding chloride tests for CEM I, GGBS, FA and SF concrete. He plotted his result with the available data concerning the time-dependent nature of the chloride diffusion coefficient as provided by Concrete Society Technical Report 61 (CSTR61) as shown Figs. 3.18 and 3.19. Hassan (2012) proposed 0.142, 0.774 and 0.437 ageing factors (defined in Chapter 7 by Eq. 7.9) for CEMI, FA, GGBS concretes in the real conditions respectively, instead of that proposed by CSTR61 (0.264, 0.621, 0.699 respectively). For SF concrete, he proposed that the same ageing formula be used as CSTR61 [ageing factor = -1 + 1.1 (w/c) but for 0.4 w/c only].

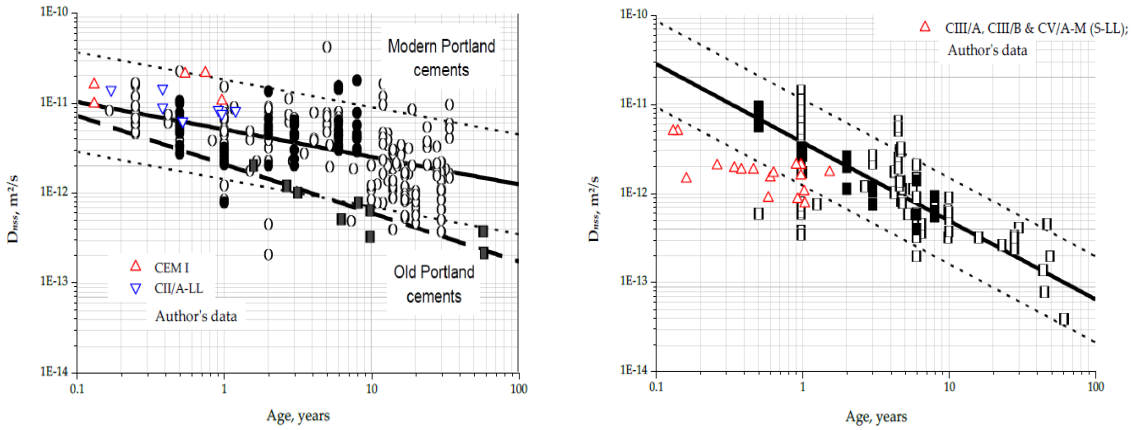

Figure 3-18 Age dependent values of D_{nss} and data in CSTR61 to derive the age factor for CEM I and GGBS concrete

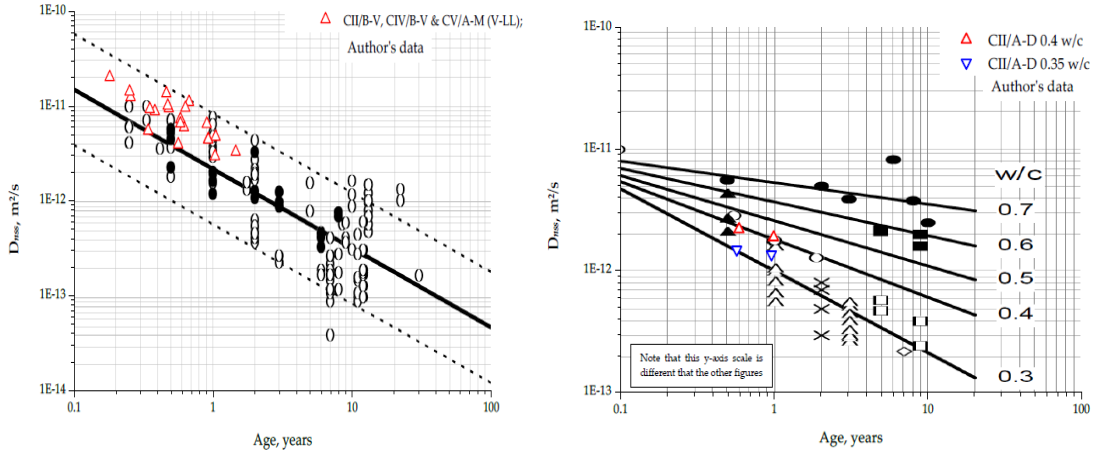

Figure 3-19 Age dependent values of D_{nss} and data in CSTR61 to derive the age factor for FA and SF concrete

3.7 Chloride ingress in medium to high strength SCC

As explained earlier in Chapter 2, it is known that the SCC has a dense microstructure and a dense cement matrix, containing reactive and non-reactive fillers, when compared to normal vibrated concrete (NVC) (Coppola et al., 2004, Yazıcı, 2008). Sometimes SCC has the same or higher water to cementitious material ratio as NVC in which case, the fillers and added workability due to the high dosage of SP may be responsible for the greater density. Sometimes SCC has lower water to cementitious material ratio, which directly contribute to the greater density and is facilitated by the SP-induced workability. Thus, the SCC could have a less easily penetrated microstructure. However, as reported by Assié et al. (2007), referencing Zhu et al. 2001, the modification of the microstructure might not be enough to assure sufficient resistance to the chloride penetration as this property might be governed by the tortuosity, the percolation and the connectivity of the internal pore network.

Although research work has been done to estimate the chloride penetration resistance as part of the durability assessment of SCC, the available experimental data about the medium to high strength SCC showed that no definite conclusion could be drawn about whether SCC has similar, larger or smaller resistance to chloride penetration than NVC at the same strength level. Assié et al. (2007) claimed that a SCC having a similar or, even better, compressive strength than a NVC, although at a higher w/c ratio, had equivalent chloride diffusion and water absorption. In their study, the SCC investigated employed limestone filler for all mixes. On the other hand, the results of Heirman et al. (2006) revealed that no definite conclusion was possible about whether SCC incorporating LP and FA has a larger or smaller chloride diffusion coefficient in comparison with NVC at medium to high strength grade. SCC3 with a compressive strength grade of 69.2 MPa exhibited good resistance against chloride ingress whilst NVC (47.6 MPa), SCC1 (57.1 MPa), SCC14 (68.4 MPa) and SCC16 (63.7 MPa) provided only moderate chloride resistance. The diffusion coefficients of three types of SCC: SCC5 (49 MPa), SCC15 (46.7 MPa) and SCC17 (39.9 MPa) exceeded 16×10^{-12} m^2/s signified their unsuitability for the use in aggressive chloride environments.

Recently, Dinakar et al.(2008) noticed that, in spite of higher permeable voids and higher water absorption, high fly ash SCC showed lower chloride penetration in comparison with NVC at any strength grade. The authors suggested that it could be as a result of a

higher chloride binding capacity of the cement matrix caused by the presence of high available C3A in the cementitious materials system with increased fly ash content.

3.8 Concluding remarks

- Carbonation can promote blocking of the pore structure of the cement matrix for concrete. For the transport properties of concrete, however, it seems that the study of the change of the geometric characteristics of pores at different scales such as pore distribution, the connectivity features of these pores and the associated microstructure change after carbonation, are more important than the reduction of the porosity value.

- There is no available investigation which studied the change of the pore structure features at different scales and the associated microstructure and chemical change of SCC after complete carbonation in a quantitative manner. The study of these phenomenon according to this approach could help to provide a useful recommendation to the use of new types of concrete in severe multi- aggressive environments (the synergistic attack of carbonation and water or chloride penetration at the same time) or in simulating the long term behavior.

- Different advanced techniques for carbonation depth measurements have been reported in the literature. The Phenolphthalein indicator is the easiest way and it is still valid for the assessments of carbonation progression or resistance as it has been used by most concrete researchers. However, the use of the XRD examination might be helpful in estimating the 100 % degree of carbonation due to the absence of CH compounds in the XRD spectra after carbonation.

- The use of mineral admixtures at relatively high partial replacement of cement might affect the carbonation progression leading to reduced service life. The theoretical bases of the carbonation phenomena and the developed accelerated tests could be a very useful tool in both the modeling of carbonation and the prediction of the long term behavior for highly carbonation resistive concretes.

- Although different chloride mechanisms have been proposed for the real exposure conditions, the most common mechanism is diffusion by which the chloride can

penetrate the concrete from high to low concentration areas until reaching the steel reinforcement.

- Taking into account the fact that SCC is a relatively new type of concrete and it has a short history in the real construction industry in severe environments, the long term durability characteristics, especially carbonation and chloride ingresses have to be studied very carefully. As compared with NVC, SCC has different chemical composition and permeation properties such as permeability, porosity and diffusivity. These properties will directly affect the carbonation progress and chloride penetration.

- Until now, the study of carbonation and chloride penetration in SCC is very limited and their velocities are a somewhat controversial topic. SCC has sometimes a larger and sometimes a smaller carbonation and chloride penetration as compared with the normal vibrated concrete (NVC) especially for medium to high strength SCC. Based on the above:
  - The investigation of the carbonation as function of both the internal chemistry and microstructural features could offer appropriate answers to the current questions about the controlling mechanism of this phenomenon and its impact on the transport properties of SCC.
  - The investigation of the chloride ingress as a function of the internal microstructure at different scales could provide a deep understanding of this complex phenomenon in SCC by establishing quantitative (macro/micro and nano internal) pore structure to chloride penetration velocity relationships.
  - Understanding of the theoretical bases of chloride ingress mechanisms, the available data from the actual concrete structure exposed to severe chloride environments and accelerated chloride tests, could be a very useful tool in modeling chloride penetration and predicting of the long term behavior for cover and durability design purposes.

3.9 References

ACI COMMITTE 222 2000. Protection of metals in concrete against corrosion. American Concrete Institute.

ACI COMMITTE 365 2000. Service-Life Prediction- State of the report. American Concrete Institute.

AHMAD, S. 2003. Reinforcement corrosion in concrete structures, its monitoring and service life prediction—a review. Cement and Concrete Composites, 25, 459-471.

ANDRADE, C., ALONSO, M., GONZALEZ, J. & FELIU, S. 1990. Similarity between atmospheric /underground corrosion and reinforced concrete corrosion. In Corrosion of Reinforcement in Concrete (edited by Page C.L., Treadway K.W.J. and Bamforth P.B.), Elsevier Applied Science, 1990, 39-48. Publication of: CICC Publications.

ANGST, U., ELSENER, B., LARSEN, C. K. & VENNESLAND, Ø. 2009. Critical chloride content in reinforced concrete — A review. Cement and Concrete Research, 39, 1122-1138.

ASSIE, S., ESCADEILLAS, G. & WALLER, V. 2007. Estimates of self-compacting concrete 'potential'durability. Construction and Building Materials, 21, 1909-1917.

ASSIÉ, S., ESCADEILLAS, G. & WALLER, V. 2007. Estimates of self-compacting concrete 'potential'durability. Construction and Building Materials, 21, 1909-1917.

ATIŞ, C. D. 2003. Accelerated carbonation and testing of concrete made with fly ash. Construction and Building Materials, 17, 147-152.

AUDENAERT, K., BOEL, V. & DE SCHUTTER, G. Year. Carbonation of filler type self-compacting concrete. In: 12th International Congress on the Chemistry of Cement (ICCC 2007), 2007.

BERTOLINI, L., ELSENER, B., PEDEFERRI, P. & POLDER, R. B. 2004. Corrosion of steel in concrete: prevention, diagnosis, repair, WILEY-VCH.

BIOUBAKHSH, S. 2011. The penetration of chloride in concrete subject to wetting and drying: measurement and modelling. UCL (University College London).

BORGES, P. H. R., COSTA, J. O., MILESTONE, N. B., LYNSDALE, C. J. & STREATFIELD, R. E. 2010. Carbonation of CH and C–S–H in composite cement pastes containing high amounts of BFS. Cement and concrete research, 40, 284-292.

CEMENT CONCRETE & AGGREGATES AUSTRALIA. 2009. Available: http://www.concrete.net.au/publications/pdf/ChlorideResistance.pdf [Accessed 17-05-2012].

CHANG, C.-F. & CHEN, J.-W. 2006. The experimental investigation of concrete carbonation depth. Cement and Concrete Research, 36, 1760-1767.

CHANG, J. J., YEIH, W., HUANG, R. & CHI, J. M. 2003. Mechanical properties of carbonated concrete. Journal of the Chinese Institute of Engineers, 26, 513-522.

CLAISSE, P. A., EL-SAYAD, H. I. & SHAABAN, I. G. 1999. Permeability and pore volume of carbonated concrete. ACI Materials Journal, 96.

COPPOLA, L., CERULLI, T. & SALVIONI, D. Year. Sustainable development and durability of self-compacting concretes. In: 8th CANMET/ACI Int. Conf. on Fly Ash, Silica Fume, Slag and Natural Pozzolans in Concrete, 2004. 29-50.

COSTA, A. & APPLETON, J. 2001. Concrete carbonation and chloride penetration in a marine environment. Concrete Science and Engineering, 3, 242-249.

DE SCHUTTER, G., BARTOS, P. J. M., DOMONE, P. & GIBBS, J. 2008. Self-compacting concrete, Taylor and Francis Group.

DINAKAR, P., BABU, K. G. & SANTHANAM, M. 2008. Durability properties of high volume fly ash self compacting concretes. Cement and Concrete Composites, 30, 880-886.

FERREIRA, R. M. 2004. Probability-based durability analysis of concrete structures in marine environment. Phd, University of Minho.

GJØRV , O. E. 2009. Durability design of concrete structures in severe environments, Taylor & Francis Group.

HANSSON, C. M., A.POURSAEE & J.JAFFER, S. 2007. Corrosion of reinforcing bars in concrete. Portland Cement Association 2007.

HASSAN, Z. F. A. 2012. Rapid assessment of the potential chloride resistance of structural concrete. University of Dundee.

HEIRMAN, G., VANDEWALLE, L., BOEL, V., AUDENAERT, K. & DE, G. Year. Chloride penetration and carbonation in self-compacting concrete. In: ConcreteLife'06-International RILEM-JCI Seminar on Concrete Durability and Service Life Planning: Curing, Crack Control, Performance in Harsh Environments, 2006. RILEM Publications SARL, 13-23.

IHEKWABA, N., HOPE, B. & HANSSON, C. 1996. Carbonation and electrochemical chloride extraction from concrete. Cement and Concrete Research, 26, 1095-1107.

JANA, D. & ERLIN, B. 2007. Carbonation as an indicator of crack age. Concrete international 29, 61-64.

JIANG, L., LIN, B. & CAI, Y. 2000. A model for predicting carbonation of high-volume fly ash concrete. Cement and Concrete Research, 30, 699-702.

KAYYALI, O. A. & HAQUE, M. 1988. Effect of carbonation on the chloride concentration in pore solution of mortars with and without flyash. Cement and Concrete Research, 18, 636-648.

KHAN, M. & LYNSDALE, C. 2002. Strength, permeability, and carbonation of high-performance concrete. Cement and Concrete Research, 32, 123-131.

LAGERBLAD, B. 2005. Carbon dioxide uptake during concrete life cycle–State of the art, Swedish Cement and Concrete Research Institute, CBI: Stockholm.

MEHTA, P. K. & MONTEIRO, P. J. M. 2006. Concrete: microstructure, properties and materials, McGraw-Hill.

MOHAMMED, M. K., DAWSON, A. R. & THOM, N. H. 2014. Carbonation of filler typed self-compacting concrete and its impact on the microstructure by utilization of 100% CO2 accelerating techniques. Construction and Building Materials, 50, 508-516.

NEVILLE, A. M. 2011. Properties of Concrete, London, Pearson Education Limited.

NGALA, V. & PAGE, C. 1997. Effects of carbonation on pore structure and diffusional properties of hydrated cement pastes. Cement and Concrete Research, 27, 995-1007.

PAPADAKIS, V. G. 2000. Effect of supplementary cementing materials on concrete resistance against carbonation and chloride ingress. Cement and Concrete Research, 30, 291-299.

PARROTT, L. & HONG, C. Z. 1991. Some factors influencing air permeation measurements in cover concrete. Materials and Structures, 24, 403-408.

RENDELL, F., JAUBERTHIE, R. & GRANTHAM, M. 2002. Deteriorated concrete: inspection and physicochemical analysis, Thomas Telford Services Ltd.

RILEM 2008. Final report of RILEM TC 205-DSC: durability of self-compacting concrete, Materials and Structures,2008, P. 225-233.

SHI, X., XIE, N., FORTUNE, K. & GONG, J. 2012. Durability of steel reinforced concrete in chloride environments: An overview. Construction and Building Materials, 30, 125-138.

SIDDIQUE, R. 2011. Properties of self-compacting concrete containing class F fly ash. Materials & Design, 32, 1501-1507.

SILVA, C. A. R. D., REIS, R. J. P., LAMEIRAS, F. S. & VASCONCELOS, W. L. 2002. Carbonation-Related Microstructural Changesin Long-Term Durability Concrete. Materials research, 5, 287-293.

SISOMPHON, K. & FRANKE, L. 2007. Carbonation rates of concretes containing high volume of pozzolanic materials. Cement and concrete research, 37, 1647-1653.

STANISH, K., HOOTON, R. D. & THOMAS, M. 2000. Testing the chloride penetration resistance of concrete: a literature review, Department of Civil Engineering, University of Toronto.

STEHLIK, M. & NOVAK, J. 2011. Verification of the effect of concrete surface protection on the permeability of acid gases using accelerated carbonation depth test in an atmosphere of 98% CO2. Ceramics–Silikáty, 55, 79-84.

THE CORROSION SOCIETY. NACE. 2012. Corrosion Control Plan for Bridges [Online]. Available: http://www.nace.org/uploadedFiles/Corrosion_Central/Corrosion_101/White_Papers/CorrosionControlPlanForBridges.pdf [Accessed].

VALCUENDE, M. & PARRA, C. 2010. Natural carbonation of self-compacting concretes. Construction and Building Materials, 24, 848-853.

WOWRA, O., SETZER, M., AUBERG, R. & KECK, H. Year. Effects of carbonation to micro structure and pore solution. In: Proceedings of the RILEM workshop on Frost Resistance of Concrete, Germany, 2002. 61-8.

YAZıCı, H. 2008. The effect of silica fume and high-volume Class C fly ash on mechanical properties, chloride penetration and freeze–thaw resistance of self-compacting concrete. Construction and Building Materials, 22, 456-462.

YOON, I. S. 2007. Deterioration of Concrete Due to Combined Reaction of Carbonation and Chloride Penetration: Experimental Study. Key Engineering Materials, 348, 729-732.

YOUNSI, A., TURCRY, P., ROZIÈRE, E., AÏT-MOKHTAR, A. & LOUKILI, A. 2011. Performance-based design and carbonation of concrete with high fly ash content. Cement and Concrete Composites, 33, 993-1000.

ZDZISŁAWA & WIOLETTA 2013. The influence of carbonation of self-compacting concrete with granulated blastfurnace slag addition on its chosen properties. Cement-Wapno - Beton.

Chapter 4:
Assessment of raw materials, experimental program and Production of mixes

4.1 General

This chapter consists of four main parts explaining: the used raw materials, the experimental program, the production of the concrete mixtures and the assessments of fresh and compressive strength results.

The first part provides the basic characteristics of the raw materials which were used for the production of normal vibrated and self-compacting concretes. For cement, fillers and mineral additions (LP, FA and SF), the microstructural and mineralogical characteristics were examined using SEM and XRD techniques respectively.

The second part includes a comprehensive review and full details of the tests performed and the experimental program, except the accelerated carbonation and chloride tests which are thoroughly reviewed and described in their respective Chapters (6 and 7).

The third part includes the mixes design, mixing procedures and the preparation of the specimens. In addition, it provides the preliminary experimental details of the mixes design, the optimization and the selection of normal vibrated and self-compacting concretes and mortars.

The fresh characteristics were assessed and the compressive strength developments up to 28 days are also debated in the fourth part. Finally, short summery and concluding remarks are given.

4.2 Materials

4.2.1 Cement

Portland cement (CEM I 52.5R) has been used widely to produce medium and high strength NVC or SCC. Each type of cement conforming to EN 197-1 is appropriate for the manufacture of SCC as recommended by the European guide for SCC (EFNARC, 2002). Therefore, in the present work, CEM I 52.5R produced by Rugby Cement

Company was used for the production of all the investigated mixtures. Physical and chemical properties of this type of cement are illustrated in Table 4.1.

Table 4.1 Physical and chemical properties of CEM I 52.5R

Chemical compounds	SiO_2	Fe_2O_3	Al_2O_3	CaO	MgO	SO_3	LOI*	IR*
Percentages %	20.09	3.87	4.84	64.02	1.15	2.83	2.36	0.34

LOI*: Loss on ignition, IR*: Insoluble residue .Specific Gravity = 3.15. Strength for 28 days = 56.40 MPa

4.2.1 Fine and coarse aggregate

Local river quartz sand with a maximum particle size of 5 mm was used as a fine aggregate. The specific gravity and the water absorption of this type of sand were 2.65 and 1.5 % respectively. Low maximum size and rounded shape of coarse aggregate are obligatory to reduce the segregation of SCC and ensure a good passing ability (Koehler and Fowler, 2006). Therefore, quartz natural uncrushed rounded gravel with a nominal maximum size of 10 mm was used as coarse aggregate for the production of normal vibrated and SCC-mixtures. The specific gravity and the water absorption of such gravel were 2.6 and 0.8 % respectively. The grading of the fine and the coarse aggregate confirms to the limitation of BS 882 (1992) as shown in Fig 4.1 and 4.2.

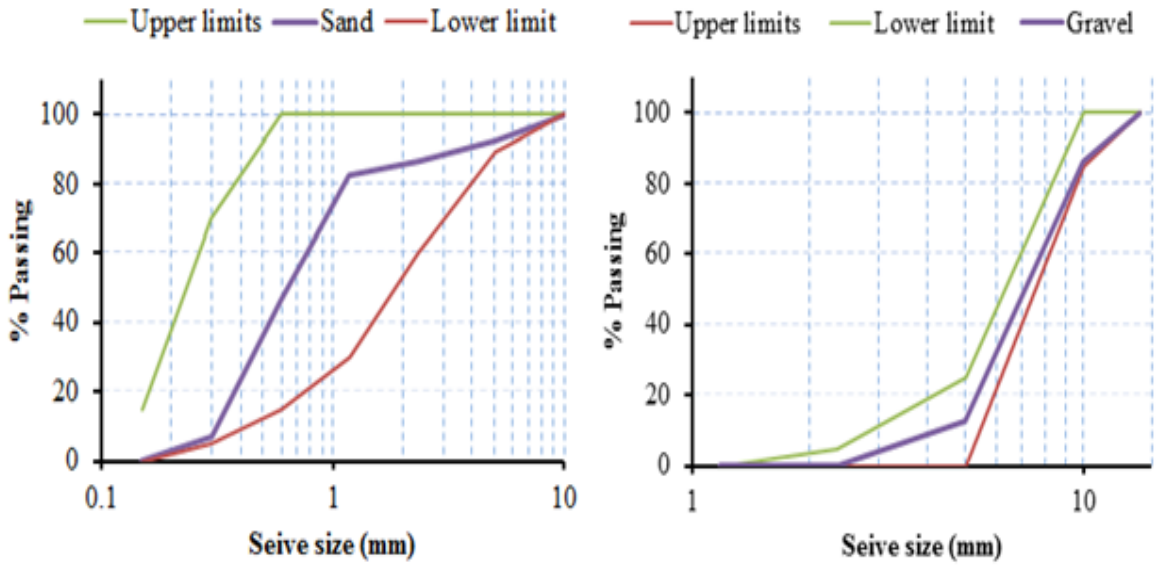

Figure 4-1 Grading curves of fine and coarse aggregate

Figure 4-2 Used fine and coarse aggregate

4.2.2 Superplasticizer (SP)

Superplasticizers or high range water reducing admixtures are modified types of water-reducing admixtures. Basically, they are water-soluble organic polymers. They dissolve in water in a complex polymerization reaction to form long molecules. These long molecules carry high negative charges, and they can be adsorbed on the surface of the cement particles which hold opposite charges. As a result of the dispersion of cement particles by electrical repulsion between these negative charges, the combined water between the cement agglomerations will be freed and hence, increase the fresh properties significantly (Neville, 2011). In SCC, the use of high percentages of SP is the main key to ensure a high deformability and moderate or high viscosity at a low water binder ratio Okamura and Ouchi (2003).

Superplasticizer based on polycarboxylic ether (PCE) polymer was used to maintain the required fresh properties with a low water to powder materials ratio for the SCC and mortars. **Table 4.2** provides the technical data for this type of SP.

Table 4.2 Technical data of SP (Appearance: yellow liquid)

Property	Sp. gr.@ 20° C	pH-value	Alkali content %	Chloride content %
Determined as	1.08 ± 0.02 g/cm^3	6.0±1	≤ 2	≤ 0.1

4.2.3 Fillers and mineral additions

In recent years, there has been an increasing interest in using high quantities of fillers as a partial replacement of cement in self-compacting concretes (SCC). By this means it helps to make SCC a more economic and sustainable material. Incorporation of a high quantity of superplasticizer (SP) and a large volume of filler materials is essential to achieve high flow ability and sufficient resistance to segregation. There are many types of fillers and mineral additions that have been used successfully to produce self-compacting concrete SCC but the most common admixtures are limestone filler (LP), fly ash (FA) and silica fume (SF). Moreover, the use of mineral admixtures and micro fillers as a partial replacement of cement may reduce the high cost of SCC effectively. These additions and the absence of vibration might give the self-compacting concrete SCC a distinct microstructure as compared with that of normal vibrated concrete (NVC). However, the durability of such types against aggressive environments needs to be studied further (Aggarwal et al.,2008,Coppola et al., 2004, Nehdi et al., 2004, RILEM ,2008).

One of main emphases of the present work is examining how the change of the filler type or /and mineral fillers at relatively high replacement of cement can affect the performance of sustainable SCC under aggressive environments of chloride and carbonation relative to a reference SCC and NVC at the same strength grade. Thus, different types of filler and mineral admixture were used: Fly ash (FA) and limestone powder (LP) in addition to the silica fume (SF).

4.2.3.1 Limestone Powder (LP)

The use of this type of filler for cementitious materials has gained an increasing interest where technical, economic, and ecological benefits could be obtained Bonavetti et al. (2003). Natural limestone filler from Longcliffe quarry, Derbyshire, UK, with a particle size less than 65 µm was used with a nominal cement content of 300 kg/m^3 for the production of LP-SCC mix. In Europe, limestone powder is considered as one of the most common additions to produce filler typed SCC. Chemically, to date, there is no reliable evidence that it can participate chemically to improve the structure of the hydrated cement paste. Physically, the finer particles of this powder can fill the pores between the cement grains. However, this filling effect depends on the surface texture,

grain size distribution of the powder and the size of the cement particles as well De Schutter G (2011). The microstructural and chemical characteristics of the cement paste and the interfacial transition zone (ITZ), using high partial replacement of a non-reactive coarser filler such as LP related to the chloride and carbonation penetration is not yet quantitatively clarified.

4.2.3.2 Fly ash (FA)

Worldwide in 2001, the estimation of coal combustion products is about 480 million tons of which the fly ash forms about 68% of these products. Mainly, FA is a byproduct (waste material) resulting from the electrostatic or mechanical precipitation of flue ash during the combustion of coal especially in the power plants Feuerborn (2005). FA and pulverized fuel ash (PFA) are two types of mineral fillers that have been used successfully in the production of SCC. In the current investigation, Fly ash type 450-S produced by Cemex Company was used. From the material datasheet provided by the supplier, the powder contains approximately 50% silica and 26% alumina. This mineral filler could be classified as Class F according to the American Society of Testing Material ASTM C-618 (1991). If the amounts of Silica plus Alumina oxides are smaller than 70%, then the FA could be classified as Class C according to this standard.

4.2.3.3 Silica fume (SF)

Silica fume is a by-product of the manufacture of Silicon metals from Ferro silicon alloys in the electric arc furnace. It has numerous form such as undensified powder if it is compiled from the filters directly, densified if it is treated to increase the bulk density and a slurry if it is mixed with water BS EN 13263-1:2005 +A1 (2009). Densified silica fume produced by the Elkem Microsilica Company was used in a combination with FA at the selected replacement ratio (See Mix design section). Some chemical and physical properties of the used cement and the admixtures are listed in Table 4.3 while Fig. 4-3 shows these materials and their particle size distribution.

Table 4.3 Some chemical and physical properties of the cement and the used filler

Chemical compounds	Cement	LP	FA	SF
SiO_2	20.09	0.3	50%	> 90
Fe_2O_3	3.87	---	6.90	---
Al_2O_3	4.84	---	26%	---
CaO	64.02	---	8.70	---
MgO	1.15	---	1.80	---
SO_3	2.83	----	0.60	---
$CaCO_3$	---	99	----	---
Loss On Ignition %	2.36	---	Category B < 3	< 3
Specific gravity	3.15	2.7	2.21	2.2
Blaine Finesse (m^2/kg)	395	550	388.5	22400

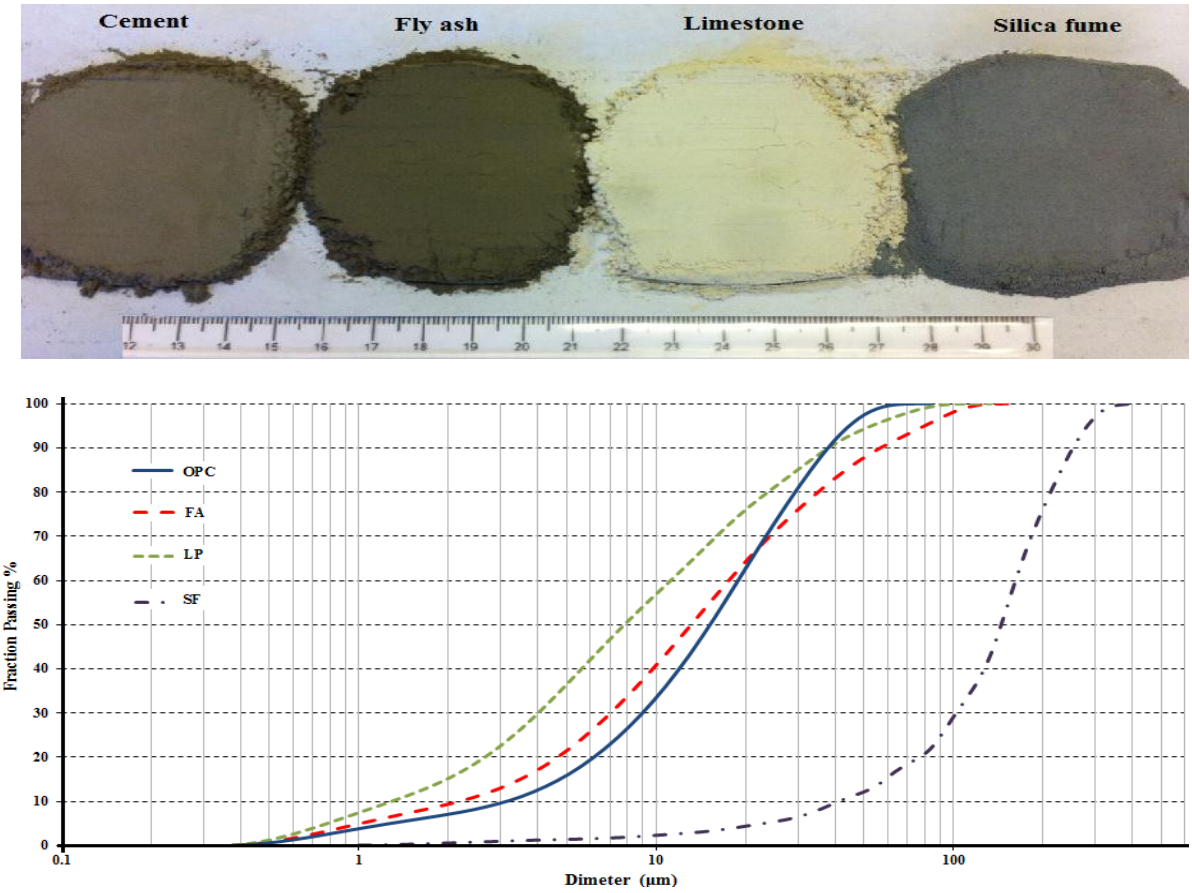

Figure 4-3 used cement, fillers and mineral admixtures and their particle size distribution

4.3 Microstructural and mineralogical characteristics of cement and fillers

4.3.1 Scanning electron microscopy images

For understanding the effect of the filler and mineral admixtures on the flow, strength, hydration and microstructural characteristics of SCC, it is important to identify the shape and the surface texture of these additions. Scanning electron microscopy images can provide suitable information about these characteristics. Images under SE mode at an accelerating voltage of 25kV were acquired with different magnifications for this purpose (See Section 3.3.6 for more details). Figs.4.4 to 4-6 shows selective SEM micrographs for cement, LP, FA and SF at high magnification. The SEM micrographs revealed that the surface texture of both the cement and LP particles are extremely rugous, the particles also being angular in shape. In contrast, the FA particles are spherically shaped with a very smooth surface texture. The SF showed two particle shapes, first: spheroid agglomerates with diameter in the range between 5 and 25 microns, second: very fine particle agglomerations with diameters in the range between approximately 0.05 and10 microns. These measurements were based on different micrographs at various magnifications. The two both exhibit a very rugous surface texture.

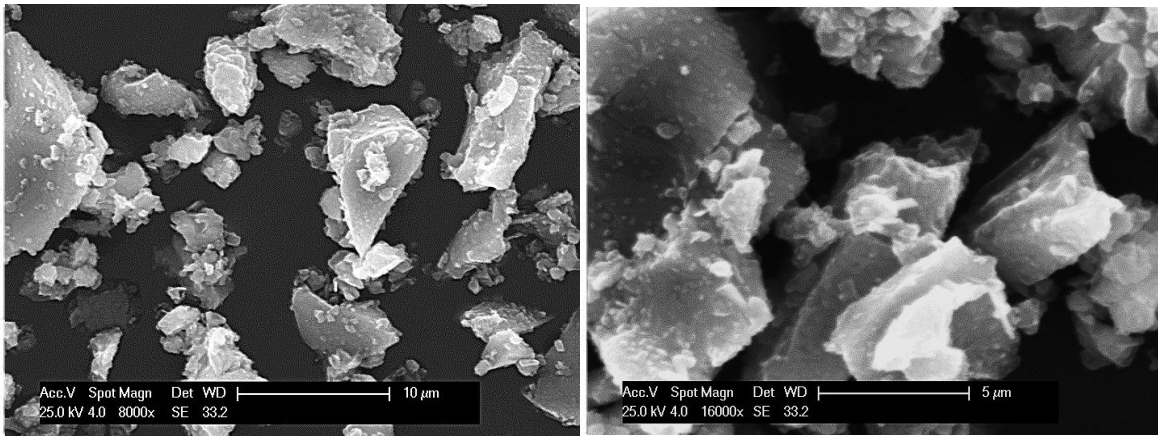

Figure 4-4 Cement particles shape and surface texture a) low magnification b) high magnification

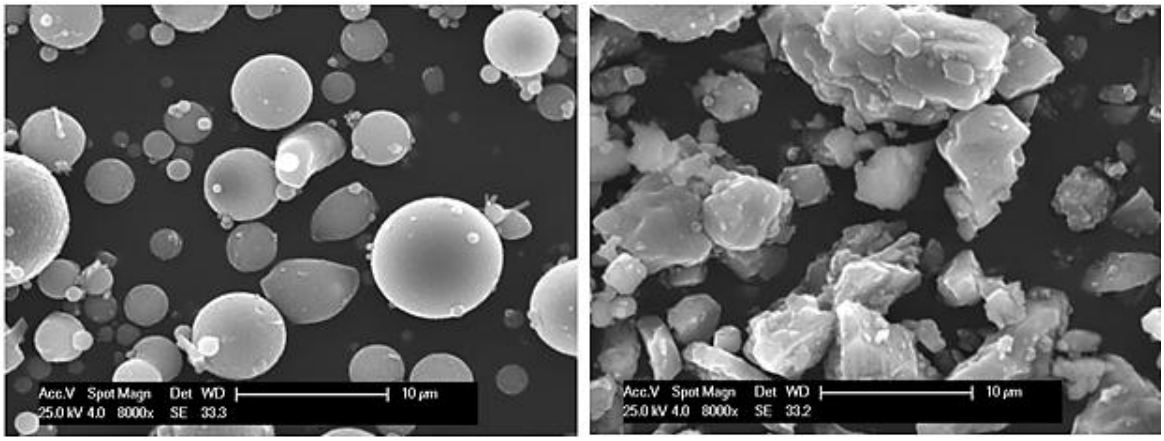

Figure 4-5 a) FA particles shape and surface texture b) LP particles shape and surface texture

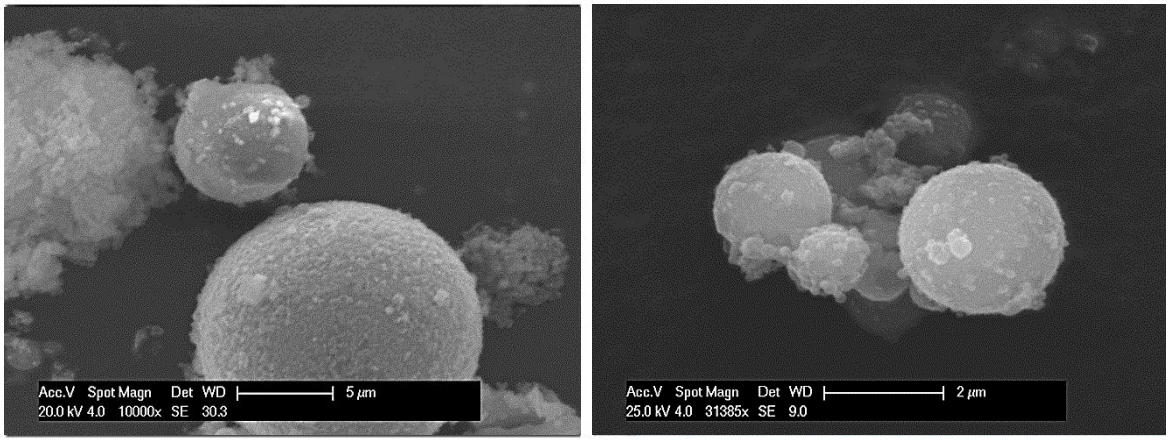

Figure 4-6 SF particles shape and surface texture a) low magnification b) high magnification

4.3.1 Mineralogical composition

The major compounds of the cement powder were identified from the XRD pattern (using the XRD technique described in Section 4.3.4.2) as C_3S, C_2S in the form of calcium silicate, C_3A in the form of calcium aluminum oxide, C_4AF in the form of the Brownmillerite phase as well as Anhydrate ($CaSO_4$) from the gypsum which is usually added to the cement to control the setting process. The XRD traces clearly indicated that the LP consisted of purely (100 %) calcite phase without any indication of the presence of amorphous material. On the other hand, the FA comprised a vitreous medium with two main crystalline phases: Quartz (SiO_2) and Mullite ($Al_6Si_2O_{13}$). However, the distinct hump between 20-34º (2-theta scale) indicated a presence of amorphous silica. The SF XRD pattern was completely different from those of LP and FA with very small peaks of Potassium Magnesium Silicate ($K_2MgSi_3O_8$) being detected. The absence of the

peaks in the XRD-spectra of the SF powder signifies a presence of very high proportion of amorphous silicon dioxide (SiO_2). Figs. 4-7 to 4-10 show the XRD spectra for the cement, filler and mineral admixture powders.

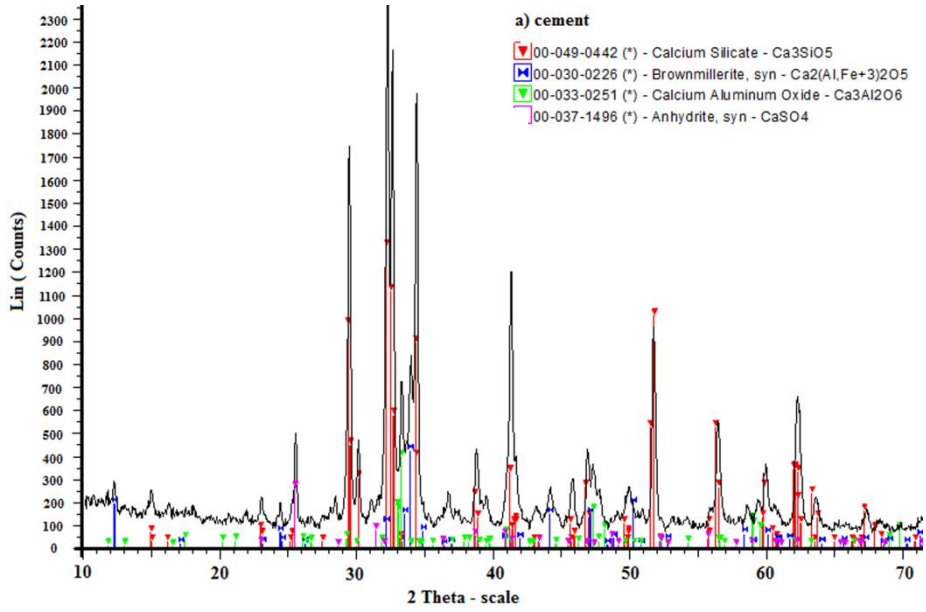

Figure 4-7 XRD spectra for cement powder

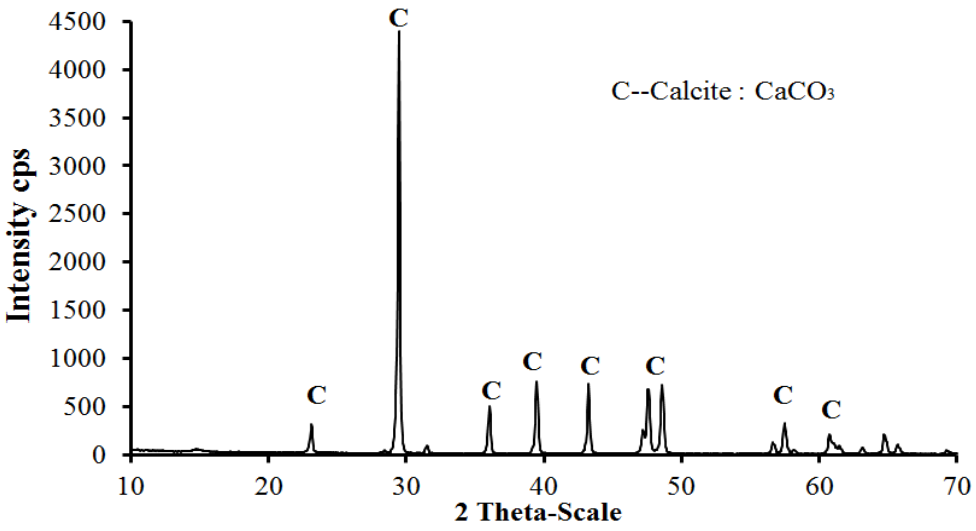

Figure 4-8 XRD spectra for LP powder

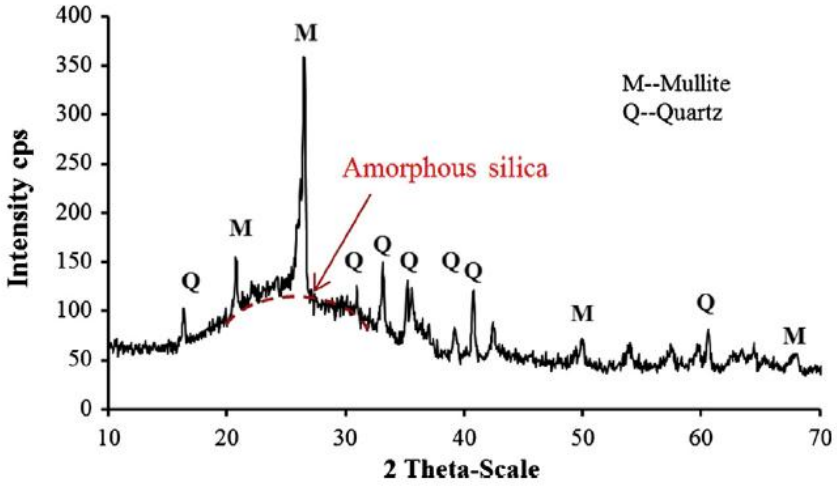

Figure 4-9 XRD spectra for FA powder

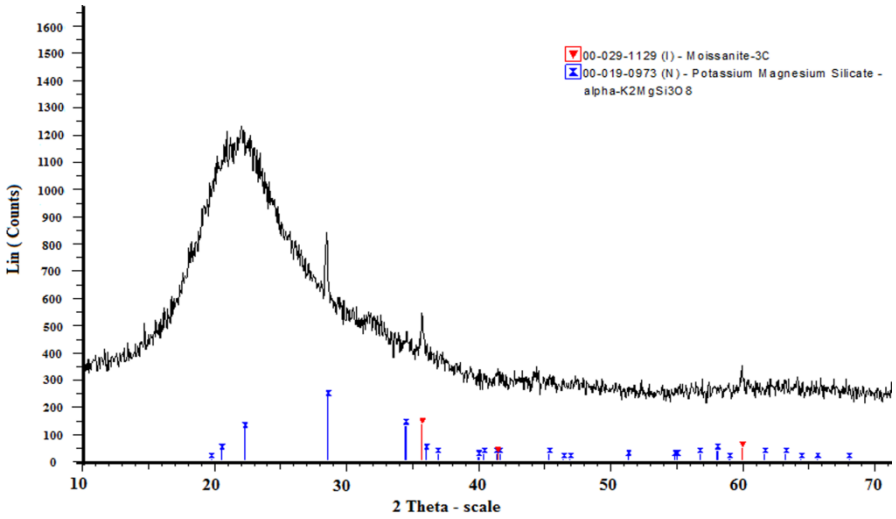

Figure 4-10 XRD spectra for SF powder

4.3 Experimental program and tests performed

4.3.1 Routine tests for fresh properties

SCC is a high flowable concrete which can totally fill the formwork under gravity action (a flowing or filling ability) even in the presence of high congestion of steel reinforcement (a passing ability) and compact totally under its own weight without segregation and bleeding (resistance to segregation) De Schutter et al. (2008).

Table 4-4 shows the classification of the SCC according to the selected tests as defined by European guide for SCC EFNARC (2005). Slump flow and T_{50} tests were used to

assess the flow ability whilst the J-ring and sieve segregation tests were conducted to ensure a good passing ability and segregation resistance respectively.

Table 4-4 Classification of (EFNARC, 2002) for the fresh properties

Class	Test type	Value	Description
SF1	Slump flow	550-650 mm	Low filling ability
SF2		660-750 mm	Good filling ability
SF3		760-850 mm	High filling ability
VS1	T_{50}	≤ 2 Sec.	Moderate to high flow rate
VS2	Slump flow	2-5 Sec.	Typical
BJ1	J-ring	≤ 10%	Low risk of blocking (Good)
BJ2		10-20 %	Moderate to high risk of blocking (Acceptable with limit obstacles)
SI1	Sieve Segregation	≤ 20	Adequate resistance
SI2		≤ 15	Good resistance

4.3.1.1 Slump, slump flow, T_{50} and Mini slump flow tests

The slump test is widely used to measure the workability of NVC mainly because this is a simple way to control the batch of fresh concrete. The sequence of the procedure is covered by ASTM C143 Mehta and Monteiro (2006). The Abrams cone in Fig. (4-12) is filled with three fresh concrete layers. Each layer is tamped 25 times using a steel rod of 16 mm Ø. The drop of the fresh concrete after the vertical removal of Abram's cone represents the slump of the mix. This test was performed to examine the slump of the NVC mixes. However, for SCC, the slump test was used in order to estimate the flowing ability by measuring the horizontal spread diameter of fresh SCC. The slump flow was used also to calculate the T_{50} which is the time required to obtain a horizontal diameter flow of 50 cm. as recommended by the European guide of SCC EFNARC (2002). According to this guide, this test can be used also to give an indication of the resistance to segregation by visual observation of the aggregate particles in the centre and the edges of the spread concrete. If there is no agglomeration of the aggregate in the centre of the spread concrete and it is homogenously distributed, the SCC-mix has an acceptable resistance to segregation. Figs. 4-11 and 4-12 show the main concepts of the slump test for NVC, slump flow test for SCC and mini flow slump for SCC mortars.

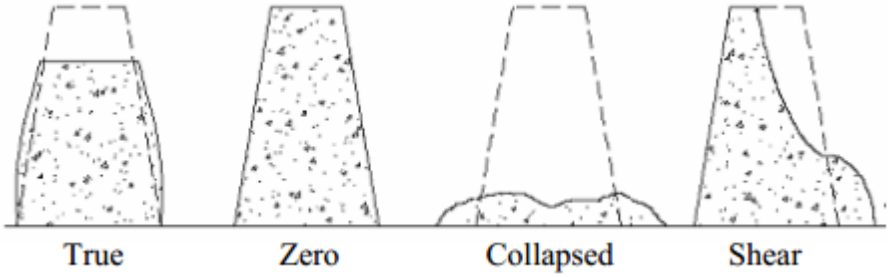

Figure 4-11 **Four types of slump for NVC according to ASTM C 143**

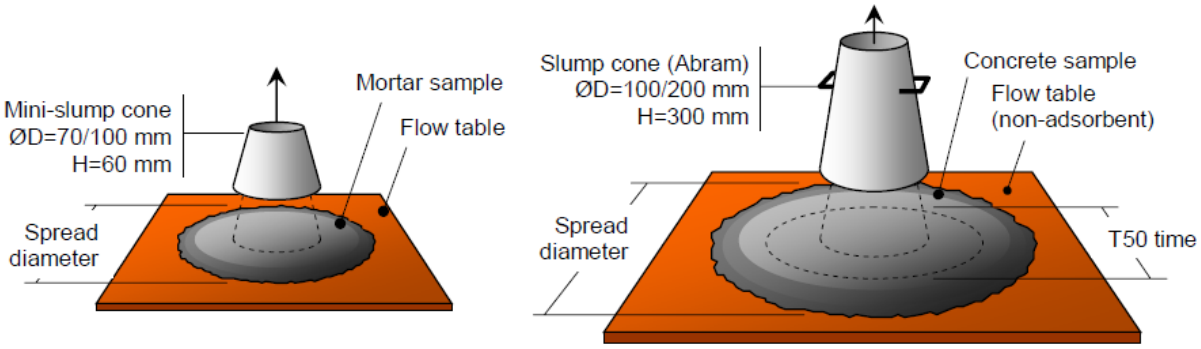

Figure 4-12 **Mini slump flow and slump flow tests for SCC** Esping (2007)

4.3.1.2 J-ring test (passing ability)

Determination of passing ability of a SCC mix is possible using the J-ring test as shown in Fig. 4-13. After removing the slump cone, the passing ability of the fresh mix was determined as a blocking step (BJ value), using Eq. 3-1, the difference between the average heights of the fresh concrete outside the restrictions of the J ring (four readings taken 90º from each other: Δhx1, Δhx2, Δhy1 and Δhy2) and the height at the centre of the ring Δh◦ (De Schutter et al., 2008).

$$BJ = \frac{\Delta hx1+\Delta hx2+\Delta hx3+\Delta hx4}{4} - \Delta h\circ \quad \text{..... Eq. 4-1}$$

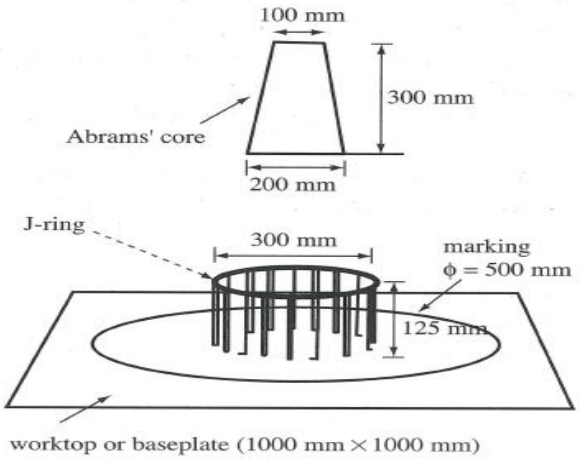

Figure 4-13 **Schematic diagram of J-ring setup**

4.3.1.3 Segregation index (resistance to segregation)

The sieve segregation test was used to assess the segregation resistance of the SCC mixtures (Fig. 4-14). It consisted of measuring the fraction of the SCC mortar that can pass a 5 mm sieve. When the mixing was completed, 10-12 L of fresh concrete is poured into a plastic bucket for 15 minutes. Then, around 5 kg is poured onto the sieve from a height of approximately 50cm. Two minutes later, the weight of the cement mortar that passed through the sieve is divided by the weight of the poured quantity, and calculated as a segregation index (SI) using Eq. 4-2 EFNARC (2002).

$$SI = \frac{W_{pass}}{W_{Total}} \% \quad \text{..... Eq. 4-2}$$

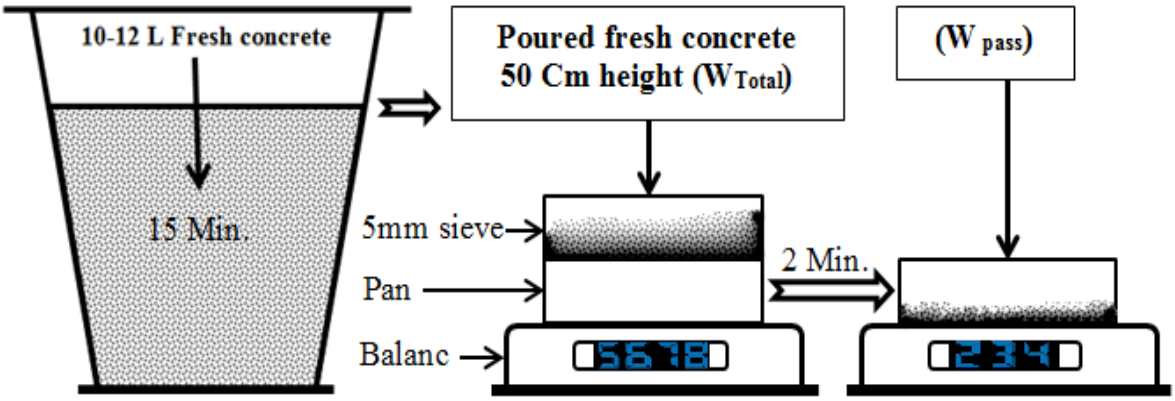

Figure 4-14 **Schematic diagram of sieve segregation test (SI index)**

4.3.2 Compressive strength and density tests

100 mm cubes were used for the compressive strength test as shown in Fig.4-15a .The test was conducting according to BS EN 12390–3 (2002) using a Hydraulic Test Machine (Bracknell, UK) as shown in Fig.4-15 b. The listed values represent an average of three readings for each age and the test was performed at 7, 14, and 28 days. The concrete bulk density was calculated using the same specimens used for the compressive strength test according to Eq. 4-3.

$$\rho = \frac{W_{air}}{W_{air} - W_{water}} \quad \text{..... Eq. 4-3}$$

Figure 4-15 a) Compressive strength cubes b) Compressive strength test machine

4.3.3 Vacuumed Saturated Porosity

The determination of the total porosity using the normal vacuum method is sensitive to the replacements of cement by cementitious materials and it can be calculated using Eq.3-4 (Mohammad Iqbal Khan,2004)**.** 60×10±5 mm mortar disks were vacuumed using 100 mb for 3 hours followed by 2 hours vacuumed with saturated $Ca(OH)_2$ solution and left to the second day (Fig. 4-16). This was done to ensure a full saturation of all the pores in the tested mortar specimens.

$$P = \frac{B-A}{B-C}\ x\ 100\% \text{..... Eq. 4-4}$$

P: Porosity, *B*: Saturated surface dry weight, *A*= Oven-dry weight, *C*= Saturated submerged weight

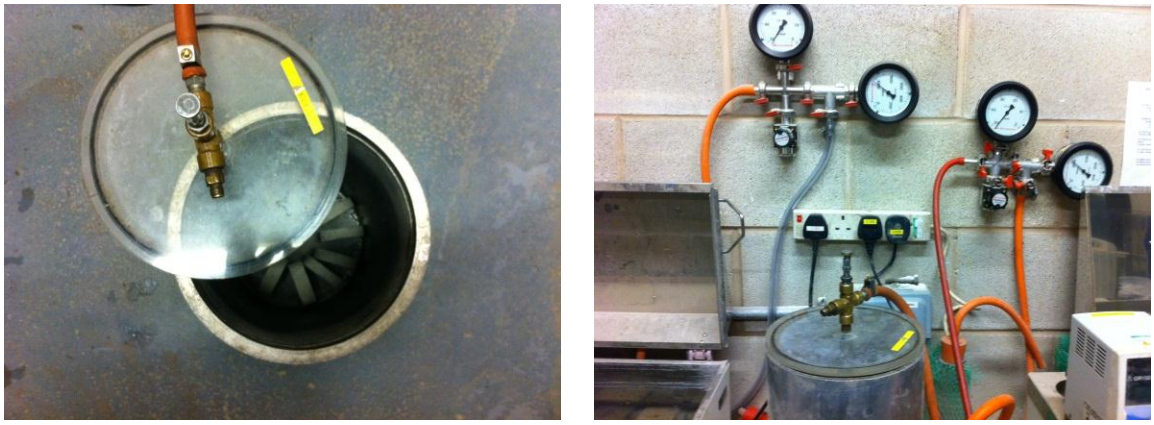

Figure 4-16 a) specimens and the vacuum chamber b) vacuum set up

4.3.4 Chemical composition tests

4.3.4.1 Thermo-gravimetric analysis (TGA)

TGA is a well-established method to study the hydration of normal and blended cementitious materials. The typical outputs of this technique are both TG (weight loss) and DTG (derivative of weight loss) curves for a reference and blended cement with SF are shown in Figs. 4-17 and 4-18 respectively (Loukili et al., 1999, Almeida and Sichieri, 2006).

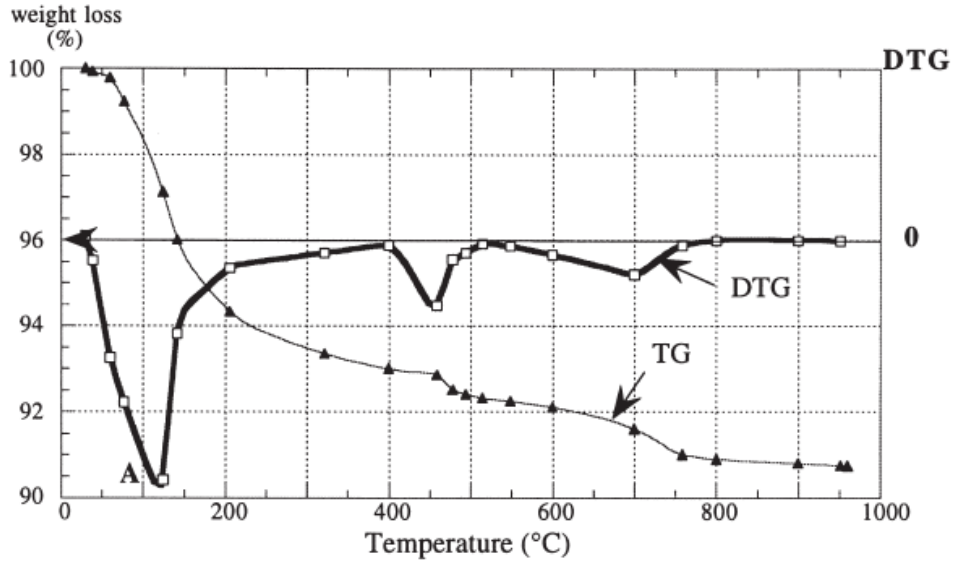

Figure 4-17 Sample TG and DTG curves for plain cement paste

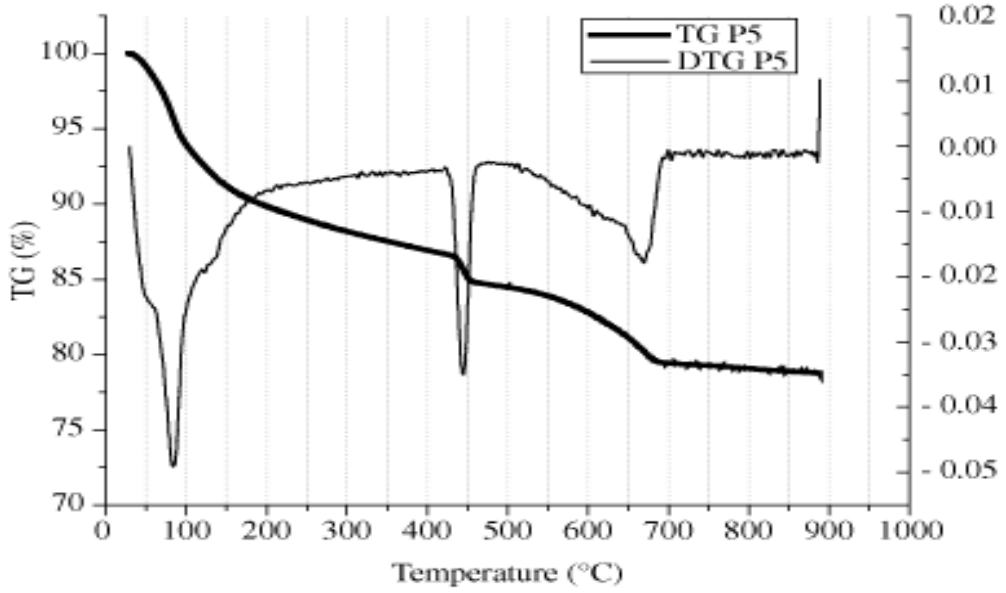

Figure 4-18 Sample TG and DTG curves for blended cement paste with SF

Generally, Almeida and Sichieri (2006) reported four zones for these curves:

- 25-123.3 °C: dehydration of pore water;
- 123.3-420 °C: dehydration of calcium silicate hydrates;
- 420-480 °C: dehydroxylation of calcium hydroxide;

$Ca(OH)_2 \longrightarrow CaO + H_2O$ **…… Eq. 4-5** [de-hydroxylation of calcium hydroxide]

- 480-730 °C: calcination of $CaCO_3$.

$CaCO_3 \longrightarrow CaO + CO_2$ **…… Eq. 4-6** [de-carbonation of calcium carbonate]

The percentages of CH% due to de-hydroxylation of calcium hydroxide and de-carbonation of calcium carbonate were calculated using powder samples weighing about 25-50 mg. The powders were taken from the middle part of 70 mm mortars cube and then passed through the 75µm sieve. This was conducted so that the powders can be as representative as possible of the mortars. A Perkin Elmer thermo-gravimetric analyzer was used as shown in Fig. 4-19.

Firstly, small ceramic pans having crooked holders were cleaned using acetone and flammable heat in order to remove any deposits from the previous experiments. The empty cleaned pans were loaded to a thermo-gravimetric analyzer holder which can carry number of samples at the same time. Secondly, the ceramic pans were weighed automatically by the thermo-gravimetric analyzer's microbalance at a precision of 0.1 µg. After that, the powder samples were loaded to the ceramic pans and the analyzer reweighed the samples again. The difference between the two weights which represents the weight of the powder sample only, was provided to the software in the control computer. Finally, the powder samples were transferred mechanically by the analyzer to a small vertical furnace to perform the experiment Fig. 4-19.

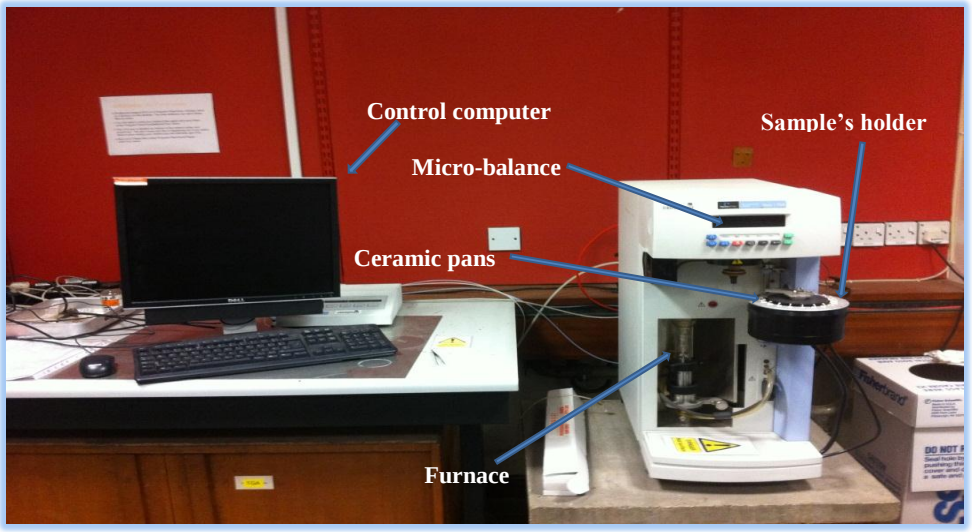

Figure 4-19 Perkin Elmer thermo-gravimetric analyzer

The software in the control computer was encoded to heat up the powder samples from 30 to 950˚C .The rate of heating were 50 ˚C per minute up to 300˚C and 20˚C per minute up to 950˚C. It has been already reported that weight loss of the cementitious materials powders between (30- 400˚C) characterizes the evaporation of the absorbed and gel waters only Ye et al. (2007). Therefore, the high rate of heating up to 300 (50 ˚C per minute) was adopted to shorten the test period.

The second and the third peaks of TG and DTG curves between 420-550 °C and 600-780 °C were used to calculate the percentages of (CH%) loss due to the de-hydroxylation of $Ca(OH)_2$ and due to the de carbonation of $CaCO_3$ respectively using Eqs. 4-7 and 4-8 respectively Borges et al. (2010):

CH% de-hydroxylation =74/18 *A ……. Eq. 4-7

CH % de-carbonation =74/44* B ……. Eq. 4-8

where: 74, 18 and 44 are the molecular weights of CH, H_2O and CO_2 respectively, **A** is the area under the DTG curve corresponding to the total mass lost due to the de-hydroxylation of calcium hydroxide, **B** is the area under the DTG curve representing the total mass lost due to the de-carbonation reaction. **A** and **B** were calculated as an average values acquired from the TG and TGA curves for each peak. An example of calculating **A** (CH % loss due to dehydration) for the R-SCC powder using (Pyris software 2009 PerkinElmer, Inc Version 10.1) is shown in Fig. 4-20.

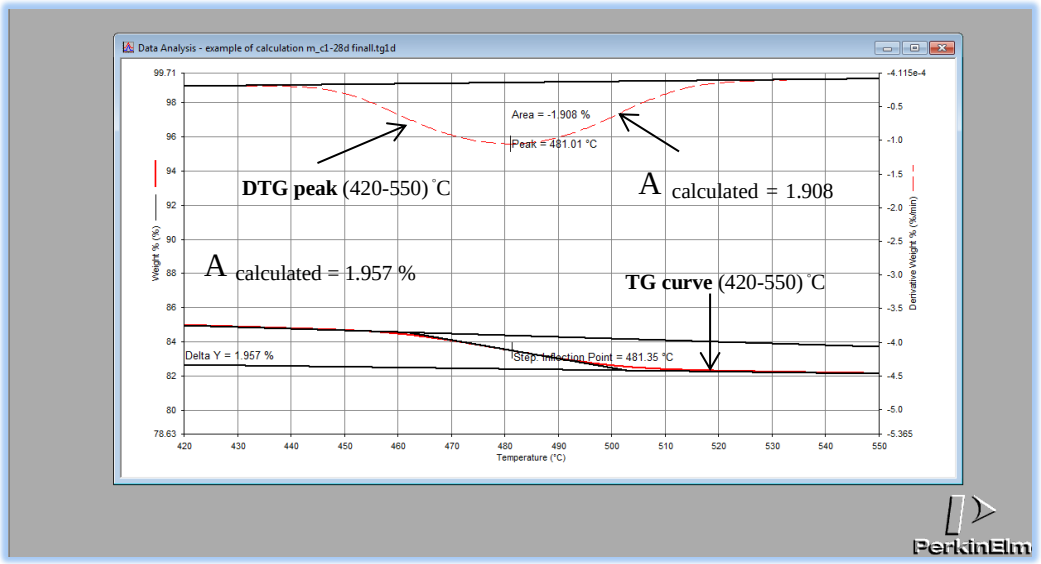

Figure 4-20 Example of calculating the area under TG and TDG (CH% loss) between 420 to 550 ˚C

4.3.4.2 X-ray diffraction analysis (mineralogy)

X-ray diffraction analysis was used to examine the mineralogical patterns and to detect the availability of the amorphous or non-crystalline solids material of the cement, fillers and mineral additions. For this purpose, XRD is considered one of the most suited techniques for identifying the crystalline phases for the powders and cementitious materials. However, the presence of amorphous material changes certain peaks in the detectable diffraction line positions and also in the sharp peaks. The distinct humps in the XRD spectra give an indication of the availability of these materials. Each atom in the orientated structure of the crystals yields detectable diffraction lines when it exposed to X-ray waves (Fig. 4-21). Bragg's Equation (Eq. 4-9) simulates the detectable diffraction lines and enables identification of the crystal structure Rendell et al. (2002).

$$2d\,Sin\,\theta = n\,\lambda \quad \text{..... Eq. 4-9}$$

d :the distance between lattice planes in the crystal

θ: is the incident/diffracted angle

n: is an integer

λ: is the wavelength of the scattered X-ray wave

\

Parts of hardened SCC specimens in section 4.3.6.1 were ground into a powder and passed through a 75µm sieve for XRD examination. The powder samples were positioned and flattened carefully in the sample holder of the XRD machine. A scanning speed of 2° per minute and a step of 0.05° were used in the range of 10 and 90° using a

Bruker –AXS D8 Advance XRD equipment as shown in Fig.4-21. This technique was also used to examine the crystalline phases of the concrete especially, the $Ca(OH)_2$. The chemical composition was evaluated before carbonation on the same powders that were used for TGA analysis whereas the kinetic of the carbonation reactions were identified after carbonation for the sustainable SCC.

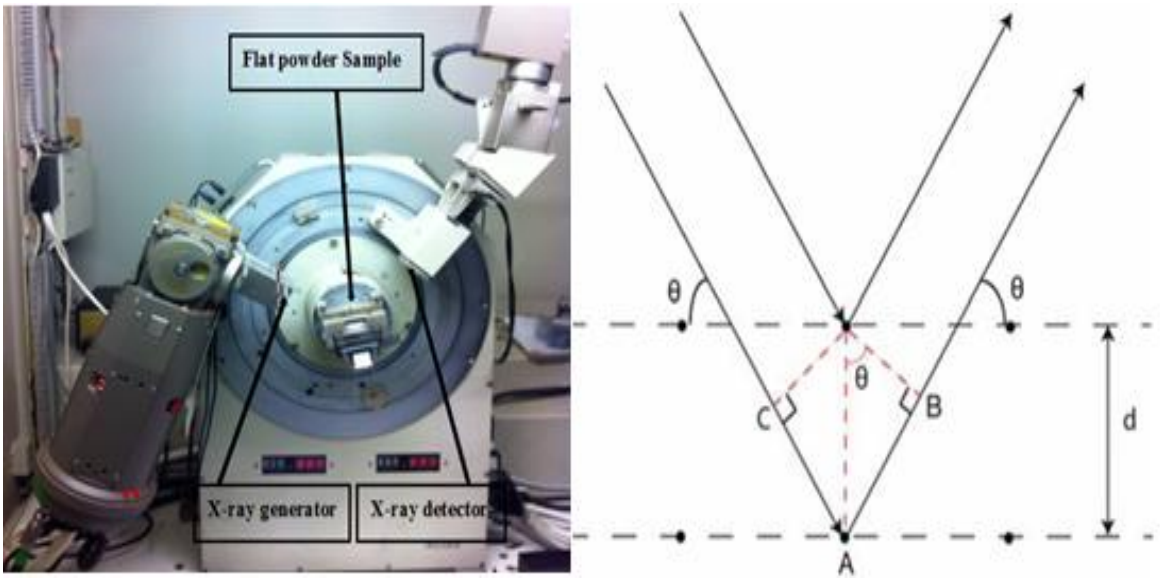

Figure 4-21 Used XRD Equipment and Schematic of X-ray diffraction.
Dots represent atoms in a lattice separated by a distance d, and arrowed lines represent X-ray beams reflecting off the atoms at angle θ Lawrence (2006)

4.3.5 MIP test (Pore structure analysis)

To date, various methods have been introduced and developed to examine the pore structure of the cementitious materials. MIP is an effective, simple and widely used method for the analysis of the pore structure system of cementitious material in comparison with the other techniques like image analysis, vapor sorption, nitrogen adsorption and thermoporometry Erdem (2012). Although there is some concern of the applicability of the ink-bottle assumption of the pore structure, different parameters such as pore size distribution, total pore volume, average pore diameter and the critical pore diameter (CPD) may be determined to characterize the internal pore structure. CPD is defined as the smallest pore diameter that can connect different pore's group to each other in the pore network of the cementitious materials and is represented by the inflection point in the derivative of the cumulative intrusion versus pore diameter curves as shown in Fig. 4-22.

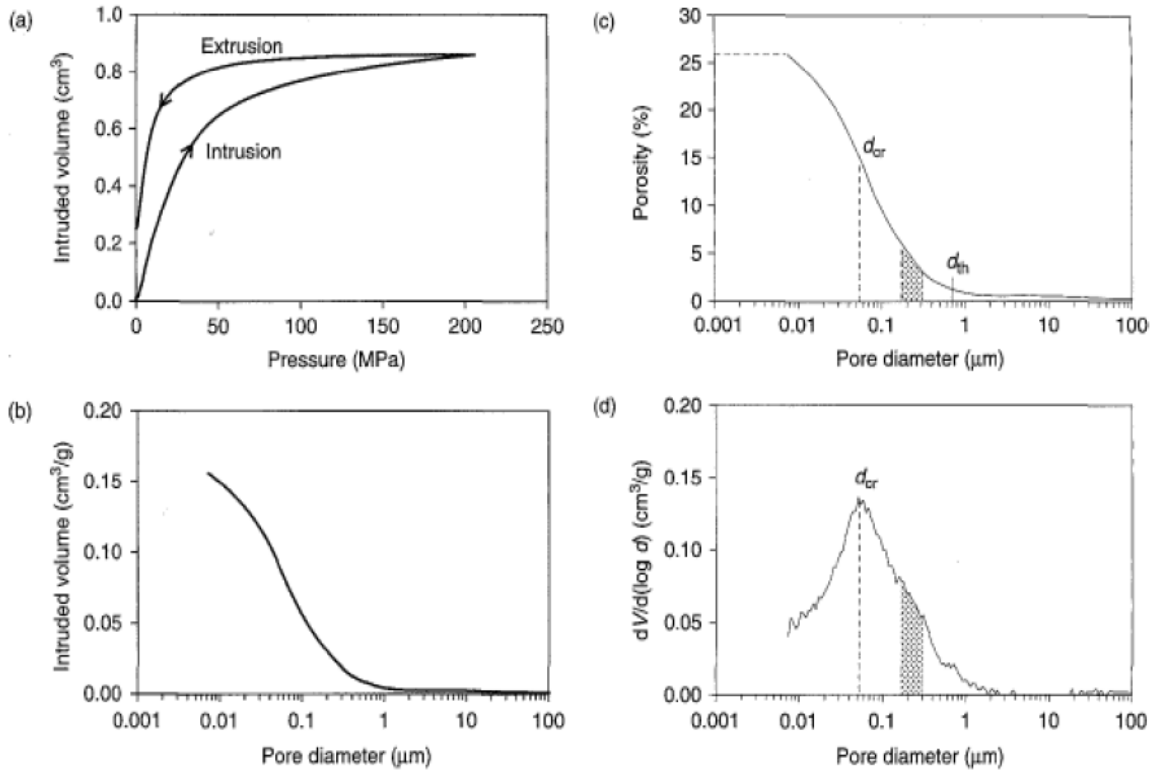

Figure 4-22 **Plots used most frequently in MIP to report experimental results (a) Pressurization curve; (b) cumulative intruded volume curve; (c) cumulative pore size distribution; (d) differential pore size distribution Ying (2013).**

Since one of the important aims of the present study is to examine:

a) The effect of the filler and mineral admixture on the internal pore structure of SCC,

b) The structure-property relationships with the chloride and carbonation propagations

c) And the impact of carbonation on the pore structure at different scales.

The MIP technique was selected to examine the above mentioned parameters before and after complete carbonation. Inaccessible or isolated pores cannot be identified because the mercury can only diffuse through the continuous pore system. However, Roy et al. (1993) claimed that these pores do not contribute effectively in the transport properties such as permeability of water and diffusivity of dissolved species. The micro porosity results detected by the MIP were evaluated and compared with macro scale porosity obtained from the vacuumed saturated test as explained in Section 4.3.3. The selection of this technique is based on the following reasons (Boel et al. ,2007, Cook and Hover 1999, Erdem, 2012):

- The results obtained from this technique could be used successfully to compare the microstructural characteristics of the internal structure of the different cement -based materials such as porosity, critical and average pore diameters and pores size distribution.
- It was successfully performed for both normal and SCC pore characterization.
- In addition, it gives appropriate information about the internal structure and the percolation of cementitious materials.

Generally, the whole MIP test comprises two main actions:

a) The intrusion of the mercury inside the pores of the specimen due to the increase of the pressure during the high pressure test.

b)The extraction process resulting from the drop of the pressure after reaching the maximum value (Fig. 4-22a). When the mercury intrusion pressure is known, the pore radius can be calculated using Washburn's equation (Eq. 4-10):

$$P = \frac{-2\gamma \cos\theta}{r} \quad \text{..... Eq. 4-10}$$

r= Pore radius

P= Intrusion pressure (MPa)

γ= Mercury surface tension (480.10-3 N/m)

θ= Contact angle (140º)

Small pieces weighing (1-3) were obtained from the middle part of 70 mm mortar specimens (near the core block that was used for preparing the flat polished sections as described in Section 4.3.6.1). They were cut by a very slow speed saw and used for MIP test. This was done to reduce the micro cracks which might occur due to the preparation process. In order to stop the hydration, the specimens were dried at 100 ˚C for approximately 24 h (until a constant weight was achieved using a high sensitivity balance) and then they were kept in sealed containers until the day of the test. A Micrometrics Autopore IV mercury porosimeter which can detect the pores as small as 7 nanometers with a maximum pressure of 414 MPa was used as shown in Fig 4-23. The test was conducted on an average of 3 water cured-samples at 28 days and 56 days after mixing and also conducted after complete carbonation using the same preparation method (See Chapters 5 and 6).

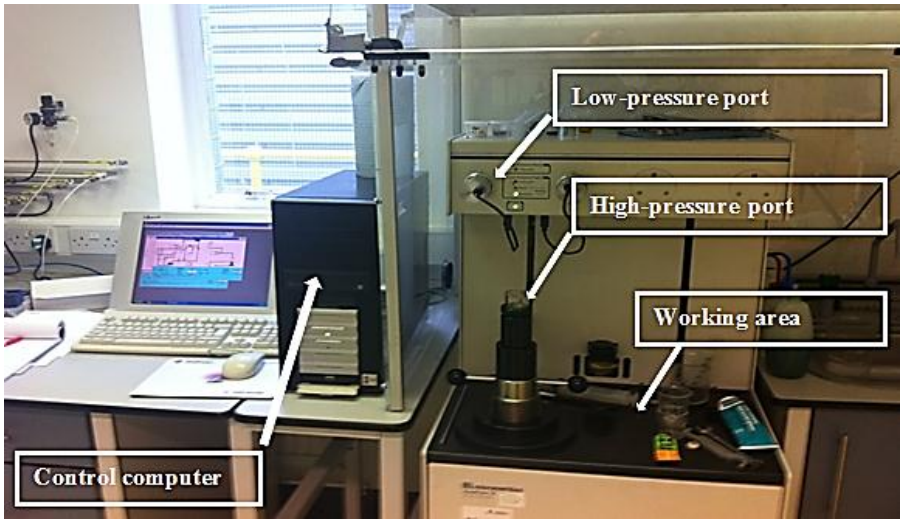

Fig. 4-23 **Autopore IV mercury porosimeter**

Prior to the test, the specimen was removed from the sealed container. After that, it was put into a standardized penetrometer. The total weight of the specimen and the penetrometer was taken. Then, the penetrometer with the specimen was loaded to the low-pressure port. At this stage, the software in the control computer was provided with the required information such as sample weight, penetrometer type, pressure and the density of the mercury at a temperature measured at the time of the test. When the low pressure cycle was completed, the penetrometer was filled with the mercury. The total weight of the filled penetrometer with the sample was taken and then it was loaded to the high pressure port and the control software was provided with the penetrometer weight only. When the high pressure cycle is completed, the system provides a report which can be saved in a spreadsheet excel sheet for data analysis.

4.3.6 Scanning Electron Microscopy (SEM)

Optical and electron microscopy are the two principle techniques which have been successfully used for assessing the microstructure of the cementitious materials. Optical microscopy has been broadly used for the purpose of evaluating the concrete and cement clinker materials. The use of normal light for the image formation in this technique gives lower resolution and depth of focus of the formed images. Thus, the use of this technique has become less popular as compared with the second one (Hemavibool, 2007).

Nowadays, scanning electron microscopy (SEM) has become one of the most widely used techniques for the purpose of identifying and analyzing the microstructure of the

concrete/mortars and cementitious material. For the cement paste phase, this technique can offer significant information about: degree of hydration, formation and distribution of the main hydration products and pores arrangement, homogeneity of cement pastes, interaction between the hydration phases. For the composite material such as cement matrices with aggregates (ITZ), the adhesion and the local features of the paste-aggregates interface could be quantitatively analyzed.

Understanding the principles of SEM work is extremely beneficial for evaluating and interpreting the data obtained. The scanning process consists of speeding up electrons, which are originally generated from the electron gun in the microscope, by using an acceleration voltage, and then focusing them (in an electron beam) to a spot on the specimen surface. The focus can be achieved with aid of deflection coils after the electrons beam has been passed through two condenser lens for voltage acceleration purposes as shown in Fig. 4-24 (Suzuki, 2002).

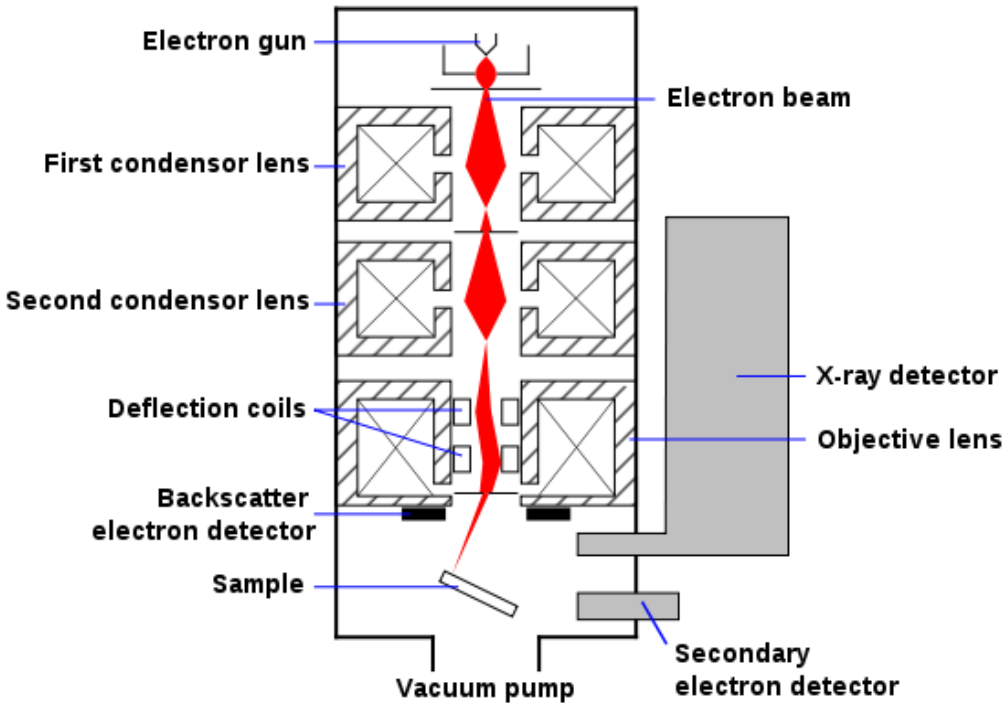

Figure 4- 24 Diagram of Scanning Electron Microscope process

In general, the interaction between the scanned specimen surface and the incident beams (electron beams) is of two types: elastic and inelastic electron scattering. In the first process, the electrons' direction might be changed and scattered by the atoms in the

specimen with no loss of their energy whilst the electrons in inelastic process suffering from energy loss. The whole interaction process generates different types of photons and scattered electrons as shown in Fig. 4-25a: X-rays and luminescence photons, secondary, backscattered, auger and transmitted electrons if a thin specimen section is used Hemavibool (2007).

Generally, the secondary electron (SE) has less energy due to the elastic scattering process as compared with the back-scattered one (BSE) and could be detected from a signal generated near the surface of the sample. In contrast, the BSE could be deduced from a deeper signal position. The high energy of the back scattered electrons might be responsible for the low resolution of the BSE image as compared to the high resolution of the SE images (Scrivener,2004, Suzuki,2002). However, quantitative analyses could be obtained from the BSE images using flat polished sections and these are more useful than the fractured or sawn surface to observe the microstructure morphology only Scrivener (2004).

Fig. 4-25b shows the signal generation position of SE, BSE and X-ray photons within a volume of tear drop shape (excitation volume) which mainly depends on the accelerating voltage and the average specimen atomic number. The energy of X-rays created in a signal generation across the tear drop shape (excitation volume) can be detected and analyzed using energy dispersive or wavelength dispersive detectors (EDS or EDX analyzer). Such information about the chemical composition of the hydrated phases of cement can be obtained in a specified position. For the cementitious materials, this volume (excitation volume) is an about 1-2 μm thick through the sample which is larger than the volume of various hydrate phases. Thus, the analysis will derive information from more than one hydration phase (combined phases) Scrivener (2004).

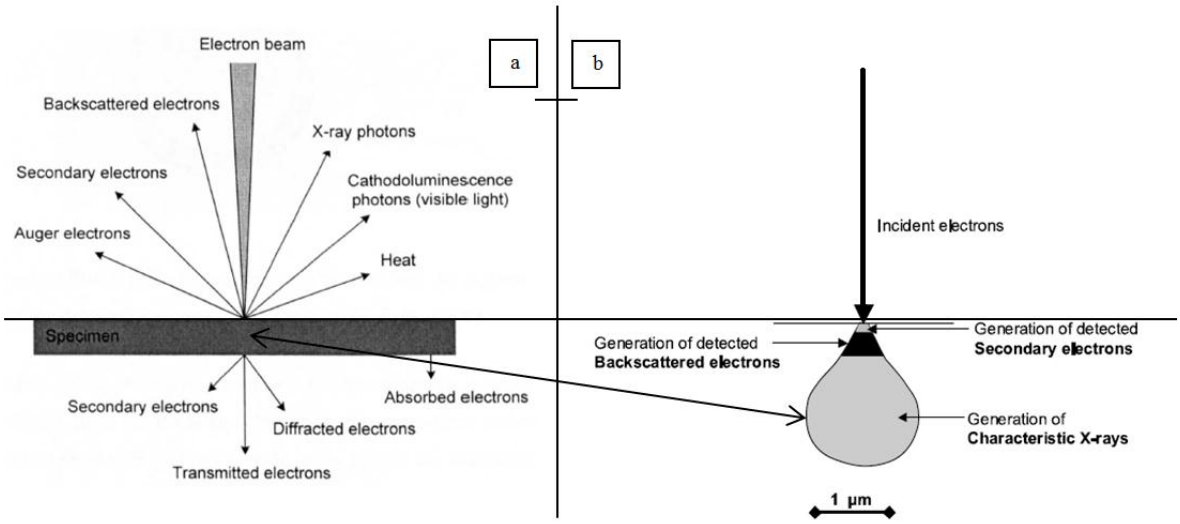

Figure 4-25 a) Interaction process Hemavibool (2007) b) Excitation volume Scrivener (2004)

In the present investigation a Philips XL 30 SEM fitted with an Oxford Instruments INCA model spectrometer for energy-dispersive X-ray (EDX) analysis as shown in **Fig.4-26** was used. It was utilized for the purpose of characterizing microstructural features of cement and fillers used as well as for the morphology observation and the quantitative microstructural analysis of the ITZ's features.

Figure 4-26 Philips XL 30 SEM fitted with an Oxford Instruments INCA model spectrometer for energy-dispersive X-ray (EDX) analysis (Scanning Electron Microscope)

4.3.6.1 Preparation of flat polished specimens (carbon coating)

In order to obtain a suitable flat section and high quality of BSE images, the following stages have been considered for this purpose Kjellsen et al. (2003):

•**Preliminary stage:**

Approximately (20×20) mm specimens were cut from a middle slice (15 mm in thick) of a 70mm cube using a diamond saw. Layers of three millimeters thick were cut by means of a low speed saw in order to avoid the distortion caused by the diamond saw. The surface of the specimens then exposed to initial polishing using a fine abrasive grinding paper (Premium SiC) to ensure a smooth and plane surface.

•**Epoxy impregnation:**

Vacuum impregnation with epoxy is an important step in the preparation of the flat polished specimens for SEM and it plays a key role in the filling of the pores prior to mechanical grinding and polishing. Epoxy resin is first prepared by mixing 30 ml with 5 ml accelerating agent to ensure the hardening of the specimens on the second day. The low viscosity epoxy is then poured into SEM moulds, covering the specimens. The moulds were then vacuumed (30 mbar) for approximately 10 minutes to ensure the intrusion of the epoxy through the voids.

•**Grinding:**

In order to eliminate any distortion and any micro cracks on the surface of the specimens, mechanical preparation followed the vacuum impregnation stage. For this stage, the specimens were first mechanically ground with 200, 400, 800 and 1200 grit abrasive papers. The grinding process was performed to a depth of 30 micron. This value was considered as a suitable depth to remove most of the micro cracks resulting from the cutting process. At this stage, all the specimens were checked in an optical microscope to ensure a flat surface with no visually detectable micro cracks.

•**Polishing, Coating and Storing:**

Polishing was conducted in three stages for approximately 3 minutes using 6, 3 and 1 μm diamond paste. At each stage, the specimens were cleaned by ethanol in order to remove any grit. However, it was not being able to eliminate all the micro-cracks due to the polishing process and the BSE images were acquired avoiding any remaining micro cracks as much as possible. Most studies of concrete microstructure in that used BSE and

x-ray modes need to coat the polishing surface with a thin film of a conductive material. This is to prevent the gathering of electrostatic charge at the sample surface during the scanning process by the electron beam. Carbon coating was adopted for acquiring the BSE and performing the EDX analysis while Platinum coating was applied for detecting the morphology of the matrices and the internal microstructure on a fracture surface. After coating, the specimens were stored in a vacuum chamber until capturing the SEM images.

4.3.6.2 Fractured surface specimens (Platinum-coated)

The microstructure and morphology of the mixtures before and after full carbonation were examined on small fractured surfaces using the secondary electron mode with various magnifications. These samples were fixed on small SEM stubs and exposed to high vacuum, and then coated with Platinum before capturing the images (Fig.4-27 E). Fig. 4-27 shows the preparation steps of the two types of the samples used for SEM examinations. The Platinum coating was also adopted for the purpose of identifying the shape and surface features of the cement and fillers (See Section 4.3.1).

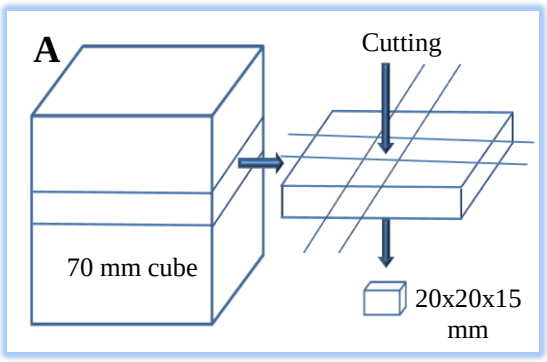

A: Diamond saw cutting B: Slow speed saw

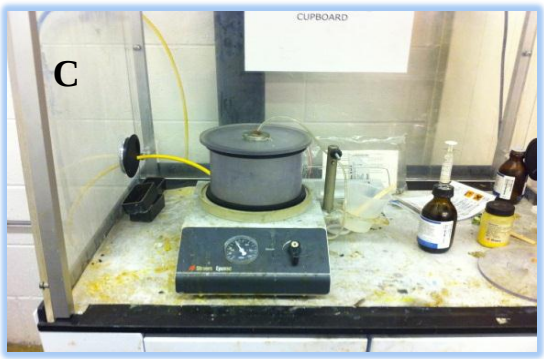

C: Vacuum impregnation with epoxy D: specimens and molds

E: Grinding with grit abrasive papers F: Polishing with diamond paste

G: Coating with platinum H: Coating with carbon

Figure 4- 27 Preparation steps of the samples for SEM examination

4.4 Mix design

4.4.1 Mix design for SCC and mortars

Various methods have been proposed for the design of SCC, each with its own advantages and disadvantages (De Schutter et al., 2008). At the moment, there is no agreement on the perfect mix design method. The use of one of these mix design methods should minimize the number of trial mixes required, and the number of the fresh property tests needed to obtain the required flow properties. Felekoğlu et al. (2007) concluded that the trial and error method could be used to produce appropriate SCC mixes according to engineering experience of the types and properties of the materials used. In addition, they suggested water to powder ratios of 0.84-1.07 by volume to avoid segregation and blocking. De Schutter and Audenaert (2007) gave the key parameters that should be taken into account to achieve a successful SCC:

- The volume of coarse aggregate should be between 30-34 % of the total volume of the SCC, which is less markedly than 40-45 % for NVC.
- The water to binder ratio by volume is recommended as 0.8-1.2 for SCC without viscosity agent.
- The water content is between 155-175 kg/m^3 for SCC without viscosity agent while it is about 200 kg/m^3 with it.
- The ratio of the paste volume to the total volume of concrete is from 34% to 40% which is very important to obtain the high flow ability.
- The percentage of the volume of fine aggregate to the mortar volume is 40-50% in order to reduce the segregation and obtain the stability for the mix. They limited the values of self-compacting concrete constituents as in **Table 4-5**:

Table 4-5 self-compacting concrete constituents' limits

Material	Coarse agg.	Fine agg.	Powder materials	Water
Content kg/m^3	750- 920	710-900	450-600	150-200 kg/m^3

Taking into the account all the above limitations, fixed amounts of water and sand (bearing in mind that 60 % of SP is water) have been considered for the design of the SCC-mixtures with a minimum binder content requirements of 450 kg/m^3. The

replacement of cement by filler or filler plus mineral admixture was fixed to about 33 % as shown in Table 4-6 and the required fresh properties were optimized using trial mixes. The flow chart (Fig 4-28) shows the adopted mix design approach. This approach was implemented in order to decrease the number of the trial mixes. Unsuccessful fresh mixes, as assessed by slump flow, were neglected for the next stage.

Table 4-6 Mix proportion and (calculated parameters*) to ensure self-concrete compatibility

Mix type	R-SCC	LP-SCC	FA -SCC	FA-SF-SCC
Cement (kg/m^3)	450	300	300	300
Coarse agg. (kg/m^3)	875	860	825	825
Fine aggregate (kg/m^3)	900			
Water (kg/m^3)	180			
Fly ash (kg/m^3)	---	---	150	120
Limestone (kg/m^3)	---	150	---	---
Silica fume (kg/m^3)	---	---	---	30
water/powder by	1.26	1.2	1.1	1.1
$V_{coarse\ agg.}/V_{total}$*	33.6	33.1	31.7	31.7
$V_{fine\ agg.}/V_{mortar}$*	51.2	50.7	49.7	49.7
$V_{cement\ paste}/V_{total}$*	32.3	33.0	34.3	34 .3

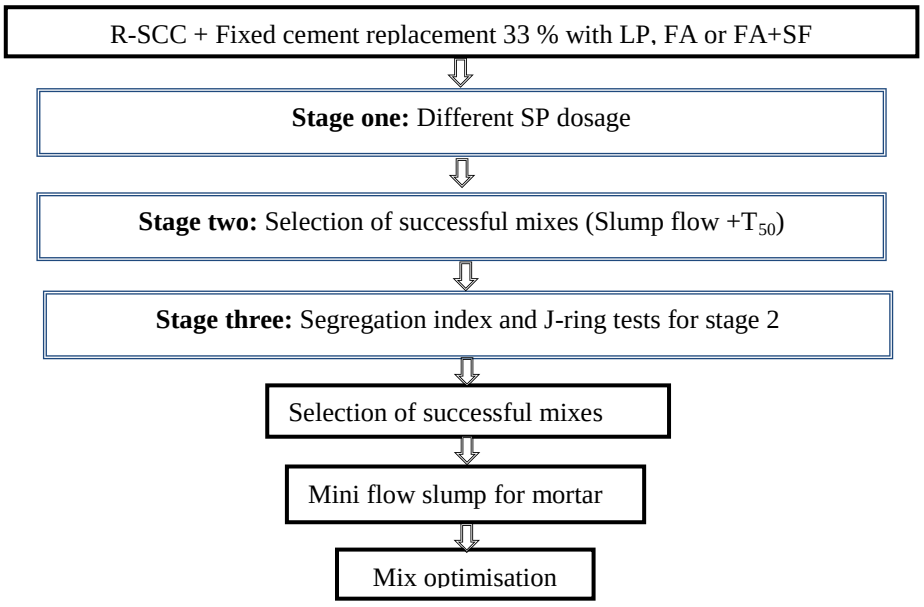

Figure 4-28 SCC Mix design approach

For the SCC mortars, the water quantity was reduced by about 0.8% (coarse aggregate absorption value) in order to ensure the same water content in the matrix. In this way, the same effective water to binder ratio was maintained for all tested fresh and hardened mortars.

4.4.2 Mix design and selection of NVC mix

For the transport properties such as carbonation and chloride penetration correlating to the mix design, it seems that the comparison between the full SCC and NVC is too complicated because of the differences of the mix design proportions. The main difference is that the coarse aggregate is much less in the SCC mix as explained in Section 3.4.1. It was decided to take the compressive strength grade as bases for making comparison with the other SCCs, taking into account the same sand to powder ratio for the mortar. This mix design approach allowed the author to focus on the effect of the cementitious materials and exclude the effect of the aggregate on most of the conducted tests.

4.4.3 Mixing procedures and preparation of the specimens

A pan type mixer of 25 kg capacity was used to mix the SCC ingredients. The dry mix ingredients (aggregate, cement and filler) were placed in the pan of the mixer, and mixed for 2 min to ensure homogeneity. Cement and filler had previously been mixed using a trowel for 5 min to ensure the dispersion of the filler grains between cement particles. The whole quantity of water was added to the dry mix in the pan and then the SP was added gradually while the mixer was running. Mixing continued for 2 min. Mixing was paused so as to check the mix before another one minute of mixing was applied. For SCC, modified mix procedures are very important so as to take advantage of the adsorption of molecules of poly-carboxylic ether, SP, by the mix Jalal et al. (2012). The same mixing procedures but without coarse aggregate, using a 20-liter Hobart mixer was adopted for the mortar works. For NVC and mortars, the dry mix ingredients were mixed for 1 minute followed by 2 minute mixing with water using the same mixers. The fresh SCC properties of each mix were checked immediately after mixing in terms of slump flow, T_{50}, J-ring test, segregation index and mini flow slump for SCC mortars whilst the slump test was adopted for the NVC mixes.

4.4.4 Casting, preparation and curing of the specimens

New concrete batches were prepared after the optimization of the fresh characteristics of each mix. After mixing, SCCs or mortars were placed in the moulds in one go whatever the shape of the moulds without any vibration whilst mechanical vibration for about 60 ± 5 sec was performed for the two cast layers in the case of NVCs. Subsequently, the surface was leveled and the moulds were covered by Polyethylene sheets and kept in the laboratory for 24 h in the case of NVCs and 48 h for the SCCs respectively. Due to the relatively high partial replacement of cement and the high dosages of SP with the minimum powder requirements, it was not possible to demould some of SCC specimens after 24h., especially for the R-SCC and LP-SCC. Thus, all the SCC's specimens were demoulded after 48h. This is not unusual for SCC and it was adopted in several investigations e.g. Jalal et al. (2012). After stripping from the moulds, the specimens were cured in water (20 ± 2 ºC) until the date of the test. Most of tests were conducted at 28 days or later except for the fresh concrete and compressive strength tests (the reasons for which are explained in the concluding remarks at the end of this chapter). In some cases, the tests were implemented up to 240 days for the unpressurized accelerated carbonation tests or at 90 days for the normal accelerated chloride diffusion tests (See Chapter 7).

4.4.5 Assessment of fresh properties

As was explained in Section 3.4.1, different SP dosages were selected to examine the slump flow and T_{50} for the first mix design stage. It was targeted to achieve the highest possible flow and lowest T_{50} time. Table 4-7 demonstrated these trial mixes that were conducted in order to define the final optimum dosage of SP.

Table 4-7 Slump flow and T50 trial mixes

MIX ID	Property	SP % by weight					
		0.5	0.75	1.0	1.25	1.5	1.75
R-SCC	Slump flow	410	525	550	600	610	615
	T_{50}	---	7.2	7	5.5	3.7	3.5
FA-SCC	Slump flow	490	720	750	750	760	---
	T_{50}	---	3.2	2.1	3.0	3.3	---
LP-SCC	Slump flow	485	550	700	680	---	---
	T_{50}	----	6.3	4.5	5.6	---	---
FA-SF-SCC	Slump flow	425	520	600	680	675	---
	T_{50}	---	5.2	4.7	3.6	4.1	---

The obtained results clearly showed that increasing of SP content, in most cases; increases the slump flow of the mixes up to a certain point. This behavior might be attributed to the cement paste reaching a saturation point with the SP with further amounts of SP not contributing to further flow enhancement. The low values of T_{50}, largely unaffected by SP percentage, may be attributed to the increased workability characteristics in the FA-SCC as compared with the other mixtures due to the spherical smooth particles of the FA which are expected to move more easily Mohammed et al. (2013). For Super Flowing Concrete (SFC), Kim et al (1996) demonstrated that excellent workability and flow ability were achieved by 30% replacement of cement by fly ash. In comparison with the fly ash particles, the rough and angular shape of the Cement, LP and SF particles could demand a higher amount of water for the same degree of surface wetting as achieved in the FA mix whereas this was not provided because the same effective water to binder ratio was adopted for the all tested mixes. Thus, a higher dosage of SP was required in these mixes to maintain the same slump flow.

The addition of SF increased the amount of SP required in FA-SF-SCC mixtures and this may be due to the very fine particles of SF (with, thus, high specific surface area) with the rough surface as detected by the SEM-images. On the other hand, R-SCC without any filler replacement showed the highest demand of SP to achieve a slump flow of only 615mm. It has already been conjectured that the SP should be absorbed only by the cement grains which carry a positive charge as compared to the negative charge of the SP

chains; although, Syed Ali Rizwan (2006) has suggested that the SP could also be absorbed by some types of fillers.

Fig 4-29 shows the relationship between the dosage of SP, slump flow and T_{50} of some selected trial mixes. In general, the results indicated that the replacement of both FA and LP at the selected replacements reduced the required SP quantity as compared with the control mix and that containing SF. Moreover, a wide range of successful fresh SCC mixes could be produced using these two filler types-LP as an example of inert filler and FA as an example of mineral filler. However, the use of FA seems to be more suitable for the production of sustainable SCC in terms of (EFNARC,2000) fresh requirements and hence could effectively reduce the cost of the production.

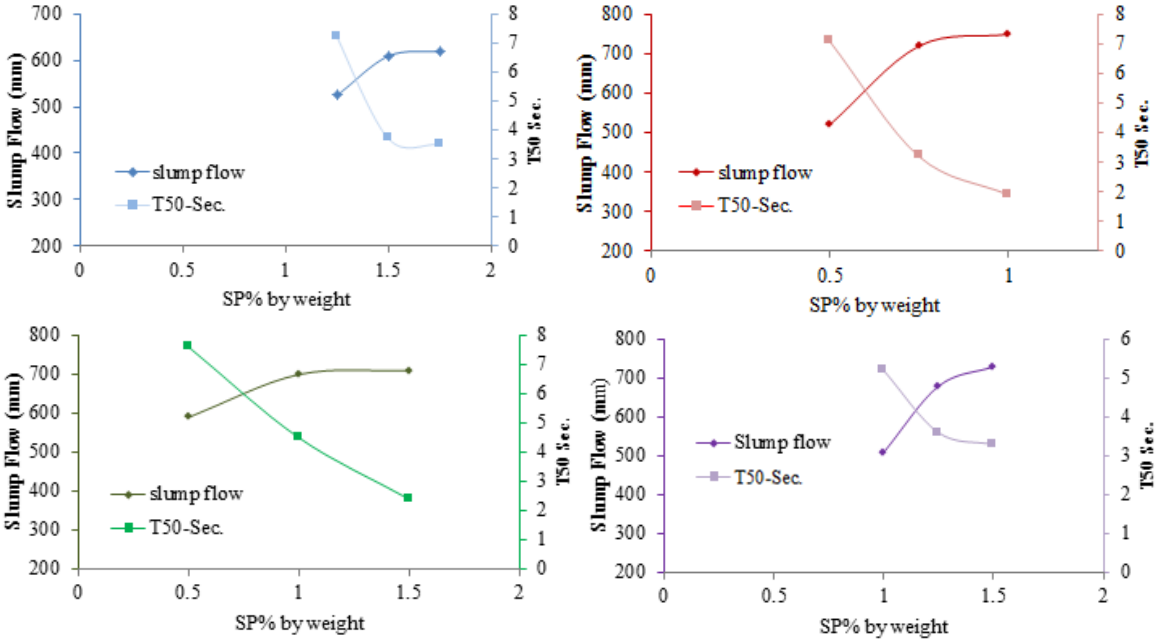

Figure 4-29 Relationship between the dosage of SP, slump flow and T_{50} of some successful trial mixes: A: R-SCC, B: FA-SCC, C: LP-SCC and D: FA-SF-SCC

The shaded trial mixes in Table 4-7 were selected for the second stage. Fig. 4-30 shows the relationship between the blocking step (BJ), SI and the dosages of SP and the limitation of the European guide for SCC EFNARC (2002).

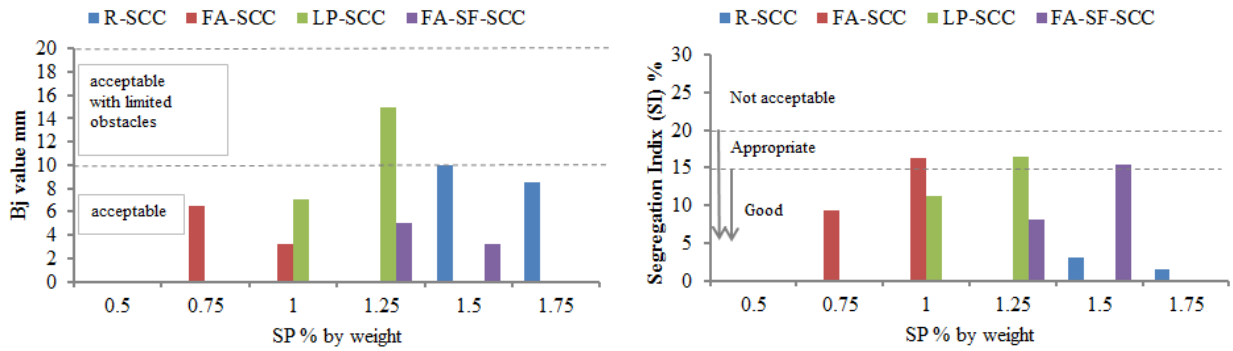

Figure 4-30 Relationship between the dosage of SP, BJ and SI for selected mixes in stage1

For SCC mortars, a wide range of flows was suggested. The European Guidelines for Self-Compacting EFNARC (2002) suggested a mortar flow between 240-260 mm while a 305-325 mm flow was recommended by BFBN (2001) as reported by Hunger (2010). However, 240-300 mm flow was achieved for all the tested mortars using the same original dosage of the SP as for full concrete.

4.4.6 Selection of the control NVC mix

The mix design of NVC is completely different from SCC. In a preliminary work, five NVC mixes were designed using the absolute volume method with a fixed mix proportion of 1:2:3 (cement: fine aggregate: coarse aggregate) and different water to cement ratios (w/c) as shown in Table 4-8. This allowed keeping approximately the same $V_{\text{fine agg.}}/V_{\text{mortar}}$ ratio (50%) as adopted for the SCC (49.7- 50.7) (see Table 4-6) so as to eliminate the effect of any variation consequent on using different fine aggregate amounts and so as to ensure a good basis for comparison with the SCC mortars. These mixes were designed to achieve a strength level of 50-60 MPa with acceptable slump for casting purposes. As reported by Neville (2011),the slump test can be used to evaluate the workability of NVC with a slump of ≥ 0 while the BS EN 206-1:2000 suggests that this test is suitable for mixes with a slump of ≥ 10 mm. However, due to the simplicity of the test, the workability of the mixes was assessed using the slump test.

Table 4-8 **Trial mixes of NVC with nominal cement content: 365 kg/m^3**

Mix ID	w/c	Slump ±5 (mm)	Slump classification	Com. St. and		Com. St. and	
				MPa	kg/m^3	MPa	kg/m^3
NVC1	0.40	Zero	---	52.0	2405	64.3	2410
NVC2	0.45	Zero	---	47.2	2385	58.5	2390
NVC3	0.50	15	S1(10-40 mm)	43.2	2355	51.3	2400
NVC4	0.60	40	S1(10-40 mm)	31.9	2355	45.2	2365
NVC5	0.70	55	S2(50-90 mm)	33.2	2310	40.4	2325

4.5 Compressive strength results

The compressive strength results of the optimized SCC and controlled NVC up to 28 days are summarized in Fig 4-31.

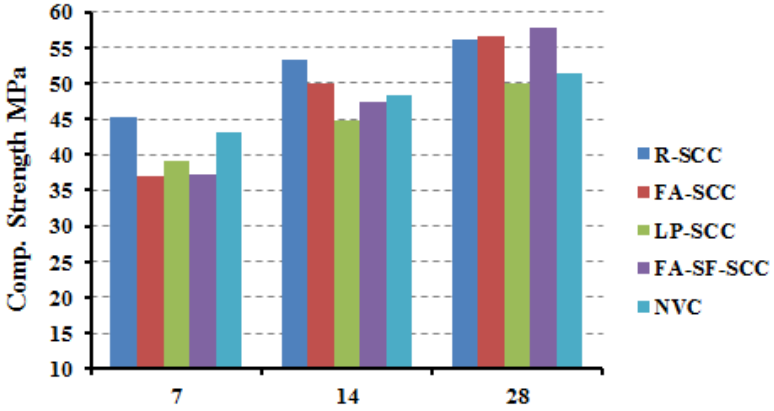

Figure 4-31 **Development of compressive strength of optimized mixes**

In general, the results indicate that all filler typed SCC showed a lower strength in comparison with the control SCC mix at early age 7 and 14. As can be anticipated, this behavior might be attributed to the high partial replacement percentages of fillers as compared with the reference SCC mix. However, it is also seen that the difference in the compressive strength between the SCC mixes becomes less at 28 days where all SCC mixes developed a compressive strength between 50-60 MPa.

At this age, the SCC made with 33% partial replacement of cement established a compressive strength of 56.5 MPa which is similar to the strength of the R-SCC. These results are consistent with Dinakar et al. (2008) who stated that for high volume fly ash SCC (HVFA-SCC), a compressive strength level between 20 and 30 MPa could be

achieved with a high level of fly ash replacement (70-85 %) while a higher compressive strength (60-90 MPa) could be obtained with 30-50 % fly ash replacement. At 28 days, FA-SF-SCC demonstrated a slightly higher strength level relative to the reference and the other SCC mixtures. This behavior may be related to the high degree of hydration for this mix as detected by the 28 days-TGA analysis (see Chapter 5). However, the most notable result is that the FA-SCC developed a higher strength at 14 days as compared with FA-SF-SCC and only a small difference in the compressive strengths was recorded at 28 days. On the other hand, NVC and LP-SCC showed approximately the same strength development trend as each other and as the R-SCC and the same strength level as each other up to 28 days.

4.6 Summary:

High strength cement CEM 1, different types of filler and mineral admixture at relatively high partial replacement, 5 mm maximum size fine aggregate and 10 mm maximum size coarse aggregates were used for the production of a wide range of medium strength normal vibrating, reference and sustainable SCC and mortars with a variety scale of fresh and hardened properties. At a minimum binder content, the special requirements of SCC mixes design were achieved both in R-SCC and in combination with the use of the relatively high partial replacement percentages using different types of filler and mineral admixture in terms of (water/powder by volume, $V_{\text{coarse agg.}}/V_{\text{total}}$, $V_{\text{fine agg.}}/V_{\text{mortar}}$ and $V_{\text{cement paste}}/V_{\text{total}}$).

The fresh properties were optimized using different dosages of SP in order to fulfill the main fresh requirements of the SCC and SCC mortars. For this attempt, the careful selection of proper materials, adequate cement replacement percentages and well design approach are important parameters to achieve the specific features of successful fresh SCC, i.e. maintaining both sustainability (minimum binder requirements) and 28 day strength (strength grade). The mix design of the normal vibrated concrete and mortars were selected carefully to achieve the same strength level of the SCC and to provide good comparison basis for the experimental program which is described in Chapter 1. In this way, it is hoped that the variation in the test results at different scales (macro, micro and nano) will be as a result of using the different cementitious material system of each

type of concrete. Based on the preliminary results obtained in this chapter, the following concluding remarks can be drawn:

- The shape and the surface texture characteristics of the filler and the mineral addition played a very important role in determining the overall fresh properties of the SCC at high percentages of cement replacement. The SCC made with FA required the smallest dosage of SP to achieve the fresh requirements indicating the consistency of the use of FA for the production of successful sustainable SCC in terms of the fresh requirements in comparison with the LP and SF additions.

- Successful economic sustainable SCC with a compressive strength grade of 50-60 MPa could be produced using a minimum binder content of 450 kg/m^3 of which approximately 33 % is either LP , FA and FA+SF cement-replacement. All the produced sustainable SCC exhibited lower compressive strength as compared with the R-SCC at 7 and 14 days except FA-SCC. However, for these three mixes, the concept of high performance SCC was achieved at 28 days regardless of mix components. Thus, this age was specified as a base point for comparing the investigated mixes and doing the accelerated carbonation and chloride tests (See Chapters 6 and 7).

- LP-SCC showed the lowest compressive strength relative to the other types of SCC and exhibited the same strength development tendency as the NVC mix up to 28 days.

- The XRD traces for the LP, FA and SF gave a reliable indication about the pozzolanic activity of the powders and their effects on the compressive strength.

- In spite of the presence of very high amorphous SiO_2 identified by the XRD pattern in the SF powder, the use of this mineral admixture (SF) in a combination with the FA as a partial replacement delayed the strength gain of SCC at early ages. Therefore, it could be suggest that the use of combined cement replacement could affect the efficiency of the SF to enhance the cement hydration process and the acquired strength level at early ages (before 28 days). The small differences in the percentages of CH amounts due to dehydration between the FA and FA-SF-SCC (TGA analysis in chapter 5) might support this conclusion.

Finally, as established by Neville (2011), each structural concrete should fulfill two principle functions. First, from the structural aspect, it must have adequate strength to resist the external loads. Second, from the durability aspect, the concrete should resist the degradation process through the service life. For SCC, the durability characteristics have been connected to the compressive strength level Parasivamurthy et al. (2012). Therefore, concrete researchers usually try to increase the strength ceiling of concrete to ensure durable concrete. However, this approach may lead to a misunderstanding of the concept of durability because of the indirect relationship between the concrete strength and impermeability, the later having the principle effect on durability, as stated by Parasivamurthy et al. (2012).

The most important question that could be raised here, especially for the modern types of concrete such as high performance and sustainable SCC, is how the complex transport properties such as chloride and carbon dioxide diffusivity could be related to the concrete internal microstructural and chemical compositions. Therefore, after the optimization and the selection of specific mixes, the proposed experimental program provided in this chapter aimed to implement quantitative chemical and microstructural assessments that may be used in combination with the current and modified accelerated tests in chapters 6 and 7 to provide further understanding of the whole performance (at various length scales) in, and interaction with, aggressive carbonation and chloride environments. In addition, these are implicated in causing concrete deterioration, so an experimental program has been commenced to predict their life span mathematically and to compare results obtained with the available standard data for different exposure status to natural aggressive conditions.

4.10 References

AGGARWAL, P., SIDDIGUE, R., AGGARWAL, Y. & GUPTA, S. M. 2008. Self-compacting concrete-procedure for mix design. Leonardo Electronic Journal of Practices and Technologies, 7, 15-24.

ALMEIDA, A. E. F. d. S. & SICIERI, E. P. 2006. Thermogravimetric analyses and mineralogical study of polymer modified mortar with silica fume. Materials research, 9, 321-326.

ASTM. C-618 1991. Standard specification for fly ash and raw calcined natural pozzolan for use as a mineral admixture in Portland cement concrete. Annual Book of ASTM Standard.

BOEL, V., AUNENAERT, K. & De SCHUTTER, G. Characterization of the pore structure of hardened self-compacting cement paste.

BONAVETTI, V., DONZA, H., MENENDES, G., CABREA, O. & IRASSAR, E. F. 2003. Limestone filler cement in low w/c concrete: A rational use of energy. Cement and Concrete Research, 33, 865-871.

BORGES, P. H. R., COSTA, J. O., MILESTONE, N. B., LYNSDALE, C. J. & STREATFIELD, R. E. 2010. Carbonation of CH and C–S–H in composite cement pastes containing high amounts of BFS. Cement and Concrete Research, 40, 284-292.

BS 882 1992. Specification for aggregates from natural sources for concrete.

BS EN 12390–3 2002. Testing hardened concrete part3: compressive strength of test specimens British Standard Institution; 2002.

BS EN 13263-1:2005 +A1 2009. Silica fume for concrete. Part 1: Definitions, requirements and conformity criteria. British Standard.

COOK, R. A. & HOVER, K. C. 1999. Mercury porosimetry of hardened cement pastes. Cement and Concrete Research, 29, 933-943.

COPPOLA, L., CERULLI, T. & SALVIONI, D. YEAR. Sustainable development and durability of self-compacting concretes. In: 8th CANMET/ACI Int. Conf. on Fly Ash, Silica Fume, Slag and Natural Pozzolans in Concrete, 2004. 29-50.

De SCHUTTER, G. & AUDENAERT , K. 2007. Report 38: Durability of Self-Compacting Concrete-State-of-the-Art Report of RILEM Technical Committee 205-DSC, RILEM publications.

De SCHUTTER G. YEAR. Effect of limestone as mineral addition in self-compacting concrete. In, 2011. 6th Conference on our world in concrete & structures. Singapore;.

De SCHUTTER, G., BARTOS, P. J. M., DOMONE, P. & GIBBS, J. 2008. Self-compacting concrete, Taylor and Francis Group.

DINAKAR, P., BABU, K. & SANTHANAM, M. 2008. Durability properties of high volume fly ash self compacting concretes. Cement and Concrete Composites, 30, 880-886.

EFNARC. 2005. The European Guidelines for Self-Compacting Concrete [Online]. Available: http://www.efnarc.org/pdf/SCCGuidelinesMay2005.pdf [Accessed 17-01-2014].

EFNARC, S. 2002. Guidelines for Self-Compacting Concrete. European Federation for Specialist Construction Chemicals and Concrete Systems, Farnham, UK, 32.

ERDEM, S. 2012. Impact Load-Induced Microstructural Damage of Concrete Made with Unconventional Aggregates. PhD thesis, University of Nottingham, Department of Civil Engineering.

ESPING 2007. Early age properties of self-compacting concrete-Effects of fine aggregate and limestone filler. PhD, Göteborg, Sweden.

FELEKOGLU, B., TURKEL, S. & BARADAN, B. 2007. Effect of water/cement ratio on the fresh and hardened properties of self-compacting concrete. Building and environment, 42, 1795-1802.

FEUERBORN, H.-J. YEAR. Coal ash utilisation over the world and in Europe. In: Workshop on environmental and health aspects of coal ash utilization, 2005. 1-5.

HEMAVIBOOL, S. 2007. The microstructure of synthetic aggregate produced from waste materials and its influence on the properties of concrete. University of Leeds.

HUNGER, M. 2010. An integral design concept for ecological self-compacting concrete. PhD, Eindhoven University of Technology, The Netherlands.

JALAL, M., POULADKHAN, A. R., RAMEZANIANPOUR, A. A. & NOROUZI, H. 2012. Effects of silica nanopowder and silica fume on rheology and strength of high strength self compacting concrete. Journal of American Science, 8.

KJELLSEN, K., MONSOY, A., ISACHSEN, K. & DETWILER, R. 2003. Preparation of flat-polished specimens for SEM-backscattered electron imaging and X-ray microanalysis-importance of epoxy impregnation. Cement and Concrete Research, 33, 611-616.

KOEHLER, E. P. & FOWLER, D. W. 2006. ICAR Mixture Proportioning Procedure for Self-Consolidating Concrete [Online].Available: http://www.icar.utexas.edu/publications/108/ICAR%20108-1%20(Proportioning).pdf [Accessed 04-05-2012].

LAWRENCE, R. 2006. A study of carbonation in non-hydraulic lime mortars. PhD, University of Bath.

LOUKILI, A., KHELIGJ, A. & RICHARD, P. 1999. Hydration kinetics, change of relative humidity, and autogenous shrinkage of ultra-high-strength concrete. Cement and Concrete Research, 29, 577-584.

MEHTA, P. K. & MONTEIRO, P. J. M. 2006. Concrete: microstructure, properties and materials, McGraw-Hill.

MOHAMMAD IQBALl KHAN for measuring porosi A Novel methodty of high .2004 .(strength concrete. Proceedings of the 7th Saudi Engineering Conference (SEC7

MOHAMMED, M. K., DAWSON, A. R. & THOM, N. H. 2013. Production, microstructure and hydration of sustainable self-compacting concrete with different types of filler. Construction and Building Materials, 49, 84-92.

NEHDI, M., PARDHAN, M. & KOSHOWSKI, S. 2004. Durability of self-consolidating concrete incorporating high-volume replacement composite cements. Cement and Concrete Research, 34, 2103-2112.

NEVILLE, A. M. 2011. Properties of Concrete, London, Pearson Education Limited.

OKAMURA, H. & OUCHI, M. 2003. Self-compacting concrete. Journal of Advances Concrete technology, 1, 5-15.

PARASIVAMURTHY, P., JAWALI, V. & VENKATAKRISNA, P. A. 2012. Study of Self-Compacting Fly Ash Concrete Using Silica Fume Admixture. Advanced Materials Research, 409, 249-254.

RENDELLl, F., JAUBERTHIE, R. & GRANTHAM, M. 2002. Deteriorated concrete: Inspection and physicochemical analysis, Thomas Telford.

RILEM 2008. Final report of RILEM TC 205-DSC: durability of self-compacting concrete, Materials and Structures,2008, P. 225-233.

ROY, D. M., BROWN, P., SHI, D., SCHEETZ, B. & MAY, W. 1993. CONCRETE MISCROSTRUCTURE POROSITY AND PERMEABILITY.

SCRIVENER, K. L. 2004. Backscattered electron imaging of cementitious microstructures: understanding and quantification. Cement and Concrete Composites, 26, 935-945.

SUZUKI 2002. High-resolution scanning electron microscopy of immunogold-labelled cells by the use of thin plasma coating of osmium. E. Journal of Microscopy 208, p. 153-157.

SYED ALI RIZWAN. 2006. High performance mortars and concrete using secondary materials. Dr.-ING, Technical University Bergakademie Freiberg.

YE, G., LIU, X., De SCHUTTER, G., POPPE, A.-M. & TAERWE, L. 2007. Influence of limestone powder used as filler in SCC on hydration and microstructure of cement pastes. Cement and Concrete Composites, 29, 94-102.

YING, W. 2013. Performance assessment of cement-based materials blended with micronized sand: microstructure, durability and sustainability.

Chapter 5:
Quantitative Evaluation of the Chemistry and Microstructure of the Concrete Mixes

5.1 General

In order to create a deeper understanding of the role of microstructure alongside the accelerated tests proposed in chapters 6 and 7, the internal microstructure was also assessed. The aims are to evaluate the following:

- The differences in the progression of carbonation and chloride penetration in chapter 6.
- The impact of carbonation on the internal concrete pore structure and the associated chemical changes of after carbonation (pore structure of the concrete as a composite material) including the chemical composition and the microstructure features of the cement matrix and the ITZ in chapter 6.
- Macro/micro and nano internal pore structure property relationships with the chloride penetration velocity in chapter 7.

The change of the chemical composition and microstructural features of the inspected concrete is probably influenced by the characteristics of the various cementious material systems in a medium strength normal vibrated concrete, in a reference SCC and in three types of sustainable SCC with relatively high partial replacement of cement. On the above bases, this chapter contains four major parts:

- Quantitative assessments of the chemical composition and the degree of hydration of the concrete mixtures using XRD, TGA and SEM techniques. This part is focused on the binder characteristics (cement matrices).
- Quantitative evaluation of the change in the internal concrete pore structure features in different scales (macro, micro and nano) using a combined results obtained from the MIP, vacuum porosity test and the SEM analysis. This section is related to pore structure of the concrete as a composite material at different scales (aggregate and cement matrices).

- Description of the microstructural techniques that have been used to characterize the change in the micro-permeation properties of the ITZ alone in terms of porosity, thickness and chemistry and the results obtained.
- General concluding remarks.

5.2 Chemical composition analysis and the degree of hydration

It is well established that aggressive agents (liquids or gases) could ingress inside the concrete from the surrounding environment through different mechanisms like capillary absorption, hydrostatic pressure and diffusion. The penetration of these substances into concrete occurs through the pore system of the cement matrix and the aggregate-cement matrix interface (ITZ) or through the micro cracks. However, the aggregate phase is usually considered as an impermeable phase (Shi et al., 2012).

The degree of hydration, which might reflect the ability of the cement matrix to produce high amount of hydration products (especially in term of CSH gel), is one of the most important factors that may control the penetration of these aggressive agents in the proposed different mechanisms. The formation of hydration products could significantly change the porosity of the concrete or block the continuity of the capillary pores at different scales in both the cement matrix and the ITZ.

Among the different methods that have already been proposed to examine the degree of hydration (such as the determining the chemically bound water, the specific gravity of the paste, the fraction of unhydrated cement and the liberated heat of hydration), the calculation of the amount of $Ca(OH)_2$ (CH) in the cement matrix is typically used to estimate the degree of cement hydration (Shafiq and Nuruddin, 2011).

The main carbonation product $CaCO_3$ (C) is originally generated from the reaction between the CH compounds in the cement matrix and CO_2 gas from the atmosphere in the presence of humidity. Thus, it is difficult to ignore the examination of the concretes' chemical composition and its degree of hydration when considers its influence on the transport properties-including the chloride and carbonation progression. The expected changes of the internal pore structure caused by carbonation reaction are highly dependent on the chemical nature of the cement matrix.

5.2.1 XRD analysis (mineralogy)

Six main crystalline phases were detected from the analysis of the typical XRD spectra of the mortar for the investigated concrete as shown in Fig. 5-1 to 5-5. These phases are as follow:

- **Portlandite ($Ca(OH)_2$)**
- **Quartz (SiO_2)**
- **Belite (C_2S) in the form of Larnite ($Ca_3 SiO_4$)**
- **Alite (C_3S) in the form of (Ca_3SiO_5)**
- **Ettringite in the form of ($Ca_6 Al_2 (SO_4)_3 (OH)_{12}.26 H_2O$**
- **Calcite ($CaCO_3$)**

The detected pure quartz in the XRD spectra does not represent one of the hydration products but it is likely to be due to the presence of SiO_2 in the sand particles as the test was conducted in mortar specimens.

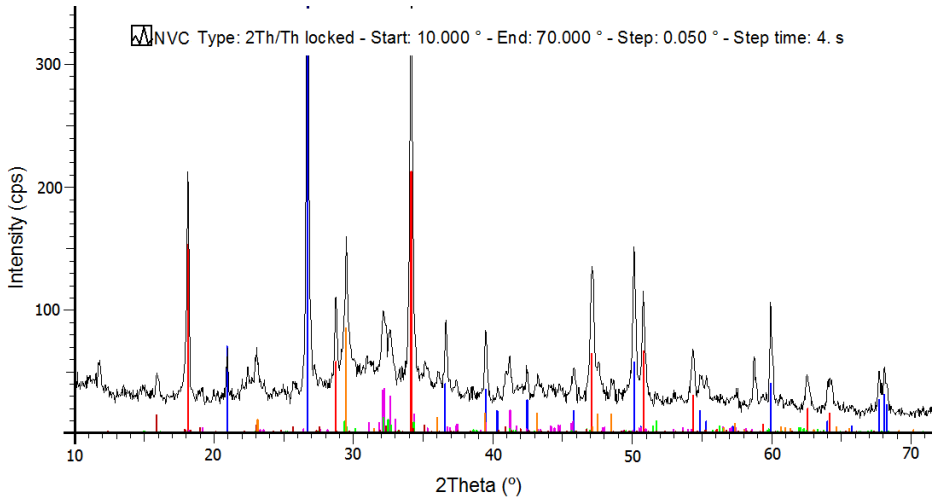

Figure 5-1 Typical XRD spectrum of NVC-mortar

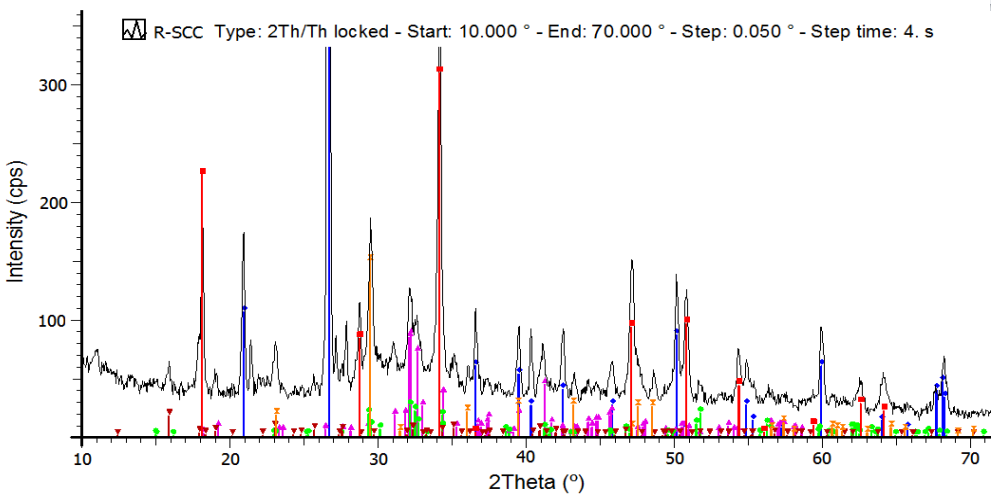

Figure 5-2 Typical XRD spectrum of R-SCC mortar

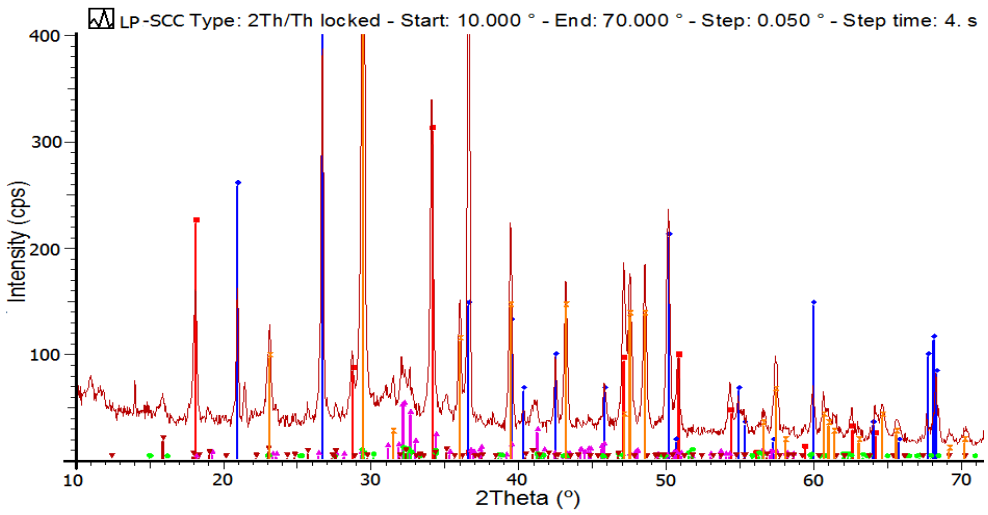

Figure 5-3 Typical XRD spectrum of LP-SCC-mortar

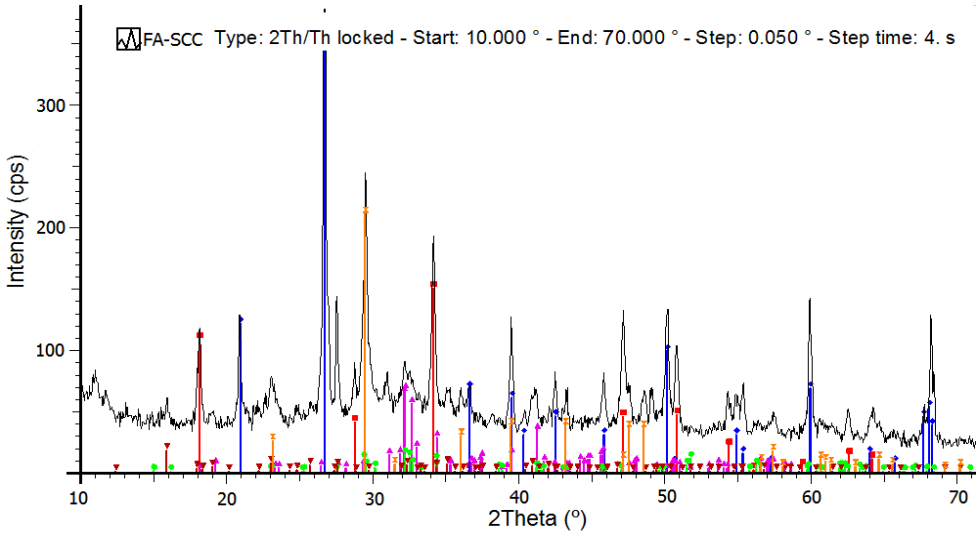

Figure 5-4 Typical XRD spectrum of FA-SCC-mortar

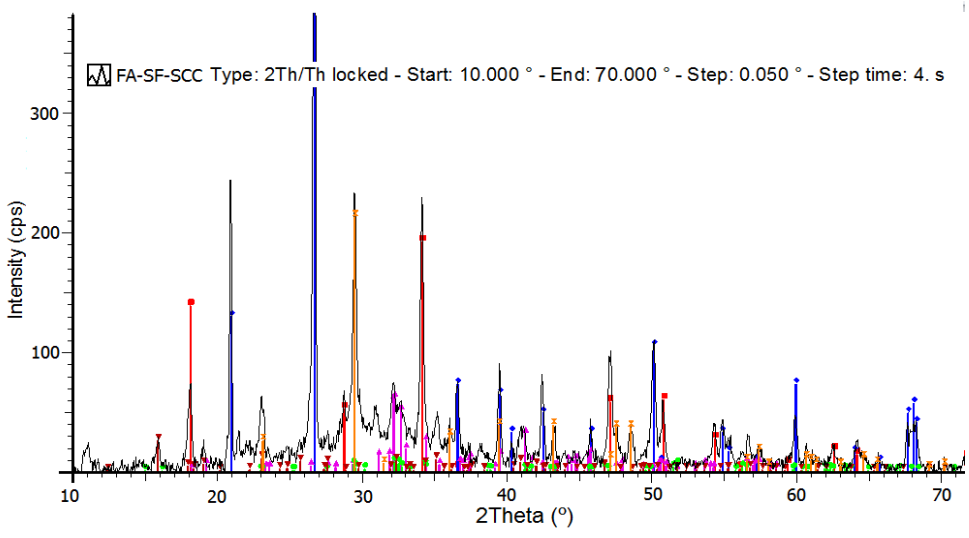

Figure 5-5 Typical XRD spectrum of FA-SF-mortar

The main focus of the discussion in this section will be on the presence and the peak intensities of the CH and C compounds. For the calcium silicate hydrate gel (CSH), Rendell et al.(2002) claimed that the various forms of this compound would comprise amorphous phases with weak and diffuse XRD peaks under normal curing conditions and hence, such compounds might not appear in the XRD diffractogram. Therefore, the existence of the CSH in both the ITZ and the cement matrix will be analyzed and discussed using the EDX analysis described in the third part of this chapter.

The CH in all the inspected mortars were identified by reference intensity peaks at 34.1º 2-theta scale. According to Rizwan(2006), the reference peak of this crystalline hydration phase can be detected at this angle by a degree sweep of (4-70 º) using Cu-kα radiation source. However, the analysis of the result presented in Figs. 5-1 to 5-5 indicated a presence of different intensity peaks on the 2-theta scale range between (10-70º). The peak intensity values, including the reference peak of CH (the highest peak), and their average values are summarized in Table 5.1.

Table 5-1 XRD peak intensity values of CH

2-theta scale	18.1º	28.75 º	34.1 º	47.1 º	50.8 º	54.4 º	62.55 º	64.15 º	Av.
NVC- mortar	212.8	95.8	**374.5**	135.0	114.8	65.8	46.3	36.5	**135.2**
R-SCC- mortar	140.3	106.8	**371.8**	147.5	117.8	69.8	50.3	54.5	**132.4**
LP-SCC- mortar	155.3	79.8	**333.0**	186.3	95.8	59.8	44.5	51.8	**125.8**
FA-SCC- mortar	118.0	78.8	**193.5**	118.5	103.5	51.0	51.0	45.3	**95.0**
FA-SF-SCC- mortar	116.0	88.8	**258.3**	122.0	79.3	67.0	47.6	48.5	**103.4**

Note: To specify the exact intensity peaks and the corresponding 2-theta scale, Appendix A provides the original XRD spectra and their data.

The results in Table 5.1 demonstrated that both the reference and the average peak intensities of the CH compound in both the NVC and R-SCC mortar's powders are roughly identical. This suggests an approximate equal degree of hydration of these two types of concrete although the higher cement content in the R-SCC relative to the NVC. However, NVC had higher water to cement ratio which might have more controlling role in the hydration process. It was deduced that the use of low water to cement ratio for a SCC without any cement replacement (R-SCC) could reduce the amount of available water to achieve a high degree of hydration at 28 days.

For the other types of sustainable SCC, the XRD results showed that the FA-SCC exhibited slightly lower reference and average CH intensity peaks compared to FA-SF-SCC followed by LP-SCC. Typical SEM micrographs of the cement matrix for these two FA-based matrices, as shown in Figs 5-6, illustrate high amounts of un-reacted FA particles (three types of FA particles were perceived: 1-rounded un-reacted, 2-partially reacted and 3-completely reacted particles). However, the lower values of the reference and average intensity peaks of CH suggest a higher degree of hydration. This behavior might be as a result of the pozzolanic reaction of the fine particles of both the FA and SF. It is well known that the reaction of such pozzolanic materials can generate additional different form of CSH due to the reaction with the CH in the presence of water (Shi et al., 2012).

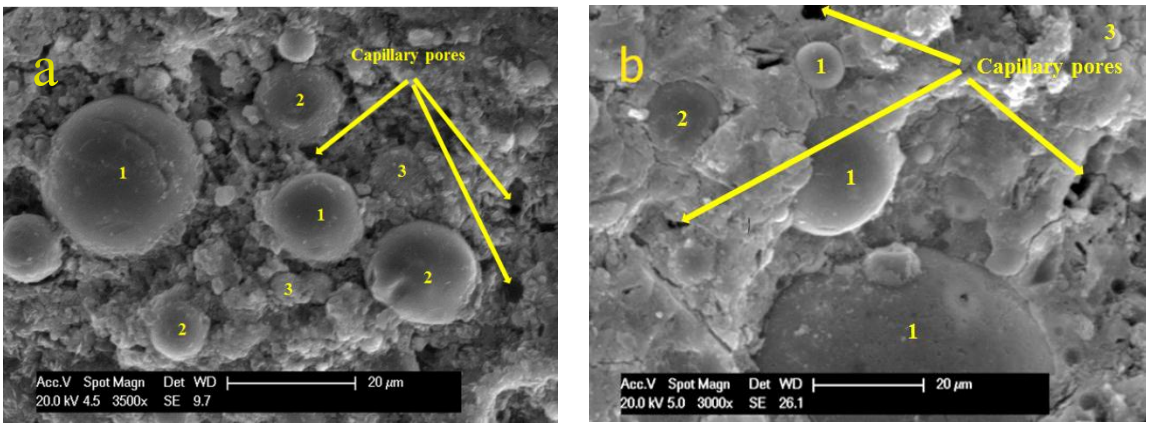

Figure 5-6 SE micrographs of the cement matrix of a) FA and b) FA-SF-SCC

Inspecting the XRD patterns also revealed that the intensities of the C- peaks were much higher in LP-SCC spectrum as compared with the other mixes. The reference peak of this compound was detected at 29.45º 2-theta scale and their values were: 159.75, 186.5, 751.5, 244.75, and 261.25 for NVC, R-, LP-, FA-, FA-SF-SCCs respectively. The higher intensity of the reference calcite peak in the LP-SCC indicates a higher proportion of this crystalline phase in this mix and this is almost certainly due to the presence of $CaCO_3$ in the original limestone.

5.2.2 TGA analysis (degree of hydration)

TGA analysis was conducted in order to calculate the percentages of the CH in each mix type. The results of the thermal decomposition of the concrete mortars are formulated in

combined TG (thermal weight loss) and DTG-curves (derivatives of the thermal weight loss) as shown in Figs.5.7.

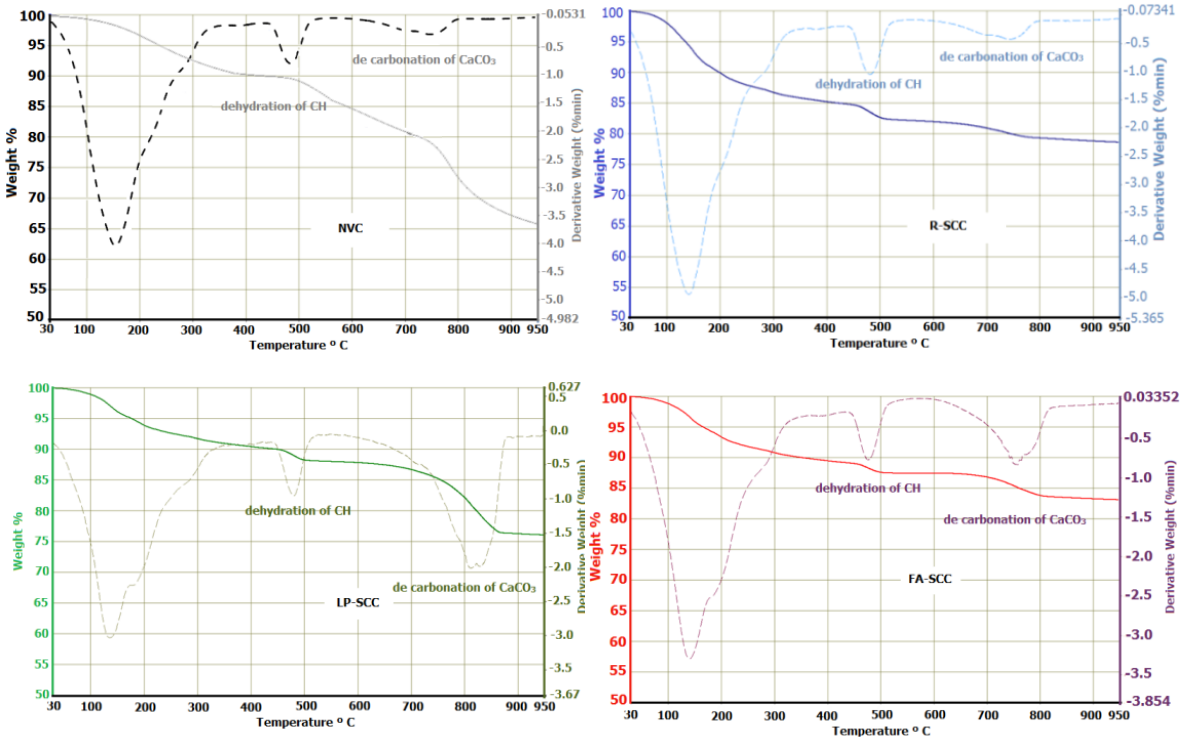

Figure 5-7 Combined TG and DTG-curves for mortars

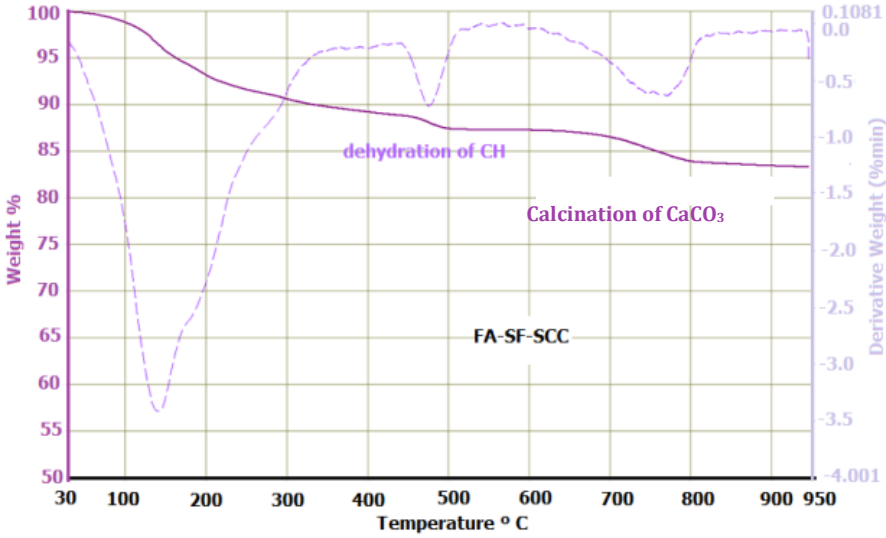

Figure 5-8 Continued combined TG and DTG-curves for mortars

The results demonstrated three main peaks in the DTG curves for all the mortars. The first peak is not of interest, as explained in Section 4.3.4.1. The second peaks were used to calculate the percentage weight losses resulting from the dehydration of CH whilst the third ones were adopted to compute the CH lost due to the de-carbonation reaction at

high temperature. These peaks verified that the decomposition of CH was in the range of (420- 550ºC) whereas the de-carbonation reaction occurred between 600 to 780 ºC for all mortar's powder. The calculated percentages of CH due to dehydration (Eq. 4-5), de-carbonation (Eq.4-6) reactions and the total amounts were summarized in Table 5-2.

Table 5-2 CH% content of the normal vibrated and SCC-mortars

Mortar ID	CH de-hydration	CH calcination	Total CH
NVC	6.9	2.7	9.6
R-SCC	7.4	2.7	10.1
LP-SCC	6.3	2.62	8.98
FA-SCC	4.7	6.1	10.8
FA-SF-SCC	4.2	4.7	8.9

A theoretical correction has been made for the sake of calculation of the total amount of CH in the LP–SCC because of the de-carbonation of the original LP at high temperature. The total weight of the powder sample in the TGA test was 25.99 mg. Therefore, 8.57 mg of this should be subtracted, representing the 33% LP content. The calculated total mass loss from the TGA curve was 8.953% between 600 and 780 ºC. Thus, CH% due to the de-carbonation of this mortar becomes = 74/44* (25.99–8.57) 8.953% = 2.62% (See **Eq. 4-8**). The greater de-carbonation reaction in the LP–SCC mortars can be compared to the corresponding ones for the other mortars as shown in Fig 5-7. This is likely to be due to the high original amount of $CaCO_3$ presented in LP–SCC and this result is consistent with those by Ye et al.(2007) who obtained the same trend for the de-carbonation reaction of SCC containing LP using TGA analysis.

The combined results of both XRD and TGA analysis confirmed the inability of the LP to make any chemical improvement to the cement matrix. However, the higher amount of detected CH due to the thermal decomposition in this type as relative to the other sustainable SCC tends to confirm the hypothesis that the hydration of C_3S is enhanced at early ages in the presence of LP due to the nucleation effect of this filler type. This is because the hydration of the C_3S is known to produce a higher amount of CH in comparison with C_2S at early ages (Gomes, 1997, Neville, 2011).

The obtained TGA results were compatible with those obtained from the XRD in term of the dehydration of the CH in a temperature range of (420- 550ºC), as shown in Fig 5-8, rather than those of the total amount of the CH. The assessed percentages of CH due to the dehydration in the SCC's that contained reactive mineral admixture (FA or FA+SF) were considerably lower than the values assessed for the NVC, reference and SCC containing LP.

Fig.5-8 displays the relationship between the CH loss percentages from the TGA analysis versus the detected reference intensity peaks in the XRD spectra for the tested mortars. As can be seen, a fairly good relationship exists. It was recently hypothesised by Rizwan (2006) that the thermal decomposition of the CH compound in the TGA should correlate to the XRD reference peak intensity considering the theoretical basis of the two tests. However, the correlation obtained was less than that obtained by Rizwan (0.98) for different cementitious systems of SCC matrices incorporating partial replacements of LP, FA, FA+SF and FA+ rice husk ash. The degree of this correlation might depend on both the reactivity of the cement in use, the type of replacement materials, the percentages of each and the equipment used. Rizwan's high correlation and the fairly good correlation in the present study might indicate that the degree of hydration of the concrete incorporating different cementitious matrices is governed by the decomposition of the CH rather than the total amount of CH obtained from the TGA analysis.

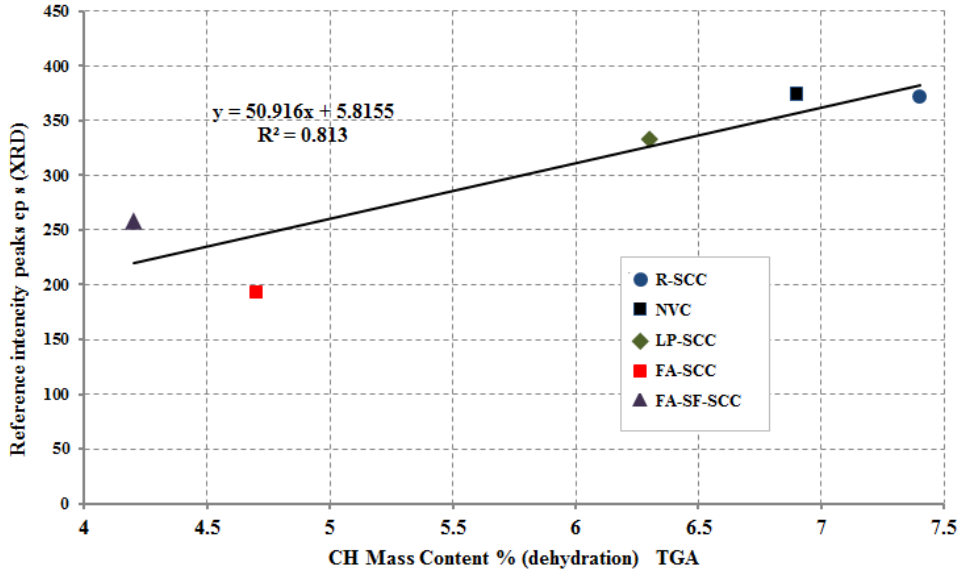

Figure 5-9 the relationship between the CH contents from TGA and the reference intensity peak of CH (XRD)

From the durability aspect, the reduction of the alkalinity of the pore water solution due to the lower amount of CH in the cement matrix could adversely affect the corrosion resistance by permitting earlier carbonation. However, carbonation rate may also depend on any modification of the pore network due to any additional cement gel generated from the use of fillers or mineral admixtures. This concern will be discussed in further specifics in chapter 6.

5.3 Pore structure characteristics of the concrete at different scales

From the physical aspect, the permeability and the water/vapour/contaminant transport properties of the concrete are highly dependent on the capillary pores and their interconnectivity. In general, the porosity of SCC is expected to be lower than that of NVC. This is due to the filling and dispersal effect of the fillers and the superplasticizer, respectively (Desmet et al., 2011). However, the type of filler and mineral additions is likely to determine the nature of the porosity at different scales (macro, micro or nano) and of the connectivity of the pores when high levels of cement replacement are used at same water to binder ratios (Malab et al., 2009). The pore classification at these different length scales are explained in details in Section 2.2.2. In addition, the ITZ's micro permeation characteristics and pore nature could be changed depending on the action of the binder used (cement, filler or the mineral admixture) to achieve a good packing to the aggregate interface and to compensate for the activity of the replaced cement.

As stated by Assié et al.(2007) referencing Zhu et al. (2001), the modification of the microstructure of the SCC might not be enough to assure sufficient resistance to the chloride penetration as this property might be governed by the tortuosity, the percolation and the connectivity of the internal pore network.

These features are expected to largely depend on the capillary pores at the micro and nano scale and their interactions with each other in the presence of constant or different amounts of the impervious phase (fine or coarse aggregate) as a composite material (concrete/mortar). The high amount of fine aggregate that is recommended for the SCC to achieve the mix design criterion in terms of mix stability and flow characteristics could have a positive or negative effect on the concrete transport properties depending on the pores network percolation as a composite material. Thus, in this section the pore characteristics will be quantitatively analyzed in different scales to establish the

macro/micro and nano internal pore structure property relationships with the chloride penetration velocity and to investigate the change of these characteristics after carbonation as well.

Fig. 5-9 illustrates an example of some mercury intrusion curves versus the pore diameter for some tested concrete mixtures at different ages whilst Fig. 5-10 shows the derivative of theses curves.

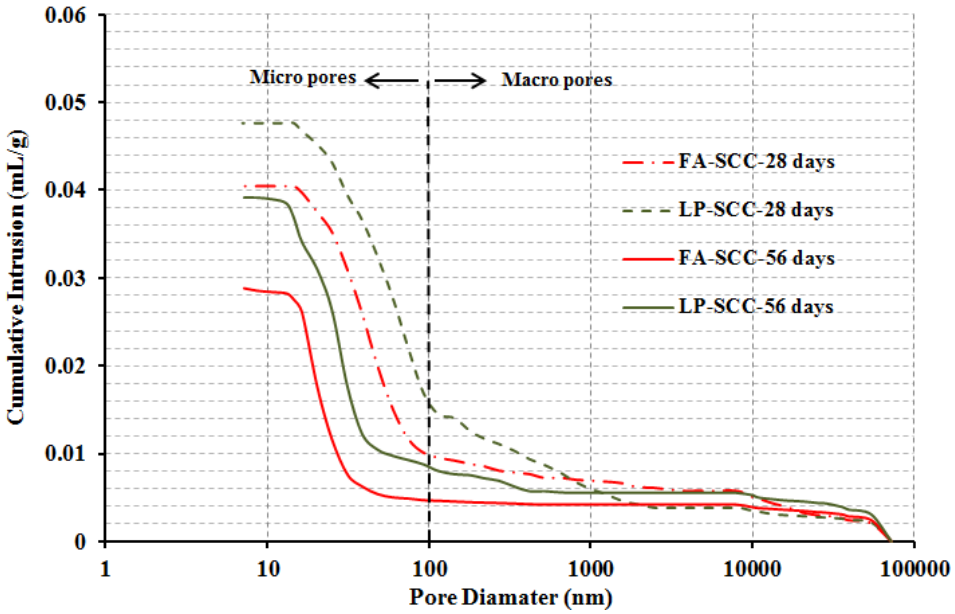

Figure 5-10 Mercury intrusion curves versus pore size diameter of LP–SCC and FA–SCC (Mohammed et al., 2013)

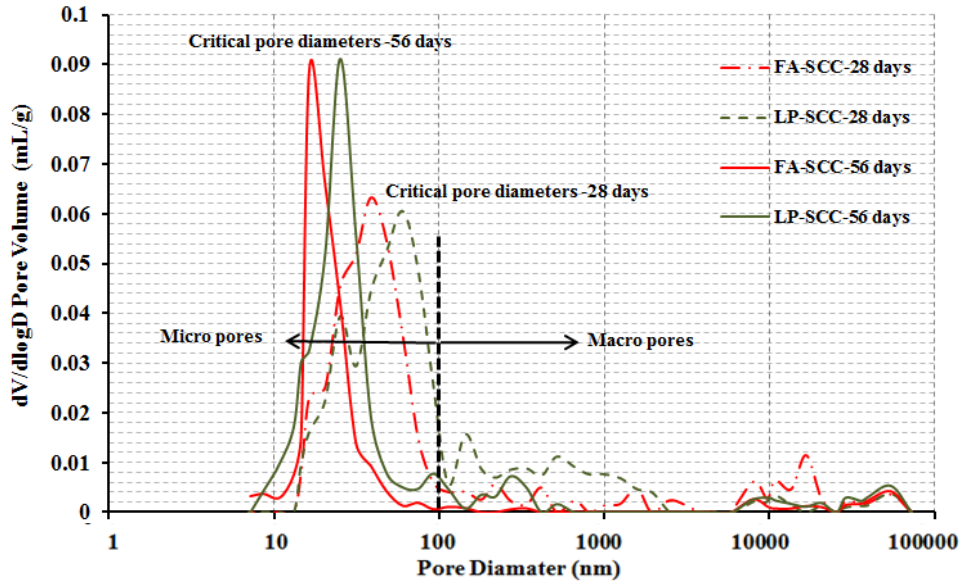

Figure 5-11 Derivative of MIP curves of LP–SCC and FA–SCC (Mohammed et al., 2013)

The porosity results of both the MIP and the vacuumed saturated porosity test were used for characterizing the pore structure of the concrete at different scales (macro, micro and nano scale) and the results are summarized in Table 5-3 and 5-4 for mix age of 28 and 56 days respectively.

The porosity natures of the concrete mixes (micro or macro) were determined in which the micro pore percentages are bigger than 65 %. From the MIP test and at this percentage, the refinement of the pore structure is expected as stated by Savas (2012). However, the macro porosity results were added to give a complete picture of the continuous pores that cannot be detected by the MIP technique. The difference between the vacuum porosity results (macro-porosity or P_V % vacuum) and that of the MIP (P% $_{MIP}$) represent the larger continuous pores. Thus, the percentage of macro pores of the mixes was re-calculated as $[(\text{Macro pore\%} \times P_{MIP}) + (P_V - P_{MIP})]/P_V$ and micro pores percentage are 100% – macro pores% as shown in Table 5-3 and 5-4.

For the R-SCC, an example of calculating the macro/micro pores percentages (Ma-P% and Mi-P %) and determining the critical pore diameter (CPD) from the MIP test is shown in Fig. 5-11. For more details, the full analysis conducted by the author for the different types of concrete at 28 days (before carbonation) and after full carbonation can be found in Chapter 6 (Section 6.5).

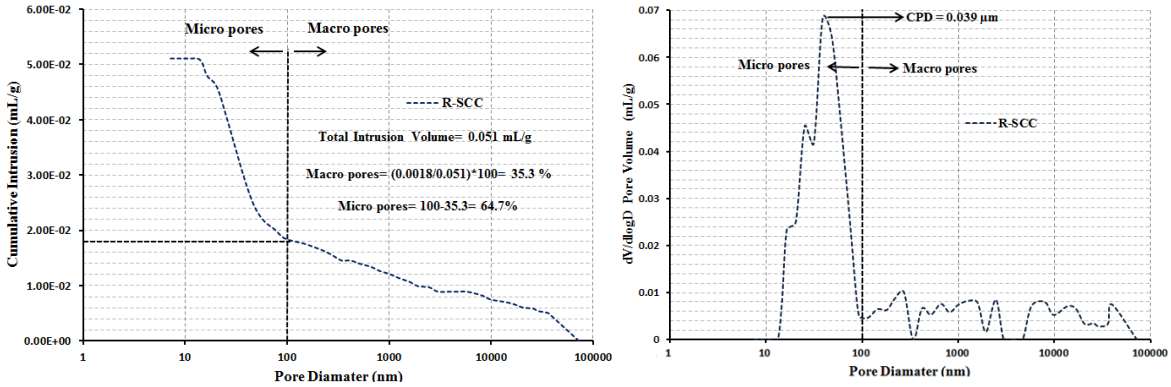

Figure 5-12 example of determination of macro/micro pores percentages and CPD

Table 5-3 Pore structure characterization at different scales (28 days)

Mix ID	Mi-P% (MIP)	Ma-P% (MIP)	CPDs (nm)	APDs (nm)	P % (MIP)	P% (vacuum)	Mi-P % (Total)	Ma-P % (Total)
NVC	76.5	23.5	60	79.4	17.9	31.2	43.9	56.1
R-SCC	64.7	35.3	39	84	19.4	21.1	67.5	32.5
FA-SCC	75	25	38	71	8.7	14.7	84.8	15.2
LP-SCC	66.6	33.4	60	88	10.5	14.1	74.9	25.1
FA-SF-SCC	71	29	31	75	9.3	12.2	77.7	22.3

Table 5-4 Pore structure characterization at different scales (56 days)

Mix ID	Mi-P% (MIP)	Ma-P% (MIP)	CPDs (nm)	APDs (nm)	P % (MIP)	P% (vacuum)	Mi-P % (Total)	Ma-P % (Total)
NVC	82.8	17.2	48	79.4	15.6	21.9	59	41
R-SCC	72.7	27.3	31	57.2	8.2	8.21	72.7	27.3
FA-SCC	82.8	17.2	16	40.3	9.8	10.3	78.8	21.2
LP-SCC	78.5	22.5	25	34.9	9.9	10.4	73.8	26.2
FA-SF-SCC	85.7	14.3	20	30.5	9.25	10.1	78.5	21.5

The pore structure analysis at 28 days indicated that the NVC and marginally R-SCC exhibited a macro porosity nature corresponding to a micro porosity of the sustainable SCC. The FA and FA+SF additions in particular achieved a refinement of the pore structure of the sustainable SCC in spite of the high cement replacement so that the detected micro pores percentages were greater than 65%. This might be attributed to the combined effect of both a tighter of packing the concrete microstructure and gel production due to the pozzolanic activity of these two mineral admixtures. For SCC, Bassuoni and Nehdi (2009) demonstrated that due to the combined filling and pozzolanic effects of the multicomponent of supplementary cementitious material system (SCMs) of different particle sizes, a dense and discontinuous pore structure could be achieved.

The analysis also indicated that all the deduced CPDs were in the nano scale with a single peak in the pore range of 10-100 nm for the all types of SCC whilst the NVC presents two peaks, one of which is in the same range as for the SCC and the other being around 10 microns (Fig 6-18). The particular monomodal structure of SCC is justified by Malab et al.(2009) who explained the refinement of the internal pores at macro and micro scales by the dense microstructure in SCC. It should be highlighted here that all the deduced CPDs should be allocated in the cement matrix away from the ITZs regions (See section 7.4). Therefore, these CPDs might represent the nature of the pore percolation of the cement matrix alone.

Despite the similar macro porosity nature of the NVC and R-SCC, the last of these exhibited a lower CPD relative to the other concretes although the approximate equal degree of hydration as identified by the chemical composition analysis (XRD and TGA). At the nano scale, this mismatch suggests that the percolation of the matrix capillary pores, defined by the smallest diameter (CPD), might be affected by: i) the interaction between the hydration products and the ability of the surrounding hydration products to pack up together with the unhydrated cement for the concrete with low degree of hydration (R-SCC and NVC) as shown in Fig. 5-12 ii) the adhesion between the unreacted particles of the filler/mineral admixture with the other hydration products for the concrete with high partial cement replacement (LP,FA and FA+SF SCCs) as shown in Fig. 5-13 and Fig 5-14. The presence of unreactive filler such as LP due to the high replacement might cause a dilution in the cement matrix leading to an increase in the CPD at this scale (LP-SCC) as shown in Fig. 5-13. The typical BSE and SE SEM micrographs in these figures of the different type of cement matrices show the differences in these interfaces.

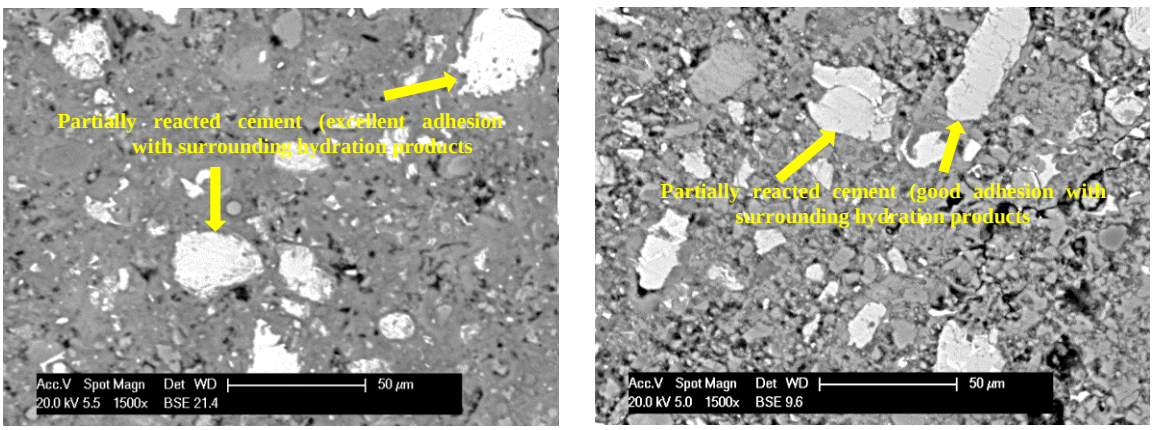

Figure 5-13 the interaction between the hydration products in the cement matrix of R-SCC and NVC (BSE images)

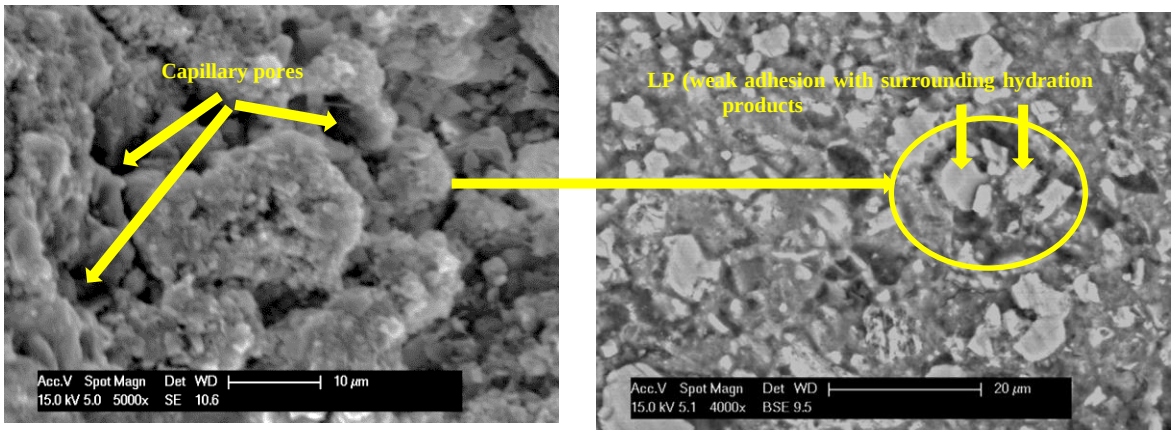

Figure 5-14 SE and BSE images showing the dilution of LP-SCC cement matrix

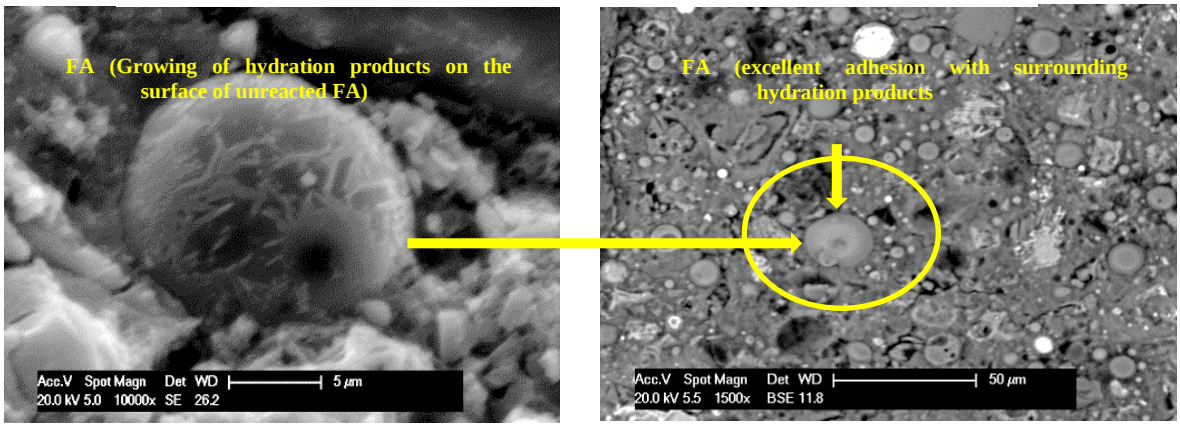

Figure 5-15 SE and BSE images showing the adhesion of unreacted FA particles and nearby hydration products

The SE and BSE micro analysis shown in Fig. 5-12 revealed a higher amount of anhydrous cement in the cement matrix of the R-SCC with an excellent adhesion with the surrounding hydration products while a porous interface was seen clearly in the case of LP replacement (Fig. 5-13). In the same manner as reported by Zhijun (2012), the result obtained from BSE imaging of LP–SCC revealed a porous interface between the limestone grains and the hydration products. In contrast, a dense interface was observed by Zhijun(2012) between unhydrated cement grains and surrounding hydration products in a high performance cement matrix. Thus, the influence of the crooked/rough surface detected by the SEM of the LP is observed at the hydrate–limestone powder interface.

In contrast, both the FA and FA-SF-SCC cement matrixes showed dense interfaces between the unhydrated fly ash particles and the closest hydration products. For these two types, a CH form growing on the surface of the fly ash particles was deduced as shown in Fig. 5-14 and hence a worthy adhesion with the near hydration products. For

blended cement with the fly ash, Rendell et al.(2002) suggest that two forms of hydration products (CSH+CH) could be formed on the surface of the unreacted fly ash particles.

With further hydration, at 56 days, the analysis of the results (Table 5-3) demonstrated that all types of concrete exhibited micro porosity nature with lower CPDs except in the case of NVC. It is anticipated that the larger micro-pores become occupied by more and more hydration products leading to more, smaller micro-pores and lower CPDs. The significant, and unexpected, result is that the LP-SCC exhibited a 58.3% decrease in the CPD corresponding to the value of 28 days, which is similar to the CPD decrease percentage in the FA-SCC (57.9%) and higher than that of FA-SF-SCC (35.5%). This remarkable reduction might be attributed to the migration of the newly generated hydration products with the continuous curing towards the rough surface of the LP, producing a less diluted matrix. This modification mightnot be related to the chemical activity of this filler type as the chemical analysis of the mortars verified the inability of the LP to enhance hydration.

In general, for SCC, Craeye et al. (2010) showed that the use of different types of filler, including mineral fillers such as FA at the same water to binder ratio, had no significant effect on the CPD of the concrete microstructure at an age of 120 days. This assertion was not tested in this study, but the available data at 56 days still shows slight differences although a noticeable difference had been recorded at 28 days. Thus, indirect support for Craeye et al.'s finding was obtained in this study.

5.4 Tests for micro permeation features of ITZ

5.4.1 Threshold criteria for the segmentation of the constituents of the cement matrix

For the normal cement paste and for the purpose of capillary pores analysis using the BSE images, pixel in the segmented or digitized image has a grey value from zero (dark) to 255(light). The porosity (capillary pores), calcium silicate hydrate CSH, dense inner hydration products DIP, calcium hydroxide CH and unhydrated cement particles can be distinguished from their lower and upper grey levels in the grey value versus number of pixels histogram of a segmented BSE image. These constituents and their threshold criteria are shown in Fig.5-15.

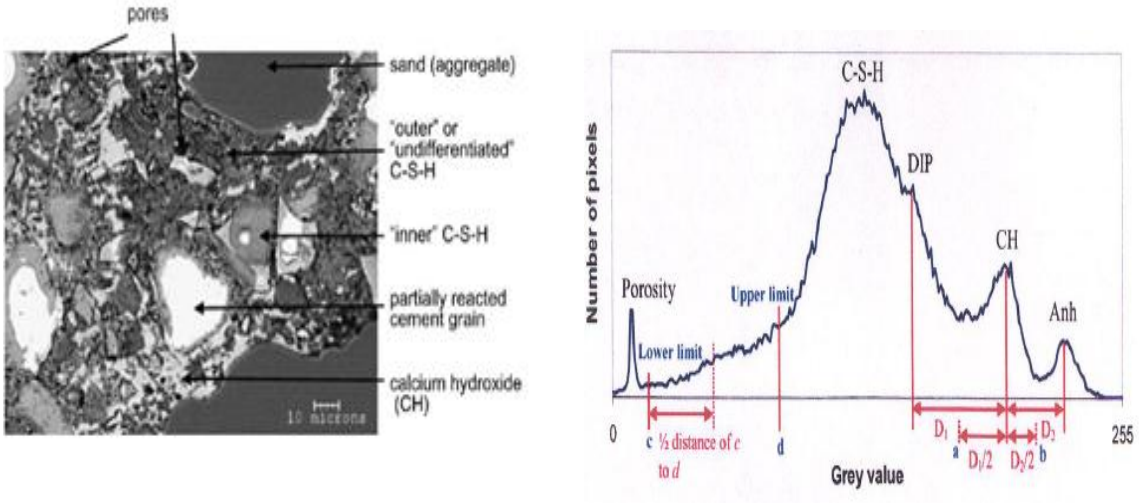

Figure 5-16 cement paste (BSE image) (Scrivener et al., 2004) and the gray levels of constituents (Hemavibool, 2007)

From the grey level histogram, the lower porosity threshold value can be fixed to a zero value (near black). However, the difficulty is how to specify an appropriate upper grey level threshold value for porosity. Many procedures have been proposed such as manual, tangent slope, minimum between peaks, and overflow criterion methods. Any error in defining the exact threshold value might give an under or overestimation of the porosity. However, very recent work has proved the accuracy of the overflow method in determining the appropriate upper grey value for the threshold of capillary pores even with the use of different cementitious material systems (Gao et al., 2013a). Fig. 5-16 shows the application of using different upper porosity threshold values for a single capillary pore of a cement matrix and the determination of the correct upper grey value as a void threshold using the over flow criteria.

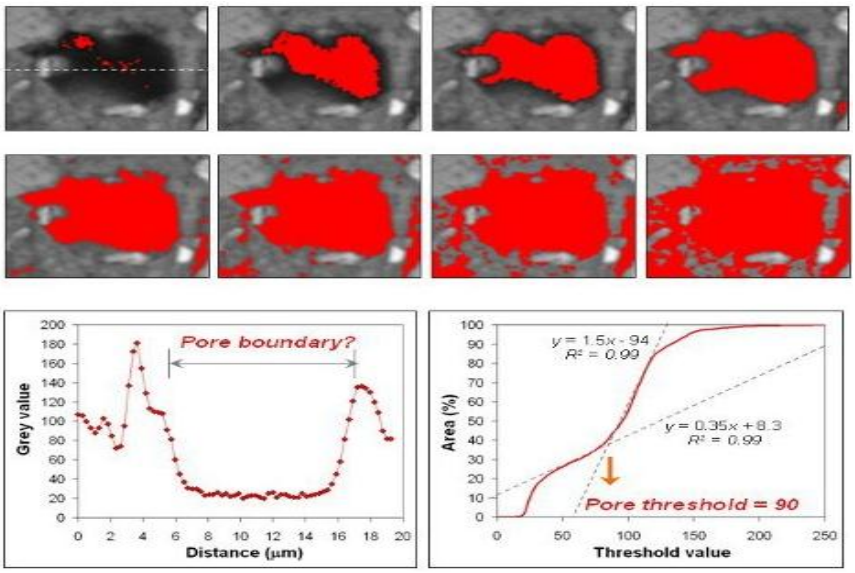

Figure 5-17 Upper threshold value of the single capillary pore in the cement matrix (overflow method) (Wong et al., 2006)

For the ITZ capillary pores (porosity) analysis, an accelerating voltage of 15–25 kV was used to capture the BSE images with a magnification of 500X which is considered the most appropriate enlargement for the cement matrix porosity analysis (Hemavibool, 2007) as shown in Fig. 5-17. The original BSE images were digitized using the Image J program with a size of 712X484 pixels and a scale of 1.18 pixels/µm.

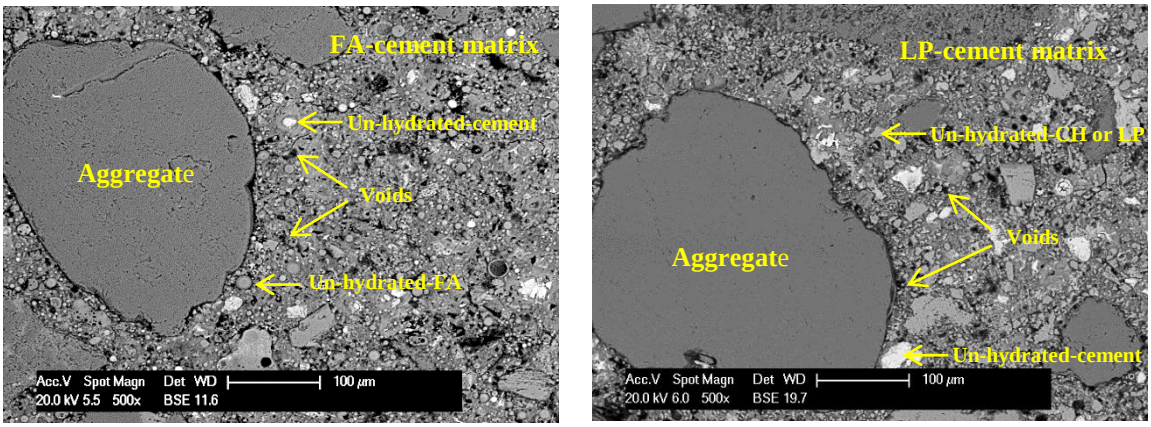

Figure 5-18 examples of original BSE images with 500X magnification of FA and LP-SCC

The ITZ porosity analyses were conducted using duplicated images with a size of 374×254 ± 0.5 pixels with the same original scale in order to keep the same segmented pixels (Fig. 5-18). First, the aggregate was removed manually from the duplicated BSE image and completely changed to white pixels (i.e. the highest grey level 255). Then, the upper threshold grey values were defined for porosity using the overflow method. The average grey values were 80, 70, 50 and 60 for cement, LP, FA and FA+SF paste systems respectively. Finally, the ITZ porosity analysis was conducted in 10 micron wide bands away from the aggregate-cement matrix interface up to a distance of 50 microns as suggested by (Diamond and Huang, 2001) using the defined upper porosity threshold.

Fig. 5-18 shows an example of a duplicated BSE image, defining the upper threshold grey value for the duplicated BSE image and also shows the direction of the ITZ porosity analysis. Eight duplicated images were selected randomly from original BSE images and analyzed for each mix. A T-distribution with a confidence interval of 95% was used to examine the accuracy of the detected porosity of each band. The details of the statistical analysis conducted by the author can be found in **Appendix B**.

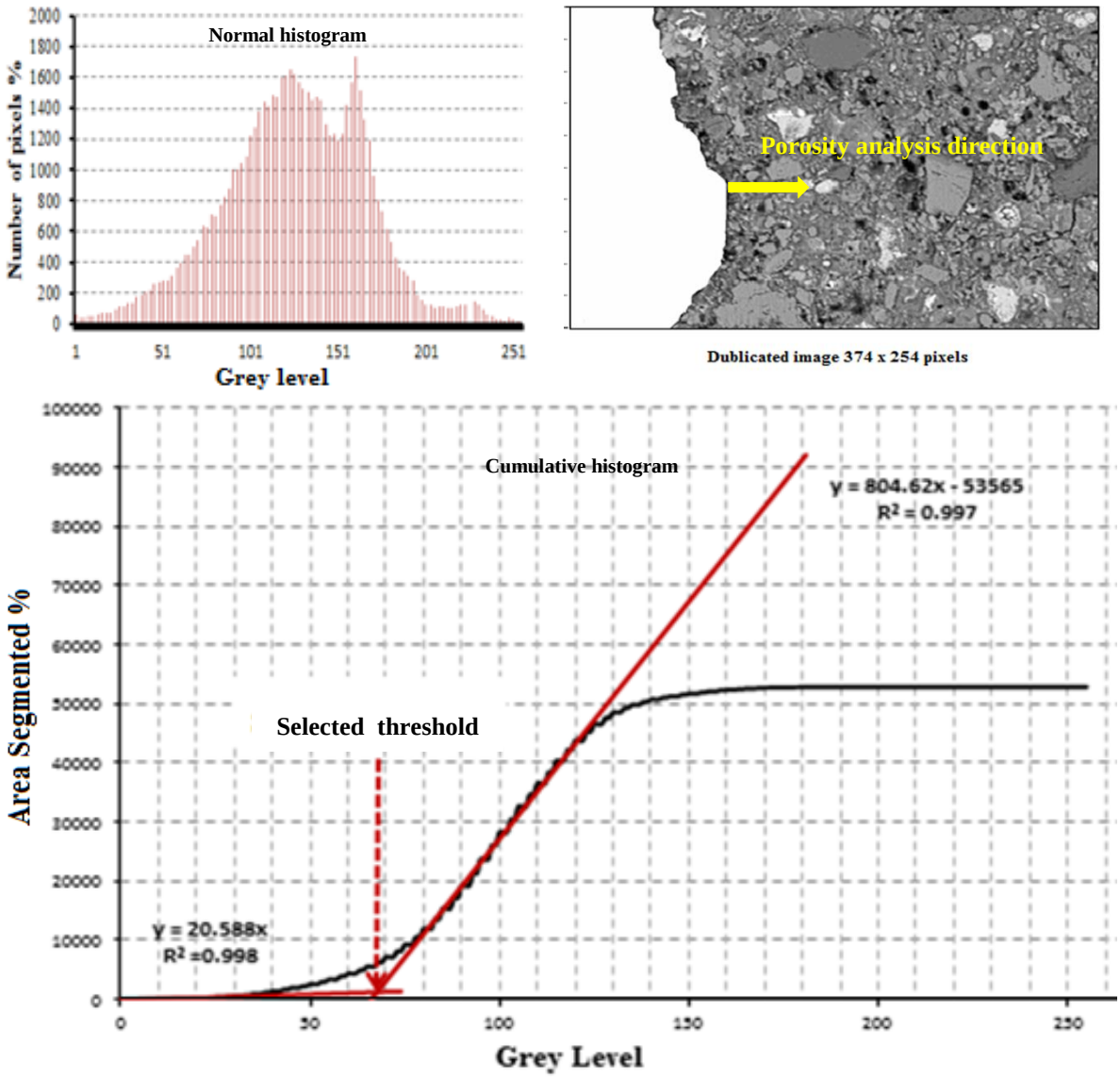

Figure 5-19 The upper threshold value of the capillary pores from a duplicated BSE image (LP-SCC) - (Overflow method)

5.4.2 ITZ-cement paste chemistry

X-ray line spectrum analysis using EDX linked with the SEM as reported by Erdem (2012) was adopted for identifying the hydration products profile in the ITZs and in the cement matrices. However, due to the heterogeneous nature of the ITZ, 3 to 4 lines were scanned and averaged in different areas of the ITZ (3 to 4 lines per different aggregate interface for each mix). This means that the average calculated atomic ratios are derived from an average of 30 to 40 analyzed spot (spectrums) in the ITZ and cement matrix regions. An accelerating voltage of 20 kV was used. The analyses were conducted for at 5µm intervals using magnifications of 3000X. Each line consisted of 14 spectra, 4 in the aggregate and the rest in the ITZ and the bulk cement matrix.

Firstly, the BSE image was rotated using the control software of the Scanning Electron Microscope so that the X-ray line spectrum was selected to be perpendicular to the ITZ. Secondly, an image was captured for the area of interest using the INCA-EDX software. Then, the spectrum line was drawn and the acquisition time for the detection of all elements of each spectrum was set to 60 seconds. This allowed detection along each spectrum in the three lines in approximately 60 to 75 minutes. Finally, ENCA-EDX software was used to assess the proportion of each of the following elements: Ca, Si, Al, S, Fe, Na, Mg, Mn, K and O. However, the oxygen was normalized by the software stoichiometry. These elements were used for the purpose of identifying the main cementitious compounds in the ITZs. An example of the analysis of one line for the R-SCC ITZ and cement matrix is shown in **Fig. 5-19**. The details of the conducted analysis can be found in **Appendix C**.

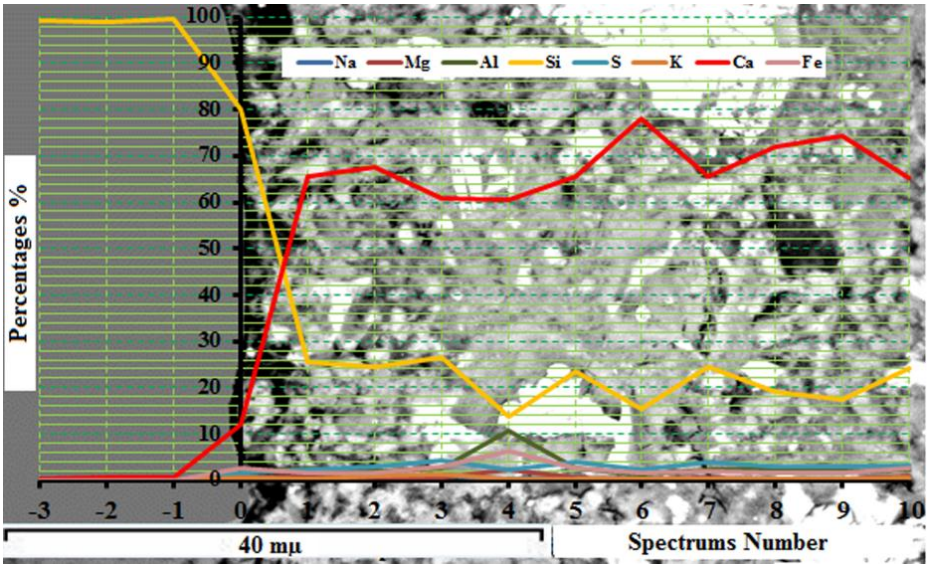

Figure 5-20 Example of X-ray line spectrum analysis (one line analysis for R-SCC)

In order to detect the main composition of the hydrated phases in the ITZ and the bulk cement matrix (C–S–H, CH and AFm), the following criteria were used as reported by several investigations i.e. Rossignolo(2009):

C-S-H $0.8 \leq Ca/Si \leq 2.5$, $(Al+Fe)/Ca \leq 0.2$

CH $Ca/Si \geq 10$, $(Al+Fe)/Ca \leq 0.04$ and $S/Ca \leq 0.04$

AFm $Ca/Si \geq 4.0$, $(Al+Fe)/Ca > 0.4$ and $S/Ca > 0.15$

5.5 Results and discussion

5.5.1 ITZ Porosity and thickness

Fig. 5-20 shows the detected porosity profiles of the ITZs regions for the NVC and the different types of SCC as a function of the distance from the aggregate-cement matrix interface up to 50 µm.

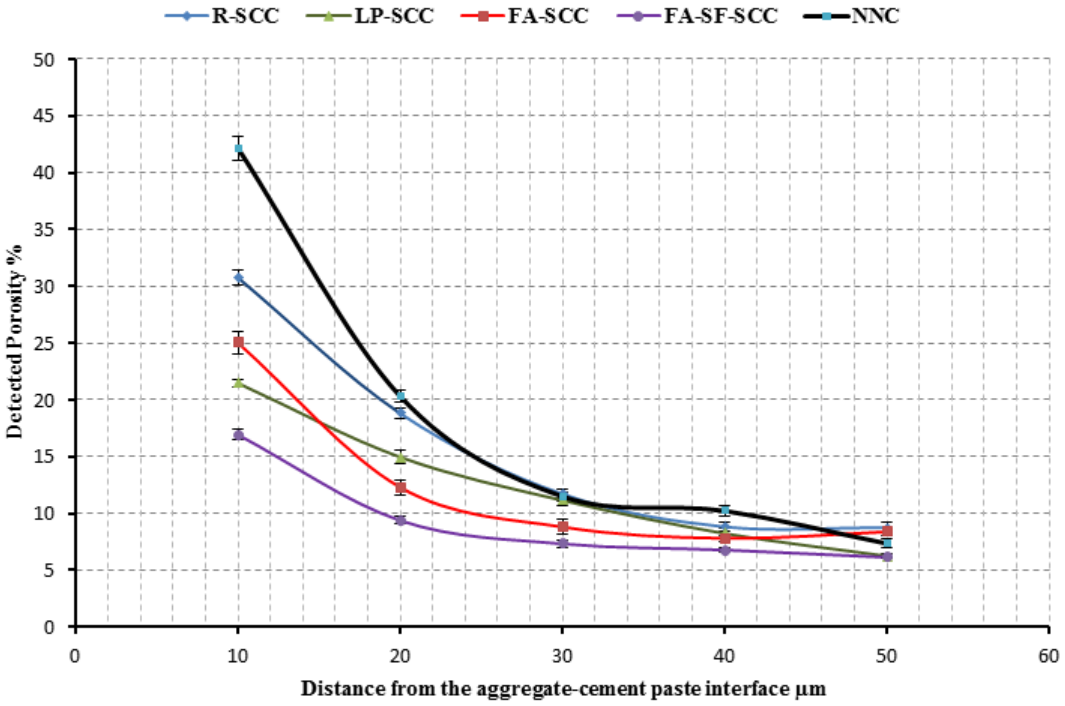

Figure 5-21 ITZs porosity profiles for the NVC and SCC

These curves were used to determine both the approximate thickness and the porosity of the ITZs. The exact determination of the ITZ thickness is so difficult and not straightforward as several investigations proposed different methods (Ollivier et al., 1995, Leemann et al., 2010, Gao et al., 2013b). In this study, the ITZ was defined as the region from the aggregate-matrix interface until the detected porosity was the same as that of the bulk cement matrix. The porosity of the bulk cement matrix was defined as the average porosity of the matrix from 50µm away from the aggregate until the end of the used duplicated BSE image. The analysis was performed using the T-distribution statistical analysis (Mohammed et al., 2013).

In general, the analysis showed that all the deduced ITZ -thicknesses were less than 30 µm for the SCC including that made with normal Portland cement (R-SCC). This is

much less than those deduced for the NVC (approximately 36 µm). They were approximately 19.9 µm, 27.5 µm, 18.5 µm and µm 15 µm for R, LP, FA and FA-SF self-compacting concretes respectively. Had the genuine ITZ thickness been greater than 50 µm this approach would not have been possible; happily this was not the case. Olivier et al.(1995) stated that the typical thickness of the ITZ region is about 50 µm for an OPC matrix in NVC. However, the absence of vibration as in SCC, could play an essential role at a microscopic scale in reducing the volume of the localized water around the aggregate surface (Leemann et al., 2006). Beside the low water content, this might explain the small thicknesses of the ITZ for all investigated types of SCC.

Recently, (Leeman et al. 2010) demonstrated an ITZ thickness between 37 and 50 mµ for SCC containing different types of cement, whereas the ITZ thicknesses determined in the present study are noticeably smaller. However, they defined the ITZ as the zone near the aggregate–matrix interface where the measured porosity is more than 15% greater than the average of the bulk paste (assessed beyond 70 µm) as well as using different binder types.

Nevertheless, relative to the R-SCC without cement replacement, the FA and FA-SF-SCC exhibited approximately similar or slightly smaller ITZ thicknesses respectively. A higher amount of anhydrous cement was observed beyond the ITZ thickness of the R-SCC (Fig. 5-19) indicating a higher local (ITZ) water to cement ratio which reduced the effective water content outside the ITZ leading to incomplete cement grain hydration. Thus, a higher ITZ thickness might be expected. It was already supposed by Laugesen (1993) quoted by Scrivener and Nemati(1996) that the difference in the amount of anhydrous cement in the bulk cement paste and the ITZ could be produced by the differences in the amount of water adhering to the aggregate surface. However, the increase in ITZ thickness in the case of using LP as a partial replacement of cement, relative to the other three mixes, could suggest a “dilution” effect provided by the large LP unreactive grains in the ITZ and the entrapped water between these grains. Also the presence of high amounts of CH or unreactive LP and the lack of sufficient CSH gels in this region was deduced for this type of SCC as explained in the nest section.

ITZs porosities between 14.5-25 % were deduced for the investigated normal and sustainable SCC with the detected ITZ thicknesses while the value was 31% for the NVC

ITZ. The higher ITZ porosity for the NVC might be as a result of the high localized water near the aggregate surface caused by internal water bleeding due to the vibration used. The higher water to the cement ratio adopted for the NVC might be responsible for the higher internal bleeding.

Although the same water to binder ratio was used for all the SCC mixes, the use of different types of fillers and mineral admixtures at high cement replacement percentages has generated different ITZ porosities. This may attributed to both a physical filling effect and the chemical activity of the used fillers and mineral admixtures. The R-SCC presented the highest ITZ porosity as compared with the other SCC mixes and this might be related to the inability of the resulting hydration products to achieve good packing due to the deduced high ITZ local water as explained in earlier.

Generally, the high porous nature of the ITZ might be related to the inability of the anhydrous cement grains to pack very well with the smooth surface of the aggregate due to the wall effect (Ollivier et al., 1995). This concept might be different when reactive and non-reactive fillers are used perhaps reducing the ITZ localized water and increasing the localized packing. However, the inability of the resulted hydration products to achieve a complete packing with the aggregate boundary might generate a porous interface. Therefore, the deduced ITZ-porosities using the image analysis were supported by an examination of the chemistry of the hydrous phases in the ITZ.

The slight reduction in the ITZ porosity for the FA-SCC relative to R-SCC might indicate the inability of the FA to improve the ITZ chemistry. In contrast, FA-SF-SCC showed lower ITZ porosity relative to the FA-SCC. This suggests that the reduction of the ITZ porosity may be as a result of the combined filling effect of the very fine grains of SF improving the packing ability of the cement particles near the aggregate surface and the modification of the chemical composition. The chemical analysis of the ITZs in the next section showed a substantial modification in the chemistry of the ITZ especially in the FA-SF-SCC.

5.5.2 ITZ-cement matrix hydration products profiles

Figs. 5-21 to 5-25 display the distribution of Ca/Si, Al + Fe/Ca and S/Ca ratios for the NVC and the different types of SCC at the 14 points in Figs. 5-19.

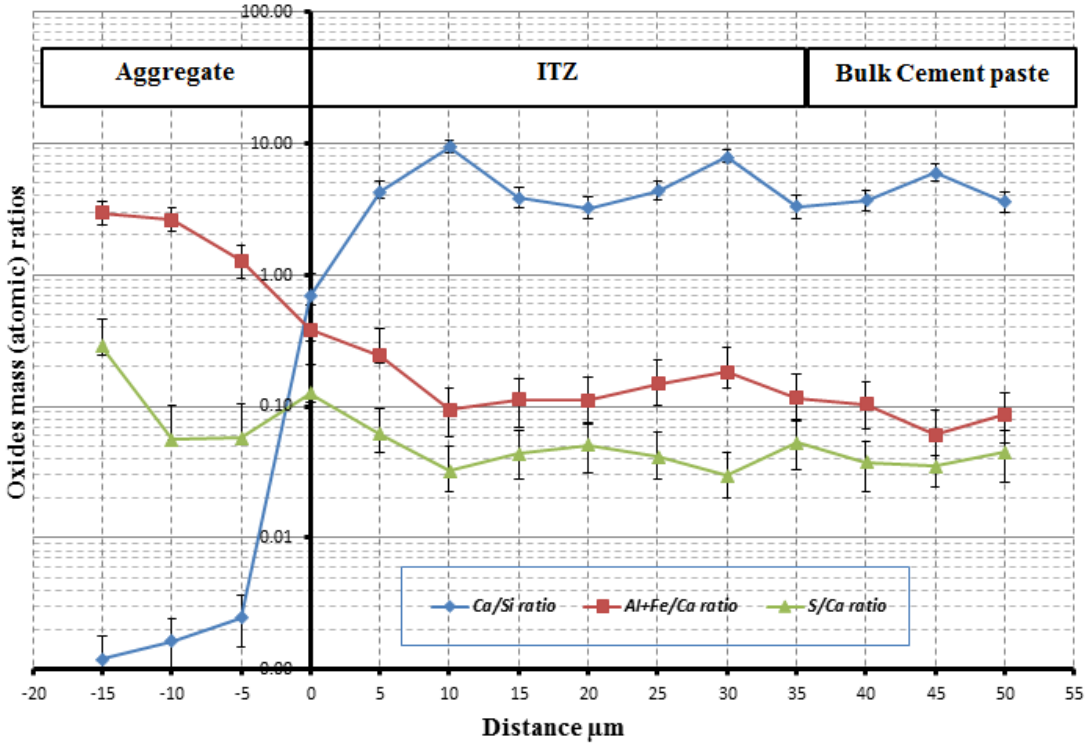

Figure 22 Atomic ratio distributions of the hydrous phases in the ITZ and bulk cement matrix (NVC)

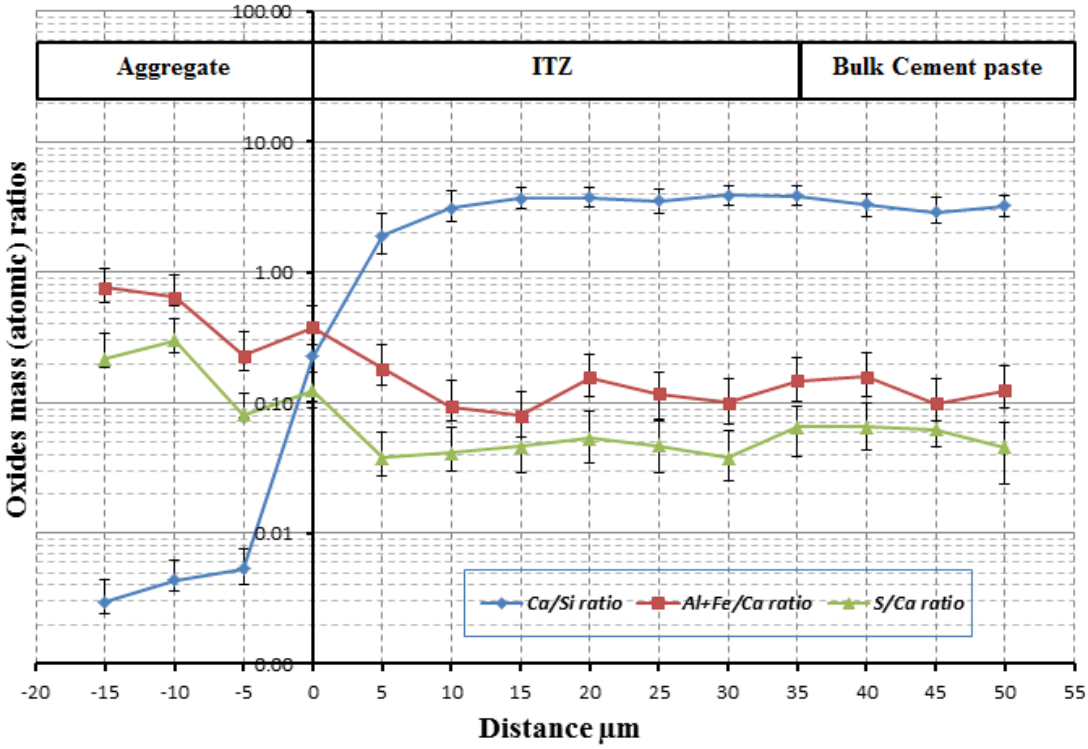

Figure 5-23 Atomic ratio distributions of the hydrous phases in the ITZ and bulk cement matrix (R-SCC)

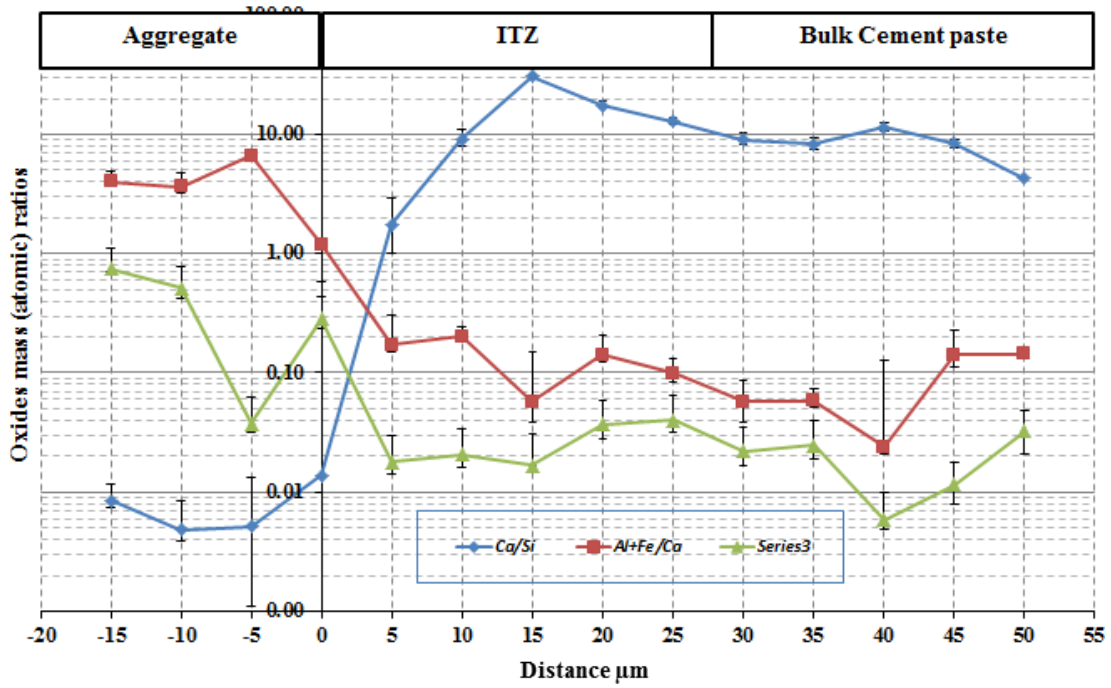

Figure 5-24 Atomic ratio distributions of the hydrous phases in the ITZ and bulk cement matrix (LP-SCC)

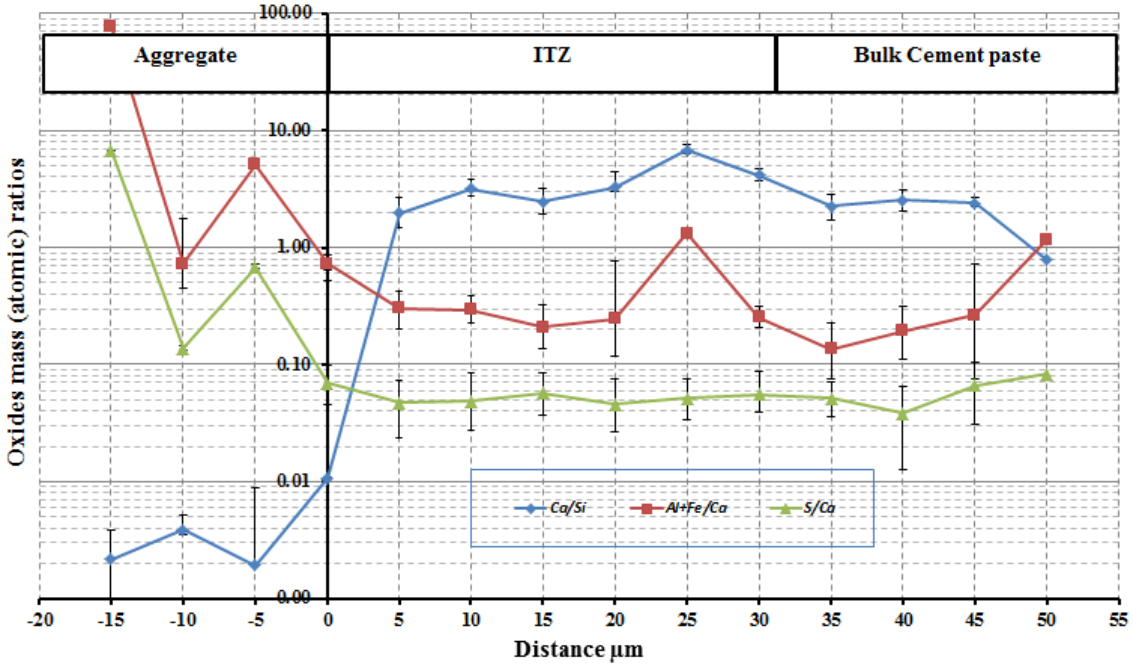

Figure 5-25 Atomic ratio distributions of the hydrous phases in the ITZ and bulk cement matrix (FA-SCC)

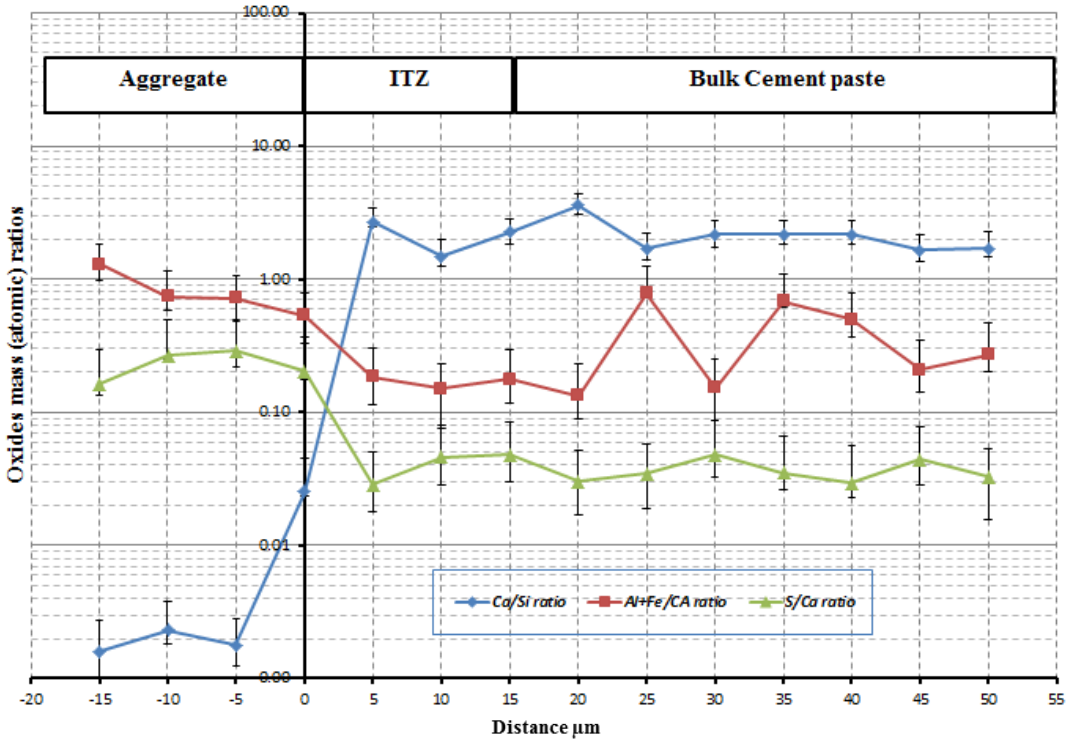

Figure 5-26 Atomic ratio distributions of the hydrous phases in the ITZ and bulk cement matrix (FA-SF-SCC)

According to the criteria used for identifying the main hydrous phases in the ITZ and the cement matrix (Rossignolo, 2009), the distribution of Al + Fe/Ca and S/Ca atoms ratios indicated there was an insignificant amount of Ettringite (AFm) both in the ITZs and in the cement matrices. Thus, the discussion will be based on the differences between the Ca/Si ratios only. For the chemical analysis only (calculating the average values of the atomic ratio in the ITZs and the cement matrices as shown in Table 5-5), the ITZ was defined as the region until the point where the Ca/Si ratio decreased below the value of 2.5 signifying the formation of CSH gel in accordance to the criteria in section 5.3.1. However, for both NVC and LP-SCC, the ITZ thickness was defined from the image analysis alone since the Ca/Si ratio exceeded 2.5 even beyond 50 µm. The higher deduced Ca/Si ratio in the ITZs of both NVC and LP-SCC signifies the presence of significant CH amount or unreacted LP grains in the case of LP-SCC ITZ. It has previously been reported that the orientation of the large hexagonal crystals of CH in the ITZ might give it a more porous structure (Ollivier et al., 1995). However, it should be emphasized that the EDX analyzer has real difficulties in differentiating between $Ca(OH)_2$ and $CaCO_3$. It was stated by Lawrence (2006) that it is difficult to distinguish between these two compounds in EDX analysis since the only differences between them

are carbon (atomic weight 12) and hydrogen (atomic weight 1). Such lighter elements are less readily detected by the EDX analyzer due to their small atomic weights as compared with oxygen (16). Therefore the analysis can give an over-estimation of the Ca/Si ratio resulting in apparently large amounts of CH in this region. Consequently, a semi-quantitative EDX analysis could be considered for the LP-SCC.

The average detected Ca/Si values, the upper and lower limits in Table 5-5 obtained from the standard deviation about the mean values of about 30 to 40 analyzed spot in both the ITZ and cement matrix of each mix type were adopted to determine the accuracy of the results in both the ITZ and the cement matrix.

Table 5-5 Average Ca/Si ratio in the ITZ and cement matrix (CM)

Mix ID	NVC	R-SCC	LP-SCC	FA-SCC	FA-SF-SCC
Upper limit	6.04	3.68	19.1	4.6	3.1
Average Ca/Si ratio- ITZ	**5.2**	**3.40**	**14.43**	**3.63**	**2.08**
Lower limit	4.27	3.12	9.74	2.63	1.1
Upper limit	5.01	3.38	9.8	2.2	2.46
Average Ca/Si ratio- CM	**4.38**	**3.16**	**8.285**	**1.99**	**2.17**
Lower limit	3.73	2.93	6.77	1.7	1.88

The ITZ's close up views in Fig. 5-26 indicated the lack of the CSH gel and the agglomeration of the hexagonal CH crystals for the NVC and the dilution that caused by the agglomeration of un-reacted coarser and angular LP particles. The finer and more spherical shapes of the small FA and SF particles might reduce this effect for the other two types of sustainable SCC. As reported by (Praveen and Kaushik, 2004), the presence of un-reacted particles of pozzolanic material in the ITZ of the SCC is not harmful compared to that of un-reacted/partially reacted particles of cement.

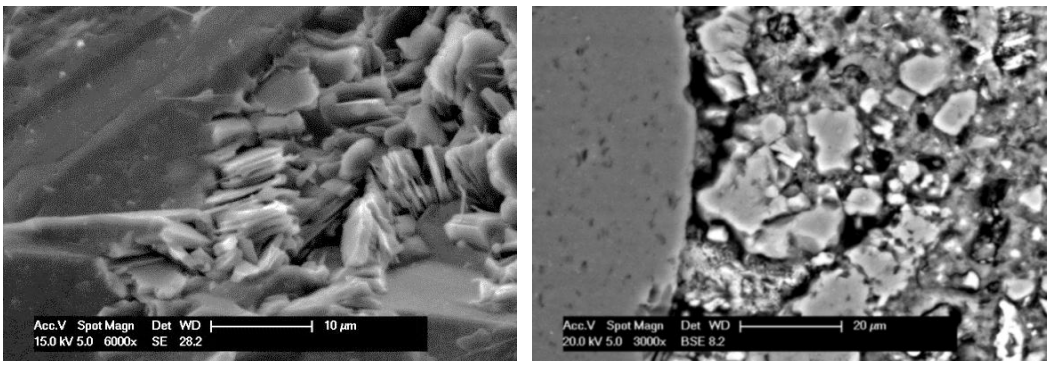

Figure 5-27 the agglomerations of CH and CH or LP in the NVC and LP-SCC ITZs

On the other hand, the analysis showed that the average Ca/Si ratio in the ITZ of the FA-SCC was greater than that which identifies the presence of CSH gel demonstrating a presence of considerable amount of CH. However, the ITZ of the FA-SCC showed a lower ITZ porosity than that of R-SCC and this may be due to the microstructural packing effect of the small spherical particles of FA. As reported by Zhang et al. (1996), the packing state might be affected by the addition of pozzolans and decrease the amount of water that is needed for void filling and this might depend on the grain size of the pozzolanic material. This proposes that the chemical improvement of the ITZ microstructure due to the high replacement of cement by FA may be attributed to the filling effect of the small particles of the FA only. However, it is known that the amorphous silica in the pozzolanic materials can consume the CH in the presence of water and produce another form of CSH gel or, at the least; it can change the orientation of the CH crystals (Zhang et al., 1996). Consequently, further microstructure development may occur. The chemical activity of the FA due to the amorphous silica detected by the XRD spectra means that full modification of the paste in this region will take longer than 28 days, hindering a full comparison with the normal SCC in which hydration will be largely complete by that time.

The chemical analysis also indicated that incorporation of the combined partial replacement of cement by SF+FA led to the formation of an extraordinary quantity of CSH gel in the ITZ where the detected Ca/Si ratio was less than 2.08%. This may explain the lower detected ITZ thickness and lower porosity in this type relative to the other mixes. It is believed by Larbi (1991) that the modification of the internal structure of the ITZ by the addition of the silica fume (only) as a partial replacement of cement may be related to the high ability of this reactive material to consume the CH amount closer to the aggregate interface. According to Scrivener et al.(2004), the addition of fine particles like SF is considered one of the most active methods to develop a dense ITZ by increasing the packing closer to the aggregate surface also.

In order to give a wide picture to each assessment presented in this chapter and the combined results obtained from the different used techniques, the relative values of the results obtained and the possible suggestions are summarized all together in Tables 5-6 to 5-8.

Table 5-6 Relative values of degree of hydration (28-days)

Cement matrices							
Mix ID / Property	NVC	R-SCC	LP-SCC	FA-SCC	FA-SF-SCC	Evidence	Comment
Degree of hydration CH% content	Low with High CH content	Low with High CH content	Moderate with High CH content	High with Low CH content	High with Low CH content	XRD ,TGA and SEM analysis	Section 5-2 and 5-3
Presence of CSH	Ca/Si=4.38 Low CSH content	Ca/Si=3.16 Low CSH content	Ca/Si=8.29 Low CSH content	Ca/Si=1.99 high CSH content	Ca/Si=2.17 high CSH content	EDX analysis	Section 5-5

Table 5-7 Relative values of pore structure (28-days)

Internal pore structure features at different scales							
Mix ID / Property	NVC	R-SCC	LP-SCC	FA-SCC	FA-SF-SCC	Evidence	Comment
Porosity % Macro/Micro	31.2 (Macro)	21.1 (Macro)	14.7 (Micro)	14.1 (Micro)	12.2 (Micro)	Vacuum saturated and MIP	Section 5-3
Pores features Nano scale (nm)	CPD/APD 60/79.4	CPD/APD 39/84	CPD/APD 60/88	CPD/APD 38/71	CPD/APD 31/75	MIP	Section 5-3

Table 5-8 Relative values ITZ micro-permeation properties (28-days)

ITZ micro-permeation properties							
Mix ID / Property	NVC	R-SCC	LP-SCC	FA-SCC	FA-SF-SCC	Evidence	Comment
ITZ porosity %	High 31	Rather high 25	Low 16.8	Low 19.4	Very low 14.5	Image and EDX analysis	Section 5-5
ITZ thickness (µm)	Thick 36	Thin 19.9	Rather thick 27.5	Thin 18.5	Very thin 15	Image and EDX analysis	Section 5-5
ITZ chemistry	Ca/Si=5.2 high CSH content	Ca/Si=3.40 Intermixed (CH+CSH)	Ca/Si=14.43 Intermixed (CH+CSH)	Ca/Si=3.63 Intermixed (CH+CSH)	Ca/Si=2.08 high CSH content	EDX analysis	Section 5-5

5.6 Concluding remarks

Based on the results presented in this chapter, the following general concluding remarks could be drawn:

- The higher water to cementitious material ratio for the NVC at the same strength level of the SCC without any cement replacement (R-SCC) had more bearing on the micro permeation features of the ITZ than the degree of hydration of the cement matrix. This might suggest the role of the internal water bleeding caused by the applied vibration for the NVC. However, it produced a dual-model to the pore structure by generating a second peak in the divertive of the intrusion mercury curve adjacent to 10 micron as compared to mono-model one of the all other types of SCC at the nano scale.

- In spite of the high cement replacement and the presence of high amounts of unreacted mineral fillers particles for the sustainable SCC made with FA and FA+SF additions, a higher degree of hydration and of refinement of the pore

structure are achieved. The lower cement matrix pores percolation at the nano scale, represented by the lower deduced CPDs of the cement matrix, might be related to the interaction and the wall adhesion of the unhydrated filler particles and the other hydration products.

- The combined microstructural and hydration studies suggest a dilution effect for both the cement matrix and the ITZ of the LP-SCC at high partial cement replacement. Therefore, it is believed that this effect might be responsible for producing a less dense ITZ and more porous nature of the SCC in general with a high probability of capillary pore interconnection in the cement matrix.
- The higher amount of CH in the LP-SCC detected by the TGA test, due to the dehydroxylation of CH and that detected by the XRD analysis, gave an indication of the accelerating effect of LP on the hydration process of C_3S in cement. However, no chemical enhancement of the cement matrix or the ITZ was deduced.

- The fairly good correlation between the results of the dehydration of the CH in the TGA curves and the detected reference peaks of CH from the XRD analysis might indicate that the degree of the hydration of the NVC and SCC containing different types of binder is related to the dehydration reaction of the CH in the TGA curves rather than the assessed total amounts of CH (dehydration plus de-carbonation reactions).

- For the sustainable SCC with high cement replacement, the ITZ micro characteristics for the investigated SCCs suggest that the use of a low water to binder ratio might offer a primary explanation for the ITZ thicknesses. However, the use of different fillers and mineral admixtures as a partial replacement of cement delivered a different microstructure nature for the ITZs. Therefore, it could be suggested that this variation in the ITZ features is governed by both the reactivity of the filler or the mineral admixtures as well as their particle sizes and surface geometrical appearances.

- In general, compared to the R-SCC, the LP addition was not able to achieve a noticeable improvement for the internal microstructure of the SCC in terms of cement matrix hydration, pore structure as composite material and ITZ

characteristics. Reasonable improvement was deduced for the FA addition while a substantial improvement of the ITZ has been deduced in the case of the combined cement replacement with SF. However, and not as expected, a slight reduction in the degree of hydration was deduced for the later addition (Tables 5-6 to 5-8).

5.7 References

ASSIE, S., ESCADEILLAS, G. & WALLER, V. 2007. Estimates of self-compacting concrete 'potential'durability. Construction and Building Materials, 21, 1909-1917.

BASSUONI, M. & NEHDI, M. 2009. Durability of self-consolidating concrete to different exposure regimes of sodium sulfate attack. Materials and Structures, 42, 1039-1057.

CRAEYE, B., DE SCHUTTER, G., DESMET, B., VANTOMME, J., HEIRMAN, G., VANDEWALLE, L., CIZER, Ö., AGGOUN, S. & KADRI, E. 2010. Effect of mineral filler type on autogenous shrinkage of self-compacting concrete. Cement and Concrete Research, 40, 908-913.

DESMET, B., SERRANO, J. H., WILLAIN, L., VANTOMME, J., FEYS, D., DE SCHUTTER, G., ELSEN, J., CIZER, Ö., HEIRMAN, G. & VANDEWALLE, L. 2011. Porosity determination of self-compacting concretes using combined forced saturation.

DIAMOND, S. & HUANG, J. 2001. The ITZ in concrete–a different view based on image analysis and SEM observations. Cement and Concrete Composites, 23, 179-188.

ERDEM, S. 2012. Impact Load-Induced Microstructural Damage of Concrete Made with Unconventional Aggregates. PhD thesis, University of Nottingham, Department of Civil Engineering.

GAO, Y., DE SCHUTTER, G., YE, G., HUANG, H., TAN, Z. & WU, K. 2013a. Porosity characterization of ITZ in cementitious composites: Concentric expansion and overflow criterion. Construction and Building Materials, 38, 1051-1057.

GAO, Y., DE SCHUTTER, G., YE, G., YU, Z., TAN, Z. & WU, K. 2013b. A microscopic study on ternary blended cement based composites. Construction and Building Materials, 46, 28-38.

GOMES, J. P. D. C. 1997. Mathematical models for assessing hydration and microstructure of cement paste. PhD, University of Leeds.

HEMAVIBOOL, S. 2007. The microstructure of synthetic aggregate produced from waste materials and its influence on the properties of concrete. PhD, University of Leeds.

LARBI, J. A. 1991. The cement paste-aggregate interfacial zone in concrete. Technische Universiteit Delft.

LAWRENCE, R. 2006. A study of carbonation in non-hydraulic lime mortars. PhD, University of Bath.

LEEMANN, A., LOSER, R. & MÜNCH, B. 2010. Influence of cement type on ITZ porosity and chloride resistance of self-compacting concrete. Cement and Concrete Composites, 32, 116-120.

LEEMANN, A., MÜNCH, B., GASSER, P. & HOLZER, L. 2006. Influence of compaction on the interfacial transition zone and the permeability of concrete. Cement and Concrete Research, 36, 1425-1433.

MALAB, S., BENAISSA, A., BOUDRAA, S. & AGGOUN, S. 2009. Drying kinetics of self-compacting concrete. Turkish J. Eng. Env. Sci, 33, 135-145.

MOHAMMED, M. K., DAWSON, A. R. & THOM, N. H. 2013. Production, microstructure and hydration of sustainable self-compacting concrete with different types of filler. Construction and Building Materials, 49, 84-92.

NEVILLE, A. M. 2011. Properties of Concrete, London, Pearson Education Limited.

OLLIVIER, J., MASO, J. & BOURDETTE, B. 1995. Interfacial transition zone in concrete. Advanced Cement Based Materials, 2, 30-38.

PRAVEEN, K. & KAUSHIK, S. K. 2004. Transition zone in self compacting concrete. Indian concrete journal, 78, 59-65.

RENDELL, F., JAUBERTHIE, R. & GRANTHAM, M. 2002. Deteriorated concrete: inspection and physicochemical analysis, Thomas Telford Services Ltd.

ROSSIGNOLO, J. A. 2009. Interfacial interactions in concretes with silica fume and SBR latex. Construction and Building Materials, 23, 817-821.

SCRIVENER, K. L., CRUMBIE, A. K. & LAUGESEN, P. 2004. The interfacial transition zone (ITZ) between cement paste and aggregate in concrete. Interface Science, 12, 411-421.

SCRIVENER, K. L. & NEMATI, K. M. 1996. The percolation of pore space in the cement paste/aggregate interfacial zone of concrete. Cement and Concrete Research, 26, 35-40.

SHAFIQ, N. & NURUDDIN, M. F. 2011. Degree of hydration of OPC and OPC/Fly ash paste samples conditioned at different relative humidity. International Journal of Sustainable Construction Engineering and Technology, 1, 47-56.

SHI, X., XIE, N., FORTUNE, K. & GONG, J. 2012. Durability of steel reinforced concrete in chloride environments: An overview. Construction and Building Materials, 30, 125-138.

SYED ALI RIZWAN. 2006. High performance mortars and concrete using secondary materials. Dr.-ING, Technical University Bergakademie Freiberg.

WONG, H., HEAD, M. & BUENFELD, N. 2006. Pore segmentation of cement-based materials from backscattered electron images. Cement and Concrete Research, 36, 1083-1090.

YE, G., LIU, X., DE SCHUTTER, G., POPPE, A. M. & TAERWE, L. 2007. Influence of limestone powder used as filler in SCC on hydration and microstructure of cement pastes. Cement and Concrete Composites, 29, 94-102.

ZHANG, C., WANG, A., TANG, M. & LIU, X. 1996. The filling role of pozzolanic material. Cement and Concrete Research, 26, 943-947.

ZHIJUN, T. 2012. Microstructure development of limestone blended cement [Online]. Available: http://www.cementscience.com/2012/06/microstructure-development-of-limestone-blended-cement.html [Accessed 04-01 2013].

Chapter 6:
Carbonation evaluation and its impact on the microstructure and service life under accelerating test

6.1 General

Carbonation of concrete is considered one of the major concrete durability problems especially with the continuous increase of CO_2 concentration in the atmosphere. Traditionally, carbonation is of concern due to its ability to reduce the service life by allowing the initiation of corrosion of embedded steel due to the neutralization of the pH value of the cement matrix as explained earlier in Chapter 3.

For medium to high strength NVC and SCC exposed to aggressive carbonation environments, there is a lack of information from a practical point of view about actual carbonation, especially for SCC, due to the relatively young age of actual structures. Recently, several laboratory studies have been performed to investigate the durability characteristics of SCC including the effects of carbonation. The most common approach has been to compare the carbonation penetration rate between SCC and NVC in different strength grades or to study the effect of the concrete age on the carbonation resistance using different cementitious materials and water contents. However, under aggressive carbonation conditions (high humidity and high concentration of CO_2), the concrete used should have an adequate strength level with a low water to cement ratio (medium to high strength structural concrete) and a minimum steel cover (to resist the degradation caused by steel corrosion promoted by carbonation) so as to provide a long service life span.

Based on the previous experimental works conducted by several researches work which were presented in Chapter 3, the results relating to the carbonation of SCC relative to the NVC are a subject of controversy. This may be due to both the differences in the chemical composition and microstructure and the fact that the carbonation in concrete is a physicochemical process. The following question may be asked: *which has the dominant effect on carbonation propensity in mature NVC and on sustainable SCC with a high rate of cement replacement: the chemical composition of the concrete represented by the CH content of the cement matrix or its pore system?* In addition, how does the

carbonation change the pore distribution, the microstructure and the chemistry of the NVC and the self-compacting concrete (SCC) with relatively high strength levels after complete carbonation? From a perspective of long-term durability in such modern types of concrete (high performance sustainable SCC), the impact of carbonation on the concrete microstructure (including the pore structure and its chemistry) may prove to be irrelevant when using different reactive and non-reactive filler materials. This is because their impact on the carbonation (due their modification of the microstructure and chemistry of the concrete) may be much more significant.

In the previous chapter, the results demonstrated that the use of different binder system in order to obtain medium strength NVC and SCC have an essential impact on the chemistry and the internal microstructure of the concrete produced in terms of the pore structure characterization, at macro/micro and nano scales, including the micro-permeation features and the chemical composition of the ITZs. In order to establish a link between the previous results, the carbonation progress, its impact on both the microstructural features and its impact on the service life of the concrete mixture, the work presented in this chapter can be classified into three main parts:

- Equipment modifications for an accelerated carbonation test with 100% CO_2 concentration to examine the carbonation process for the normal, high performance and sustainable SCC over a practical time-frame.
- Evaluation of the carbonation progression of the concrete/mortar to deliver a deep understanding of the role of the chemical composition and the microstructural features on the carbonation progression and prediction of the actual carbonation rates and depths.
- Examination of the microstructural impact of the carbonation on the pore structure at macro/micro and nano scales and the associated change in the chemistry of the hydration products in the cement matrices. Simulating long term exposure in a quantitative manner, taking into account the microstructural and chemical issues.

6.2 Equipment development for carbonation accelerating test

6.2.1 Review of accelerated carbonation techniques with low and high concentration of CO_2

It is well known that carbonation is a very slow process in concrete, especially in HPC. It may take a very long time to occur. Therefore, the use of accelerated carbonation becomes necessary for most concrete researchers investigating this topic. Accelerated carbonation testing is crucial to accelerate the very slow reaction between CO_2 from the atmosphere and the hydration products in the cement matrix.

The BS EN 13295 standard (BS EN 13295, 2004) recommends use of (4 ± 0.5)% by volume of carbon dioxide concentration, a temperature of (20 ± 2)° C and relative humidity of (55 ± 5)% for the evaluation of the carbonation depth. Other standards propose similar conditions. Nevertheless, accelerated carbonation tests have been utilized by many researchers using different CO_2 concentrations and relative humidity. This is in order to investigate the carbonation process, to compare carbonation rates of different types of cementitious materials, to predict the actual carbonation rate and to study the effect of this phenomenon on the microstructure of the concrete.

For low concentrations of CO_2, Roy et al. (1999) stated that the use of 6% CO_2 concentration with five different humidity levels in the accelerated carbonation test should increase the carbonation rate (K) ten times compared to those obtained from normal exposure (considering 0.06% as the concentration of CO_2 in the natural environment). This is suggesting that K is approximately proportional to the square root of CO_2 concentration. Fig 6.1 shows their laboratory setup for the accelerated carbonation test.

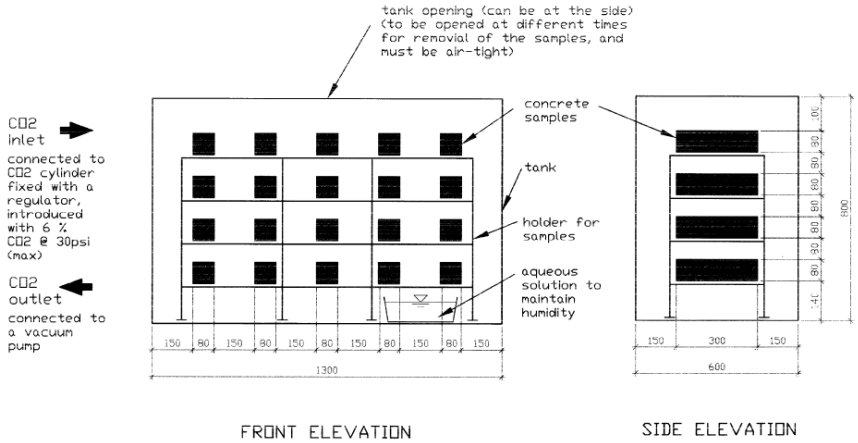

Figure 6-1 Laboratory setup for an accelerated carbonation test Roy et al. (1999)

Atiş (2003) concluded that a long curing time leads to a reduction in the carbonation depth of high performance fly ash concrete under accelerated carbonation. His accelerated test was started at different curing ages 3,7,28 and 90 days for different high levels of FA cement replacement. A 4.70% CO_2 concentration at 1 bar above ambient and 65% relative humidity was used for the proposed accelerated test (Fig 6.2). The author found that a concrete with low potential for carbonation could be produced with less than 50% replacement of fly ash, and that the use of superplasticizer in the produced HPC did not affect the carbonation depth.

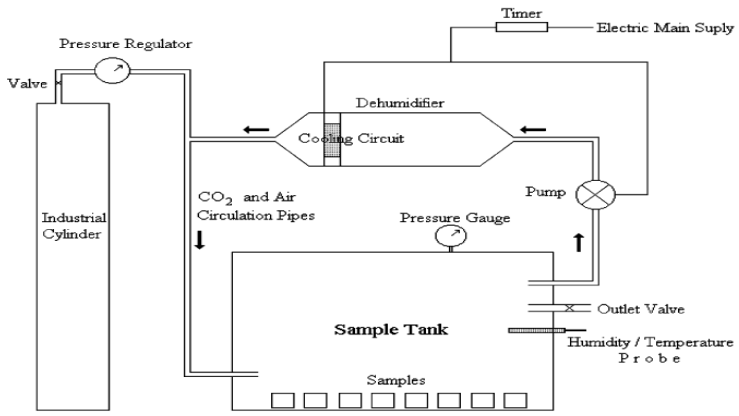

Figure 6.2 schematic diagram of the accelerated carbonation testing set-up Atiş (2003)

As reported by Khunthongkeaw et al. (2006), from a practical point of view, it is advantageous to estimate the carbonation depth in the natural environment from accelerated tests. The temperature and the relative humidity inside their carbonation chamber were controlled at 40ºC and 55%, respectively. However, no information has been provided by the authors about the accelerated chamber used and its operating system. They obtained a strong relationship between the accelerated carbonation depth (with 4% CO_2 concentration) and the depth observed in the natural environment. In this study the authors proposed a mathematical method to predict the actual carbonation depth based on a square root time relationship (discussed further in Section 6.4).

Chang and Chen (2006) used different advanced techniques (TGA, XRD and Fourier transformation infrared spectroscopy (FTIR)) to examine concrete carbonation depths. An accelerated carbonation test subjected the concrete specimens to carbonation for 8 and 16 weeks after 28 days curing at 70% relative humidity, 23ºC and 20% CO_2 by volume. There was no information about the test equipment in this study. However, the

authors suggest that in general, the depth of carbonation detected using phenolphthalein indicator was twice that determined by the other used techniques. In addition, the XRD analysis demonstrated the complete absence of CH crystals for the fully carbonated zone as compared to the uncarbonated and partially carbonated areas Fig 6.3.

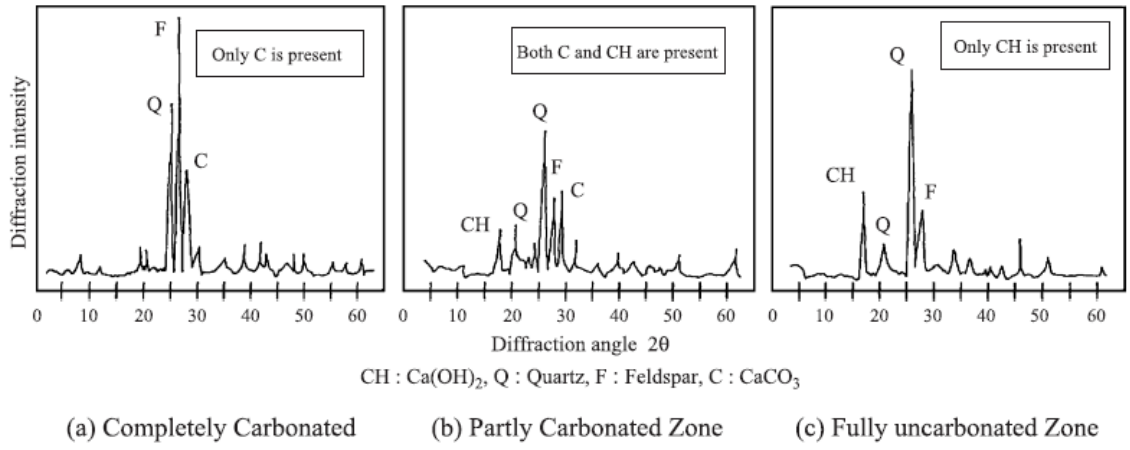

Figure 6.3 Results of accelerated carbonation test assessed by X-ray diffraction (Chang and Chen 2006)

Recently, Ji et al. (2010) have examined the validity of using high CO_2 concentrations in order to compare the carbonation process of the concrete with the natural environment using the XRD and TGA techniques at 20% of CO_2 with a relative humidity of 70 % and 20º C temperature. The accelerated carbonation experiments were performed in a fully controlled testing room in the carbonation laboratory at the China University of Mining Technology. They concluded that it was acceptable to simulate the natural carbonation condition using artificially high CO_2 concentrations because they discovered that both the high concentration of CO_2 and the duration of the accelerated test had no effect on the progression of carbonation from un-carbonated or semi-carbonated zone to achieve complete carbonated one.

For very high CO_2 concentration, it can be argued that the higher concentration of CO_2 might increase the carbonation velocity whereas it may lead to rapid carbonation of the concrete surface thereby blocking the pores and, consequently, this could reduce the penetration of CO_2. However, a 98% CO_2 concentration (Fig 6.4) was successfully used by Stehlik and Novak (2011) when making a correlation between the carbonation in the natural environment and in an accelerated test using Fick's first law of diffusion. The authors reveal that the carbonation speed increased regularly in an environment of

concentrated 98% CO_2 relative to the natural environment containing 0.03% CO_2. In addition, Sanjuan et al. (2003) pointed out that the rate of carbonation under 100% CO_2 and a relative humidity of 60% was 40 times that of the natural condition. This was when testing of normal vibrated concrete with cement contents of 250 kg/m^3 and 350 kg/m^3 with w/c ratios of 0.69 and 0.49, respectively.

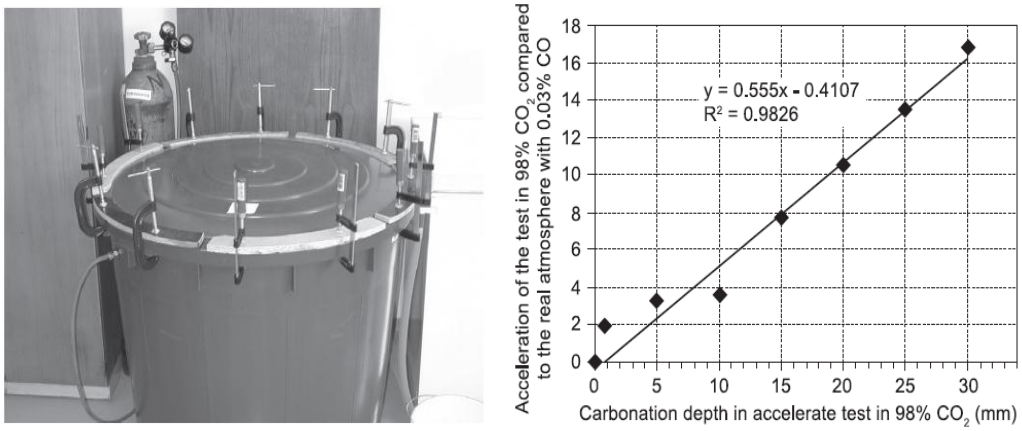

Figure 6-4 Pressurized tank with an atmosphere of 98 % CO_2 and the constant carbonation increase relative to natural conditions Stehlik and Novak (2011)

In order to investigate the effect of the compaction pores on the sorptivity and carbonation of concrete, Gonen and Yazicioglu (2007) used both an accelerated carbonation with 40% CO_2 for 0.25, 1 and 3 days after 28-days of water curing (with different relative humidities, 35%, 55% and 80%) and natural carbonation (0.03% CO_2 with relative humidity of 35% for 575 days). The authors established a relationship between the carbonation rate (K) in both natural and accelerated conditions, which was obtained from a square root time relationship for both type of exposure, and the different porosity results (Fig 6.5). The trend of this relationship in the accelerated conditions was similar to the actual carbonation condition with natural exposure (0.03% CO_2). This suggests that the accelerated carbonation coefficient (K_{acc}) obtained is constantly proportional to the actual one (K_{act}), and its value depending only on the CO_2 concentration. Thus, it is believed that the proposed relationship linking carbonation penetration to the square root (See section 6.4) should be valid in a 100% CO_2 concentration environment in the same way as has already been proposed for the low CO_2 concentrations (3% and 6%) by Roy et al. (1999) and Sisomphon and Franke (2007) respectively. Only the coefficient of carbonation, K, will change.

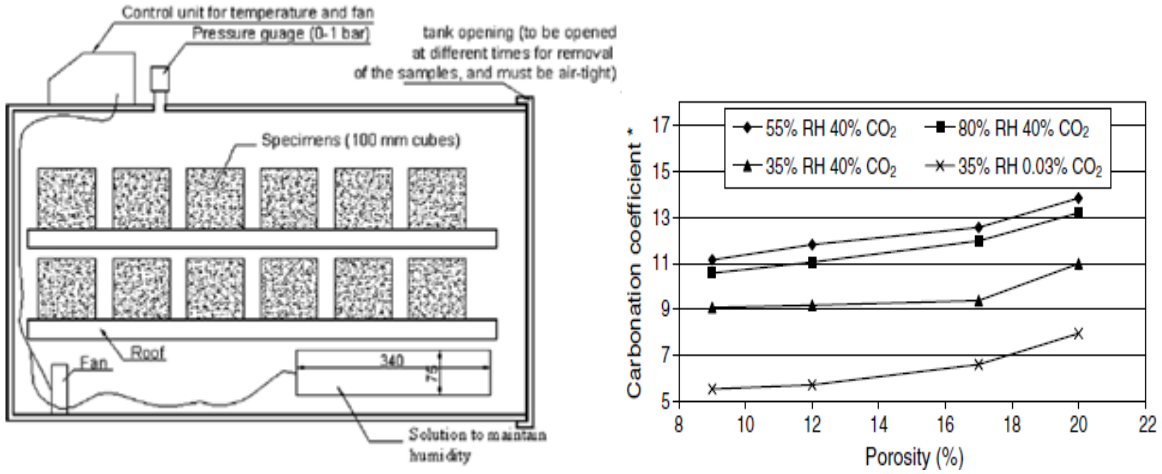

Figure 6-5 Cross selection of the accelerated chamber with 40% CO_2 and K_{acc}/K_{act} – porosity relationship Gonen and Yazicioglu (2007)

The carbonation-related microstructural changes of a medium strength NVC with a strength grade of 40 MPa were investigated by Silva et al. (2002). A 100 % CO_2 atmosphere accelerated carbonation test was used to simulate the long-term durability of the concrete. Their results of indicated that carbonation was enhanced and that the carbonation products closed the pore structure for all pores range. The threshold diameter of the pores in the carbonated samples was half that of the control samples without carbonation. A microstructural examination showed the presence of few pores and fissures in the carbonated samples. The Mercury intrusion curves for both the control and the carbonated samples are shown in Fig 6.6.

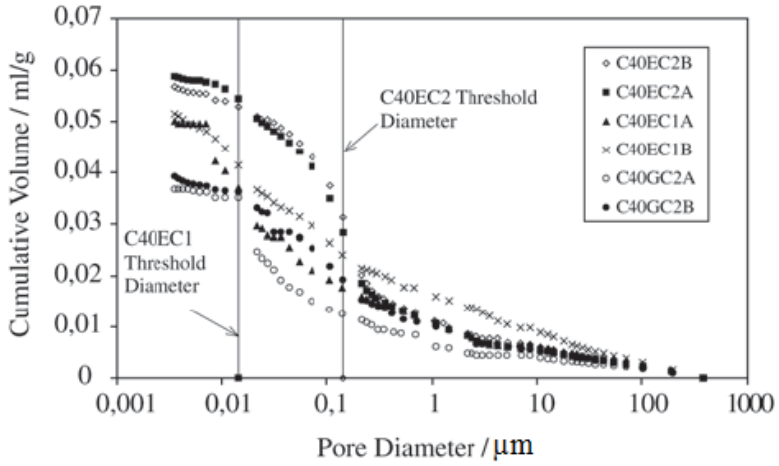

Figure 6-6 Mercury intrusion curves for carbonated (100% CO_2) and controlled specimens of a medium strength NVC (40) MPa (Silva et al., 2002)

For studying the carbonation-induced corrosion and electrochemical re-alkalization after carbonation, Al-Kadhimi et al. (1996) proposed a pressurized accelerated carbonation procedure with an atmosphere of 100 % CO_2 and a pressure up to 15 bars. They revealed that the microstructural characteristics of concrete carbonated at high pressure used agreed closely with those obtained from naturally carbonated concrete. Thus, their proposed accelerated technique could be useful for examining the vulnerability of cementitious materials to carbonation.

Accordingly, taking the work of all the researches reviewed above, their methods and conclusions and the strength grade of the NVC and SCC mixtures produced, two types of accelerated testing with 100% CO_2 were developed and utilized in the present investigation to study the carbonation phenomenon and so as to obtain the results in a practical frame time.

6.2.2 Accelerated carbonation test modification in the present study

6.2.2.1 Normal pressure accelerated carbonation test with 100% CO_2

A plastic box with dimensions 605×370×355 mm was used to design a simple carbonation chamber. It had one inlet for providing the gas from a CO_2 tank and one outlet for releasing any pressure inside the box. A saturated NaCl solution was used to maintain a humidity of 75 ± 5% as recommended by Kubo (2007) for 100% CO_2. However, the recorded humidity actually varied between 50% and 80% through the period of the accelerated test with a temperature of between 19 and 24 ºC. The specimens were stored over a steel mesh, to avoid contact with the saturated NaCl solution and the chamber was filled by CO_2 each two weeks (by allowing the exhaust valve to vent while CO_2 is injected from the inlet valve) and sealed very well to ensure 100% concentration of CO_2. A schematic diagram and photograph of the chamber are shown in Fig. 6-7. More details about the parts and the operating process of the modified chamber can be found in the MSc thesis by Saeed (2013) which is appended on the attached CD. This MSc was performed in parallel with the current study to examine the carbonation of normal and high strength Portland cement concrete.

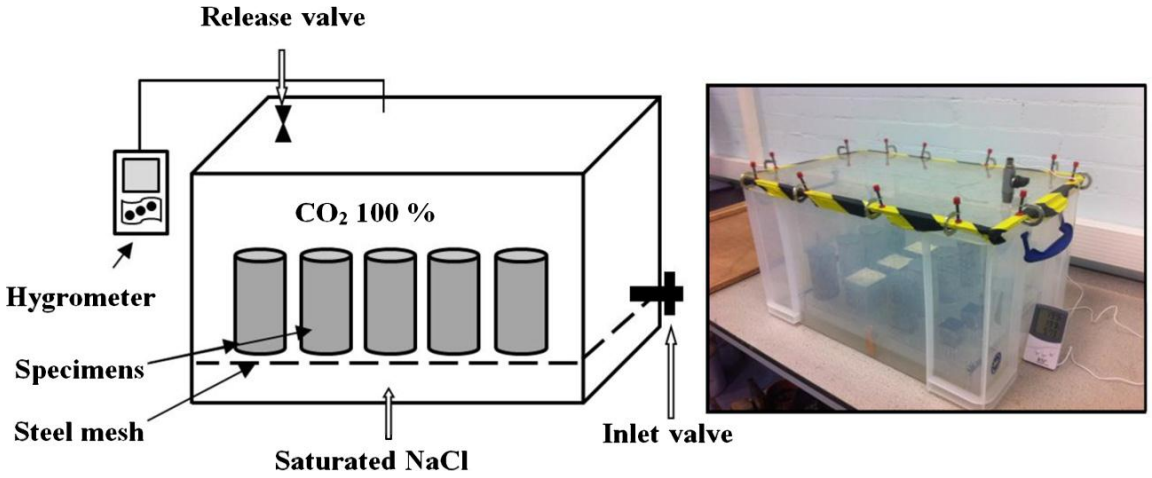

Figure 6- 7 Schematic diagram and photograph of the normal pressure accelerated carbonation test with 100% CO2.

6.2.2.1a Carbonation depth measurement

Among different proposed procedures to determine the carbonation depth of concrete, the depth of carbonation is traditionally determined by spraying phenolphthalein indicator to the surface of a freshly split concrete as recommended by RILEM CPC-18 (1988). The pink color will disappear completely from the carbonated area indicating the drop of the pH value below 9.5. Cylindrical concrete and mortar specimens were prepared for carbonation depth measurement. The specimens had a diameter of 60 mm and a height of 120 mm. After water curing for 28 days, the top and bottom ends of the cylinders were sealed using plastic caps to ensure the radial movement of the carbonation. They were stored inside the unpressurised chamber with 100% CO_2 environment for 240 days. At ages of 30, 60, 90, and 120 and 240 days, the specimens were removed from the chamber and the following steps were conducted to observe the progression of the carbonation depth:

- After removing the plastic caps, a 15 mm long (60 mm diameter) disks were cut from the bottom of each cylinder using a machine saw.
- The sectioned surface was cleaned from any dust and the depth of carbonation through the circumference of the disks was detected by a phenolphthalein indicator.

- The depth of carbonation was recorded as an average value of four readings taken 90º from each other on the disk. In some cases, especially for the concrete samples, another two readings were added to evaluate the minimum depth of carbonation.
- The shortened cylinders were then sealed at their ends again and loaded into the chamber for further carbonation.

The procedure for preparing, detecting and measuring the carbonation depth of the specimen's disks are shown in Figs. 6-8 and 6-9 respectively.

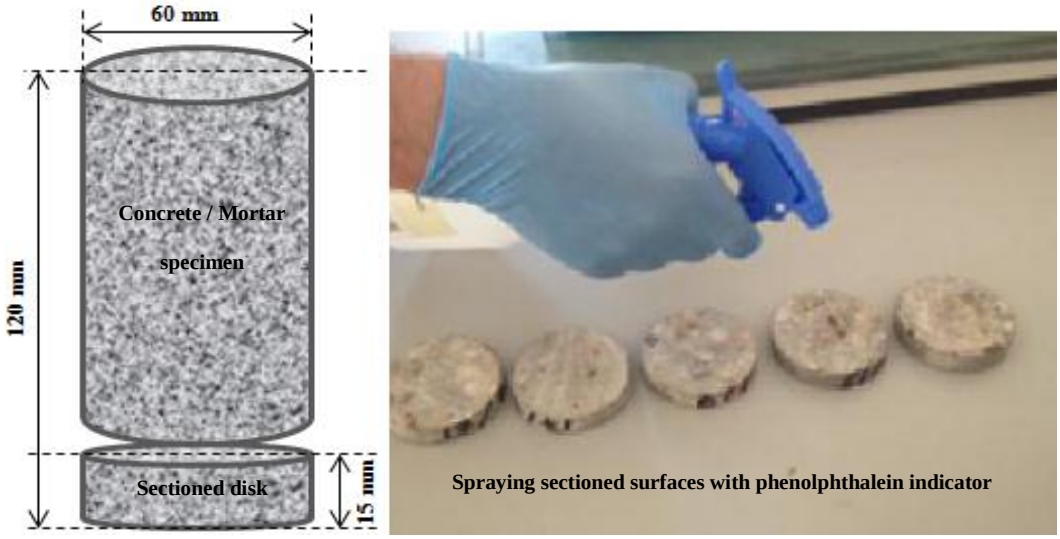

Figure 6-8 cutting of specimens and spraying the sectioned surface of the discs with phenolphthalein

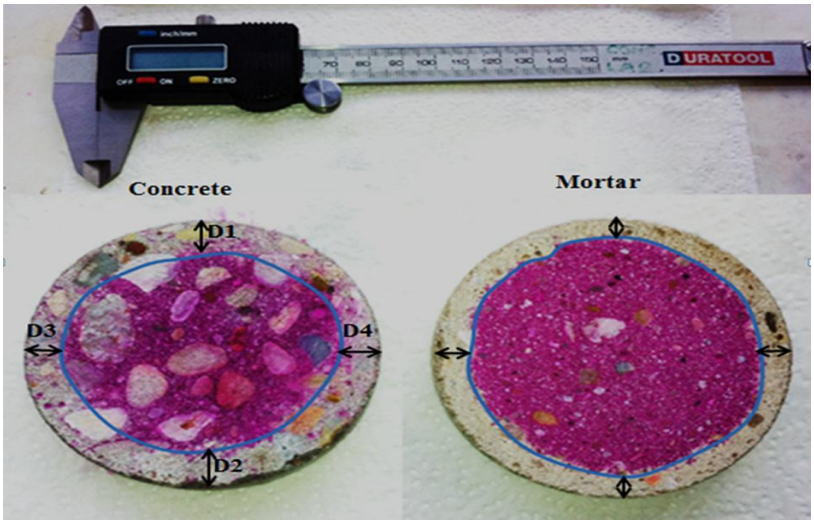

Figure 6-9 Phenolphthalein carbonation depth measurements

6.2.2.2 Pressurized accelerated carbonation test with 100% CO_2

The Pressure Aging Vessel (PAV) which is mainly used to simulate the long term aging of asphalt binder was modified as a pressurized accelerated carbonation test vessel (Fig. 6-10). The original oxygen cylinder was replaced by a CO_2 cylinder to provide the vessel with 100% concentration of CO_2 at a pressure of 2.8 bars. Three mortar samples discs 60 mm in diameter by 10 ± 3 mm high with between 50% and 70% partial saturation, cut from cylinders (60×120 mm), were used for each mix as shown in Fig. 6-10. One was used for monitoring the progress of the carbonation using the phenolphthalein indicator through the cross section of the specimen and the others were kept inside the vessel until complete carbonation. After approximately 15 days, full carbonation was achieved for LP-SCC, FA-SCC and FA-SF-SCC mixes when the phenolphthalein pink color of a specimen disappeared completely indicating the drop of the pH value below 9.5. However, approximately 30 days were needed to obtain fully carbonated specimens for both NVC and R-SCC mixes.

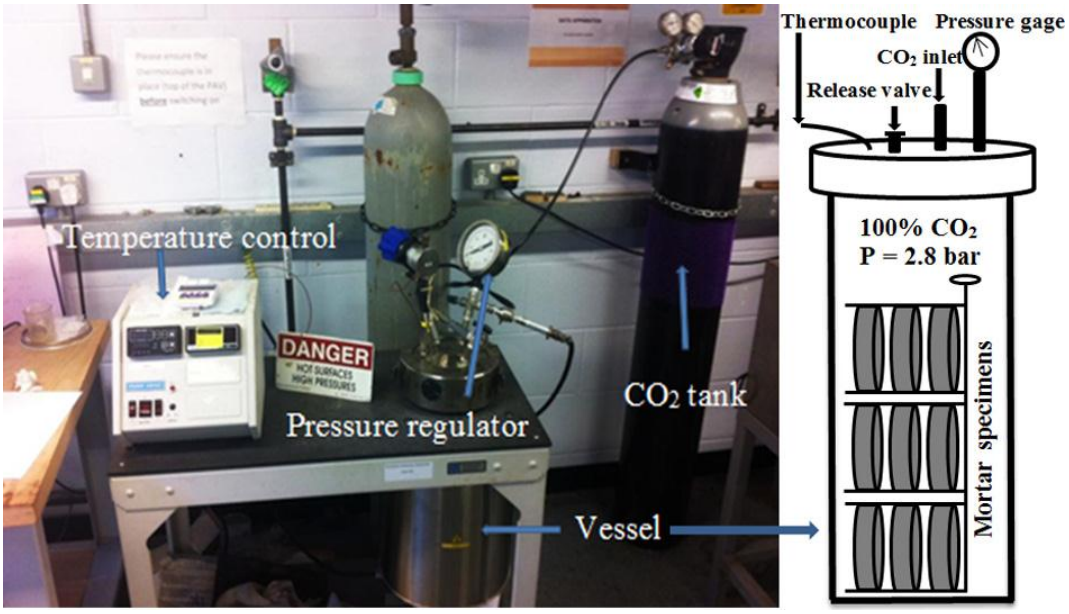

Figure 6-10 Schematic diagram of the pressurized accelerated carbonation test with 100% CO2 and the samples used

In contrast to the partially carbonated specimens obtained in the normal pressure container, 100% carbonated specimens were obtained from the pressurized accelerated carbonation. Three types of tests were conducted on these carbonated samples:

- Small pieces weighing 1–3 g from the middle part of fully carbonated mortar samples were used for the MIP test in order to detect the change of the internal pore structure compared to that of mortars already evaluated at 28 day age before carbonation.
- SEM images were acquired to check the change of the morphology of the carbonated sample and to detect any change of the chemistry inside the pores using platinum-coated fractured surfaces. These were compared to similar images obtained before carbonation.
- XRD analysis of powder samples for the sustainable SCC mixes to examine the associated chemical change of the hydration products after carbonation and to define the kinetics of the carbonation reaction.

6-3 Carbonation progress linked with the chemistry and the microstructure analysis

Fig.6-11 represents the change of the carbonation depth of the normal and self-compacted concretes and mortars with time as a result of testing under the normal pressure test with 100% CO_2 conditions for up to 240 days. The control SCC/mortars (R-SCC) did not exhibit any carbonation by the end of the test. The reason for that is unknown. However, in previous work as stated by Siddique and Khan (2011), the examination of carbonation depth for 72 days in a high performance concrete (HPC) with high cement content (550 kg/m^3) under accelerated carbonation showed no indication of any depth of carbonation. The authors stated that this unexpected behavior might be as a result of the high relative humidity at the beginning of the accelerated test (80-90%). The inspection of their HPC specimens' surface zones also indicated the presence of a cement laitance, rich in water, which might prevent the CO_2 penetration completely.

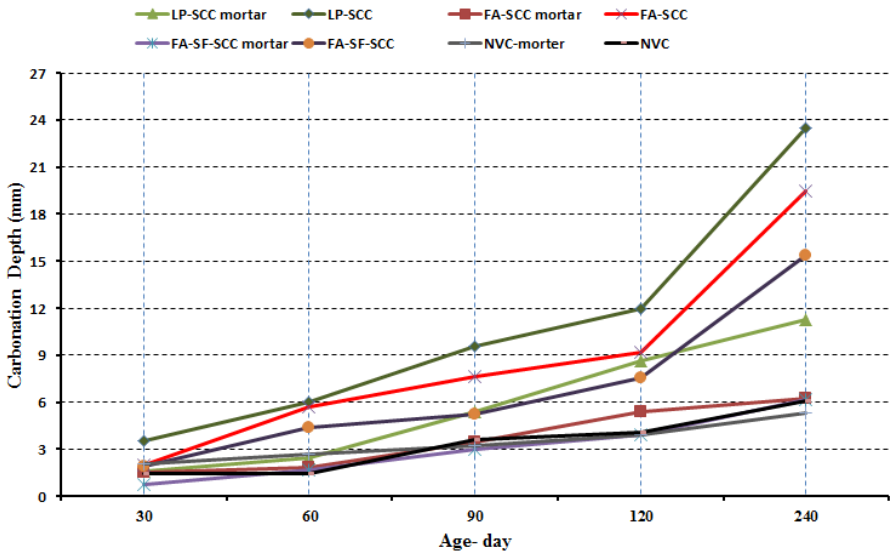

Figure 6-11 carbonation depth of NVC and SCC and mortars versus the exposure time

In general, the results shown in Fig. 6-11 demonstrated that all the concrete types exhibited a higher depth of carbonation in comparison with their respective mortar specimens. This might suggest that the ITZ around the coarse aggregate has a role in facilitating CO_2 diffusion through concretes (See section 7.4).

The results also indicated that the NVC and mortars exhibited the lowest carbonation depth at all tested ages relative to the other sustainable SCC mixes with high filler and mineral admixture content. Physically, the analysis of the pore structure at different scales and the porosity results obtained for this mix before exposure to the accelerated test at 28 days (Table 5-1) and the permeation characteristics of its ITZ as examined in Chapter 5 (Section 5.4.1 and thereafter) suggest that the NVC would exhibit greater carbon dioxide diffusion and, hence, higher carbonation depth. However, from a chemical point of view, the CH is considered as the most soluble phase forming the $CaCO_3$ in the carbonation reaction. One suggestion is that if the calcium ions penetrate more slowly than the carbonate ions, the $CaCO_3$ resulting from the carbonation may make a shell around the CH and delay further carbonation reaction at that site. However, the resulting product appears to be porous and therefore might not be able to delay the progression of carbonation to the next site (Lagerblad, 2005). On the other hand if the carbonate moved faster than the calcium ions the CH might dissolve completely to form $CaCO_3$. This might then block the pores and prevent penetration of the carbonation front to deeper sites (Lagerblad, 2005).

The SEM micrographs in Fig. 6-12 illustrate the transformation of the CH crystals that occurred in the capillary pore of the NVC mix before carbonation to the prismatic crystal shaped $CaCO_3$ after carbonation. The resulting microstructure of the $CaCO_3$ seems to support the second assumption of Lagerblad. However,

- The higher CH content detected by the chemical analysis of the cement matrix of the NVC (TGA analysis section 5.2.1).
- The participation of this compound in the cement matrix' pores before carbonation as shown in Fig. 6-12.
- The presence of high amounts of this compound in the ITZ region (EDX analysis section 5.4.2).

These could have essential roles in delaying the diffusion of the CO2 through the pores of both the cement matrix and the ITZ. It is therefore believed that the chemistry of the NVC mix has a controlling effect on the carbonation process rather than the pore structure characteristics or the micro-permeation features its ITZ.

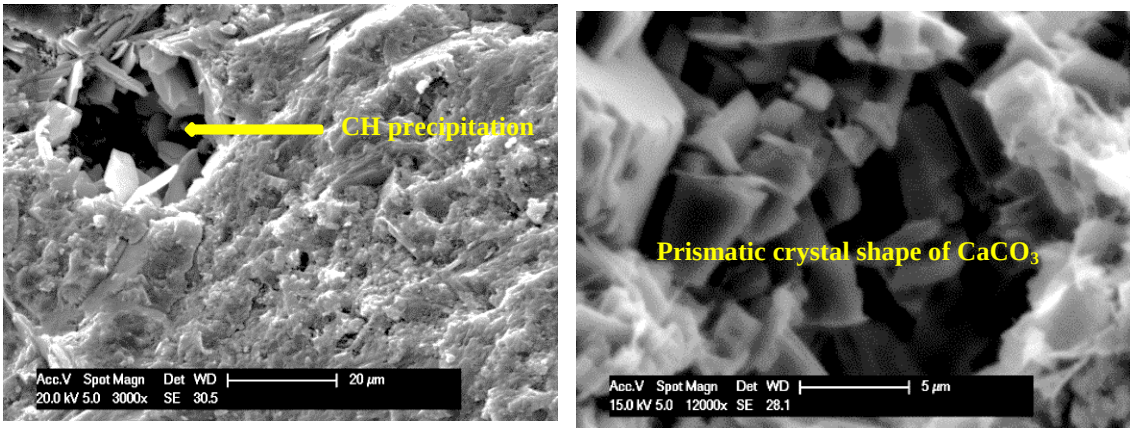

Figure 6-12 SEM micrographs of NVC cement matrix a) before carbonation b) after carbonation

In contrast, those SCCs and mortars made with high partial cement replacement appear to have their carbonation response more controlled by pore structure than by chemistry. This is explained as follows. SCC and mortar made with high partial cement replacement of LP showed the highest carbonation depth at all ages. This was followed by FA-SCC (which exhibited approximately the same 28 day compressive strength as the FA-SF-SCC). The FA-SF-SCC revealed the lowest carbonation depth at all test ages. Before the exposure to the accelerated carbonation, the TGA analysis conducted by the author also demonstrated that LP-SCC exhibited the highest amount of CH due to dehydration relative to the other two filler typed SCCs, followed by FA-SCC and FA-SF-SCC. However, it was less than that detected in the NVC.

Based on the discussion above for the NVC, in comparison to the other types of SCC, the LP-SCC should have the highest resistance to carbonation due to the high amount of CH in the cement matrix which can dissolve to form a dense pore structure and prevent the CO_2 from further diffusion. However, it showed lower resistance as shown in Fig. 6-11. Physically, the analysis of the pore structure before carbonation clearly showed that this type exhibited a more porous microstructure than the other SCC mixes (see Table 5-1). Thus, the results appear to demonstrate that modification of the pore structure in both the FA and FA-SF-SCC increases the mix's resistance to carbonation and eliminates the

effect in both the cement matrix and ITZ of CH content reduction. This modification of the pore structure is attributed to the reactivity of the filler or the mineral admixture.

6-4 Carbonation modeling and predicting of actual carbonation depth

The monitoring for eight months of the carbonation depth of the NVC and filler- and mineral admixture -typed SCC and mortars was used to predict the carbonation depth in a natural environment and the results are summarized in Table 6-1 and 6-2 respectively.

Table 6-1 Predicted carbonation depths for NVC and SCC in natural environment

Mix ID	$K_{acc.}$ mm/(year)^1/2	$K_{act.}$ mm/(year)^1/2	Carbonation depth (mm) after number of years				
			10	20	30	40	50
NVC	9.6	0.19	0.60	0.85	1.04	1.20	1.34
LP-SCC	38.6	0.77	2.43	3.44	4.22	4.87	5.44
FA-SCC	32.6	0.65	2.05	2.91	3.56	4.11	4.60
FA-SF-SCC	25.5	0.51	1.61	2.28	2.79	3.22	3.61

Table 6-2 Predicted carbonation depths for NVC and SCC mortars in natural environment

Mortar ID	$K_{acc.}$ mm/(year)^1/2	$K_{act.}$ mm/(year)^1/2	Carbonation depth (mm) after number of years				
			10	20	30	40	50
NVC	6.2	0.124	0.40	0.55	0.68	0.78	0.88
LP-SCC	19.9	0.40	1.26	1.79	2.2	2.53	2.83
FA-SCC	9.9	0.20	0.63	0.9	1.1	1.27	1.4
FA-SF-SCC	6.2	0.124	0.40	0.55	0.68	0.78	0.88

The accelerated rate of carbonation (K) for the concrete/mortar was calculated as the slope of the carbonation depth-square root time relationship as shown in Figs. 6-13 and 6-14 respectively according to Fick's first law in **Eq. 6-1** which is mainly used for

carbonation modeling (Bertolini et al., 2004). It is possible to determine accelerated K values from only three readings (for example, first 3 months only after 28 days water curing). However, this method would need the carbonation speed to be constant with time, whereas, due to the effect of continuous hydration with time during the extended time of the test and due to the small variations in the relative humidity inside the carbonation chamber. Constant behavior probably is not a realistic assumption. Thus, it was decided to take into account the carbonation depth results for up to 8 months in order to obtain more accurate accelerated K values.

$$X = K_{acc.}\sqrt{t} \quad \ldots\ldots\ldots \textbf{Eq. 6-1}$$

where X is the depth of carbonation (mm), $K_{acc.}$ is the accelerated carbonation coefficient (mm/year), t is time (year)

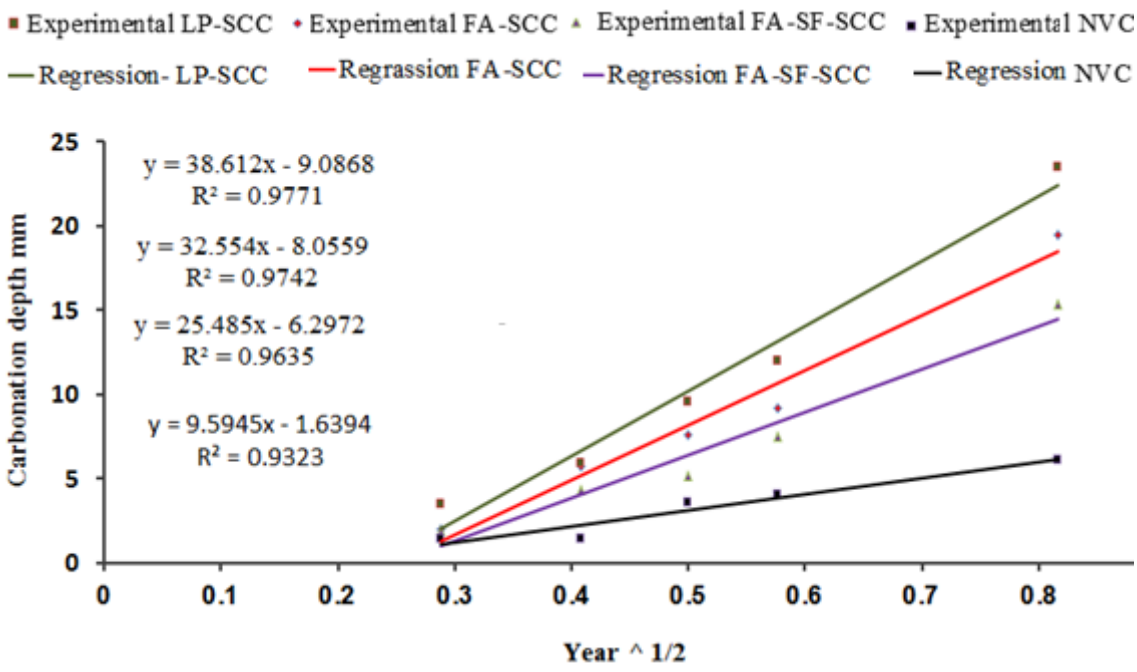

Figure 6-13 Carbonation depths versus the square root of time (year) relationships of concrete

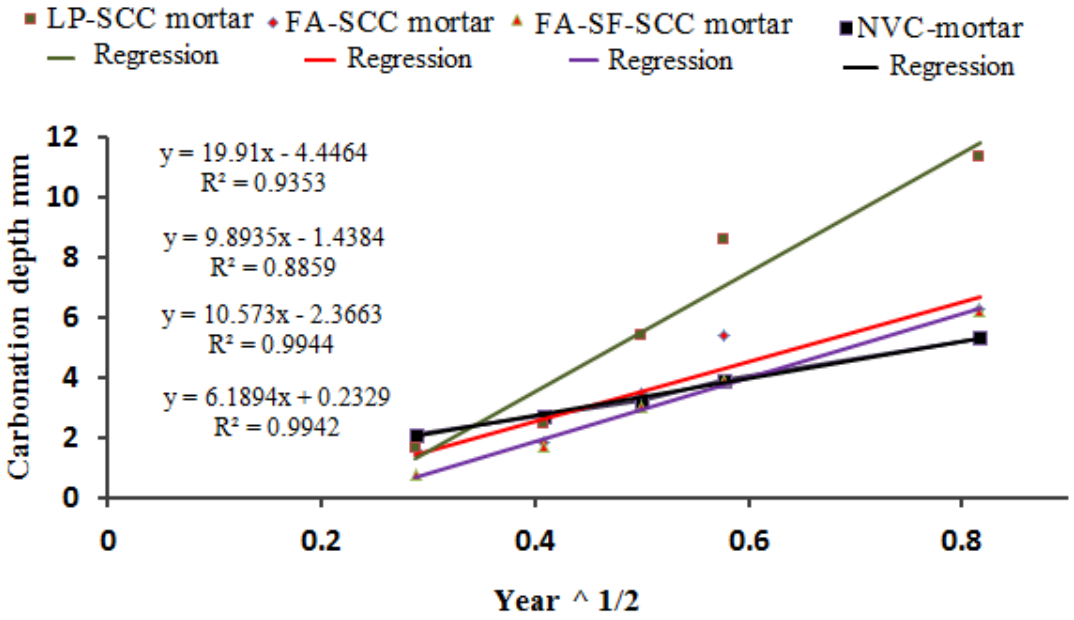

Figure 6-14 Carbonation depths versus the square root of time (year) relationships of mortars

The carbonation depth does not seem to be linearly proportional to the square root time during the first month of measurements. The reason for this is not known, although it might be because of an initial delay in carbonation propagation due to different density or packing at the smooth surface of the specimens, especially in the case of SCC specimens. Thus, the regression was performed from the beginning of the second month of measurement.

The experimental results under accelerated test showed an excellent correlation factors with the regression lines (at least 96.37% for the concrete specimens and 88.59% for the mortar ones). The actual rate of carbonation ($K_{act.}$) was calculated using the formula developed by Sisomphon and Franke (2007) for the accelerated test under 3% CO_2 concentration but here altered for 100% CO_2 concentration. The use of such a square root relationship is supported by the study of two authors using different CO_2 concentrations Roy et al. (1999) and Sisomphon and Franke (2007) as explained earlier. Therefore, the ratio of the accelerated and the actual diffusion coefficients could be stated in terms of CO_2 concentrations under accelerated and natural conditions considering that 0.04% is the actual CO_2 concentration in the atmosphere. Fig. 6-15 shows the CO_2 concentration increase in the atmosphere from 1955 to June 2013 measured at Mauna Loa observatory by U.S. Department of Commerce-National Oceanic and Atmospheric Administration (ESRL, 2013). According to this measurement, May 2013 is the first time that the

atmospheric CO_2 concentration has reached to 400 ppm. $K_{acc.}$ is 50 times greater than $K_{act.}$ considering 100% CO_2 (Eq. 2):

$$\frac{K_{acc.}}{K_{act.}} = \sqrt{\frac{[CO_2]100\%}{[CO_2]0.04\%}} = 50 \quad \text{..... (Eq. 6-2)}$$

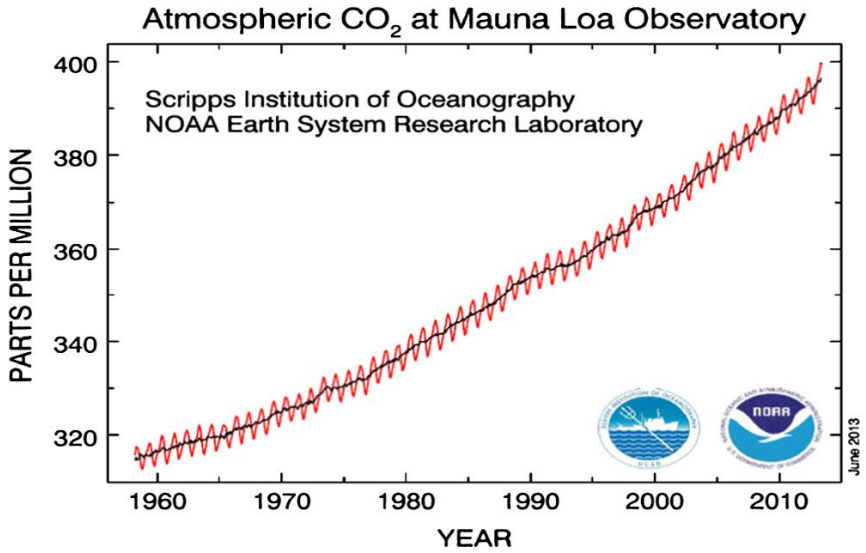

Figure 6-15 CO2 concentration increase in atmosphere from 1955 to June 2013 (ESRL, 2013)

BS EN 206-1:2000 classifies the exposure classes related to aggressive carbonation environments and the minimum required cover for structural concrete class S4 (the Euro code for structural concrete) for a service life of 50 years as shown in Table 6-3.

Table 6-3 exposure classes and minimum cover requirements for 50 years life span (BS EN 206-1:2000)

Class	Minimum cover (mm)	Environment	Type of structure
XC1	15	Dry or permanently wet	Concrete inside building with air low humidity. Also concrete permanently submerged in water
XC2	25	Wet, rarely dry	Concrete surface subject to long-term water and many foundations
XC3	25	Moderate humidity	Concrete inside building with moderate to high air humidity and External concrete sheltered from rain
XC4	30	Cyclic wet and dry	Concrete surface subject to water content, not within exposure class XC2

XC: exposure class (corrosion due to carbonation)

The analysis, Table 6-1, demonstrates that the predicted carbonation depths were only 1.34 mm, 5.44 mm, 4.60 mm and 3.61 mm for NVC, LP-, FA- and FA-SF-SCC after 50 years of exposure to natural environment. Therefore, there is no risk of carbonation-induced corrosion during this service life. If atmospheric carbon should rise to 0.06% in 50 years' time [refer to the Intergovernmental Panel on Climate Change (IPCC) worse case estimate] then these predictions rise to 1.7, 6.7, 5. 66 and 4.42 for the NVC, LP-, FA- and FA-SF-SCC respectively (conservative assumption as concentration is taken as 0.06% through those 50 years). Therefore, even increased greenhouse gas is not likely to lead to the initiation of steel corrosion over that time scale in structural concrete class S4 for 50 years' service life (Table 6-3).

The results obtained clearly show that the use of high partial cement replacement for the sustainable SCC increased the carbonation rate and reduce the service life as compared to the NVC at the same strength level (50-60) MPa. Holland (2012) proposed that, for precast pre-stressed concrete piles in severe marine environments (concrete exposed to both carbonation and chlorides), if the concrete cover suffers from cracks and there is no chance for the self-healing of these cracks, the design life span of a HPC with blended cement should be greater than 100 years and the estimated service life in excess of 1000 years. This is due to the combined effect of the use of low water to cementitious material ratios and the use of blended cement with reactive mineral admixture. Thus, to ensure such a service life, the theoretical recommended required cover distance, using Eq. 6-1 and duration of 1000 years, should be 24.4 mm, 20.6mm and 16.1mm for the LP-, FA- and FA-SCC respectively (Some of these values are not applicable for the concrete depending on the aggregate size).

6-5 Quantitative analysis of the pore structure (MIP) before and after carbonation

In general, the carbonation can promote blocking of the pore structure and decrease the concrete porosity. This is because of the higher volume of the carbonation products as compared to the original hydration products. However, the incorporating of fine reactive and non-reactive filler and higher amounts of SP, such as in the case of SCC, change the chemical composition and modify the pore structure to a large extent as detected in Chapter 5. For this reason and the impact of the carbonation on the internal structure of the SCC might be different from that in a NVC. Thus, it is interesting to identify the

change in pore characterization after carbonation of both the NVC and the SCC mixes. Changes in the pore connectivity and pore concentration after carbonation could have a major impact on the diffusivity of water and of other aggressive agents through the concrete cover.

Fig. 6-16 and 6-17 show the cumulative MIP intrusion volume against the pore diameter of the LP–SCC and the frequency distribution of these pores before and after carbonation while Fig. 6-18 displays the obtained results for the NVC, R-SCC, FA and FA-SF-SCC mixtures respectively.

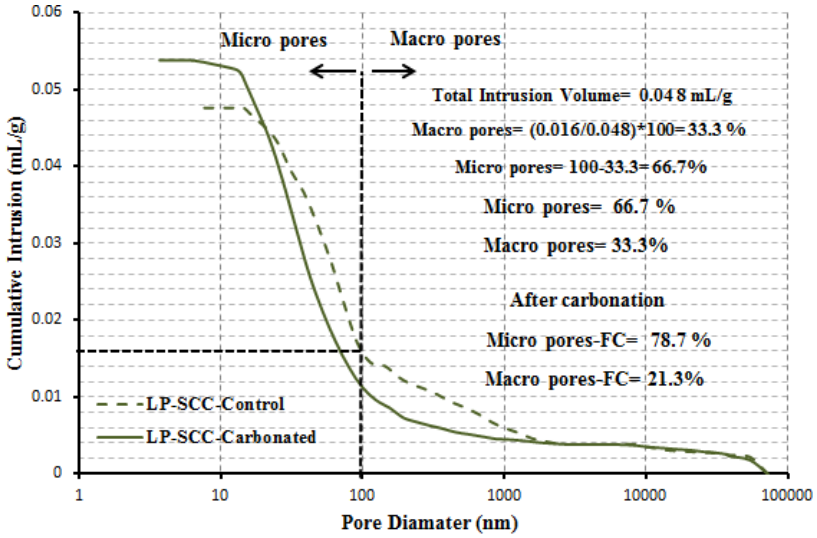

Figure 6-16 MIP intrusion volume against the pore diameter curve of LP-SCC

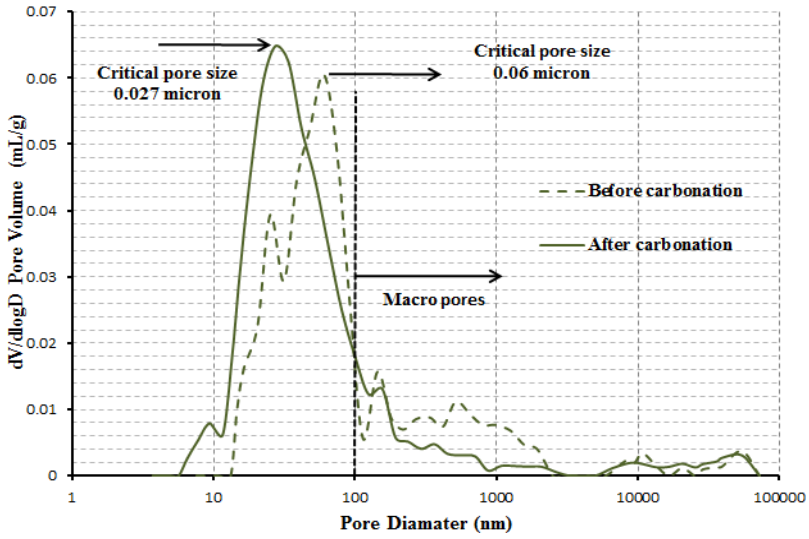

Figure 6-17 Frequency distributions of the pores in LP-SCC

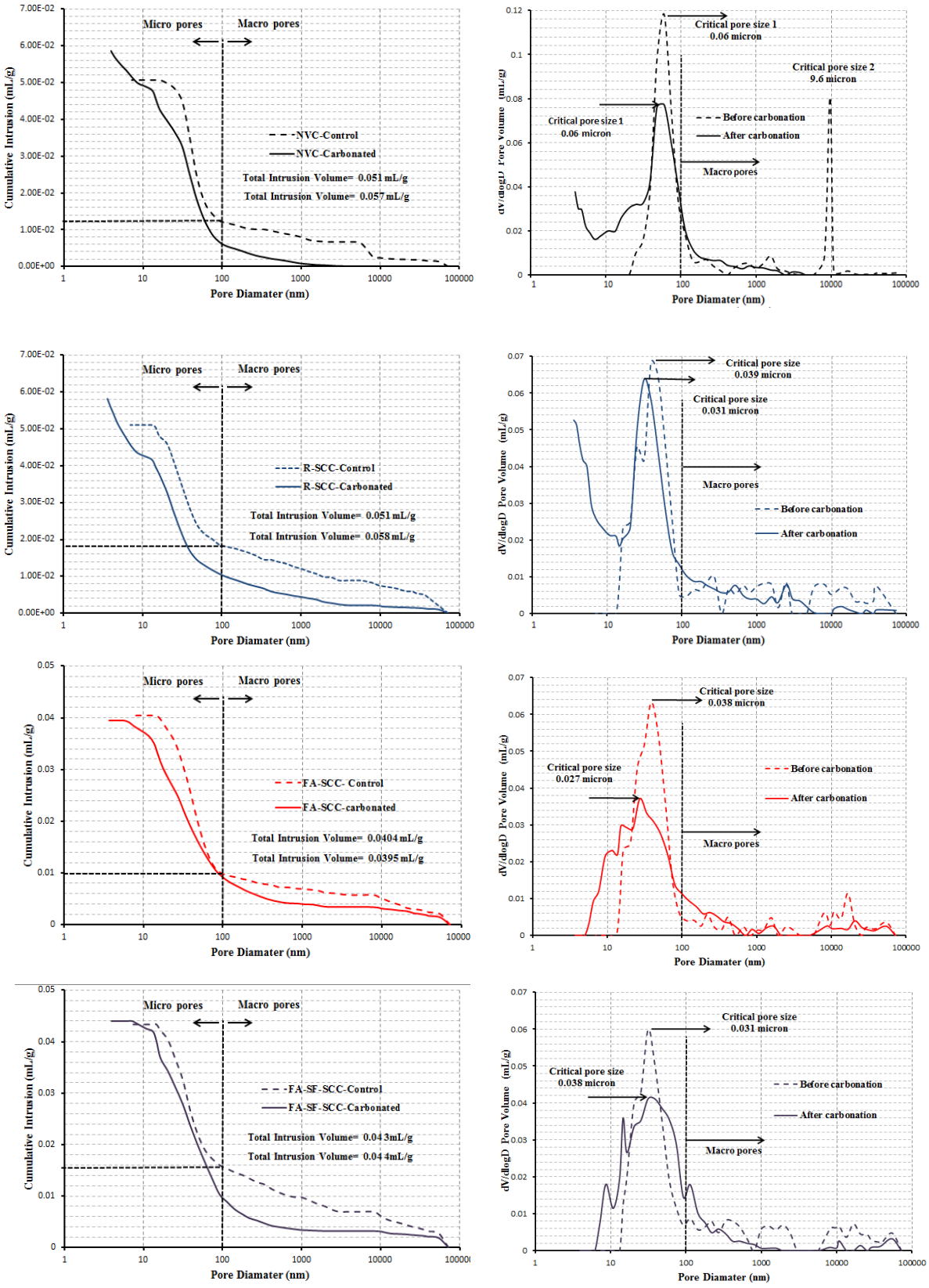

Figure 6-18 MIP intrusion curves and the frequency distribution of these pores for the NVC, R-SCC, FA and FA-SF-SCC

In general, the results of MIP after carbonation demonstrated a noticeable redistribution of the pore structure of the all concrete mixtures. The calculated percentages of the total pores (micro and macro pores considering 0.1µm to be the boundary between these pore classes) before and after carbonation and the critical pore diameter (CPD) are presented in Table 6-4.

Table 6-4 Characterization of pore structure at different scales (macro/micro and nano) before and after carbonation

Mix ID	Before carbonation			After carbonation		
	Micro pores %	Macro pores %	CPD (nm)	Micro pores %	Macro pores %	CPD (nm)
NVC	76.5	23.5	60	89.8	10.2	60
R-SCC	64.7	35.3	39	82.8	17.2	31
LP-SCC	66.7	33.3	60	78.7	21.3	27
FA-SCC	75	25	38	77.3	22.7	27
FA-SF-	71	29	31	79.5	20.5	38

From Table 6-4, the analysis of the results of the NVC indicated that the carbonation increased the proportion of micro pores to about 15%. In addition, the CPD was the same even after carbonation. This suggests that there was no effect of the carbonation on the nature or the pore connectivity of the cement matrix at the nano scale. This is explained in more details using the microstructural evidence discussed in the next section (Section 6-6). The micro pores of the R-SCC were increased by about 28% after carbonation with a slight decrease in the CPD from 39 nm to 31 nm.

For the sustainable SCC, the carbonation of the LP-SCC increase the proportion of micro pores by about 18% from the original micro pores' proportion. In addition, the critical pore diameter (CPD) reduced significantly from 60 nm to 27 nm (the evidence for this substantial decrease at this scale is provided in the next section). The corresponding development of the micro pores was about 3.1% for the FA-SCC while it showed a small decrease in the CPD from 38 nm to 27 nm as compared with the LP-SCC.

For the FA-SF- SCC the micro pore proportion only increased a little from 71% to 79.5%. However, the most surprising result was the slight increase of the CPD for this

type after carbonation from 31 nm to 38 nm. This may be as a result of the carbonation of the CSH gel which is expected to have been present at a higher percentage in this type of SCC due to the high activity of SF in consuming the CH and producing further CSH. The EDX microstructural analysis of this mix type in Chapter 5 demonstrated the presence of a high amount of the CSH in both the ITZ and the cement matrix as well. Perhaps the carbonation of CSH in the cement matrix of this type explains the changes observed, especially at the micro pores level (See Fig. 6-19).

Recently, the work conducted by Borges et.al (2010) to investigate the carbonation of CH and CSH in composite cement pastes containing high amounts of blast furnace slag (BFS) indicated that overall porosity and permeability may increase if the main phase (CSH) is attacked by CO_2. If the resistance of the cement matrix is sufficiently high to prevent a constant CO_2 penetration, the probability of the reaction between CO_2 and CSH might increase. On the other hand, for blended pastes with low resistance to the CO_2 access, they pointed out that carbonation of CSH having a low Ca/Si ratio (< 1.6) might not cause a significant change in the capillary pores structure. The combined result of the EDX microstructure analysis and the carbonation progress of this type of SCC indicated the presence of high amount of CSH with an average Ca/Si ratio of about (2.08 for the cement matrix and 2.17 for the ITZ) and the highest carbonation resistance relative to the other types of sustainable SCC. The corresponding deduced Ca/Si ratios for the other types of concrete are presented in Table 5-5.

6.6 Pore structure change linked with the SEM observation and XRD analysis after carbonation

The quantitative results obtained from the cumulative MIP test intrusion volume against the pore ranges before and after carbonation are summarized in Fig. 6-19.

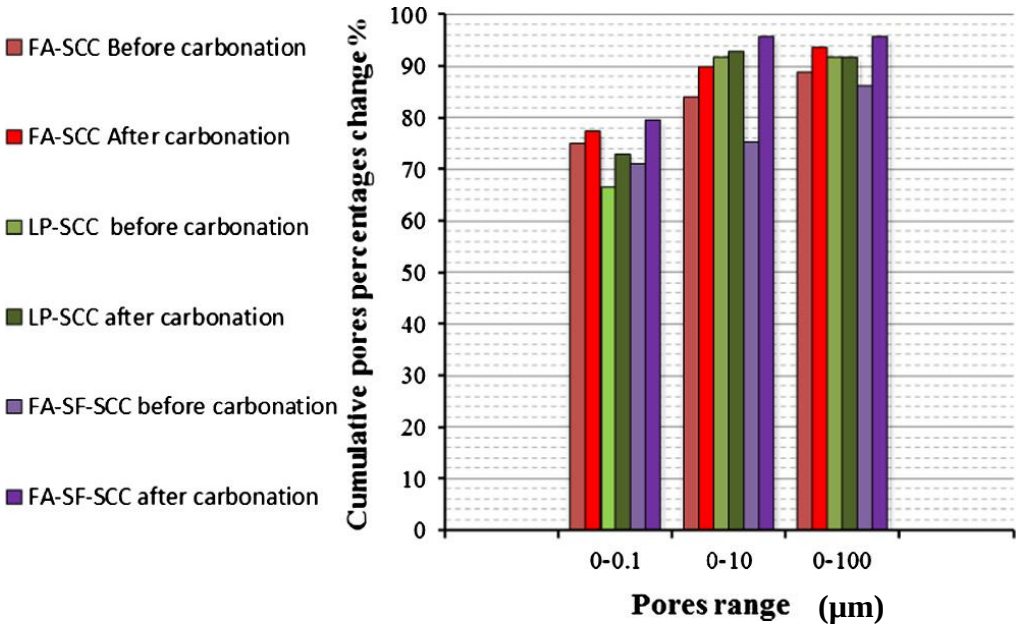

Figure 6-19 Quantitative analysis of pores percentages change% versus different pores ranges before and after carbonation MIP test.

On one hand, the MIP results for the NVC (Fig. 6-20) confirmed that the impact of the carbonation was more pronounced on the macro capillary pores than on the micro one. The carbonation also changed the dual mode of the pore structure distribution as detected by the MIP before carbonation by eliminating the CPD_2 at the macro range of around 10 µm. In addition, there was absolutely no effect on the nature of the pores at the nano scale (CPD_1) where the same value was deduced before and after carbonation (Fig 6-18). On the other hand, a slight reduction is recorded for this parameter in the case of R-SCC with obvious changes in the macro pores as well. This implication is that the carbonation was able to alter practically all pore sizes distribution of the R-SCC whilst there were a more micro/macro changes in the case of NVC but no changes were deduced at the nano scale. In contrast, Silva et al. (2002) stated that the carbonation could change all the pore size distribution for a medium strength NVC (40 MPa). However, the author used CPII E 32 (composite cement added with 25% slag and 10% limestone) with a w/c ratio of 0.42 and a slump flow of 85 to obtain the required

strength level. Further, the deduced threshold diameters for the different types of concrete before carbonation were between (0.0144 - 0.1443) µm. In this prospective, the type of the cement used for their NVC might determine the change of the pore structure after carbonation.

The analysis also shows noticeable changes in the cumulative pore percentages especially in the range of (0-100) µm for the FA-SF-SCC matrix as compared with the other two types of sustainable SCC mixes (LP-SCC and FA-SCC). The SEM observations of the matrix of the FA-SF-SCC after carbonation indicated the presence of coarse pores in several areas in comparison with the matrices of the LP- and FA-SCC.

The detailed SEM examination of the pores after carbonation of the R-SCC, LP- , FA- and FA-SF-SCC matrices are illustrated in Figs. 6-20 to 6-22.

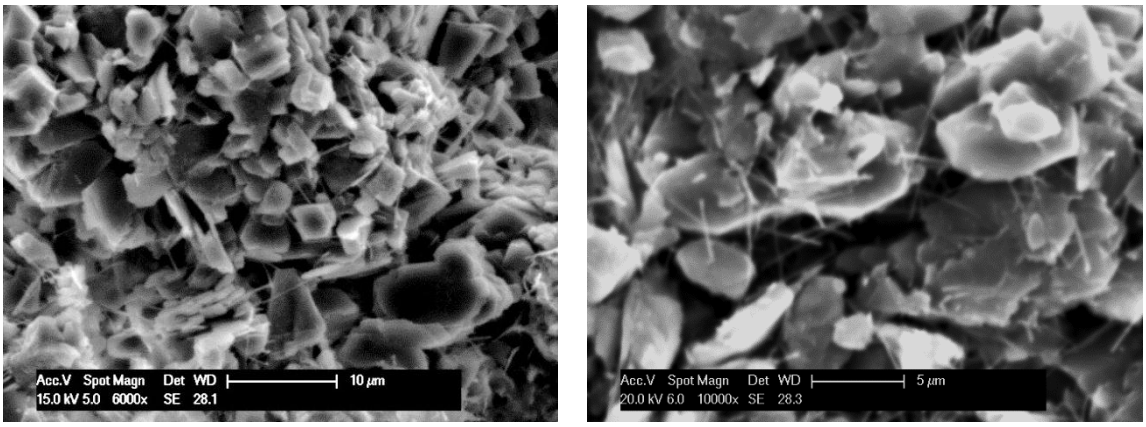

Figure 6-21 Monosulfate form (needles) after carbonation in the pores of R-SCC (a) low magnification and (b) high magnification

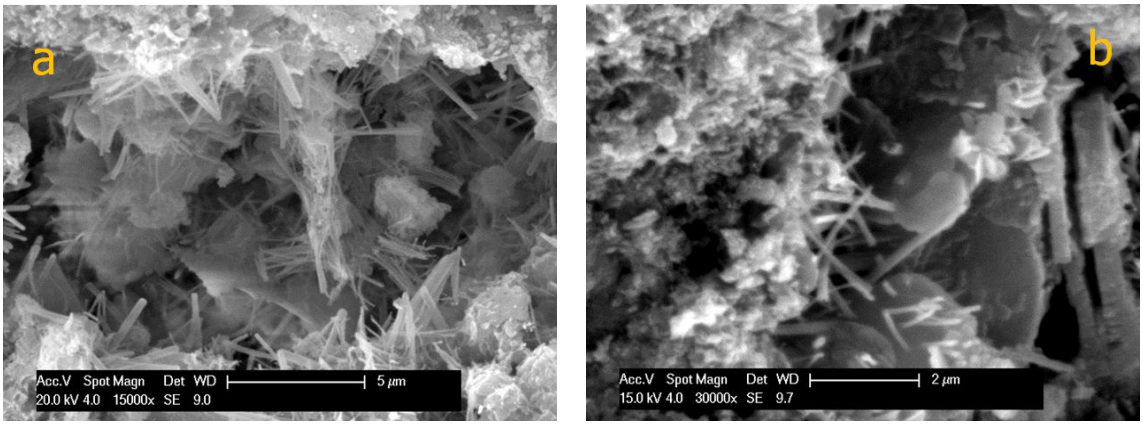

Figure 6-21 Monosulfate form (needles) after carbonation in the pores of (a) LP-SCC and (b) FA-SCC

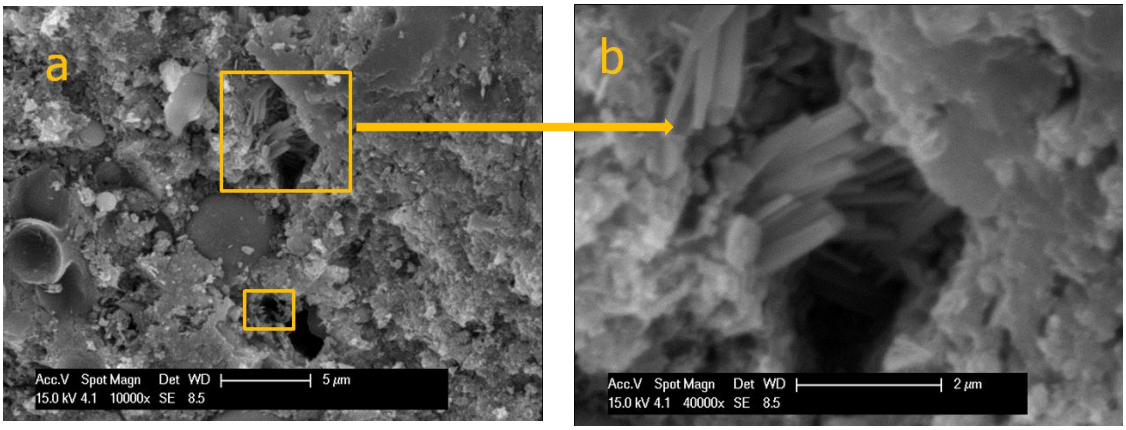

Figure 6-22 DEF (Ettringite) after carbonation in the pores of FA-SF-SCC (a) low magnification and (b) high magnification.

The results revealed that the Ettringite occurred in the capillary pore structure in two forms after carbonation. Monosulfate needles, which are not an expansive form, were found in both LP- and FA- SCC cement matrices after carbonation. However, this compound was much more prominent in the pores of the LP -SCC rather than in those of the FA-SCC.

The transformation of the monosulfate into the hexagonal Ettringite shape is associated with an approximately 2.3 times increase in the volume (Stark and Bollmann, 2000). This form of Ettringite (hexagonal platelet shape) was found in the pores of the FA-SF-SCC. The presence of the first form in addition to the original $CaCO_3$ resulting from the carbonation reaction of CH/CSH could lead to an additional increase in the proportion of micro pores in the LP-SCC and FA-SCC matrices and a considerable decrease in the CPD, especially for the LP-SCC (Table 6-4). The occurrence of the second form of the Ettringite in the FA-SF-SCC might have caused a kind of microscopic damage to the pore structure due to the expansion pressure caused by the volume increase as this form of Ettringite developed. This might, thus, be responsible for a substantial change of the pores in the range of 0.1-100 mμ (Fig. 6-19) and the slight increase in the CPD at the nano scale as detected by the MIP test.

Delayed Ettringite formation (DEF) (i.e. Ettringite not found during initial curing) could be associated with pore changes after heat-treatment, freeze-thaw attack with and without de-icing salt, sulphate attack and as a result of the combined action of the CO_2 and water (carbonation) in the cement matrix due to the low pH value. Ettringite results

from the decomposition of the monosulfate in the cement paste to produce $CaCO_3$, $Al(OH)_3$,gypsum, and water. A part of original monosulfate then combines with the liberated gypsum to form the Ettringite. However, whether the formation of the this compound during the carbonation has a practical impact or not is a subject of controversy (Stark and Bollmann, 2000).

The microstructural analysis after carbonation also indicated the complete absence of these two types of Ettringite in the capillary pores of the NVC (See Fig. 6-12). However, a very small amount of the monoslfate type was detected in the R-SCC capillary pores (See Fig. 6-20). This might support the previous conclusion derived by the author, which conflicts with Silva et al. (2002). It should be mentioned that the DEF could significantly affect the capillary pores connectivity at the nano scale (the size of the Ettringite crystals is only about 10-15 nm) whilst the resulting Calcite ($CaCO_3$) and forms of other carbonation products (other forms of $CaCO_3$ such Aragonite and Vaterite) could have an essential role in occupying the macro pores and in increasing the micro pore percentages. The equivalent volume increase due to the carbonation of the original CH to form different types of $CaCO_3$ is illustrated in Table 6-5 (Arandigoyen et al., 2006).

Table 6-5 Properties of minerals that can be involved in the carbonation process

Mineral	Density (g/cm^3)	Molar volume (cm^3)	Crystal shape	Volume variation
Portlandite (CH)	2.23	33.2	Lamminer	----
Calcite ($CaCO_3$)	2.71	36.93	Prismatic	11.2%
Aragonite ($CaCO_3$)	2.93	34.16	Fibrous	2.9%
Vaterite ($CaCO_3$)	2.54	39.4	Spherical	18.9%

The typical XRD patterns of the powder samples obtained from the carbonated sustainable SCC-mortars are shown in Figs. 6-23 to 6-25.

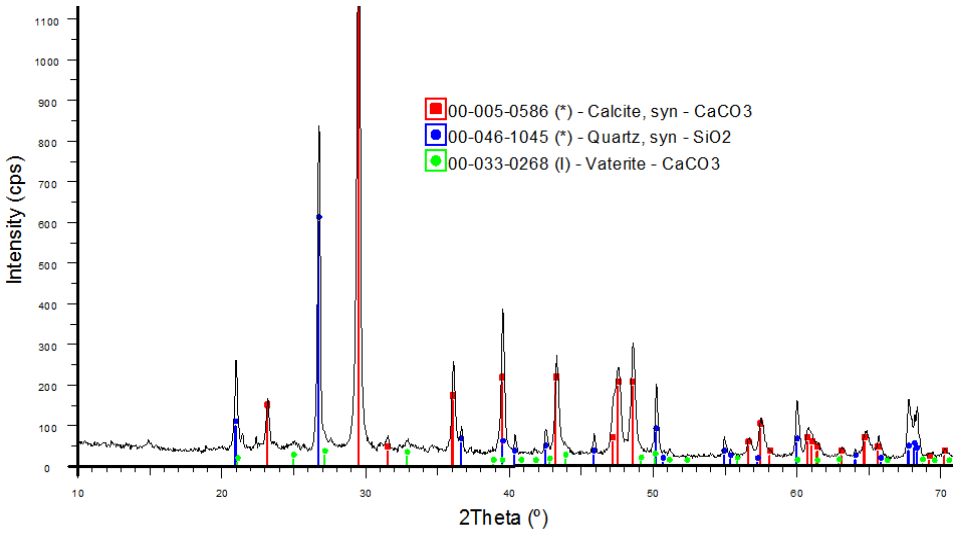

Figure 6-23 Typical XRD spectra of carbonated LP-SCC mortar

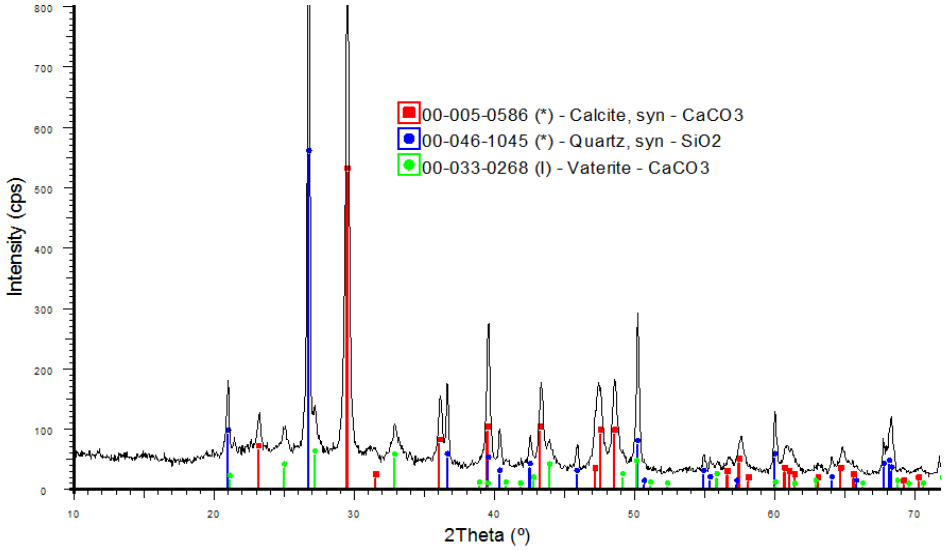

Figure 6-24 Typical XRD spectra of carbonated FA-SCC mortar

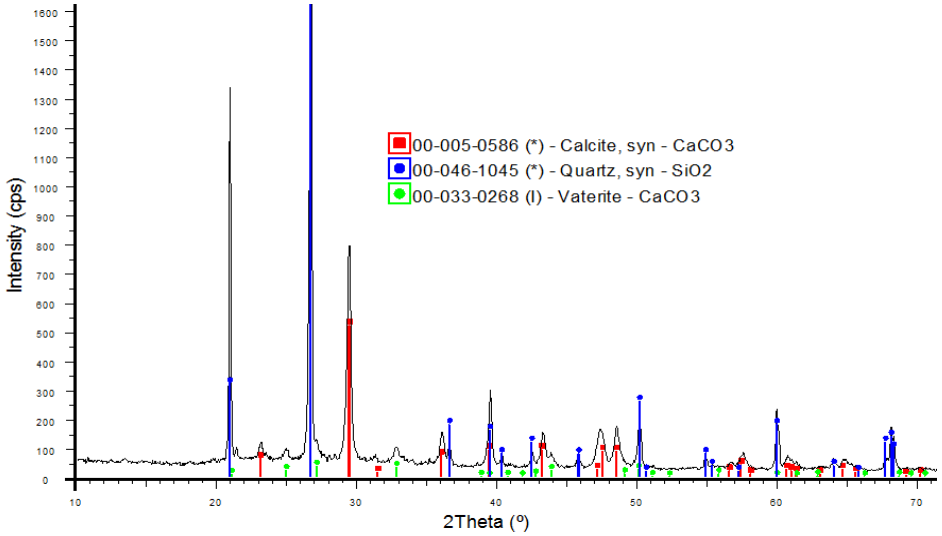

Figure 6-25 Typical XRD spectra of carbonated FA-SCC mortar

The XRD analysis indicated the absence of the CH compounds which were deduced using the same technique before carbonation (Section 5.2.1) signifying the full carbonation of the mortar matrices. The analysis also demonstrated that two forms of Calcite have been detected due to the carbonation reaction: Calcite and Vaterite. However, the Vaterite form was more pronounced in the case of the FA-SCC with higher intensity peaks in comparison with the carbonated products found in LP- and FA-SF-SCC. Thus, the results appear to indicate that the kinetic factors predominate in controlling the carbonation reaction of all types of sustainable high performance SCC rather than the thermodynamic factors.

It was already reported by Arandigoyen et al. (2006), that if the CH compound is transformed to the Calcite form (only) due to the full carbonation, then the carbonation reaction is thermodynamically controlled. This is in contrast to the formation of different forms of Calcite when kinetic factors dominate. More details could be obtained from the micro analysis of thin carbonated samples, using the petrographic microscope, to investigate the associated change of the hydration phases due to the carbonation. Unfortunately, it was not possible to include this type of in-depth micro-chemical analysis in this study due to absence of the facilities used for the preparation of such thin carbonated samples.

6.7 Concluding remarks

Based on the result obtained from this chapter, the following general concluding remarks could be drawn:

- Under normal pressure 100% CO_2 accelerated testing, the carbonation depth of the NVC and mortars was lower than all types of the sustainable high performance SCC. The carbonation depth of LP-SCC or mortars was higher than FA- and FA-SF-SCC or mortars at all ages of the test. In contrast, the FA-SF-SCC revealed the lowest carbonation depth.
- The combination of chemical, microstructural analysis before and after the exposure to the accelerated test suggest that the carbonation progress was chemically controlled in the NVC whilst the carbonation propensity in

sustainable SCC is only practically chemically controlled, with the pore structure playing a substantial role in determining the progression of the carbonation.

- The differences in the carbonation depth between the concrete and mortar specimens suggest a significant role of the ITZ around the coarse aggregate in facilitating the diffusion of CO_2 and increasing the carbonation depth.

- Whatever the type of the filler, whether non-reactive (LP) or reactive (FA and SF) with 33% replacement of binder, the actual predicted carbonation diffusion coefficient did not change much after 28 days water curing. Stating the finding in another way, the change of the chemistry of the matrix due to the addition of different fillers had little impact on the actual carbonation rate. Therefore, none of the filler-and mineral admixture typed SCC mixes is at risk of carbonation induced corrosion in natural exposure. The predicted carbonation depths were only 5.44 mm, 4.6 mm and 3.61 mm for LP-, FA- and FA–SF–SCC respectively after 50 years in the natural environment.

- The theoretical recommended minimum required cover distance should be 24.4 mm, 20.6mm and 16.1mm for the LP-, FA- and FA-SCC respectively in order to avoid the risk of steel corrosion in a service life of 1000 years.

- The extrapolated carbonation depth due to unpressurised 100% CO_2 testing could be used for estimating the actual carbonation depth of concrete that has a high resistance to carbonation, such NVC and SCC with a strength grade of 50–60 MPa, in a fairly short time. However, carbonation depth results from actual structures should be monitored to check the validity of the predicted results. Unfortunately, the time scale of the current study is not enough to do that.

- The modification of the internal pore structure in LP and FA–SCC after carbonation was more pronounced in comparison with the FA–SF–SCC. This modification was less in the NVC and this was likely related to the presence of more macro pores before carbonation and the nature of the carbonation products.

- The combined results of the MIP test and SEM observations after carbonation suggest that the addition of SF could have a positive effect on modifying the internal pore structure and producing high resistance to carbonation while it had a

negative effect on the connectivity of the capillary pores after carbonation especially, at the micro and nano scales level. Therefore, carbonation may have an important effect on the permeation characteristics of such concrete cover if interacted with water or other aggressive substances.

- The two forms of the Ettringite observed in the SEM examinations in the pore structure of the filler-and mineral admixture typed SCC after carbonation could play a significant role in determining the nature of the internal pores and its connectivity after carbonation, especially at the micro and nano level scales. At the nano scale, this effect was less in R-SCC without any cement replacement and it was not observed at all in the pores structure of the NVC.

6.8 References

AL-KADHIMI, T., BANFILL, P., MILLARD, S. & BUNGEY, J. 1996. An accelerated carbonation procedure for studies on concrete. Advances in Cement Research, 8, 47-59.

ARANDIGOYEN, M., BICER-SIMSIR, B., ALVAREZ, J. I. & LANGE, D. A. 2006. Variation of microstructure with carbonation in lime and blended pastes. Applied surface science, 252, 7562-7571.

ATIŞ, C. D. 2003. Accelerated carbonation and testing of concrete made with fly ash. Construction and Building Materials, 17, 147-152.

BERTOLINI, L., ELSENER, B., PEDEFERRI, P. & POLDER, R. B. 2004. Corrosion of steel in concrete: prevention, diagnosis, repair, Vch Verlagsgesellschaft Mbh.

BORGES, P. H. R., COSTA, J. O., MILESTONE, N. B., LYNSDALE, C. J. & STREATFIELD, R. E. 2010. Carbonation of CH and C–S–H in composite cement pastes containing high amounts of BFS. Cement and concrete research, 40, 284-292.

BS EN 13295 2004. Test method determination of carbonation.

CHANG, C.-F. & CHEN, J.-W. 2006. The experimental investigation of concrete carbonation depth. Cement and Concrete Research, 36, 1760-1767.

DILOVAN M. SAEED. 2013. Carbonation of medium to high strength portland cement concrete. MSc, Nottingham University.

ESRL. 2013. Earth System Research Laboratory;U.S. Department of Commerce [Online]. Available: http://www.esrl.noaa.gov/gmd/ccgg/trends/ [Accessed 17/06/2013].

GONEN, T. & YAZICIOGLU, S. 2007. The influence of compaction pores on sorptivity and carbonation of concrete. Construction and Building Materials, 21, 1040-1045.

HOLLAND, R. B. 2012. Durability of precast prestressed concrete piles in marine environments.

JI, Y., YUAN, Y., SHEN, J., MA, Y. & LAI, S. 2010. Comparison of concrete carbonation process under natural condition and high CO2 concentration environments. Journal of Wuhan University of Technology-Mater. Sci. Ed., 25, 515-522.

KHUNTHONGKEAW, J., TANGTERMSIRIKUL, S. & LEELAWAT, T. 2006. A study on carbonation depth prediction for fly ash concrete. Construction and Building Materials, 20, 744-753.

KUBO, J. 2007. Methods of remedial treatment for carbonation-induced corrosion of reinforced concrete. PhD, University of Leeds.

LAGERBLAD, B. 2005. Carbon dioxide uptake during concrete life cycle–State of the art, Swedish Cement and Concrete Research Institute, CBI: Stockholm.

RILEM RECOMMENDATION CPC-18 1988. CPC-18 Measurement of hardened concrete carbonation depth. Mater. Struct, 21, 453-455.

ROY, S. K., POH, K. B. & NORTHWOOD, D. O. 1999. Durability of concrete—accelerated carbonation and weathering studies. Building and environment, 34, 597-606.

SANJUAN, M., ANDRADE, C. & CHEYREZY, M. 2003. Concrete carbonation tests in natural and accelerated conditions. Advances in Cement Research, 15, 171-180.

SIDDIQUE, R. & KHAN, M. I. 2011. Supplementary cementing materials, Springer.

SILVA, C. A. R. D., REIS, R. J. P., LAMEIRAS, F. S. & VASCONCELOS, W. L. 2002. Carbonation-Related Microstructural Changesin Long-Term Durability Concrete. Materials research, 5, 287-293.

SISOMPHON, K. & FRANKE, L. 2007. Carbonation rates of concretes containing high volume of pozzolanic materials. Cement and concrete research, 37, 1647-1653.

STARK, J. & BOLLMANN, K. 2000. Delayed ettringite formation in concrete. NORDIC CONCRETE RESEARCH-PUBLICATIONS-, 23, 4-28.

STEHLIK, M. & NOVAK, J. 2011. Verification of the effect of concrete surface protection on the permeability of acid gases using accelerated carbonation depth test in an atmosphere of 98% CO2. Ceramics–Silikáty, 55, 79-84.

Chapter 7:

Chloride penetration - microstructural relationships and the service life prediction under accelerating tests

7.1 General

The aims of this chapter can be divided into two main parts:

- To quantitatively analyze the correlation between the microstructural features, in terms of internal pore structure at different scales, and the local micro-permeation properties of the ITZ, in relation to the chloride penetration velocity. The pores' macro/micro and nano characteristics and the ITZ micro-permeation features were already assessed in Chapter 5. Establishing pore structure property-chloride penetration relationships in conjunction with ITZ local micro-characteristics could contribute to provide further understanding of the microstructure of the sustainable SCC and the part it plays in determining the resistance to chloride ingress.

- To examine the ability of using relatively high dosages of different types of filler such as LP, FA and the combined partial replacement of cement by FA plus SF in improving the chloride resistance and the service life of a medium to high strength sustainable-SCC. In addition, compared the chloride resistivity to two reference mixes (NVC and SCC) at the same design strength level (50-60 MPa) at 28 days.

For the purposes of achieving the above two central aims which will form the second and the third parts of the current chapter, two types of accelerated chloride penetration tests were selected in this investigation based on the recommendation of Nordtest methods (NT BUILD 492, Nordtest,1999, NT BUILD 443, Nordtest,1995). It seems here that a brief and general overview of the established accelerated chloride penetration tests is needed in addition to the results obtained. This will help to explain:

- *Why the author selected these tests?*

- *How the modifications were performed?*
- *How the results were obtained?*

Thus, the first part of this chapter will begin with a very short overview of the available accelerated chloride techniques, the tests details and the modifications performed in the present investigation.

7.2 Review of natural and accelerated chloride penetration techniques

In general, the chloride penetration tests in concrete (natural ponding or electrical accelerated tests) can be classified into two kinds: steady and non-steady state tests. Steady-state means that the chloride penetrates the concrete at a constant rate of flux causing the concentration to increase at a constant rate. In contrast, the rate of chloride ion concentration will change continuously with the time at any position in none-steady state conditions as shown in Fig. 7-1 (Djerbi et al., 2008).

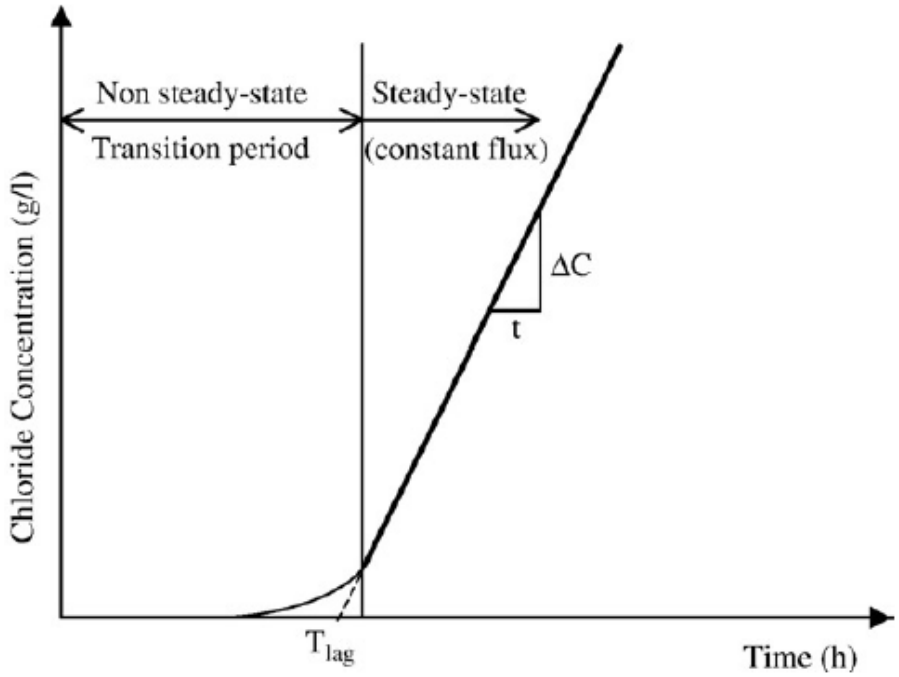

Figure 7-1 Schematic representation of non-steady and steady-state conditions of chloride ingress

The process of chloride diffusion is governed by Fick's first law in the steady-state condition (Eq. 3.13) (Cement Concrete & Aggregates Australia, 2009). However, especially with the use of high performance concrete, a long time is needed to estimate

the steady-state chloride diffusion coefficients as reported by several investigations i.e. Heirman et al.(2006) for SCC. Non-steady state diffusion process which is mainly controlled by Fick's second law is normally used for high performance concrete (Eq. 3.27) (Stanish et al., 1997, Cement Concrete & Aggregates Australia, 2009). For the above reason, only non-steady state conditions were adopted to calculate the chloride diffusion/migration coefficients in the present study.

7.2.1 Stimulating Chloride penetration

7.2.1.1 Natural ponding and accelerating diffusion techniques

The AASHTO T_{259} test as shown in Fig.7-2 was designed to examine the chloride diffusion phenomena in the concrete. It is based on one-dimensional chloride penetration (non-steady state). According to this standard, the concrete sample should be cured for (14 days moist cure plus 14 days in 50 % relative humidity) followed by ponding the concrete specimens with 3% NaCl solution for 90 days) (Stanish et al., 1997). In order to avoid some of the shortcuts in the AASHTO T_{259} diffusion test, the bulk diffusion test has been modified as the Nordtest version (NT BUILD 443, Nordtest,1995) which is considered to be the first officially standardized test for the bulk chloride diffusion. Among the different proposed laboratory accelerated chloride tests such as ASTM C1202 (steady state), NT Build 355(steady state), NT Build 492 (non-steady state-Electrical migration) and NT Build 443(non-steady state), the last is considered as the most similar test method to the real condition for the submerged concrete structure where the apparent non-steady state chloride diffusion (D_{nss}) and the surface chloride concentration (Cs) could be obtained (Kim et al., 2009).

This standard recommends curing the concrete specimen for 28-days followed by ponding with 2.8 M (165gm/L) NaCl solution for minimum of 35 days. At the end of the above two tests, the chloride concentration (C) in specified depth increments (x) would be calculated and plotted versus the depth. The setups of these two tests are shown in Fig.7-2 (Stanish et al., 2000).

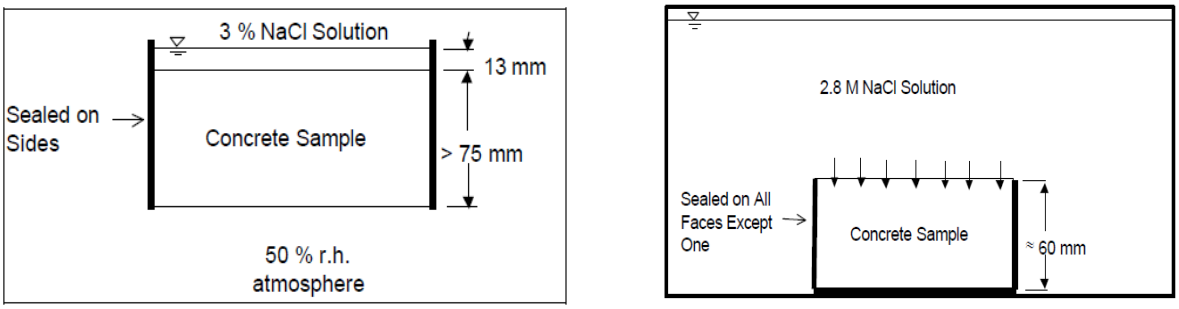

Figure 7-2 AASHTO T_{259} and NT Build 443 setups

Based on the Fick's second law, the both natural or accelerated chloride diffusion tests could be used for the purpose of investigating the chloride penetration resistance of the concrete. In addition, the apparent chloride diffusion coefficient, D_{app} in the non-steady sate based on the calculation of chloride concentration in different depths (both combined chloride with the hydration products and free soluble chloride in the pore water) can be used for modeling the chloride penetration and calculating the time of corrosion initiation (service life). This is based on using different suggested solutions to Fick's second law of diffusion Eq. 3.27. These tests required two important assumptions: no applied external voltage (natural diffusion) and stable moisture in the pore structure in the concrete (vacuumed saturated) (Song et al., 2008). Fig.7-3 shows a typical output data from these a ponding tests and an example from ponding test with 4M NaCl for 400 days respectively.

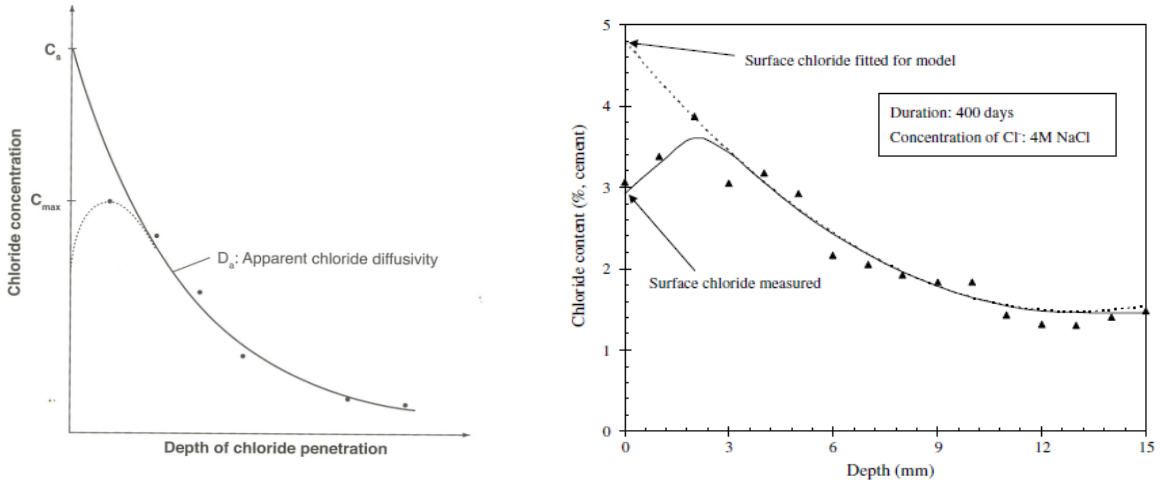

Figure 7-3 Typical chloride concentrations versus penetration depth from natural and accelerating ponding tests (Gjørv 2009, Song et al., 2008)

Kim et al.(2009) claimed that the chloride diffusion coefficients obtained from the NT Build 443 accelerated ponding test demonstrated the highest correlation with the ACI

(Life 365) model, which was introduced to design concrete structures that are exposed to chloride attack as shown in Fig.7-4a and b.

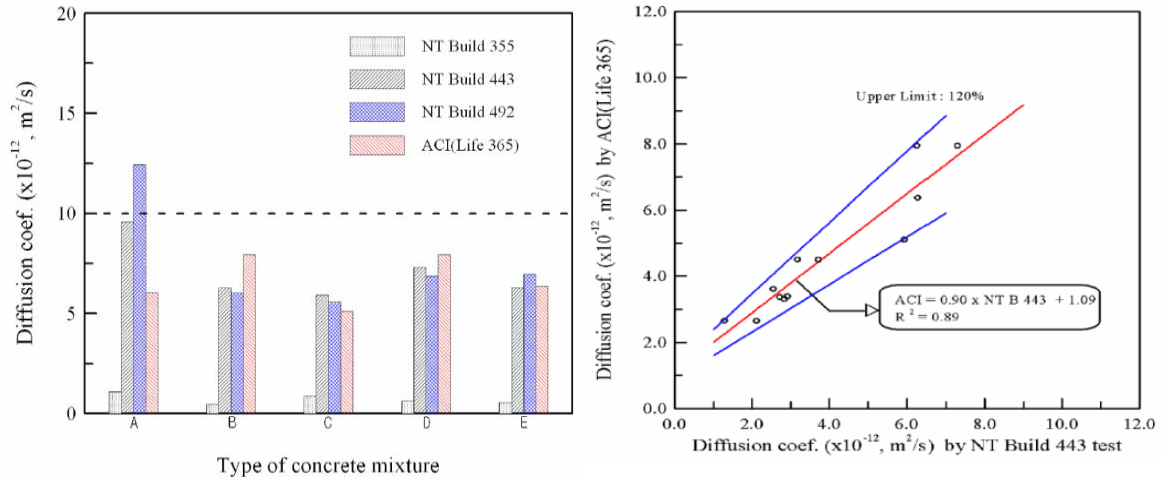

Figure 7-4 Chloride diffusion coefficients (D) obtained from different tests and the correlation between D from NT Build 443 and ACI (Life 365) model (Kim et al., 2009)

Further, according to Frederiksen et al. 1997 quoted by Nilsson, 2001(Nilsson, 2001), a relation between the field exposure and the laboratory exposure according to this accelerated chloride penetration test has been found for the concrete. Thus, for the above reasons, this method was selected in the present study for examining the chloride penetration resistance of the NVC and SCC mixes, the numerical modeling of the chloride ingress process and, hence, for estimating the service life of all concrete types.

7.2.1.2 Electrical Chloride Migration Techniques

Electro-chemical accelerated tests have been developed such as AASHTO T_{277} (steady-state) (ASTM, 2000 vol. C04.02) and the NT Build 492(NT BUILD 492, Nordtest,1999) (none-steady-state) and NT Build 355-Nordtest as shown in Fig.7.5 respectively.

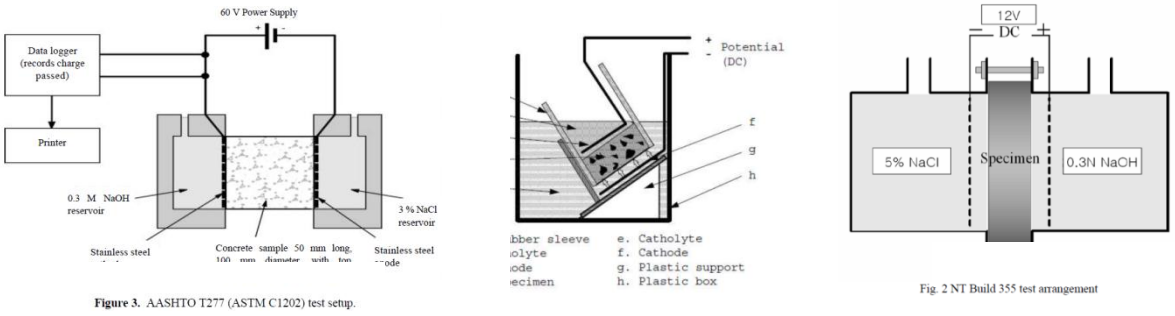

Figure 7-5 Different exciting methods for electro-chemical chloride penetration tests in concrete (Stanish et al., 2000, NT BUILD 492, Nordtest,1999, Kim et al., 2009)

The main idea of these electro-chemical tests is to apply an external voltage for the purpose of accelerating the migration of the chloride through the concrete/mortar from a catholyte solution (NaCl) to an anolyte solution (NaOH) with different applied voltages and concentrations. Thereby, the contribution of the pure diffusion process can be neglected and the chloride ingress process will be mainly controlled by an electrical migration of the chloride ions through the concrete as defined in Eqs. 7.1 to 7.3 for the accelerated steady-state condition (Stanish et al., 2000) and Eq.7.5 for the non-steady state conditions as described in section 7.3.1(NT BUILD 492, Nordtest,1999).

$$Flux = Pure\ diffusion + Electrical\ migration + Convection \quad \textbf{.....Eq. 7.1}$$

$$J_i = D_i \frac{\partial C_i\,(x)}{\partial x} + \frac{Z_i\,F}{RT}\,DC_i \frac{\partial E(x)}{\partial x} + C_i V_i\,(x) \quad \textbf{.....Eq. 7.2}$$

By neglecting the pure diffusion and the convection (no pressure or moisture gradients):

$$J_i = \frac{Z_i F D C_i}{RT} \frac{\partial E(x)}{\partial x} \textbf{.....Eq. 7.3}$$

J_i: is the flux of the ionic species i, D_i : the diffusion coefficient of the ionic species i, $Ci\ (x)$: is the concentration of ionic species i as a function of location x, Zi: is the valence of ionic species i, F: Faraday's constant, R: the universal gas constant, T: is the temperature, $E(x)$: is the applied electrical potential as a function of x and Vi: is the convection velocity of i

The typical setup of the rapid chloride penetrability test method (RCPT) is according to ASTM C1202 as shown in Fig.5a. In this standard, the current (I) driven by the external voltage (60V) through the concrete sample can be measured and plotted at several time intervals i.e. ($I_{0min.}$, I_{30min}, ……, $I_{360min.}$). The integrated current over the test period gives the charge passed (number of coulombs) which can be used for identifying the chloride ion penetrability resistance using Table7.1.

Table 7.1 rapid chloride penetration test (RCPT) ratings (per ASTM C1202)

Charge passed (coulombs)	Chloride ion penetration
>4000	High
2000-4000	Moderate
1000-2000	Low
100-1000	Very low
<100	Negligible

For NT Build 355, one to two months is required to maintain the steady-state due to the lower applied voltage (12V) as compared to (60V) for ASTM C1202. By knowing the differences on the concentration of the chloride ions between the catholyte and the anolyte with time, the chloride flux (J) should be calculated and the chloride diffusion coefficient can be obtained according to the equation in Table 7.2. For NT Build 492 (non-steady state), the chloride migration coefficient (D_{nssm}) can be obtained in accordance to Eq.7.5 presented later.

Although the above methods do not represent the real circumstances of chloride diffusion and the outputs of these tests are qualitative, they have been related to non-electric accelerated diffusion test methods (Audenaert et al., 2007). In very recent work, for example, the chloride diffusion coefficients from the NT Build 492-Nordtest have been used for the service life design of a sustainable concrete type containing blended micro-sand as a partial replacement of cement following the "DuraCrete" methodology as designed by Eq. 7.4 (Ying, 2013) which is a modified version of Eq. 3.28:

$$C(x,t) = C_s^d - (C_s^d - C_i).\left[erf\left(\frac{x}{\sqrt{4kD_0\left(\frac{t_0}{t}\right)^n t}}\right)\right] \quad \textbf{.....Eq. 7.4}$$

$C(x,t)$ = the chloride content at depth x at time t;

C_s^d = the design value of surface chloride content , % by mass of binder

C_i = the intial chloride content, % by mass of binder;

k = a correction factor;

n = the aging factor;

D_0 = the reference diffusivity at reference time t_0, m^2/sec (NT Build 492-Nordtest Method);

t_0 = the refernce time = 28 days (sec.);

erf = Gauss error fuction,

Table 7.2 summarized the chloride accelerating test methods.

Table 7-2 Accelerating test methods and conditions for assessing chloride ions diffusivity in concrete (Kim et al., 2009)

Test method	Measuring item	Required time	Electrolyte solution	Applied voltage	Equation
ASTM C 1202 Standard test method for electrical indication of concrete's ability to Resist chloride ion penetration[1)] **(KS F 2711)**	Total passed charge	6 hours	(+) 0.3N NaOH (-) 3.0% NaCl	60V	$Q_{tatol} = 900 \cdot (I_0 + 2I_{30} + \sim + 2I_{300} + I_{360})$
NT Build 492 Chloride migration coefficient from non-steady-state migration experiments[2)]	Penetration depth	24~48 hours	(+) 0.3N NaOH (-) 10.0% NaCl	10~60V	$D = \frac{RT}{zFE} \cdot \frac{x_d - \alpha\sqrt{x_d}}{t}$
NT Build 355 Chloride diffusion coefficient from migration cell experiments [3)]	Concentration. Increase rate	1~2 months	(+) 0.3N NaOH (-) 5.0% NaCl	12V	$D = \frac{JRTL}{z_{ci}F\Delta EC_1}$
NT Build 443 Accelerated chloride penetration[4)]	Penetration profile	Minimum 1 month	2.8N NaCl Solution	-	$C(x,t) = C_s \cdot erf(x/\sqrt{4 \cdot D \cdot t})$

Nowadays, the use of electrically accelerated chloride penetration tests has become a very useful tool for establishing the relationship between the microstructural features in general, estimating the diffusion coefficient of the ITZ region and the velocity of the chloride penetration as a function of its micro features. They have been used successfully for both experimental and numerical models of this approach by several investigations i.e. (Yang and Su, 2002, Yang and Cho, 2005, Yang, 2005, Zheng et al., 2009). However, for the NVC or mortars, most recent investigations have employed accelerated steady state conditions. For high performance concrete incorporating different types of fillers and mineral admixture, a very long time might be needed to maintain the steady state to assess the chloride migration coefficients. Thus, a non- steady state test was modified and used for this purpose to calculate the non-steady chloride migration coefficients (D_{nssm}) of the different concrete types in order to establish pore structure-chloride ingress relationships (Section7.4 and Section 7.5).

7.3 Tests performed and modified for chloride migration and diffusion tests

For calculating the non-steady state chloride migration coefficient (D_{nssm}), the chloride movement was achieved using a modified rapid migration test. This modification, as described in Section 7.3.1, was mainly performed in order to reduce the time of the test to, as much as possible, 6hr or somewhat more (depending on the applied voltage in Table 7.2). The need for a modified none-steady state test was based on electro-chemical issues related to the migration of OH^- ions during the chloride migration test, as explained in more detail in Chapter 2 Section 2.3.2.

7.3.1 Rapid chloride migration test

The same type of specimen that was used for the Marco porosity test in Section 3.1.2 was used to determine the none-steady state chloride migration coefficient (D_{nssm}). Before the test, the mortar discs were vacuumed and saturated with a $Ca(OH)_2$ solution. The same arrangement as suggested by the Nordtest standard (NT BUILD 492, Nordtest,1999) as shown in Fig.7-5, was adopted in performing the experiment. However, the main difference is the dimension of the specimens, especially the thickness, which can affect the chloride penetration depth considerably. According to the standard, the time of the test should be determined dependent on the initial reading of the current under an applied voltage of 30V.

First, preliminary work was conducted on one sample of each mix with an external voltage of 30V to find the initial current (I_{30v}) and, hence, a suitable time for the modified test so that chloride does not breakthrough nor achieve only a shallow penetration depth through the sample. None of these samples produced an initial current in the range suggested by the standard due to the difference in thickness of the specimens used leading to different electrical resistances. The initial currents were all in the range 80-320 mA. Thus, the challenge was to find an appropriate time that would keep the chloride penetration within the thickness of the specimen (10-15) mm under the initial current. As stated by McGrath and Hooton (1996), the calculated non-steady chloride penetration coefficient was reasonably constant over the voltage range tested up to 30V.

For the modified arrangement just described, 30V would cause a considerably greater voltage gradient and this gave cause for concern regarding possible heat generation and

consequential specimen damage which would affect chloride ingress. For this reason during the preliminary work, the temperature of the anolyte (0.3M NaOH) and the catholyte (10% NaCl) solutions was measured continuously using a thermocouple. The range of the recorded temperatures was 18.6 - 25.4 °C showing that there was no substantial change in the temperature of the specimen during the test. The standard (NT BUILD 492, Nordtest,1999) stipulates an operating temperature range of 20 to 25 °C, thus the modified arrangements appear acceptable in this respect.

Several trials were performed on each specimen for 6, 5, 4, 3, 2 or 1 hours. Finally, the test duration then was specified to be 1 h as the chloride penetration was within the thickness of specimen for all types of NVC and SCC mortars whereas complete breakthrough of the chloride occurred for larger test durations.

Fig.7-6 shows examples of some samples broken in half to expose an internal cross section and then coloured by the use of 0.1 M silver nitrate solution indicator ($AgNO_3$). White silver chloride precipitation (AgCl) on the split surface appeared clearly after 5-10 minutes where the chloride ions have penetrated. Then, the D_{nssm} was calculated as an average value of duplicated successful samples for each mix using the modified Nernst-Planck equation Eq.7.5 (NT BUILD 492, Nordtest,1999):

$$D_{nssm} = \frac{0.0239(273+T)L}{(U-2)t}\left[X_d - 0.0238\sqrt{\frac{(273+T)LX_d}{U-2}}\right] \quad \textbf{.....Eq. 7.5}$$

D_{nssm}: Non-steady-state migration coefficient, $\times 10^{-12}$ m^2/s;

U: Absolute value of the applied voltage, V;

T: Average value of the initial and final temperatures in the anolyte solution, °C;

L: Thickness of the specimen, mm;

X_d: Average depth of penetration over central zone as revealed by AgCl coloring, mm, and t: Test duration, hr.

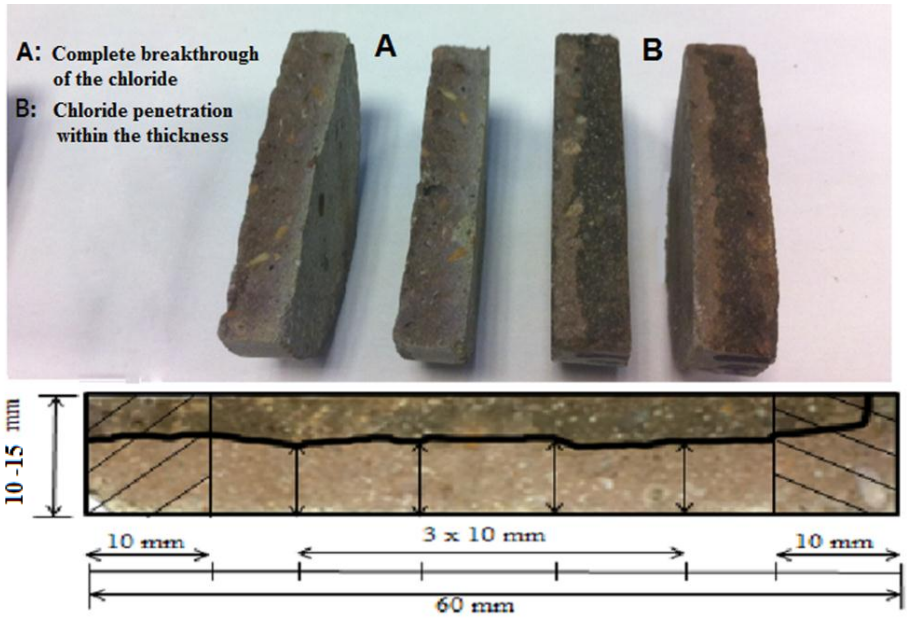

Figure 7-6 some tested specimens and the chloride penetration distance (X_d) revealed by AgCl

Using the ACTM C1202 (steady state) test to assess the chloride penetration in normal vibrated carbonated concrete samples with three different water to cement ratios (w/c) (0.4, 0.5 and 0.6), Chang et al (2004) demonstrated that the assessed total charges (coulombs) decreased for these samples as compared to the healthy ones (with no carbonation). This indicates a delay of the chloride penetration due to the carbonation. The authors justified this by the denser microstructure of the concrete matrix observed in their SEM images after carbonation. However, the assessed carbonated samples in this study were not completely carbonated except those of 0.6 w/c ratio.

It should be noted here that an attempt has been made by the author to address the effect of carbonation on the chloride penetration using the modified arrangement. This was done by using fully carbonated NVC and SCC mortar samples (see Section 6.2.2.2). However, the chloride penetration assessed by AgCl coloring change indicated a noticeable ingress of the chloride through the samples for all the concrete types assessed in this study. These results are totally against the prevailing opinion that the carbonation produced a denser concrete microstructure and hence would delay the chloride penetration in natural condition or even with the use of chloride electrochemical accelerated tests, as stated by Chang et al (2004). However, the carbonation can reduce the chloride binding and can remove charge carriers effectively if it happens in chlorides contaminated concrete.

From an electro-chemical point of view, the observed results of the present work might be attributed to the complete change of cement matrix chemistry and the pH of the pore water solution after carbonation. These changes could increase the migration of the free and the combined chloride ions as well that induced by the external applied voltage and thus apparently increase the chloride penetration velocity. Therefore, care should be taken to address the effect of carbonation on the chloride ingress in concrete using the electrochemical chloride accelerated test, in particular for saturated concrete.

7.3.2 Chloride penetration test (immersion test)

The chloride penetration test was performed in accordance to the recommendation of NT Build 443 standard (NT BUILD 443, Nordtest,1995) using 70mm mortar cubes. This was done in order to reduce any variation in the chloride penetration path resulting from differences due to coarse aggregate proportion in the mix design of full NVC and SCC. The NVC and SCC mortars have the same proportions of the fine aggregate with approximately the same $V_{fine\ agg.}/V_{mortar}$ (See Sections 4.4.1 and 4.4.6). To a large extent this should minimize the effect of the aggregate phase in determining the chloride penetration path taking into account that the aggregate (fine/coarse) is considered as an impermeable phase for the chloride ions as compared to the cement matrix. Further, the diffusion of the free chloride ions occurs in the pore water solution through the continuous capillary pores of the cement matrix and the percolated pores of the Interfacial Transition Zones (ITZs) formed around the aggregate (both fine and coarse) as will be discussed in Section 7.4.

After casting and demoulding, the mortar specimens were cured for 28 days in potable water before full immersion in NaCl solution with a 2M concentration (165 gm/L). Prior to the immersion, the mortar cubes were vacuumed using 100 mb for 3 hours and then left in a saturated $Ca(OH)_2$ solution for three days to ensure full saturation, which is essential for the chloride diffusion test. Finally, five faces of the mortar cubes were sealed very well, to ensure only one direction of chloride penetration which was perpendicular to the casting direction, and then the cubes were submerged in the salt solution. The containers were covered by polyethylene and kept in the laboratory for 90

days. The NT Build 443 standard proposed an immersion period of at least 35 days for low quality concrete and 90 days for high quality ones (Stanish et al., 2000).

7.3.2.1 Preparing of concrete powder sample and titration test

After 90 days, the specimens were extracted from the salt solution and kept in the laboratory for a suitable time for drying. The specimens then were placed in a grinding machine to remove 1mm layers and the resulting powder was collected with the aid of a hand vacuum device. 0.3 to 1 gm from the powders sample were weighed using a high sensitive balance with an accuracy of 0.0001 gm and kept in a sealed glass containers up to the day of titration tests to calculate the their chloride contents.

Among the different proposed techniques to determine the chloride contents of the powdered cementitious material, the titration method is recognized to be an accurate method for calculating the chloride concentration/content. As reported by Dhir, 1990 (Dhir et al., 1990), this method is able to detect up to 94% of the total chloride content (free plus combined ions). Thus, the standard Volhard titration method was used for this purpose. The profiled powder samples were dissolved in 50 ml distilled water and acetified with 10ml of nitric acid (HNO_3, 5M).

The beakers and the solution were boiled to about 150 ºC for 4-5 minutes with continuous stirring to allow complete dissolution of the chloride ions from the powder samples. Then, the solutions were filtrated using a filtration paper and an additional 40ml of distilled water was added to maintain a total volume of 100ml of the solution. The 100ml solutions were kept in well-sealed standard plastic bottles and provided for the titration test. Four solution samples (each 25 ml) were used for the titration test against a standard titrant ($AgNO_3$, 0.041M) after adding 3-5 drops of Potassium dichromate ($K_2Cr_2O_7$).

The calculated chloride content represent an average of three titration trials of each solution sample where (V_1-V_2) is ± 0.02 ml. The chloride content was calculated using Eq. 7.6:

$$Cl^{-}gm = [0.041 \times (V_1 - V_2)/25] \times 35.5 \quad \textbf{……Eq. 7.6}$$

V1: the volume of the titrant in the burette before titration

V2: the volume of the titrant in the burette after titration up to the equilibrium point when the solution color changed from yellow to brown, as shown in Fig.3.

35.5: atomic mass of the chlorine

25: the volume of the solution (ml)

0.041: molarity of the titrant ($AgNO_3$)

The preparation of the profiled powder samples and the titration steps are summarized in Fig.7-7.

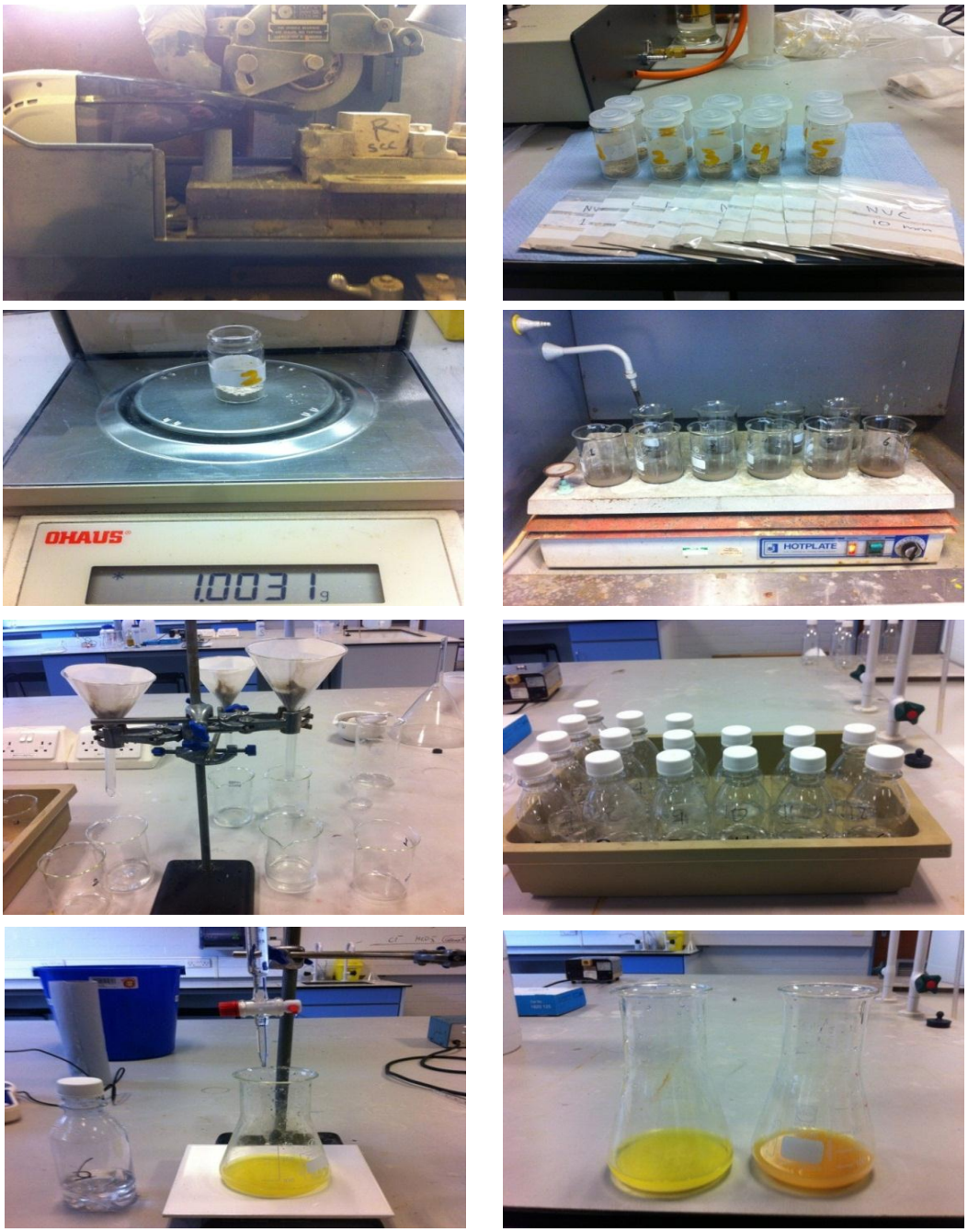

Figure 7-7 Powder samples collection and titration process

7.4 General discussion of the pore structure and the percolation degrees of the ITZ

Before establishing the relationships between the obtained D_{nssm} and the pore structure features at different scales (Table 5-3). It would be interesting to determine the pore percolation degrees of the analyzed ITZ's micro-features to consider their effects on the overall chloride penetration response of each concrete type.

For the MIP test which was used as part of the quantitative analysis of the pore structure at different scales in Chapter 5, it is already reported by Shane et al.(2000) that the mercury is expected to intrude into the large pores in the ITZ region if they are percolated. Consequently, the smaller pores (including the smallest ones (CPD)) will be allocated in the nearby cement matrix. Conversely, this is not the case for non-percolated ITZ as shown in Fig.7-8 (Shane et al., 2000).

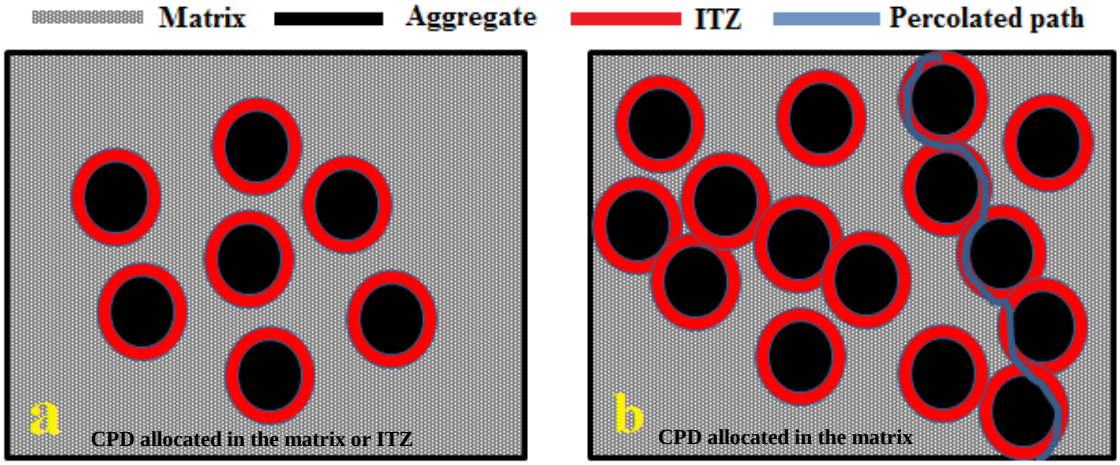

Figure 7-8 a) Non-percolated ITZs with low volume fraction of aggregate b) percolated ITZs with high volume fraction of aggregate after (Shane et al., 2000)

The results of the present study (Table 5-3) showed that in spite of the marginally macro porosity nature, the R-SCC exhibited similar or lower CPD as compared to the FA-SCC and LP-SCC respectively. However, the FA-SF-SCC demonstrated the lowest critical pore diameter, signifying the lowest cement matrix' pore percolation.

For the SCC mortars, the volume fraction of the fine aggregate should be between 40-50% in order to reduce the segregation and obtain the stability for the mix as reported by published guidance and research findings (EFNARC, 2002, Okamura and Ouchi, 2003, Koehler and Fowler, 2006, De Schutter et al., 2008). Therefore, the probability of

the ITZ having percolating pores is likely to be high even when ITZ thickness is small. For the adopted aggregate : mortar volume fraction (49.7-51.2%) for all concrete types, the experimental results obtained for the minimum detected ITZ-thickness (15µm for FA-SF-SCC) was analyzed in conjunction with a numerical model adopted by et al. (1994) for concrete mortars with different aggregate volume fractions and ITZ thicknesses. The outputs of this model are summarized in Fig.7-9.

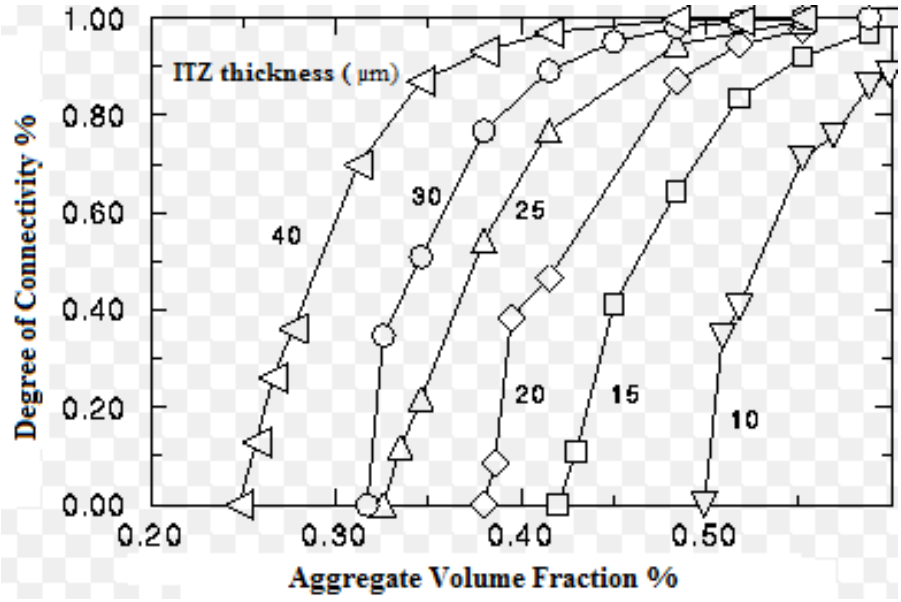

Figure 7-9 outputs of Winslow et al. model 1994

The analysis revealed that the degree of ITZ pores interconnectivity is more than 78%. These degrees were approximately greater than 90%, 88%, and 95% for the R, FA, and LP-SCC respectively. The ITZ's interconnectivity degree in the NVC was more than 99% (Fully interconnected). Thus; the chloride penetration might largely be governed by ITZ pores percolations in such a way that the tortuosity effect of the aggregate could be neglected due to the use of the same fine aggregate volume fractions of all the mixes. The change in tortuosity effect of the aggregate is not entirely eliminated, but should be rather small. The presence of the coarse aggregate in the concrete matrix is expected to increase the percolation degree of the original percolated ITZs for the mortars and hence increase the ingress of the water or the aggressive substances such as Cl^- and CO_2, relative to its mortar.

7.5 Macro/micro and nano internal pore structure property relationships with the none-steady state chloride diffusion D_{nssm}

7.5.1 D_{nssm} – ITZ micro-features relationships

Fig.7-10 plots the relationships between ITZ porosity and thickness of the different types of concrete and the none-steady sate chloride migration coefficient obtained from the analysis of the modified rapid chloride migration test (Section 7.3.1).

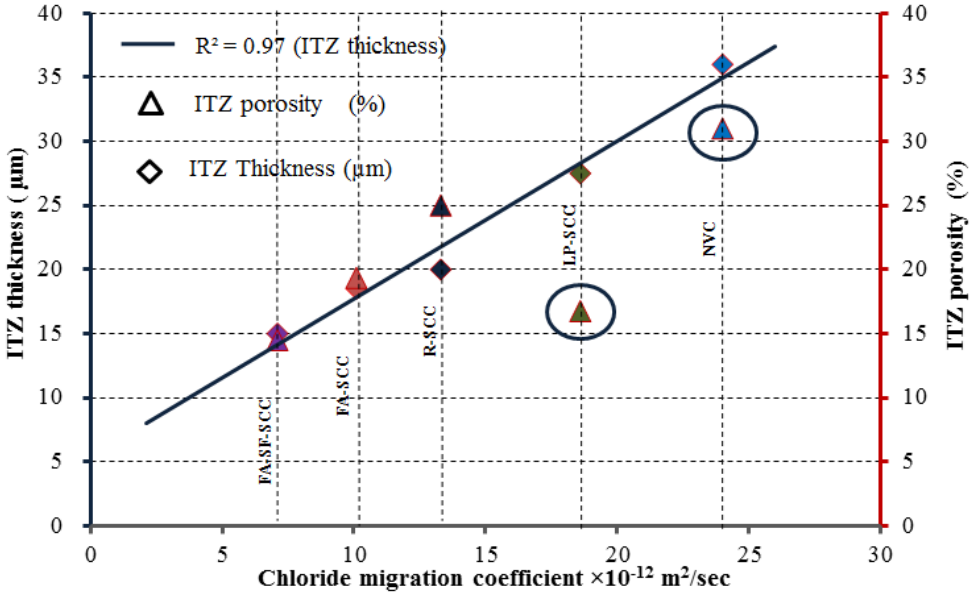

Figure 7-10 D_{nssm} – ITZ micro-features relationships

It can be seen clearly that the chloride migration coefficient is simply related to ITZ thickness and, with the exception of the anomalous LP-SCC and NVC results, to the ITZ porosity. The latter relationship is in line with Jiang et al. (2012) who stated that the increase of the porosity of the ITZ could facilitate the penetration of destructive agents including chloride and carbon dioxide. Taking the two relationships together, and assuming the distribution of the pores through the ITZ thickness around the aggregate, this might suggest that the chloride penetration in all types of SCC is likely to be controlled by the pore percolation in the ITZs, as a high degree of interconnected pores were deduced (78-95 %) in this region (Section 7.4). For LP-SCC and NVC, the higher ITZ thickness allows more capillary pores to be interconnected to adjacent ITZs in these two mix types. Thus, a more porous path is anticipated and, thus, a decreased chloride resistance is found for these two mixes.

7.5.2 D_{nssm} – Pore structure features relationships

Fig.7-11 plots the relationships between the critical pore diameters (CPDs), the average pore diameters (APDs) and the non-steady chloride migration coefficients obtained from the analysis of the modified rapid chloride migration test (Section 7.3.1) of the concrete mixes.

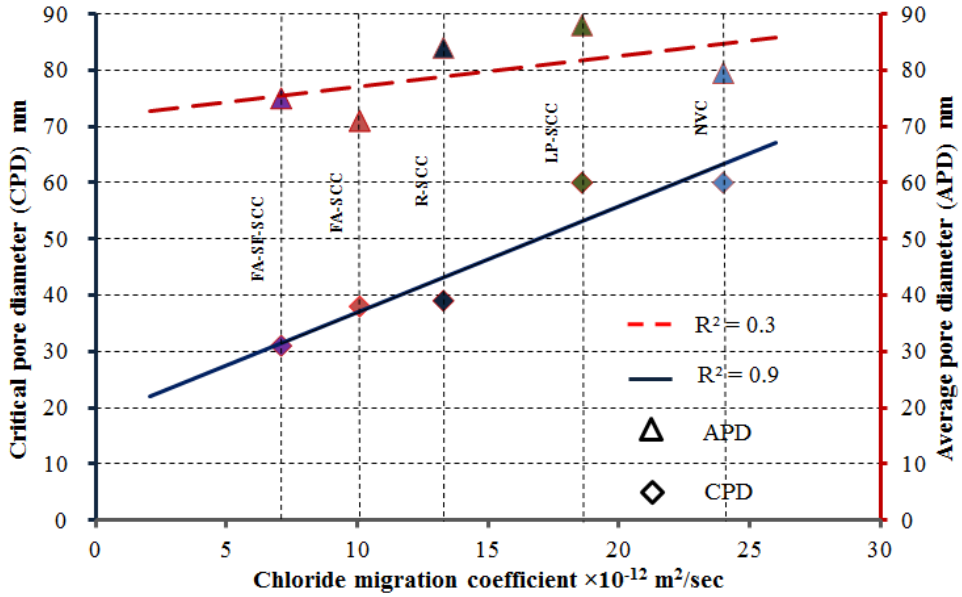

Figure 7-11 D_{nssm} – Pore structure features relationships

A broadly linear relationship was observed in both cases. Although the figure shows that the chloride migration coefficient had much higher correlation with the CPDs than the APDs, there are insufficient data to assess the relative reliability of these correlations. Moon et al. (2006) observed a very high correlation (0.91) between the APD and the chloride diffusion coefficient for some high performance concrete specimens. On the basis of the present investigation alone, it would seem that the CPD in the cement matrix is a more important factor than the APD in controlling the chloride penetration velocity of SCC. Therefore, it is proposed that the chloride resistance of a SCC with high replacement of cement could be increased /decreased according to the ability of its filler or mineral admixture to alter the interconnectivity nature of the pores in the cement matrix (CPD at the nano scale). This is independent on the resulting average capillary pores diameter in the ITZ or in the cement matrix at this scale, or the porosity value/nature of the pore diameters at the micro or macro scales as listed in Table 5-3.

7.6 Chloride penetration resistance, modeling and predicting of the service life-NT Build443

The apparent chloride diffusion coefficients (D_{nss}) and surface chloride concentrations (Cs) values for the NVC and SCC were calculated from the non-linear curve best fitting the chloride content (% by weight of concrete) versus the depth in (mm) data. The curve fitting was based on a numerical solution using the least squares method for minimizing errors between the obtained experimental results and the theoretical model with the aid of the Excel solver tool. This tool and the steps of the non-linear regression implementation are included in the same Excel sheet as for the chloride ingress modelling (Section 7.7) for each concrete type. An example of the best curve fitting is given in Fig.7-12 for the NVC. The theoretical model in this figure is a plot of the solution of Fick's second law of diffusion (as used by Nordtest method NT BUILD 443) as shown in Eq. 7.7. Due to the burdensome quantity of data obtained and the numerical analysis performed, all the details of the titration tests results, the steps of the implementation of the non-linear curve-fitting using the Excel solver tool and the numerical simulation of the chloride ingress for each types of investigated concrete are attached in **Appendix D**.

$$C(x,t) = C_s - (C_s - C_i) \cdot \operatorname{erf}\left(\frac{x}{\sqrt{4D_{nss}\,t}}\right) \quad \text{.....Eq. 7.7}$$

$C(x,t)$ = chloride content measured at depth x at exposure time t, % by weight of concrete

C_s = calculated surface chloride content, % by weight of concrete

C_i = initial chloride content, % by weight of concrete

x = depth, mm

D_{nss} = apparent chloride diffusion coefficient (non-steady state), m^2/sec

t = exposure time, sec

erf = error function= $\operatorname{erf}(z) = \frac{2}{\sqrt{\pi}} \int_0^z \exp\ (-u^2)\, du$

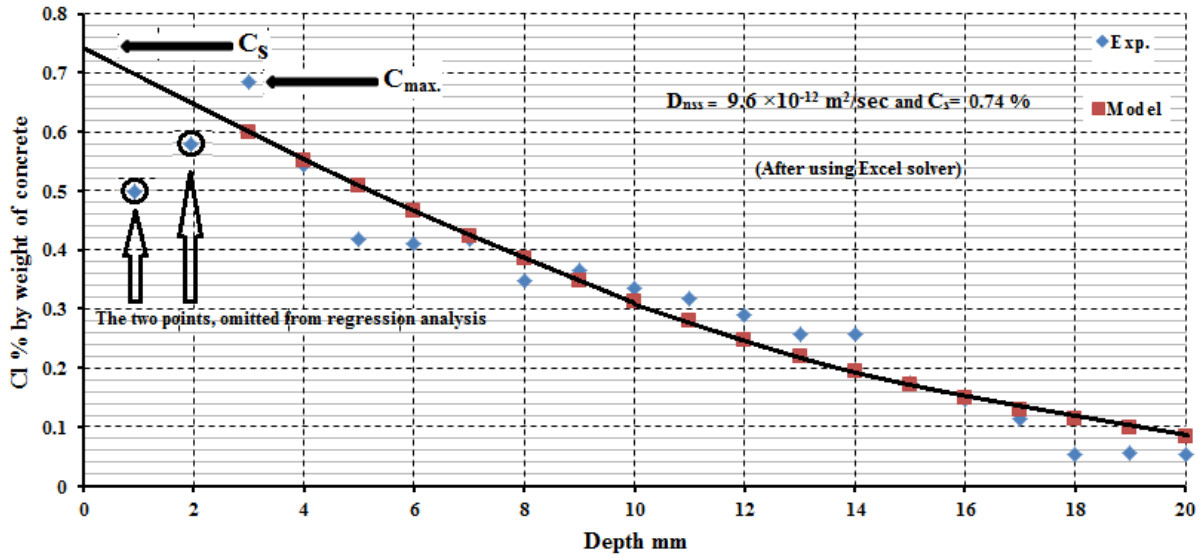

Figure 7-12 Curve fitting data after using Excel solver

The lower chloride contents than the maximum detected one was omitted from the non-linear regression as shown in Fig.7-12.These values are normally appear in chloride content-depth relationships (Gjørv 2009) perhaps because of the leaching of the chloride ions to the surface of the specimen during the drying period. Two such points were observed for the NVC-mix and one point for all the other types of SCC. D_{nss} and C_s values for the all concrete types are summarized and listed in Table 7-3. The penetration parameter (K_{cr}) in mm /$\sqrt{year}$ which takes into account both the effect of the resulting surface chloride contents and the computed diffusion coefficients is considered more relevant for chloride resistance comparison purposes although it does not represent the actual chloride penetration velocity. Thus it was calculated and listed in the same table according to the Eq. 7.8 as reported by the 5FP Growth Program (2002):

$$K_{cr} = 2\sqrt{D_{nss}}\ \mathrm{erf}^{-1}\left(\frac{C_s - C_r}{C_s - C_i}\right) \quad \textbf{.....Eq. 7.8}$$

erf^{-1} = the inverse of erf

C_r = critical chloride content =0.05% by weight of concrete and

K_{cr} is defined only when $C_s > C_r > C_i$

Table 7-3 D_{nss} , C_s and K_{cr} values of the concrete mixes

Mix title	$D_{nss} \times 10^{-12}$	C_s (% by wt. concrete)	K_{cr} (mm / $\sqrt{year}$)
NVC	9.60	0.74	47.2
R-SCC	8.35	0.31	34.5
LP-SCC	16.03	0.40	51.8
FA-SCC	9.26	0.49	34.9
FA-SF-SCC	8.46	0.31	34.5

The results in Table 7-3 demonstrated that all the concrete types show approximately similar apparent diffusion coefficients (8.35-9.60) $\times 10^{-12}$ m^2/sec including the NVC but with the exception of LP-SCC. In all mortar samples assessed, except the LP-SCC, the ratio of the active binder (cement, cement plus FA, cement plus FA-SF) to fine aggregate was 1:2, and these four mixes all exhibited similar diffusion coefficients. In contrast the LP-SCC mortar, with an active binder to fine aggregate ratio of 1:3, had a significantly higher diffusion coefficient although the mortar's mix design maintained approximately the same volume of the fine aggregate to the total volume of the cement matrix (50.7% for LP-SCC mortar and 49.7-51.2% for the other mortars). Therefore, it seems likely that chloride diffusion is reduced by interaction with an active binder. Chemically, the matrix of the LP-SCC might not have a similar chloride binding ability as compared to the cement itself in NVC and R-SCC and cement plus active fillers even with the low water to cementitious material ratio used. Physically, the quantitative analysis of the pore structure of this type of concrete and the micro-features of its ITZ (by the author et.al.) indicated a more open microstructure, with less homogeneity ITZ (Mohammed et al., 2013, Mohammed et al., 2014).

The NVC exhibited the highest surface chloride content (Cs) as compared to the other SCC types. At the same time, it showed a slightly higher chloride resistance (lower penetration parameter) as compared to the LP-SCC. The calculation of the penetration parameter K_{cr} helps to explain these results. The LP-SCC showed the highest K_{cr} signifying the lowest chloride resistance followed by NVC with only a little greater resistance. All the SCCs containing fully active cementitious material (i.e. cement or active-cement replacement) show much greater, and broadly similar, resistance to

chloride penetration. Thus, it is apparent that the SCCs mixes provide a denser matrix more resistance to chloride penetration, but that this improvement is undermined when some of the active filler (cement) is replaced by passive filler (LP). Thus, in part, resistance to chloride penetration is provided by interaction of the chloride with hydration products. Given that hydration is progressive, this implies a non-constant diffusion coefficient.

7.7 Modelling of chloride penetration, prediction of service life and cover design

The estimation of the service life of the normal and SCC mixes was performed numerically for different ages to find $C(x,t)$, based on the solution of Fick's second law (Eq. 7.7) as shown in Figs. 7-13 to 7-17. As indicated above hydration and diffusion are interacting mechanisms for the chloride movement through concrete. Therefore, to predict long-term diffusion, which is the most familiar controlling mechanism for the chloride ingress process (submerged concrete structure) (Stanish et al., 2000), the values obtained in the short term (D_{nss} at 90 days as given in Table 7-3) must be adjusted to a time-dependent value. This is achieved using the formula presented as Eq. 7.9 (Hassan, 2012):

$$D_a(t) = D_{ao}(t)\left(\frac{t_0}{t}\right)^{\alpha} \quad \textbf{.....Eq. 7.9}$$

$D_a(t)$: Time dependent chloride diffusion coefficient

t : Maturity age and t_0 : Reference maturity age (when concrete exposed to chloride)

$D_{ao}(t)$: Achieved apparent chloride diffusion coefficient (D_{nss}) at maturity age (t_0)

α : Aging factor (reduction in D_{nss} with time due to continuous hydration plus binding effect.

Current experience indicated that the aging factor of CEM I based concretes and of FA based concrete is 0.4 and 0.6 respectively and may still be used for the estimation of a proper aging factor (Gjørv 2009). The aging factor of LP based concrete is not available in the literature. Therefore, it is assumed to be similar to the NVC mix (i.e. 0.4) due to the same trend in compressive strength development up to 28 days (see Section 4.5). For the FA-SF SCC the FA aging factor has been adopted (0.6). The critical chloride content for the steel corrosion initiation is between 0.05-0.07 by weight of concrete for different exposure humidity and conditions and normally is taken as 0.05% by weight of concrete (Gjørv 2009, Bioubakhsh, 2011) (See horizontal lines on Figs. 7-13 to 7-17).

It can be noted that Nilsson, 2001 (Nilsson, 2001) quotes Frederiksen et al. 1997 who reported that the relationship between the NT Build 443 laboratory exposure and the field exposure has been established for plain concrete. The result of the present investigation shows that the values of the surface chloride concentrations were between 0.31 and 0.74 which is typical for various types of concrete structure exposed to severe natural chloride environments over a range of different exposure ages as reported by (Gjørv 2009).

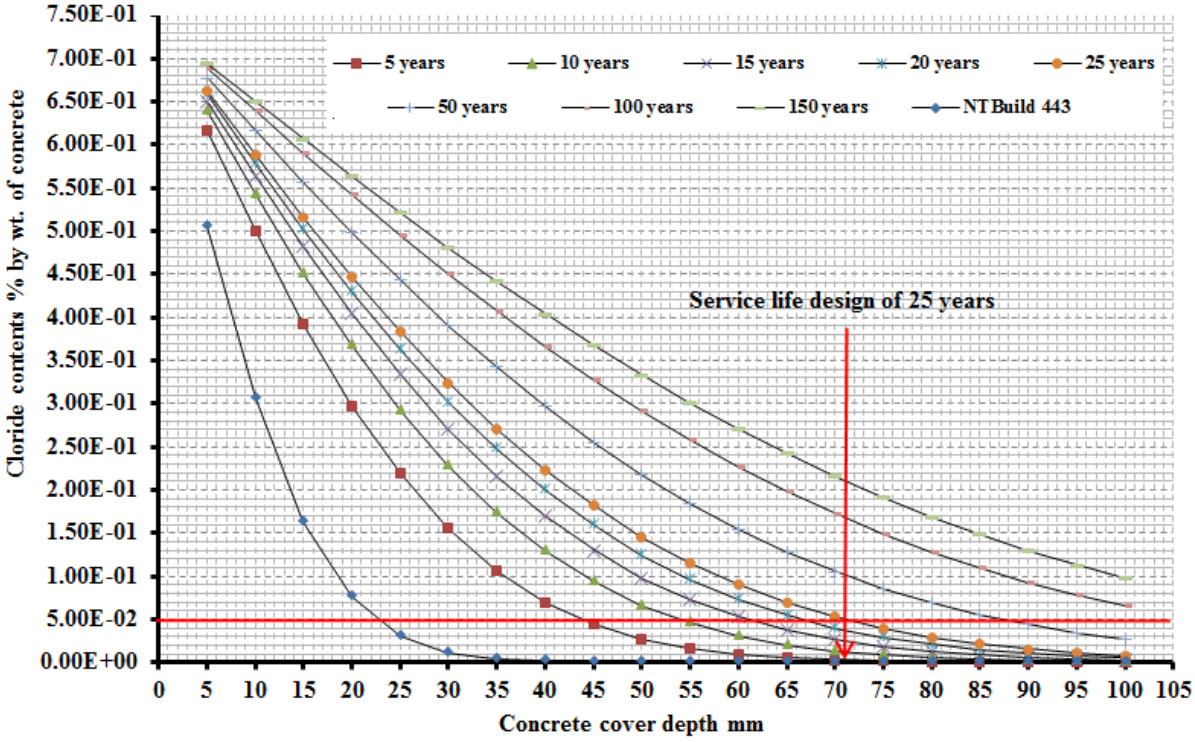

Figure 7-13 chloride ingress model - NVC

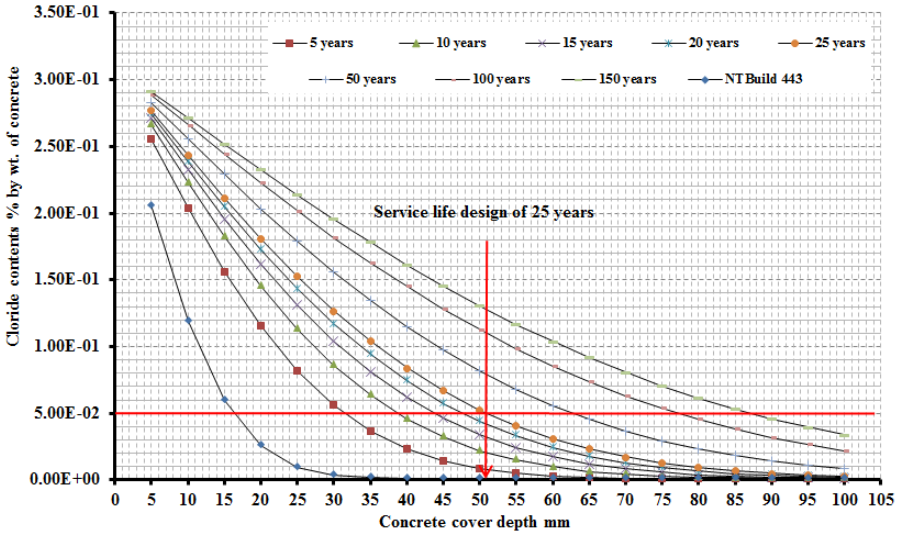

Figure 7-14 chloride ingress model: R-SCC

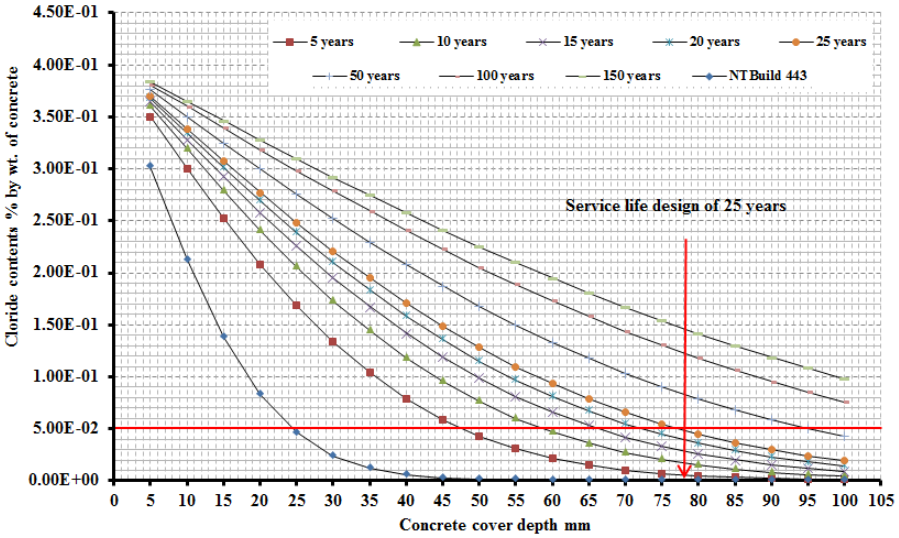

Figure 7-15 chloride ingress model: LP-SCC

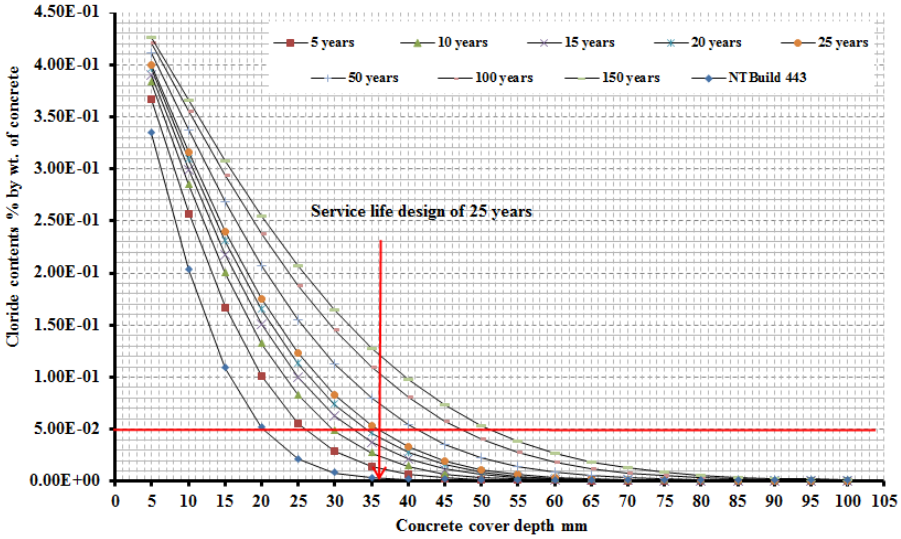

Figure 7-16 chloride ingress model: FA-SCC

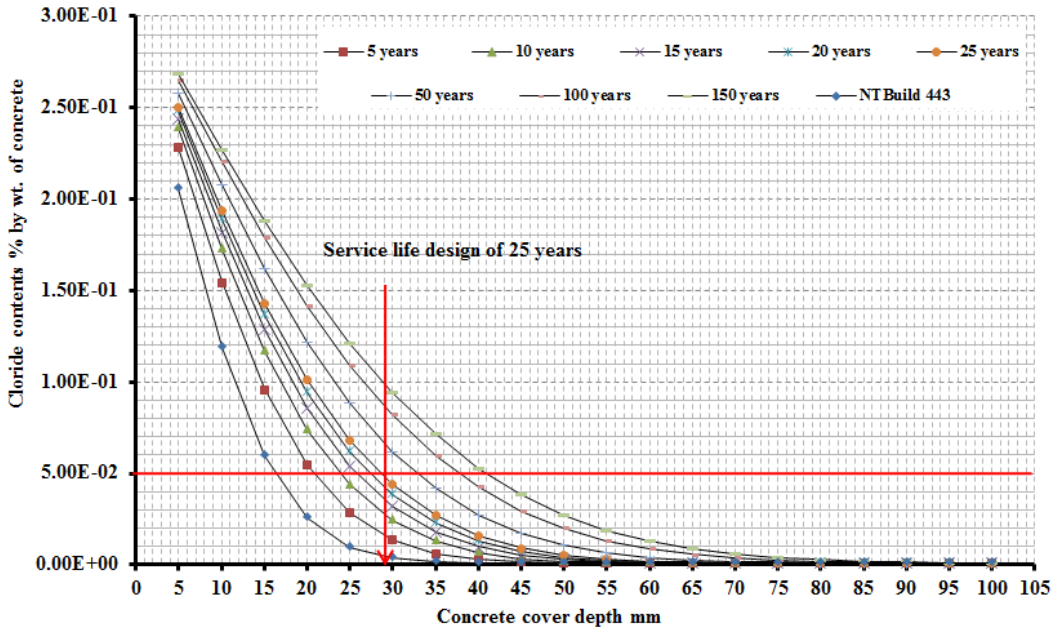

Figure 7-17 chloride ingress model: FA-SF-SCC

Using these approaches, Figs. 7-13 to 7-17, show that, in order to achieve a service life design of 25 or 50 years, the theoretical designed concrete cover for the NVC mix should be 71mm or 87 mm respectively while it should be 51mm or 63 mm for the R-SCC. Further, for the LP-SCC, to achieve 50 years' service life would require excessive concrete as much as 78mm being needed even for 25 years protection. It should be borne in mind that the increase of the cover thickness beyond 70 mm could have an adverse effect, as it can increase the probability of the concrete cover cracks due to the external load, depending on the design purpose, and it will increase the whole cost of concrete element construction. The FA-SCC and FA-SF-SCC decrease the required cover thicknesses to about 36mm and 29mm for 25 years' service life and 42mm and 33mm for 50 years' service life respectively.

To assess the validity of using all types of concrete produced in this study for aggressive natural chloride environments (from the predicted cover design) and to compare the results with the available standards and codes for structural concrete used for bridges construction, Table 7-4 summarized the exposure classes related to chloride environment in EN 206:1 (BSI, 2000b).

Table 7-4 Table describing exposure classes related to chloride environment in EN 206:1 (BSI, 2000b) (Hassan, 2012)

Class designation	Description of the environment	Informative examples where exposure classes may occur
3. Corrosion induced by chloride other than from sea water		
Where concrete containing reinforcement or other embedded metal is subject to contact with water containing chlorides, including de-icing salts, from sources other than from sea water, the exposure shall be classified as follows: NOTE Concerning moisture conditions, see also section 2 of this table.		
XD1	Moderate humidity	Concrete surfaces exposed to airborne chlorides
XD2	Wet, rarely dry	Swimming pools. Concrete exposed to industrial waters containing chlorides
XD3	Cyclic wet and dry	Parts of bridges exposed to spray containing chlorides. Pavements. Car park slabs.
4. Corrosion induced by chlorides from sea water		
Where concrete containing reinforcement or other embedded metal is subject to contact with chlorides from sea water or air carrying salt originating from sea water, the exposure shall be classified as follows:		
XS1	Exposed to airborne salt but not in direct contact with sea water	Structures near to or on the coast
XS2	Permanently submerged	Parts of marine structures
XS3	Tidal, splash and spray zones	Parts of marine structures

Table 7-4 lists the degradation classes for the corrosion induced by chlorides from sea water as XS1, XS2 and XS3 for different environments whilst Table 7-5 gives the minimum cover requirements for durable concrete for these three classes according to Eurocode2: Part2 (Hendy and Smith, 2007). The structural class of the produced NVC and SCC is S2 according to this code. Therefore, the minimum cover requirements for the durable concrete are 25mm, 30mm and 35 mm for XS1, XS2 and XS3 class degradations respectively (shaded cells).

Table 7-5 Minimum cover requirements $C_{min,dur}$, for durability(reinforcing steel) (Hendy and Smith, 2007)

Environmental requirements for $C_{min,dur}$ (mm)							
Structural class	Exposure class						
	X0	XC1	XC2/XC3	XC4	XD1/XS1	XD2/XS2	XD3/XS3
S1	10	10	10	15	20	25	30
S2	10	10	15	20	**25**	**30**	**35**
S3	10	10	20	25	30	35	40
S4	10	15	25	30	35	40	45
S5	15	20	30	35	40	45	50
S6	20	25	35	40	45	50	55

X0=No corrosion, XC=corrosion induced by carbonation, XD=corrosion induced by chloride other than sea water and XD=corrosion induced by chloride from sea water

The predicted results for 25 years' service life revealed that only FA-SF-SCC showed less cover thickness (29mm, See Fig. 7-17) than proposed by Eurocode2. This in both XS2 and XS3 degradation classes, whilst FA-SCC required approximately the same minimum cover as for the XS3 class (36mm, See Fig. 7-16). On the other hand, for 50 years' service life, only FA-SF-SCC exhibited less cover value (33mm) than the XS3 class. The result obtained demonstrates the benefits of using relatively high dosages of active by-product fillers as partial replacement of cement in improving both the sustainability of the SCC constructions and in delivering economic of concrete elements that could be exposed to severe chloride environments. However, care must be taken in both the selection of a proper mix design to obtain the required fresh properties and to gain the designed strength level in the short term at 28 days.

7.8 Concluding remarks

Based on the work reported in this chapter, it can be concluded that:

- The use of LP at relatively high replacement of cement increased the chloride penetration velocity of LP-SCC (in terms of both the obtained chloride migration coefficient (D_{nnsm}) in the short term and in the apparent chloride diffusion coefficient (D_{nns}) in the long term as compared with both the use of cement only in NVC and R-SCC (no replacement) and the incorporating of active fillers and mineral admixture such as FA and FA+SF respectively at the same replacement percentage at 50-60MPa design strength (28 days).

- Care should be taken to address the effect of carbonation on the chloride ingress in concrete using the electrochemically- accelerated chloride penetration test, in particular, for saturated concrete due to the probable change of the pH value of the pore water solution after carbonation.

- The chloride migration coefficient (D_{nssm}) was usually proportional to both the thickness and the porosity of the ITZ. However, the ITZ porosity of the LP-SCC and NVC did not fit with this relation. This suggests that high deduced ITZ thickness increased the capillary pore's percolation in the ITZ and thus ITZ thickness was more responsible than ITZ porosity alone in determining the chloride ingress.

- The internal pore structure analysis at different scales revealed that the macro or micro porosity natures of the NVC and SCC did not relate to the chloride penetration diffusivity (D_{nssm}) as it is the interconnectivity of the pores in the cement matrix (represented by the change in the CPD) and the percolation degree of the pores in the ITZ that play a more important controlling role.

- At the nano-scale, the comparison of the results of the chloride migration assessment (in terms of D_{nnsm}) and of the characteristics of the internal pore structure demonstrated that the chloride penetration velocities were more closely related to the change in the CPDs in the cement matrix than to the APDs, including the capillary pores, in both the ITZ and the cement matrix.

- The incorporation of relatively high replacements of cement by LP increased the apparent diffusion of chloride through SCC and increased the penetration parameter (K_{cr}) as compared to NVC for the same design strength. The K_{cr} of this LP-SCC was slightly higher than that of the NVC, even with the use of lower water to cementitious material ratio.

- The NVC exhibited the highest surface chloride content assessed by Nordtest method NT BUILD 443 test among all the tested types of SCC. However, it achieved a slightly lower penetration parameter than that in the LP-SCC.

- A simplified service life model for the chloride ingress in concrete has been proposed based on simple diffusion theory and a time-dependent factor (α) for the

chloride diffusion coefficient. The chloride penetration through concrete was numerically modelled with the aid of a numerical tool developed in Excel solver to calculate the diffusion coefficient and surface chloride content according to the NT build 443 accelerated tests.

- According to this model, the theoretical thicknesses for the concrete cover design were 71mm, 51 mm, 78mm, 36mm and 29mm for 25 years' service life for NVC, R-SCC, LP-SCC, FA-SCC and FA-SF-SCC (having the same design compressive strength, 50-60 MPa) respectively. The corresponding values were 87mm, 63mm, more than 95mm, 42mm and 33mm for 50 years' service life. Thicknesses greater than 70mm are often viewed as undesirable, thus only the mixes with cement or cement plus active fillers achieve practical resistance to chloride penetration in the long term.

- For natural aggressive chloride environments, the predicted cover thicknesses for all assessed concrete types demonstrated how the use of relatively high dosages of active by-products fillers as partial replacement of cement could improve both the sustainability of the SCC constriction and economically provide concrete element construction that will withstand exposure to severe chloride environments. However, with appropriate selection and mix design, the replacement of cement by active by-product fillers need not interfere with the development of concrete strength. In this way, the modified mix can still obtain a medium to high design compressive strength at 28 days.

7.9 References

ASTM 2000 vol. C04.02. C1202 Electrical indication of concrete's ability to resist chloride ion penetration. Annual Book of American Society for Testing Materials Standards.

AUDENAERT, K., BOEL, V. & DE SCHUTTER, G. Year. Chloride migration in self compacting concrete. In: Proceedings of the 5th International Conference on Concrete under Severe Conditions Environment and Loading (CONSEC 07), 2007. 291-298.

BIOUBAKHSH, S. 2011. The penetration of chloride in concrete subject to wetting and drying: measurement and modelling. UCL (University College London).

CEMENT CONCRETE & AGGREGATES AUSTRALIA. 2009. Available: http://www.concrete.net.au/publications/pdf/ChlorideResistance.pdf [Accessed 17-05-2012].

CHANG, J. J., YEIH, W., HUANG, R. & CHEN, C. T. 2004. Suitability of several current used concrete durability indices on evaluating the corrosion hazard for carbonated concrete. Materials Chemistry and Physics, 84, 71-78.

DE SCHUTTER, G., BARTOS, P. J. M., DOMONE, P. & GIBBS, J. 2008. Self-compacting concrete, Taylor and Francis Group.

DHIR, R., JONES, M. & AHMED, H. 1990. Determination of total and soluble chlorides in concrete. Cement and Concrete Research, 20, 579-590.

DJERBI, A., BONNET, S., KHELIDJ, A. & BAROGHEL-BOUNY, V. 2008. Influence of traversing crack on chloride diffusion into concrete. Cement and Concrete Research, 38, 877-883.

EFNARC, S. 2002. Guidelines for Self-Compacting Concrete. European Federation for Specialist Construction Chemicals and Concrete Systems, Farnham, UK, 32.

EU FUNDED RESEARCH PROJECT UNDER 5FP GROWTH PROGRAM 2002. Guideline for practical use of methods for testing the resistance of concrete to chloride ingress.

GJØRV , O. E. 2009. Durability design of concrete structures in severe environments, Taylor & Francis Group.

HASSAN, Z. F. A. 2012. Rapid assessment of the potential chloride resistance of structural concrete. University of Dundee.

HEIRMAN, G., VANDEWALLE, L., BOEL, V., AUDENAERT, K. & DE, G. Year. Chloride penetration and carbonation in self-compacting concrete. In: ConcreteLife'06-International RILEM-JCI Seminar on Concrete Durability and Service Life Planning:

Curing, Crack Control, Performance in Harsh Environments, 2006. RILEM Publications SARL, 13-23.

HENDY, C. R. & SMITH, D. A. 2007. Designers' Guide to EN 1992-2: Eurocode 2: Design of Concrete Structures. Concrete Bridges, Thomas Telford.

JIANG, J.-Y., SUN, G.-W. & WANG, C.-H. 2012. Numerical calculation on the porosity distribution and diffusion coefficient of interfacial transition zone in cement-based composite materials. Construction and Building Materials.

KIM, H.-S., AHN, T.-S., KIM, C.-H. & JEON, B.-S. 2009. Quality Control of Chloride Diffusivity of the High Durable Concrete for Approaching Road of Incheon Bridge.

KOEHLER, E. P. & FOWLER, D. W. 2006. ICAR Mixture Proportioning Procedure for Self-Consolidating Concrete [Online]. Available: http://www.icar.utexas.edu/publications/108/ICAR%20108-1%20(Proportioning).pdf [Accessed 04-05-2012].

MCGRATH, P. & HOOTON, R. 1996. Influence of voltage on chloride diffusion coefficients from chloride migration tests. Cement and Concrete Research, 26, 1239-1244.

MOHAMMED, M. K., DAWSON, A. R. & THOM, N. H. 2013. Production, microstructure and hydration of sustainable self-compacting concrete with different types of filler. Construction and Building Materials, 49, 84-92.

MOHAMMED, M. K., DAWSON, A. R. & THOM, N. H. 2014. Carbonation of filler typed self-compacting concrete and its impact on the microstructure by utilization of 100% CO2 accelerating techniques. Construction and Building Materials, 50, 508-516.

MOON, H. Y., KIM, H. S. & CHOI, D. S. 2006. Relationship between average pore diameter and chloride diffusivity in various concretes. Construction and Building Materials, 20, 725-732.

NILSSON, L.-O. Year. Prediction models for chloride ingress and corrosion initiation in concrete structures. In: Prediction models for chloride ingress and corrosion initiation in concrete structures, 2001. Chalmers university of technology, Building Materials.

NT BUILD 443 Nordtest,1995. Accelerated Chloride Penetration.

NT BUILD 492 Nordtest,1999. Concrete mortar and cement based repair materials:chloride migration coefficient from non-steady-state migration experiments.

OKAMURA, H. & OUCHI, M. 2003. Self-compacting concrete. Journal of Advances Concrete technology, 1, 5-15.

SHANE, J. D., MASON, T. O., JENNINGS, H. M., GARBOCZI, E. J. & BENTZ, D. P. 2000. Effect of the interfacial transition zone on the conductivity of Portland cement mortars. Journal of the American Ceramic Society, 83, 1137-1144.

SONG, H.-W., LEE, C.-H. & ANN, K. Y. 2008. Factors influencing chloride transport in concrete structures exposed to marine environments. Cement and Concrete Composites, 30, 113-121.

STANISH, K., HOOTON, R. & THOMAS, M. 1997. Testing the chloride penetration resistance of concrete: a literature review. FHWA contract DTFH61, 19-22.

STANISH, K., HOOTON, R. D. & THOMAS, M. 2000. Testing the chloride penetration resistance of concrete: a literature review, Department of Civil Engineering, University of Toronto.

WINSLOW, D. N., COHEN, M. D., BENTZ, D. P., SNYDER, K. A. & GARBOCZI, E. J. 1994. Percolation and pore structure in mortars and concrete. Cement and Concrete Research, 24, 25-37.

YANG, C. & SU, J. 2002. Approximate migration coefficient of interfacial transition zone and the effect of aggregate content on the migration coefficient of mortar. Cement and Concrete Research, 32, 1559-1565.

YANG, C. C. 2005. Effect of the percolated interfacial transition zone on the chloride migration coefficient of cement-based materials. Materials chemistry and physics, 91, 538-544.

YANG, C. C. & CHO, S. W. 2005. Approximate migration coefficient of percolated interfacial transition zone by using the accelerated chloride migration test. Cement and Concrete Research, 35, 344-350.

YING, W. 2013. Performance assessment of cement-based materials blended with micronized sand: microstructure, durability and sustainability.

ZHENG, J.-J., WONG, H. S. & BUENFELD, N. R. 2009. Assessing the influence of ITZ on the steady-state chloride diffusivity of concrete using a numerical model. Cement and Concrete Research, 39, 805-813.

Chapter 8:
Conclusions, suggestions and recommendations

8.1 General

Despite the long history of studying the concrete damage caused by corrosion of steel reinforcement as a result of carbonation and the chloride penetration, these phenomena have to be re-examined with the invention of modern types of concrete. The relationships between these two physico-chemical durability features and both the internal chemical composition and the microstructure of the concrete at different length scales are not established clearly. Thus, the present research has attempted to quantitatively analyze these relationships using a combined approach of experimental and modeling works. These were undertaken with the aid of some selected and modified chloride and carbonation accelerated tests in order to obtain the result in a practical time frame.

Due to the very heterogeneous nature of the concrete as a composite material at all scales, several parameters related to its cement matrix and ITZ phases were quantitatively analyzed, considering the aggregate phase to be impermeable to aggressive agents. Hydration products (i.e. concrete chemical composition), the capillary pores nature of these two phases (Macro/micro and nano scales) and the pore characterizations of the two in the presence of the aggregate were linked with the carbonation and chloride penetration. Accordingly, a possible mechanism at different length scales explaining the overall response of both normal and sustainable SCCs, at medium to high strength grade, to the degradation caused by carbonation and chloride penetration in harsh environments are proposed. Even so, the work and the results presented in this dissertation are still too limited to fully understand the response mechanisms to these two environmental phenomena and cover all types of normal and sustainable SCC.

It is possible to derive the following main and key conclusion from the current research: The macro tests (observation of carbonation and chloride penetration progression) and the modeling results based on these observation showed that sustainable SCC exhibited lower carbonation resistance than NVC in short term. However, the modification of the

internal micro structure in this type of concrete enables it to resist CO_2 penetration in the longer term over the service life. In aggressive chloride environments, sustainable SCC should have greater suitability than NVC except when using unreactive filler. However, to produce sustainable SCC with high resistivity to the aggressive agents such as carbon dioxide and chloride as well as to lengthen its service life in very severe environments, vital enhancement of the concrete internal pore structure at both micro and nano scales is needed by selecting the proper filler type. The significant improvement of the internal pore structure at the nano scale by using multi-active fillers and mineral admixtures is not recommended for the sustainable SCC which might be exposed to severe combined environments (carbonation and chloride). Further, the features of the internal pore structure and the strength level at the macro scale had less effect on the whole response of sustainable SCC to carbonation and chloride ingress in both short and long term tests. More details of this final and main conclusion can be summarized as follows:

8.2 Carbonation progression response

In terms of internal chemical composition and pore structure characterization, the results obtained demonstrate that the carbonation propensity in sustainable SCC is not only chemically controlled. But, instead, the modification of the internal pore structure plays a substantial role in determining the progression of carbonation especially when the SCC is less alkaline. On the other hand, NVC tends to produce more alkaline pore water solutions by depositing considerable amounts of CH compound in the concrete pores. Thus, in the case of NVC, chemical control of carbonation is more important, regardless of the more open internal pore structure of this concrete type.

Whatever the type of the filler or mineral admixture that may be used to produce sustainable SCC, whether non-reactive or reactive, the computational modeling using data obtained from the unpressurized accelerated carbonation test predicts that the carbonation diffusion coefficient will not change much after 28 days water curing. Stating the finding in another way, the change of the chemistry of the matrix (lower pH due to lower CH content) as a result of the addition of different fillers will have little impact on the actual carbonation rate under long term exposure. This will keep the steel in sustainable SCC passivated and in safe conditions throughout a concrete service life of at least 50 years as for the NVC.

In sustainable SCC the matrices have less CH and fewer and finer micro-pores than are encountered in the matrices of the NVC and less than in the ITZs of both SCC and NVC. The consequence is that CO_2 is preferentially penetrated to the ITZs in sustainable SCC, whereas in NVC it takes place more generally through the whole system.

8.3 Carbonation- microstructure footprints

The more open internal structure revealed by the presence of greater macro pore percentages in the NVC, in the reference SCC (without cement replacement) and in the SCC with non-reactive filler, had a positive impact on the microstructure after carbonation. This benefit arises because the proportion of macro capillary pores reduces and micro capillary pore proportion increases after carbonation with very little or no change of the nano pores. The same trend was recorded for the sustainable SCC with denser structures using reactive fillers and mineral admixtures. However, the delayed Ettringite formation after carbonation had a negative effect in increasing the percolation of the nano pores by producing bigger critical pore diameters after carbonation. This was particularly noticeable in the sustainable SCC with combined cement replacement by FA plus SF (i.e. reactive filler and a mineral admixture).

Accordingly, it is possible to conclude that the impact of carbonation on the sustainable SCC microstructure is more noticeable in denser concrete having multi filler and mineral admixture additions in its cement matrix. On the one hand, this denser microstructure reduces the carbonation penetration rate. On the other hand, carbonation affects the nano permeation characteristics of the carbonation front in denser concrete more significantly than it does in lower density concrete. This might facilitate the concrete cover deterioration in the case of the interaction of carbonation with water or other aggressive substances leading to more rapid initiation of steel corrosion. The previously accepted norm that carbonation, itself, has a non-harmful effect - its effect being limited to the reduction of the pH value of the concrete, causing the steel de-passivation (as explained previously) - might need to be revised for concretes having complex cement matrix chemistries.

8.4 Chloride progression response in short term test

According to the quantitative analysis performed for characterizing the internal microstructure, the calculation of chloride migration coefficients and the proposed relationships between them, it may be concluded that the chloride resistivity of the investigated normal and sustainable SCC is independent of the porosity values or capillary pore structure nature (whether macro or micro). The ability of the cementitious materials used (cement, fillers and mineral admixtures) to alter the capillary pore structure or chemistry of the cement matrix at nano scale may cause the chloride resistivity differences.

From a physical point of view, the microstructural analysis suggested that the use of unreactive filler at relatively high cement replacement in sustainable SCC might effectively dilute the active chemistry that could react with the chloride. This would be the case for both the cement matrix and the ITZ at micro and nano scales and hence, might facilitate the chloride migration and ingress in a short term test. Supporting the above hypothesis of a relationship between chloride resistivity and the pore structure of the concrete as a composite material in the short term, the chloride migration coefficients obtained were much more related to the critical pores diameters of the cement matrix than to the average pore diameters in both the ITZ or cement matrix.

It is found that the local micro permeation features (porosity and thickness) of the ITZs and their pore percolations often play a significance role in controlling the overall response to chloride ingress in SCC. The high connectivity of ITZs as a result of using a high volume of fine aggregates in the SCC (for achieving the mix design and fresh properties criterion) probably increased the sensitivity of the transport characteristics to the ITZ features. The assessment of the chloride migration coefficients demonstrates that chloride ingress increased significantly with the increase in ITZ porosity and, especially, with an increase of the ITZ thickness. Therefore, it is proposed that the ITZ thickness might be primarily responsible in determining the chloride ions' migration velocity, especially when high water to cement ratio or coarse and unreactive filler is used. The ITZ of the NVC had greater local water content than in other mixes; the sustainable SCC with limestone filler had greater non-reactive material in the ITZ. Both of these

disturbances to their respective mixes caused thick and more porous ITZs than in other mixes. This explains the much greater pore percolation observed in these two mixes.

8.5 Chloride progression response in long term and numerical results

The chloride diffusion features of the concrete were assessed by determining the chloride diffusion coefficients for short term exposure and by the numerical simulation for the long term chloride penetration. These assessments revealed that the SCC had a greater chloride resistivity than the NVC at medium strength grade in the aggressive chloride environments, especially when reactive by-products were used at relatively high percentages of cement replacement. However, the use of unreactive filler demonstrated lower chloride penetration resistance even with the use of low water to binder ratios. It is concluded that chemically active binders are an important contribution to the ability of a SCC to resist chloride penetration for natural long term exposure. The predicted service life and the proposed cover designation might confirm the above conclusions.

8.6 Recommendations for more durable sustainable SCC

Based on the work presented in this dissertation, the following recommendation should be consider for producing sustainable SCC that is more resistive to carbonation and aggressive chloride environments:

8.6.1 Aggressive carbonation environment

Although CO_2 levels are increasing, the study has shown that a design service life of 100 years or more against steel de-passivation is possible when sustainable SCC with reactive or non-reactive fillers (at relatively high dosage of cement replacement) is used. However, some pre-stressed concrete products need be designed to achieve a very long service life i.e exceeding 1000 years in very harsh environments. Normally, the carbonation is not the sole cause of deterioration of the concrete cover. Interactions with water and other aggressive agents such as Cl^- are highly probable in very severe exposure conditions.

Therefore, to maintain the defense against steel corrosion beyond 100 years, it is recommended to keep the cement matrix phase of the sustainable SCC simple in term of chemistry. The use of a binary blend with reactive or non-reactive filler at relatively high

cement replacement may be enough to protect the steel from the de-passivation. For this case, carbonation products are expected to be limited to the blocking of macro and micro pores of the concrete with very little effect on the nano permeation features. More complex cement matrix phases might have an adverse effect on the nano pore structure features of the carbonation front, producing expansive carbonation products that thus provide easy penetration pathways.

Being a composite material at macro scale, sustainable SCC with low maximum coarse aggregate size might be more desirable for the use in the aggressive carbonation environment because of the lower percolated internal pore structure revealed by the present study. The presence of coarse aggregate produced a lower overall carbonation resistance of the concrete as compared to its mortar. For the same volume of coarse aggregate, minimizing the size of that coarse aggregate will increase the tortuosity, and hence length, of the carbonation diffusion path at macro scale. However, it will increase the total volume of the ITZ at micro scale and this might allow easier carbonation progression. Therefore, reducing the volume of coarse aggregate is also required, as well as size reduction, to ensure good carbonation resistance.

8.6.2 Aggressive chloride environment

To increase suitability of the sustainable SCC in chloride aggressive environments, the results of the rapid chloride assessments, when considered in terms of the micro and nano internal structure features, lead to a recommendation that the fine aggregate volume fractions should be minimized as much as possible. However, this reduction should not be enough to interfere with the desirable flow characteristics of the concrete produced. An optimum fine aggregate volume fraction at macro scale might reduce the role of the ITZ effectively in producing more percolated internal structures at both micro and nano scales. Therefore, work is required to define this optimum volume fraction.

To improve the chloride resistivity of sustainable SCC, and to achieve long service life, the cementitious materials should be selected on the basis of their ability to make significant changes at nano and micro scales for both the cement matrix and the ITZ phase’s pores, rather than the to change the pores of the concrete at macro scale. Thus, the optimization of the cement matrix phase characteristics is probably enough to achieve

significant reductions in chloride ingress. By using low water to cement ratios for cement-based SCC, or low water to cementitious material ratio when cement is blended with active fillers with the optimum dosage of SP, it is possible to obtain the desired fresh characteristics, the required strength level and reduced chloride penetration.

However, for sustainable SCC with non-reactive filler based, both the short and long term chloride assessments results imply that the use of ground-up, or very fine, fillers needs to be employed in producing sustainable SCC more relevant to chloride penetration. The low water to powder materials ratio with the aid of optimum SP dosage was not enough to improve the chloride diffusivity. The long-term chloride penetration assessments also suggest that the chloride binding capacity of the cement matrix of this type of concrete mix might not be enough to improve the chloride resistivity of sustainable SCC and to produce long service lives in aggressive chloride environments, even when compared to NVC. Thus, it is strongly recommended to use of ground-up or very fine non-reactive fillers at least in order to avoid undesirable disturbance of the cement matrix and the ITZ phases of sustainable SCC that is to be used in severe chloride environments.

8.7 Suggestions and recommendations for future works

The following points are recommended for any future research work:

- The quantitative results obtained from the TGA and XRD chemical analysis and the pore structure characterization at different scales before and after carbonation could be combined together with the accelerated carbonation progression results to develop a multi-phenomenon model to describe this complex response.
- There is a need to develop a multi- phenomenon model to describe the chloride penetration in sustainable SCC with regard to both short and long terms behaviour. The proposed relationships between the internal microstructure and the concrete chloride resistivity in short term assessments, the proposed simple diffusion model from the long term evaluation and the quantitative assessment of the cement matrix chemistry in the present study might be considered as starting points in developing such a model.

- In the present investigation, the most common fillers and mineral admixtures to produce sustainable SCC were considered. However, further work could be done to evaluate the effect of using relatively high replacement of cement by other types of fillers and mineral admixtures on the carbonation and chloride penetration of sustainable SCC using the same existing approach. Non-reactive fillers based on brick and glass by products and slag, Metakaolin (M) and rice husk ash (RHA) as moderately active fillers or mineral admixtures have become attractive materials to produce sustainable SCC recently.
- As the medium to high strength sustainable SCC has become increasingly used and planned for different applications, more research work is needed to evaluate the long term resistivity of such concrete to the sulfate attack and freeze-thaw cycling. The research addressing the combined impact of these two types of deterioration processes and their interaction with chloride and carbonation would be a very interesting topic.
- The present study has been unable to determine to what extend penetration of SCC by external chemicals can be treated generically and to what extent individual chemical interaction should be consider. A wide range of chemical 'stresses' might help to develop such understanding.
- The electro-chemical behavior of the embedded steel in sustainable SCC has to be investigated in detail due to the concern of the reduction of the original pH value of such concrete, especially when high percentages of reactive fillers are used. Any reduction in the pH value of the concrete could terminate the steel passivation at early ages and hence very high deterioration rates would be expected when the concrete is exposed to aggressive environments over the longer term.
- The main concern in the use of SCC is an economic one due to the use of high binder contents including cement. Therefore, the impact of using various aggregates in terms of their types and quantities were excluded from the present investigation. However, nowadays sustainable concrete can also made with totally or partially recycled aggregate. Thus, future work could consider these two parameters as the main variables in the evaluation of carbonation and chloride penetration in

sustainable SCC made with natural and artificial aggregate by-products and constant cement contents. Slag, brick, glass, rubber and sintered fly-ash-based aggregate are recommended for such future work.

- Cost analysis of the increased/decreased predicted cover thicknesses due to the use of sustainable SCC in aggressive chloride environments is needed in the future work to evaluate the economy of concrete material required to meet the service life. The most efficient filler might not produce the most economical solution for the desired service life.

Appendices

Due to the burdensome quantity of data obtained and analysis performed, all the relevant appendices were included in a CD attached with the current thesis. These appendices, their description and the file types are listed as follow:

ID	Description	Files type
Appendix A	XRD analysis (Cement, fillers and Mixes) + TGA Data	Word, Excel and Text
Appendix B	ITZ thickness and Porosity analysis	Excel (Analysis)
Appendix C	ITZ hydration products profiles- EDX analysis	Word (Data) + Excel (Analysis)
Appendix D	Titration tests results, numerical calculation in Excel Solver and chloride ingress modeling	Excel (Analysis)
Appendix E	Published researches	Pdf
MSc thesis	Full MSc thesis 2013	Pdf